UNIVERSITY OF
BIRMINGHAM

Changes in Cellular Phenotype and Resistance to Cisplatin in an Oral Squamous Carcinoma Model Over-Expressing Cytoglobin

by

Lorna Susan Thorne

A thesis submitted to

The University of Birmingham

for the degree of

DOCTOR OF PHILOSOPHY

School of Biosciences

The University of Birmingham

September 2015

ABSTRACT

Although cytoglobin is widely considered a tumour suppressor, re-expression plays a role in disease progression in a subset of oral squamous cell carcinomas (OSC), but the mechanism of action is not understood. In this thesis, we developed a new OSC cell model to study the effects of cytoglobin over-expression on cellular phenotype and resistance to cisplatin. Microarray analysis of cytoglobin-expressing cells showed significantly altered transcripts related to stress response, adhesion and locomotion, and metabolism. Treatment of cytoglobin-expressing cells with cisplatin revealed a greater response in p53-regulated target expression (*MAP3K5, NQO1, CDKN2A* and *GADD45A*) compared to non-expressing cells. Further investigation showed this was associated with higher CHK1, p53 and p21 protein levels, suggesting enhanced activation of p53 signalling pathways. Furthermore, cytoglobin-expressing cells were more resistant to cisplatin-induced apoptosis and altered their cell cycle distribution. These changes were linked to reduced total cellular and mitochondrial superoxide. Collectively, these findings demonstrate for the first time that cytoglobin over-expression is associated with resistance to cisplatin-induced cytotoxicity and that the mechanism involves p53 signalling. In conclusion, we propose expression of cytoglobin may afford tumours cells a survival advantage in the harsh environmental conditions of the developing tumour as well as resistance to drugs like cisplatin.

I wish to dedicate this thesis to my nan, Kathleen Ellen Millichamp,

who sadly passed away from colon cancer before she could

see me complete my doctoral studies.

~

ACKNOWLEDGEMENTS

Thanks are firstly due to my supervisor, Dr. Nikolas Hodges, for his support during my PhD and the trust he has shown in allowing me to develop this research. I am also grateful for the kind assistance of Dr. Lakis Liloglou and the team at the Roy Castle Lung Cancer Research Centre who made me feel very welcome during my visits, and for their invaluable help in analysing my microarray data. I would like to thank Dr. Timothy Williams who gave his time to teach me the basics of array analysis and helped me trawl through the data, and also to Dr. Christopher Weston who assisted with the motility studies. I am indebted to Dr. Farhat Khanim for her guidance and much-needed motivation during the troubleshooting days of this PhD. I would also like to express gratitude to Dr. Fiona McRonald who first helped me navigate through the sometimes treacherous waters of Cytoglobin research and was always on hand for a cup of tea.

Special thanks are due to my many Tower labs colleagues who brightened my long laboratory days and made my PhD such a cheerful experience (you know who you all are!). My frequent trips to genomics were made so much more enjoyable with lively conversations with Laine Reynolds, Fay Williams, and Norman Day. When I collected my orders, the wonderful guys in stores, Alan and Grahame, were always able to help me return back to the lab smiling. I could not have survived without the lasting friendship, infectious happiness and craziness of the many people I shared this PhD with, especially: Zahra Khan, Louise Stone, Katarzyna Koczula, Rachael Kershaw, Chibuzor Uchea, Leda Mirbahai, Mohammed Shuwaiken, Bob Harris, Abiola Domasu, Shrikant Jondhale, Jaspreet Kaur, Nicola White, Jack Charlton, Allan West and James Haycocks.

My brilliant parents have been my rock throughout my PhD rollercoaster of highs and lows as a first generation academic, and I thank them for everything; from their unwavering enthusiasm to inspiring me to aim high by pursuing science at University. I owe them so much. I also wish to thank my boyfriend, Nick Martin, who has preserved my sanity with his encouragement and cheesy comic relief to help me through the difficult times. Without the love and support from these special people I would be lost, and I thank them whole-heartedly for helping me through.

CONTENTS

LIST OF FIGURES

LIST OF APPENDIX FIGURES

LIST OF TABLES

LIST OF EQUATIONS

LIST OF ABBREVIATIONS

ΔNp63	Tumour suppressor protein 63, delta N isoform (amino deleted)
$^{\bullet}OH$	Hydroxyl radical
53BP-1	p53 binding protein
AhR	Aryl hydrocarbon receptor
AKT	V-Akt murine thymoma viral oncogene homolog 1
AP1	Activator Protein 1 (c-Jun/c-Fos)
ARE	Antioxidant response element
ARHGAP18	Rho GTPase activating protein 18
ASK1	Apoptosis signal-regulated kinase 1 (aka. MAP3K5)
ATP	Adenosine triphosphate
BNIP3L	BCL2/adenovirus E1B 19kDa interacting protein 3-like
BSO	Buthionine sulfoximine
CCND1	Cyclin D1
CDKN2A	Cyclin-dependent kinase inhibitor 2A
cDNA	Complementary deoxyribonucleic acid
c-Ets-1	Cellular erythroblastosis virus E26 oncogene homolog 1
CHK1	Checkpoint kinase 1
CO	Carbon monoxide
COL1A1	Collagen 1α1
COX7C	Cytochrome c oxidase subunit VIIc
CYGB	Cytoglobin
CYGB+	Cytoglobin over-expressing PE/CA-PJ41 clones
Cysteine	Cysteineteine
DEN	N,N-diethylnitrosamine
DNA	Deoxyribonucleic acid
DNMT1	DNA methyltransferase 1
DTT	Dithiothreitol
ECM	Extracellular matrix
ERK1/2	Extracellular signal related kinase 1/2
ETC	Electron transport chain
FAK	Focal adhesion kinase
Fe^{2+}	Ferrous iron
Fe^{3+}	Ferric iron
G1	Growth phase 1 (cell cycle)
G2	Growth phase 2 (cell cycle)
GADD45A	Growth arrest and DNA-damage inducible alpha
GFP	Green-Fluorescent Protein

GPX	Glutathione peroxidase
GSH	Glutathione, reduced
GSSG	Glutathione, oxidised
GST	Glutathione transferase
H_2O_2	Hydrogen peroxide
HDAC	Histone deacetylase
HIF1	Hypoxia Inducible Factor 1
HIF1A	Hypoxia Inducible Factor 1, alpha subunit
His	Histidine
HRE	Hypoxia response element
HSC	Hepatic Stellate Cell
IP3	Inositol triphosphate
ITGA2	Integrin alpha 2 subunit
JNK	c-Jun N-terminal kinase
LMW-PTP	Low molecular weight protein tyrosine phosphatases
LPA	Lyophosphatidic acid
M	Mitosis (cell cycle)
MAP3K5	Mitogen-activated protein 3 kinase 5 (aka. ASK1)
MB	Myoglobin
MDA	Malondialdehyde
MMP	Matrix metalloprotease
MMR	Mismatch repair
mPTP	Mitochondrial permeability transition pore
mRNA	Messenger ribonucleic acid
MTT	3-(4,5-Dimethyl-2-thiazolyl)-2,5-diphenyl-2H-tetrazolium bromide
NAD(P)+	nicotinamide adenine dinucleotide (phosphate), oxidised
NAD(P)H	nicotinamide adenine dinucleotide (phosphate), reduced
NCE	No Cytoglobin Expressing PE/CA-PJ41 control clones
NER	Nucleotide excision repair
NFAT	Nuclear factor of activated T cells
NFκB	Nuclear Factor kappa B
NGB	Neuroglobin
$NO^{\bullet}$	Nitric oxide
NOD	Nitric oxide dioxygenase
NQO1	NAD(P)H dehydrogenase quinone 1
Nrf2	Nuclear factor E2-related factor 2
NSCLC	Non-small cell lung cancer
$O_2^{\bullet-}$	Superoxide
OSC	Oral squamous cell carcinoma

p21	Tumour suppressor protein 21
p38	Tumour suppressor protein 38
p53	Tumour suppressor protein 53
PCNA	Proliferating cell nuclear antigen
PCR	Polymerase chain reaction
PDGF	Platelet-derived growth factor
PHD	Prolyl hydroxylases
PRPF40	Splicesome assembly factor 40
RNA	Ribonucleic acid
RNS	Reactive nitrogen species
ROS	Reactive oxygen species
RTqPCR	Real time quantitative PCR
S	S phase (cell cycle)
SOD	Superoxide dismutase
Sp1	Stimulatory Protein 1
SRB	Sulforhodamine B
STAP	Stellate cell activation-associated protein (former name of Cytoglobin)
TAA	Thioacetamide
TAp73	Tumour suppressor protein 73, TA isoform (transcriptional domain containing)
TBP	TATA-Binding Protein
TGFβ1	Transforming growth factor beta 1
TRX	Thioredoxin
TSA	Trichostatin
UCP	Mitochondrial uncoupling protein
VDAC	Voltage dependent anion channel
αSMA	alpha Smooth Muscle Actin
γH2AX	Gamma histone H2 variant

CHAPTER ONE:

General Introduction

1.1 Cytoglobin as a Hemeprotein

Heme (ferriprotoporphyrin IX) is a critical cofactor that mediates the function of many heme-containing proteins within aerobically respiring cells. Its biosynthesis occurs in the mitochondria through the incorporation of a ferrous (Fe^{2+}) iron atom into the protoporphyrin-IX complex by ferrochelatase (Ajioka et al., 2006; Tsiftsoglou et al., 2006) and this moiety is then subsequently incorporated into apoproteins to produce hemeproteins such as cytochromes (e.g. cytochrome P450), metabolic enzymes (e.g. peroxidases) and oxygen-binding globins (e.g. hemoglobin) (Ponka, 1999) (Figure 1). The globin protein superfamily includes a collection of heme-bound metalloproteins that are able to bind to diatomic ligands such as oxygen, carbon dioxide and nitric oxide and share a characteristic globin fold, comprised of eight α-helical chains in a 3-over-3 arrangement (Wajcman et al., 2009) (Figure 2).

The two most studied globins are the oxygen transporter hemoglobin and oxygen storing, nitric oxide-metabolising myoglobin, and both have been found to also exhibit a peroxidase function (Vinogradov and Moens, 2008; Wajcman et al., 2009). These globins are pentaco-ordinated; that is, the iron atom has its 5 co-ordination sites occupied by nitrogen atoms within the heme and a proximal histidine residue of the globin protein (highly conserved His113) whilst its distal 6^{th} bond is freely available to reversibly associate with diatomic ligands (Wilson and Reeder, 2008) (Figure 1c). Other members of the globin superfamily; neuroglobin (NGB) and cytoglobin (CYGB), contain hexaco-ordinated hemes where all co-ordination sites are bonded and the distal 6^{th} site is bound by another histidine residue (highly conserved His81) that directly competes with the ligand to bind the heme (Gorr et al., 2011; Weber and Fago, 2004). The presence of

conserved cysteine residues within these hexaco-ordinated globins (at Cys46 and Cys55 in NGB, at Cys38 and Cys83 in CYGB) have been found to form a redox-sensitive disulfide bond (Hamdane et al., 2003; Tsujino et al., 2014). Dithiothreitol (DTT)-mediated reduction of the disulfide bond in CYGB, for instance, re-positions His81 slightly away from the heme increasing ligand access to the heme and permits regulation of their affinity (Hamdane et al., 2003; Lechauve et al., 2010; Makino et al., 2011). Studies investigating the oxygen affinity of hexaco-ordinate globins have found both His81 binding and disulfide bond formation affects ligand affinity, with overall CYGB oxygen affinity (P_{50}) greater than that of myoglobin, being ~1 Torr and 2.8 Torr, respectively (Fago et al., 2004; Hamdane et al., 2003; Wright and Davis, 2015).

1.2 Cytoglobin Discovery and Structure

CYGB was initially identified in a proteomic screen of a fibrotic rodent liver that aimed to develop understanding of the hepatic stellate cell (HSC) activation process (Freitas et al., 2005; Kawada et al., 2001). The globin was significantly up-regulated in activated HSCs, in association with other activation markers alpha smooth muscle actin (αSMA) and collagen 1α1 (COL1A1) (Kawada et al., 2001). The protein has since been found in a number of vertebrates including fish, birds, amphibians, mice, and humans, of which the latter two share 95% primary sequence similarity (Asahina et al., 2002; Burmester et al., 2002; Kugelstadt et al., 2004; Pesce et al., 2002; Wawrowski et al., 2011; Xi et al., 2007). Phylogenetic profiling of globin family proteins suggests that CYGB is most closely related to avian Globin E and is likely to share a common ancestor with Myoglobin, with which it has ~25 % sequence similarity (Burmester et al., 2002; Burmester et al., 2004; Kawada et al., 2001; Kugelstadt et al., 2004; Pesce et al., 2002).

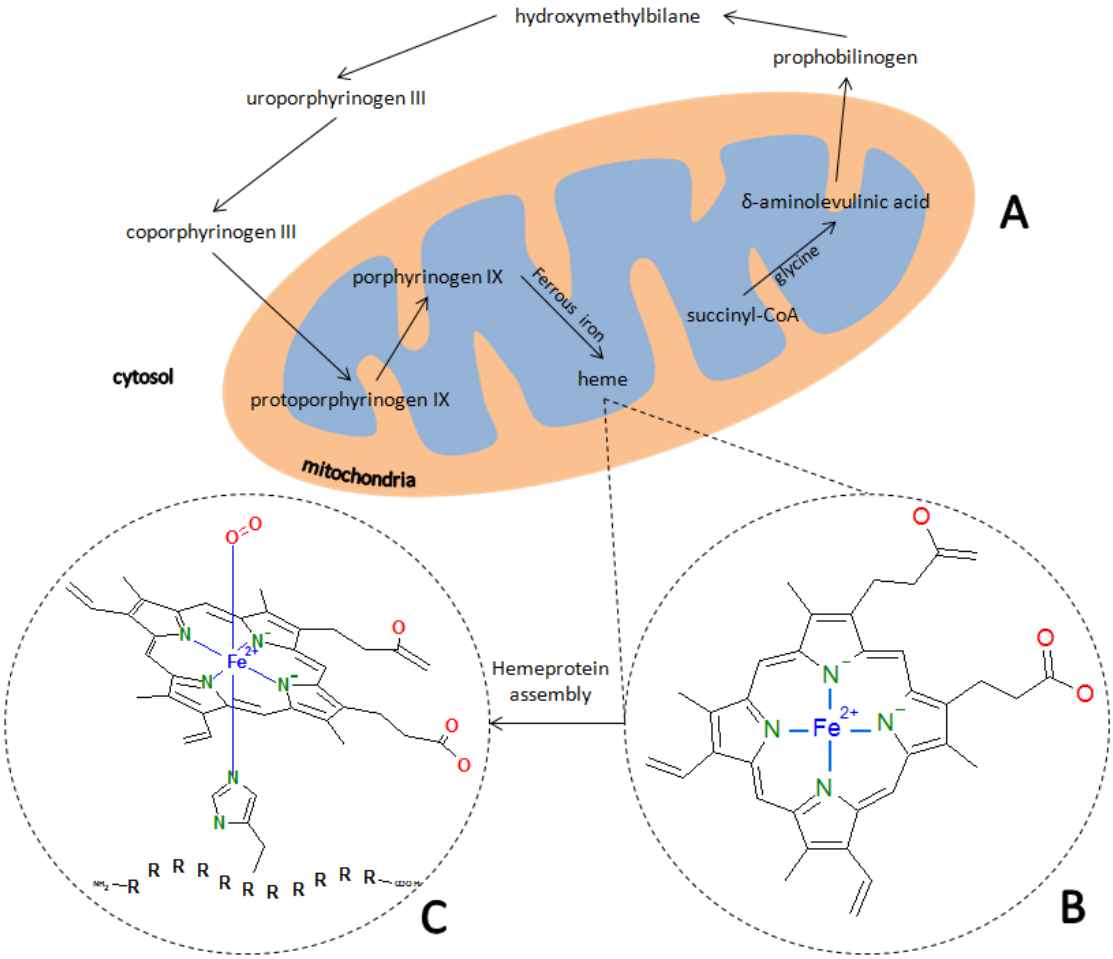

Figure 1 - Heme synthesis and its incorporation into protein.
(**a**) The heme biosynthetic pathway takes place in both the mitochondria and cytosol, starting with the conversion of succinyl coenzyme A (CoA) supplied by the tricarboxylic acid cycle into δ-aminolevulinic acid that then is shuttled into the cytosol for further processing into the protoporphyrinogen IX complex that is returned to the mitochondria for manufacture into heme. (**b**) The heme is planar with a central ferrous (Fe^{2+}) iron atom held in place by four co-ordination bonds (*blue lines*) to nitrogen atoms of a tetrapyrrole complex. In its ligand-bound state, the iron is ferrous and in its unbound state is ferric (Fe^{3+}). (**c**) Heme forms the prosthetic group of proteins such as globins where the heme is tethered to a histidine residue of the protein (*shown as part of polypeptide chain*, *[R]n*) via its 5th co-ordination bond of the iron atom, leaving the remaining 6th co-ordination site available to bind diatomic ligands such as oxygen, carbon monoxide and nitric oxide. Figure adapted from Tsiftsoglou et al. (2006) and molecular structures created with Isis Draw v. 2.3.

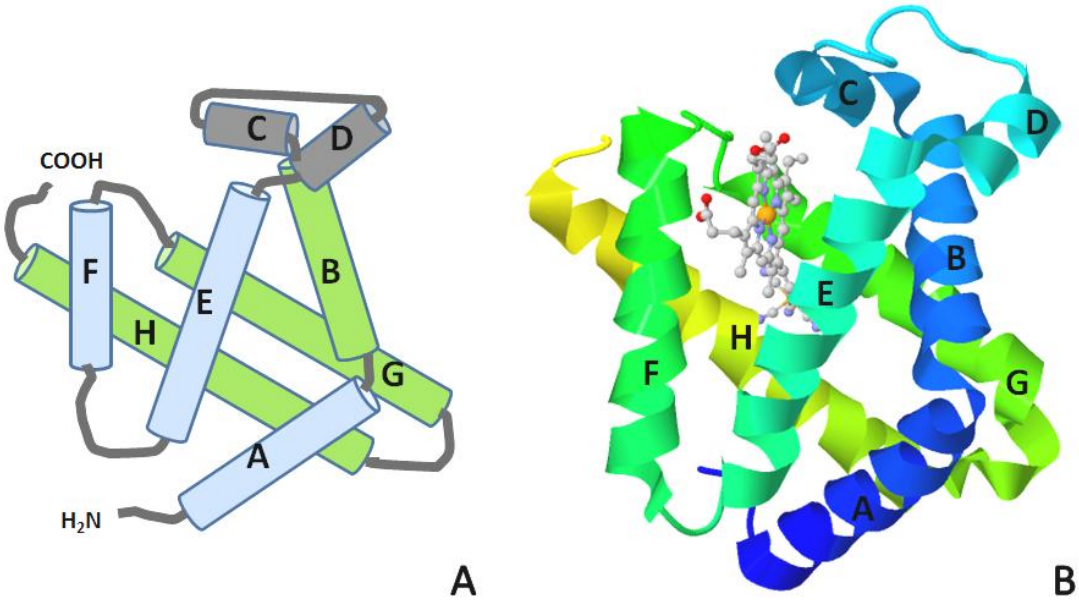

Figure 2 - Globins share a conserved 3/3 fold assembly in their tertiary structure.
(**a**) The globin fold is made of eight α-helices arranged so there are three stacked above each other (each set shown in blue and green), with two α-helix hinges (shown in grey) between them. The heme is anchored by the conserved His113 residue between helices E and F. (**b**) CYGB protein structure adapted from the RCSB protein databank (PSB ID = 1URV), showing the eight helices labelled A to H and the position of the heme moeity.

Like the other globins, CYGB contains the conserved globin fold and a heme group (Figure 2b) within its active site that is surrounded with non-polar residues to create a hydrophobic environment to tightly regulate the redox state of the central iron atom (de Sanctis et al., 2004; Sawai et al., 2005). CYGB is 190 amino acids in length; almost a third longer than the average length of the other globins (Pesce et al., 2002; Trent and Hargrove, 2002). The increased size is due to the presence of extended N and C termini, suggested to be due to a direct seven codon duplication event and acquisition of an additional exon, respectively, during its evolution (Burmester et al., 2002). The longer termini have potential to be protein interaction sites that may regulate or permit CYGB function, but the actual purpose for these extensions is unknown. It has, however, been recently suggested that the N terminus offers some stability to CYGB (Tangar, 2015) and further that the termini may be responsible for facilitating lipid binding to cardiolipin and oleate (Reeder et al., 2011). The quaternary structure of CYGB has been under debate. Crystal structures indicate it exists as a homo-dimer with the interaction interface at the E helix mediated in part by intermolecular disulfide bonding and the heme pockets extending outwards (de Sanctis et al., 2004). However, later studies using a laser light scattering technique found this conformation was far less common than monomeric CYGB at physiological concentrations (Lechauve et al., 2010). Recent work has also shown the existence of CYGB monomers, dimers and tetramers and that polymerisation is associated with lower affinity for carbon monoxide and cyanide (Tsujino et al., 2014).

1.3. Cytoglobin Gene Structure and Expression

The locus encoding *CYGB* in humans is at chromosome position 17q25 and consists of four exons separated by three intronic sequences; B12-2 (i.e. the second amino acid of

the 12th codon in the B α-helix), G7-0 and H36-2, the latter of which does not occur in other hexaco-ordinate globin sequences (Trent and Hargrove, 2002) (Figure 3). Compared with other vertebrate globin family members, the *CYGB* gene has the lowest mutation rate, suggesting that the gene encodes a protein with a highly conserved function (Trent and Hargrove, 2002; Wystub et al., 2004). There are several transcription factor binding sites in the regulatory region of *CYGB* (but notably not one for TATA-binding protein (TBP)) and these include sites for Hypoxia Inducible Factor 1 (HIF1), Stimulatory Protein 1 (SP1), Activator Protein 1 (AP1), Nuclear Factor kappa B (NF_kB) and cellular erythroblastosis virus E26 oncogene homolog 1 (c-Ets-1) sites (Guo et al., 2006; Guo et al., 2007; Wystub et al., 2004) NF_kB and Sp1 transcription sites are situated in the CpG-rich island in the promoter, suggesting that epigenetic control of *CYGB* expression is possible (Oleksiewicz et al., 2011). Most recently, members of the tumour suppressor protein 53 (p53) family, ΔNp63 and TAp73, have been found to directly regulate expression of *CYGB* (three recognition sites for ΔNp63 were found in the promoter) and this was associated with diminished oxidative stress and apoptosis (Latina et al., 2015).

Important mechanisms of *CYGB* gene regulation include promoter hypermethylation (Shaw et al., 2009) and histone modification. Expression of *CYGB* in cancer cell lines can be restored; at least partially, by treatment with de-methylating agents (Shivapurkar et al., 2008; Xinarianos et al., 2006), such as 5-aza-2-deoxycitidine as demonstrated in head and neck cancer cell lines (Shaw et al., 2006; Shaw et al., 2009). *CYGB* transcripts were increased in 12/14 lung cancer cell lines and decreased in 7/8 of normal bronchial cell lines following 18 h incubation with 100 nM trichostatin (TSA), which is a type 1 and 2

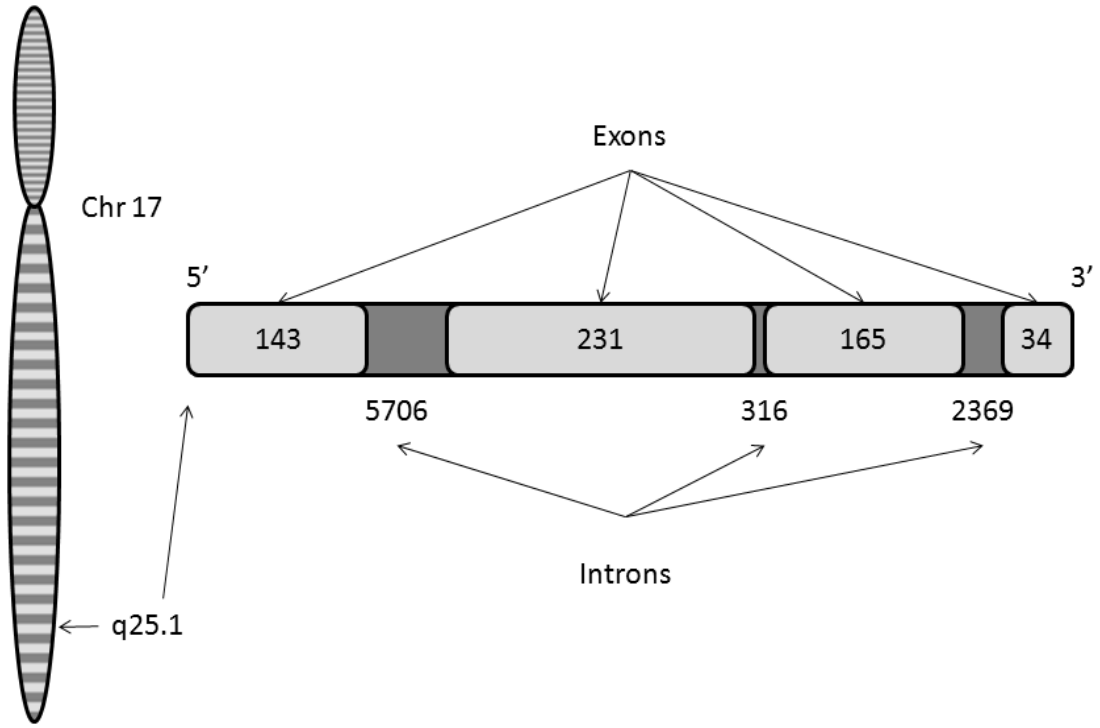

Figure 3 - Cytoglobin Gene Structure.
The *CYGB* gene is located on chromsome 17q25 and is made up of four exons and three introns, two of which are conserved with other hexaco-ordinated globin members. The numbers depict the number of bases (not to scale) within each region of the sequence. Figure adapted from Asahina et al. (2002) and Trent and Hargrove (2002).

histone deacetylase (HDAC) inhibitor (Oleksiewicz et al., 2013). It is proposed that either TSA interferes with normal HDAC function of chromatin decondensation and enhances access to the transcription machinery (Dokmanovic et al., 2007) or modifies transcription factors like HIF1α or NFκB, which result in altered *CYGB* expression (Oleksiewicz et al., 2013; Xu et al., 2007). Recently, rodents with reduced thyroid function have been shown to down-regulate *CYGB* within their hippocampus and transcripts could be restored to normal levels (and protein increased, but not to control levels) 24 h after an intravenous injection of triodothyronine (T3), indicating hormonal regulation is a component of controlled *CYGB* expression (Oliveira et al., 2015).

1.4. Cytoglobin Distribution

CYGB expression has been reported within a range of organs for example the liver, oesophagus, brain, retina and heart (Burmester et al., 2000; Fordel et al., 2004; Geuens et al., 2003; Hundahl et al., 2010; McRonald et al., 2012; Nakatani et al., 2004; Schmidt et al., 2004; Shigematsu et al., 2008). The globin has been found to be mainly expressed within fibroblast-related cell types including myofibroblasts, osteoblasts and HSCs, but expression has also been detected within neurones and epithelial cells (Hundahl et al., 2010; Nakatani et al., 2004; Schmidt et al., 2004; Shigematsu et al., 2008). The cellular location of CYGB is still debated. CYGB has been reported to be in the cytoplasmic compartment within epithelial cells (Gorr et al., 2011; Shigematsu et al., 2008), hepatocytes (Shigematsu et al., 2008), hepatic stellate cells (Kawada et al., 2001), osteoblasts and fibroblasts (Schmidt et al., 2004). However, there has also been nuclear CYGB staining reported in the brain (Geuens et al., 2003; Man et al., 2008), liver, cardiac, lung, and kidney tissues (Geuens et al., 2003), as well as in hepatocytes (Shigematsu et al., 2008), melanocytes (Fujita et al., 2014), and muscle progenitor cells (Singh et al.,

2014). Therefore, it remains unclear where in the cell CYGB localises, and this may be dependent upon context and cell type. Interestingly, CYGB has been observed in both cytoplasmic and nuclear regions in some cell types (Fujita et al., 2014; Man et al., 2008; Schmidt et al., 2004). Although work with a CYGB-GFP (GFP, Green-Fluorescent Protein) fusion construct failed to find a nuclear targeting motif or any evidence of active nuclear import (Hodges et al., 2008; Hundahl et al., 2010; Kawada et al., 2001; Schmidt et al., 2004), splicing of a nuclear localisation signal of a known nuclear protein to the N terminus of CYGB does however enable nuclear localisation of the globin (Itoh et al., 2013). This indicates CYGB has the potential to move across the nuclear envelope but the mechanism may be independent of a nuclear localisation sequence and may even involve simple diffusion (Geuens et al., 2003) or binding to other nuclear-targeted proteins.

1.5 Possible Cytoglobin Functions

Although the exact functions of CYGB are presently unknown, there is accumulating evidence in favour of a cytoprotective role. The most recent view of CYGB function is that it is involved in protecting cells against oxidative, fibrotic and hypoxic stress and thus has a tumor suppressor nature (Oleksiewicz et al., 2011). The vast array of potential functions for CYGB in normal cells seems to depend on specific cellular contexts and includes regulation of oxygen status, an antioxidant function through the detoxification of both ROS and RNS, a molecular oxygen shuttle to prolyl hydroxylases and other metabolic processes, cell survival and oxidative DNA damage protection (Asahina et al., 2002; Halligan et al., 2009; He et al., 2011; Hodges et al., 2008; Man et al., 2008; Mimura et al., 2010; Nakatani et al., 2004; Singh et al., 2009; Smagghe et al., 2008; Stagner et al., 2005; Tateaki et al., 2004; Xu et al., 2006). Very few downstream effectors

of CYGB have been identified, but there are transcripts that have been found to be regulated in response to CYGB over-expression, including collagen 1α1 (*COL1A1)*, mitochondrial uncoupling protein 2 (*UCP2*), cyclin D1 (*CCND1*), DNA methyltransferase 1 (*DNMT1*) and splicesome assembly factor 40 (*PRPF40*) (see Table 4).

1.5.1 Oxygen Sensing and Storage

It was logically assumed that as a globin protein, CYGB was involved in oxygen metabolism, and it had already been shown to bind oxygen with high affinity (see section 1.1). CYGB also shares some structural similarity with myoglobin (MB), especially in the primary structure of the heme-binding site (Trent and Hargrove, 2002) and has an oxygen affinity similar to that of MB (Fago et al., 2004; Hamdane et al., 2003). Therefore, early suggestions were that CYGB would operate to store and transport oxygen intracellularly to the mitochondria in cells lacking MB (Fago et al., 2004; Kawada et al., 2001; Trent and Hargrove, 2002). Expression of CYGB has also been found induced following hypoxia and fibrosis (see sections 1.6.1 and 1.6.2), which implied that it may act as an oxygen reserve during hypoxia. However, the fact CYGB is present at low concentrations within cells (Liu et al., 2012) and has slow ligand dissociation rates (Lechauve et al., 2010; Smagghe et al., 2008) makes a MB-like role seem unlikely. Also, the cell types where CYGB is expressed are not associated with high metabolic rates unlike the occurrence of MB or NGB in smooth muscle cells and neurones, respectively, and this further implies a role outside of simple oxygen transport and storage. However, the idea of CYGB acting to supply oxygen to particular biochemical reactions has recently resurfaced with the observation that CYGB expression in murine hepatic stellate cells can impair paracetamol metabolism and hepatocyte necrosis was lessened, particularly after low oxygen stress (Teranishi et al, 2015). Upon binding carbon

monoxide (CO) or oxygen, the expected movement of the distal His81 residue away from the heme is accompanied with distortion of the E helix and adjustments in the positions of amino acids within the CD-D helix region of CYGB (Makino et al., 2011). This conformational change has been hypothesised to form the basis of a signalling pathway where ligand-bound CYGB translates information about the oxygen status of the environment into a structural rearrangement that in turn leads to the downstream modulation of factors related to the oxygen response; potentially through altered gene expression (Geuens et al., 2003). However as stated by Schmidt et al (2004), there is no clear explanation for why a gas sensor should be restricted to fibroblast-like cells.

1.5.2. Enzyme Activity

CYGB from rodent HSCs were found to exhibit peroxidase activity and could metabolise linoleic acid hydroperoxide and hydrogen peroxide (H_2O_2) (Kawada et al., 2001), the latter of which was later confirmed by (Asahina et al., 2002). Most recently, CYGB's peroxidase ability was reported to involve production of an intermediate tyrosine free radical, which was inhibited by glutathione (Ferreira et al., 2015). There have also been reports to suggest CYGB has some limited superoxide dismutase (SOD) activity. A CYGB construct that lacked the N and C terminal extension sequences found in wildtype CYGB was reported to exhibit SOD activity that was lost almost completely when using double cysteine mutated CYGB (Trandafir et al., 2007). Although this study found the activity of the truncated construct was a fraction (~ 6 %) of that shown by bovine SOD, it was still higher than the activities of MB (0.2 %) or NGB (<0.1 %). Studies have additionally shown CYGB operates as an effective nitric oxide dioxygenase (NOD) in the presence of electron donor reduced cytochrome b_5 (Gardner et al., 2010; Smagghe et al., 2008). This was associated with improved preservation of aconitase activity after continuous nitric

oxide treatment; an enzyme that metabolises citrate within the tricarboxylic acid cycle (Tortora et al., 2007). Nitric oxide inhibits complex IV activity within the mitochondrial electron transport chain (ETC) when oxygen is in short supply (Petersen et al., 2008). CYGB expression was additionally reported to show an inverse correlation with intracellular nitric oxide concentration in vascular fibroblasts and CYGB's NOD activity was able to mediate protection against nitric oxide-induced apoptosis (Jourd'heuil et al., 2012) and improve nitric oxide-impaired respiration rates (Halligan et al., 2009), so CYGB detoxification of nitric oxide might restore respiratory function. Other detrimental consequences of chronic nitric oxide treatment include aberrant hypoxic signalling in normal oxygen conditions through inhibition of prolyl hydroxylase that regulates HIF1A activity (Berchner-Pfannschmidt et al., 2007; Metzen et al., 2003). CYGB is known to afford cells protection against hypoxic stress (see section 1.6.1), so the NOD activity of CYGB may facilitate this in part by hindering the nitric oxide-activated hypoxia response.

Under oxidising conditions, CYGB was found to cause lipid peroxidation of lecithin liposomes (Reeder et al., 2011). This study found oxidation of lipids by CYGB was five times more rapid than that by MB, suggesting this reactivity may be critical to CYGB's *in vivo* function. Although this seems to contradict observations that show CYGB to be an antioxidant (see section 1.5.3.2) and reduces lipid peroxidation biomarkers after oxidative stress (Kawada et al., 2001; Xu et al., 2006), the physiological level of CYGB is low enough that a signalling; rather than cytotoxic, role for the CYGB-generated lipid peroxides is possible (Ascenzi et al., 2013). Lipids are the basis of many important signalling molecules and lipid rafts provide a scaffold for certain proteins to transduce signals from activated membrane-associated receptors, such as integrins and RasGTPase (Santos and Schulze, 2012; Simons and Toomre, 2000). Peroxidation of lipids generates

intermediate signalling molecules such as inositol triphosphate (IP_3) and lyophosphatidic acid (LPA) that serve to regulate various processes like cell survival, migration and inflammatory responses (Hannun and Obeid, 2008; Leonarduzzi et al., 2000; Mills and Moolenaar, 2003). Indeed, binding of ligands has been shown to induce a structural change in CYGB (see section 1.1) and the binding of lipids such as cardiolipin and oleate to Fe^{3+} CYGB causes a shift towards the pentaco-ordinated iron state (Reeder et al., 2011), so together these might initiate signalling pathways through either binding other proteins and/or enhancing production of lipid second messengers. In conclusion, even though CYGB shows enzymatic potential as a peroxidase, NOD and SOD, the activities reported for these are relatively low, so it is unclear yet whether these have physiological importance.

1.5.3. Antioxidant

1.5.3.1. Defining Oxidative Stress and the Antioxidant Response

Oxidative stress describes a cellular environment that consists of significantly elevated reactive oxygen species (ROS) and/or reactive nitrogen species (RNS) that are generated from, for example, aerobic mitochondrial respiration and as a by-product of xenobiotic metabolism (Ray et al., 2012a; Schieber and Chandel, 2014). ROS are free radicals with at least one unpaired outer shell electron that reacts more readily than molecular oxygen. ROS have many endogenous extracellular functions (this is reviewed in detail by Janssen-Heininger et al., 2008). For instance, critical signalling factors involved in cell survival such as the regulator of the mitogen-activated protein kinase cascade, apoptosis signal-regulated kinase 1 (ASK1, aka. MAP3K5, Ray et al., 2012a) and transcription factor NF_kB (Wang et al., 2002) are redox-regulated. However, ROS in excess are

extremely damaging to cellular components, oxidising DNA bases, proteins and lipids that in turn detrimentally lead to mutations, changes in activity and compromise membranes, respectively.

There are a wide variety of free radicals with different half lives and properties that influence the molecules they can interact with. These include superoxide ($O_2^{\bullet -}$), H_2O_2, hypochlorous acid (HClO), peroxyl radicals (HOO^-), hydroxyl radicals ($^\bullet OH$), nitric oxide ($NO^\bullet$) and peroxynitrite ($ONOO^-$) (Murphy et al., 2011). A major endogenous source of ROS is the mitochondria and production pathways are shown in Figure 4. The mitochondrial complexes 1 (NADH:ubiquinone oxidoreductase) and complex 3 (ubiquinol:cytochrome c oxidoreductase) are the primary sources of superoxide and can be responsible for both oxidative stress and the increased conductance of mitochondrial uncoupling proteins (UCP) for protons during thermogenesis (Brand et al., 2004). In contrast to H_2O_2, $^\bullet OH$ cannot diffuse very far, has a short half life and is very reactive, making it one of the most toxic cellular radicals (Klaunig et al., 2011; Schieber and Chandel, 2014; Valko et al., 2006). For instance, $^\bullet OH$ initiates the lipid peroxidation chain reaction, whereby the fatty acid hydrocarbon tails of phospholipids are oxidised leading to amplified ROS generation that compromise membrane structure and function (Valko et al., 2006). Surplus of ROS also damages DNA through base oxidations and promoting lesions such as strand breaks and cross-links, each of which; if unrepaired, contribute to genetic instability, mutation and aberrant cell signalling - factors strongly implicated in tumorigenesis (Hanahan and Weinberg, 2011; Klaunig et al., 2011). Proteins can be

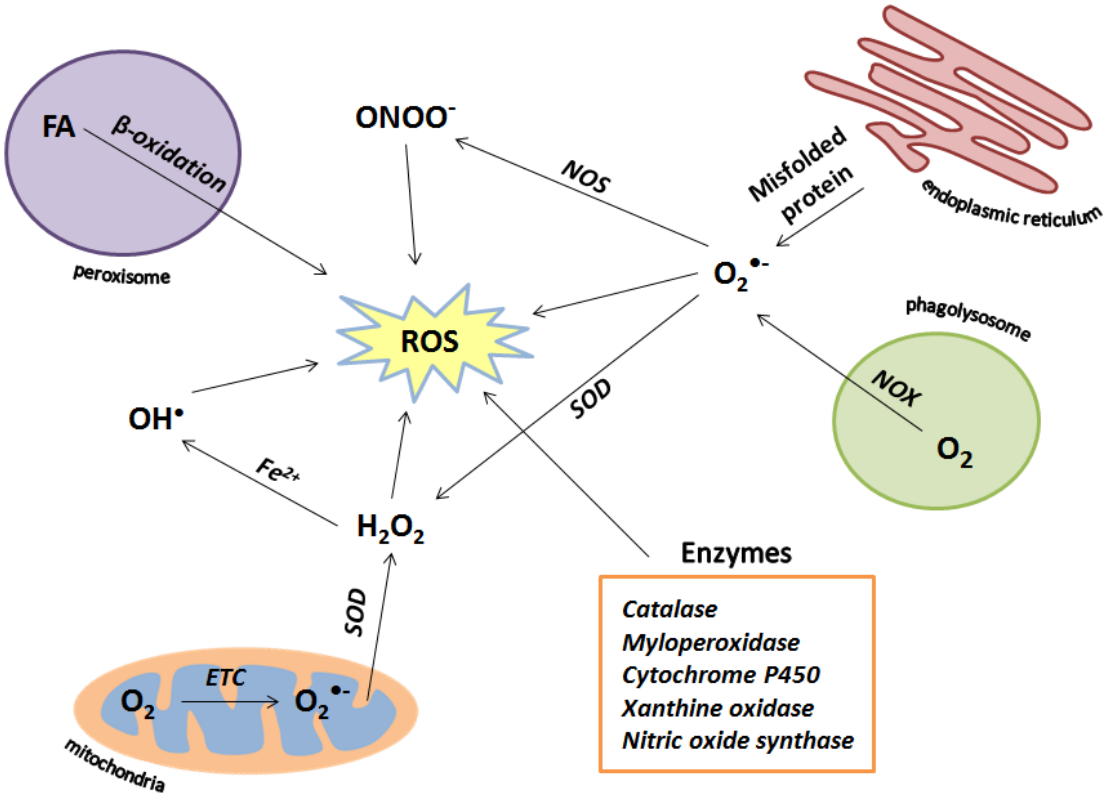

Figure 4 - Endogenous Sources of ROS.
The mitochondria are a major source of ROS within cells. Under aerobic conditions, oxygen is reduced to water by accepting a pair of protons and two pairs of electrons within the electron transport chain, whilst ATP is produced from the energy release caused by the transfer of electrons between the four mitochondrial complexes. However, electron transfer can be uncoupled from the complexes 1 and 3 and reduces molecular oxygen to form superoxide which is subsequently metabolised by superoxide dismutase in both mitochondrial and cytosolic compartments to form hydrogen peroxide. This can be further metabolised by redox-active transition metal ions to form hydroxide (i.e. the Fenton reaction that uses ferrous ions (Fe^{2+}) obtained from local storage pools within cells). Figure adapted from Holmstroem et al. (2014) and information provided in Hamanaka and Chandel (2010), Kamata et al. (1999) and Sena et al. (2012). Electron transport chain (ETC), Peroxynitrite (ONOO-), FA (Fatty acids), superoxide ($O_2^{\bullet-}$), superoxide dismutase (SOD), hydrogen peroxide (H_2O_2), hydroxide (•OH), nitric oxide synthase (NOS) and NADPH oxidase (NOX).

post-translationally modified or damaged by ROS through oxidation of Cysteine thiols that can react with other oxidised Cysteine residues to form disulfide bridges or oxidised further into sulfenic acid, which can subsequently react with nitrogen of a local amino acid to form sulfenyl amide, with glutathione or irreversibly with H_2O_2 to generate sulfonic acid (Ray et al., 2012a). Such structural modifications would alter protein activity and adversely affect intracellular signalling, as well as changing transcription factors activity and thus gene expression. In all, oxidative stress contributes to the development of a host of pathologies such as inflammation, neurodegenerative disease and cancer (Vurusaner et al., 2012).

In order to evade or delay the deleterious effects of oxidative stress on cellular macromolecules and address the redox homeostatic balance, a variety of defensive proteins are activated that are collectively referred to as antioxidant response factors. Expression of these antioxidants is implemented by redox-sensitive Keap1 that has over 20 Cysteine thiol groups, of which some are highly vulnerable to oxidation by electrophiles or ROS (Niture et al., 2010; Yamamoto et al., 2008). Oxidation of Keap1 causes a conformational change, such that the associated transcription factor Nuclear Factor E2-related Factor 2 (Nrf2) - the major regulator of the antioxidant response - is liberated and translocates into the nucleus where it assembles with other factors to bind antioxidant or electrophile response elements (AREs or EpREs, respectively) (Copple et al., 2008; Niture et al., 2010). These regulatory sites are upstream of an array of enzymatic and non-enzymatic antioxidants that ultimately result in senescence, and repair or apoptosis. Keap1 normally sequesters Nrf2 in the cytosol via an interaction with E3 ubiqutin ligase Cul3 that targets Nrf2 for proteasomal degradation, while in the

nucleus Bach1 competes to bind ARE and thereby represses antioxidant gene expression in non-oxidising conditions (Niture et al., 2010). There are hundreds of Nrf2-inducible antioxidant factors and these include glutathione peroxidase (GPX), glutathione-S-transferase (GST), SOD, thioredoxin (TRX) and several drug efflux transporters (Holmstroem and Finkel, 2014).

Nrf2 also controls glutathione (GSH) synthesis via increasing expression of glutamylcysteineteine synthetase (Trachootham et al., 2008). GSH is a tripeptide of critical importance, acting as the primary non-enzymatic reductant within cells (concentrations can reach 10 mM) and it can efficiently detoxify ROS (Reuter et al., 2010). GSH is maintained in the cytosol in its reduced state by an NADPH-dependent glutathione reductase, whilst in the endoplasmic reticulum it is oxidised to GSSG that may enable the formation of disulfide bonds required for some protein assemblies (Chakravarthi et al., 2006). As GSH contains a Cysteine residue and thus a sulfydryl group, it can be used to reduce a number of oxidising molecules through enzyme-mediated reactions (e.g. GPX conversion of H_2O_2 to water) or directly conjugating to oxidants via GST, producing oxidised GSSG (López-Mirabal and Winther, 2008). The reversible reaction between GSH and GSSG enables redox homeostasis to occur as under oxidative stress, so when GSH is readily available it detoxifies ROS and oxidised proteins.

Thioredoxin (TRX) is another critical antioxidant that contains two oxidisable Cysteine residues and has overlapping functions with the GSH antioxidant system in reducing protein disulfides (Holmgren and Lu, 2010). TRX is NADPH-dependent and transfers electrons from this cofactor to its active site to supply to antioxidant enzymes like TRX-peroxidase and promote their activity (Lu and Holmgren, 2014). TRX maintains the

activity of transcription factors like p53 and NF_kB in this manner that allows a response to altered cellular redox state to be mounted. NF_kB is another transcription factor activated in response to oxidative stress through ROS-activation of I_kB kinase that is responsible for targeting the NF_kB inhibitor I_kB for ubiquitin-mediated degradation and thus liberating the factor to enter the nucleus and initiate changes to gene expression (e.g. *GADD45* for inhibition of apoptotic c-Jun N-terminal kinase (JNK)) (Trachootham et al., 2008).

HIF1 is another transcriptional factor that responds to oxidative stress and regulates cell survival. It is a heterodimer of HIF1α and HIF1β (aka. ARNT), the latter of which is constitutively present in cells, unlike its partner HIF1α that is only stabilised in low oxygen conditions. This occurs because prolyl hydroxylases (PHD); dependent on ascorbate, 2-oxoglutarate, and oxygen for their function, have limited oxygen available to hydroxylate the degradation domain of the HIF1α subunit that normally promotes ubiquitin-mediated proteasomal degradation through the Von-Hippel Lindau protein (D'Angio and Finkelstein, 2000; Harris, 2002; Myllyharju, 2013). ROS can regulate HIF1 through promoting the Fenton reaction (Figure 4) that inactivates PHD that relies upon Fe^{2+} for its activity, but also by direct S-nitrosylation of HIF1 that stabilises the protein (Trachootham et al., 2008). HIF1 enhances the transcription of genes containing the hypoxia response element (HRE; sequence RCGTG) and includes numerous targets involved in regulating apoptosis, cell cycle progression, angiogenesis and glycolysis (Harris, 2002; Majmundar et al., 2010; Semenza, 2000).

1.5.3.2. Cytoglobin as an Antioxidant

Expression of CYGB decreases cellular ROS and its expression was down-regulated in Nrf2 knockout diabetic murine heart tissue (He and Ma, 2012), suggesting CYGB is a component of the Nrf2-regulated antioxidant response system. CYGB can detoxify ROS through its peroxidase, SOD and NOD activities (see section 1.5.2) and the disulfide bond formed between Cys38 and Cys83 of the globin has been shown to be redox regulated (see section 1.1), which together suggest CYGB has importance in detecting changes to oxygen tension and elicits antioxidant functions to enable the cell to maintain redox homeostasis.

Indeed, *CYGB* expression increases after exposure to oxidative stressors and is associated with protection against oxidative damage. Peroxide-treated MCF7 human breast cancer cells showed an up-regulation of a number of antioxidant genes; including *CYGB* (Chua et al., 2010). *CYGB* is also up-regulated in N27 rodent mesencephalic cells following treatment with nitric oxide-generating paraquat (Moran et al., 2010). N2a neuroblastoma cells also showed a time-dependent H_2O_2-inducible *CYGB* expression, and stable *CYGB* knockdown after treatment with H_2O_2 caused significantly impaired viability as determined by reductase turnover of MTT (see section 2.9.2) (Li et al., 2007). CALU1 and H358 human lung cancer cells also showed enhanced viability following treatment with H_2O_2 after *CYGB* transfection that also corresponded with reduced depletion of cellular GSH (Oleksiewicz et al., 2013). G361 human melanoma cells with high levels of CYGB expression have elevated total cellular ROS levels when *CYGB* is knocked down and this sensitised cells to H_2O_2-induced apoptosis (Fujita et al., 2014). Viability after H_2O_2 treatment was also increased in CYGB over-expressing NRK49F rodent kidney fibroblast cells and was reversed by *CYGB* knockdown (Nishi et al., 2011).

Mimura et al (2010) confirmed CYGB over-expression increased protection against oxidants in CYGB over-expressing, H_2O_2-treated NRK49F cells and also showed this in H_2O_2-treated HEK293T rodent kidney fibroblasts. This study also found CYGB expression increased in rodent remnant kidney models and transgenic over-expression of CYGB in these rodents protected them against nephrectomy-induced oxidative stress damage, including reduced excretion of oxidised deoxyguanosine (Mimura et al., 2010). This confirmed oxidative stress protection exhibited by CYGB *in vitro* also occurred *in vivo*.

CYGB expression has also been linked to protection against DNA damage. In liver tumours of *CYGB* knockout C57BL/6 mice with chronic choline deficiency, the absence of CYGB was associated with enhanced levels of p53 binding protein (53BP-1) and gamma histone H2 variant (γH2AX) (Thuy et al., 2015) and these proteins are known to be key biomarkers of DNA damage (Mohammad and Yaffe, 2009). In TE671 human medulloblastoma cells, transfection with CYGB-GFP resulted in lower total cellular ROS concentrations after treatment with synthetic oxidant Ro19-8022; a cell-permeable photosensitiser that generates singlet oxygen (Will et al., 1999), and this correlated with decreased oxidative DNA damage (Hodges et al., 2008). Protection against oxidative DNA damage was also demonstrated after buthionine sulfoximine (BSO) treatment in TE-8 human oesophageal cancer cells with CYGB over-expression but not in NE-1 normal oesophageal cells showing physiological levels of CYGB (McRonald et al., 2012), which suggests the protective effect depends on a threshold level of CYGB being reached. CYGB over-expression in C2C12 murine myoblasts treated with menadione increased viability by almost 20 % relative to controls and siRNA-mediated *CYGB* knockdown was able to reverse this effect (Singh et al., 2014), indicating oxidant protection in these cells

was CYGB-regulated. Furthermore, *CYGB* knockdown in these oxidant-treated cells also correlated with depleted GSH, indicating decreased oxidative stress. The nitric oxide-impaired respiration of NIH3T3 murine fibroblasts was increased with stable *CYGB* knockdown, which could be reversed by stably transfecting *CYGB* into these cells (Halligan et al., 2009), which suggests the NOD activity reported for CYGB (see section 1.5.2) has physiological relevance.

The physiological importance of CYGB's peroxidase activity (see section 1.5.2) was shown with the over-expression of CYGB enabling increased cell survival in SH-SY5Y human neuroblastoma cells following H_2O_2 treatment (Fordel et al., 2006) and in rodent HSCs after treatment with ferric nitrilotriacetate or arachidonic acid (Xu et al., 2006). Most recently, H226 human keratinocytes with *CYGB* knockdown showed increased apoptosis following treatment with H_2O_2 and were also shown to have higher ROS levels after doxorubicin treatment (Latina et al., 2015). Xu et al (2006) found CYGB expression blocked ROS-induced differentiation of the cells into myofibroblasts and decreased concentrations of the products of lipid peroxidation; namely malondialdehyde (MDA) and 4-hydroxynoneal, which together support an antioxidant function. The study by Hodges et al (2008) also showed CYGB over-expression caused reduced lipid peroxidation, as determined by using *cis*-paranaric acid, which is a fatty acid that can integrate into membranes of the cell and lose its fluorescence upon oxidation (Steenbergen et al., 1997). Reduced MDA levels were also reported in CYGB over-expressing transgenic Sprague-Dawley rats with hypoxia-ischemia brain injury compared to control groups (Tian et al., 2013).

Together, these data strongly support the hypothesis that CYGB promotes cell survival through homeostatically modulating oxidative stress, although the exact mechanism by which CYGB does this remains to be determined. Functions determined to date are summarised in Figure 5.

1.6 Pathologies Linked to Cytoglobin

1.6.1. Hypoxia

CYGB has also been implicated in the hypoxic signalling pathway. The *CYGB* promoter region contains two HIF1-binding HRE sites at positions -141 and -448 upstream of the transcriptional start site and an erythopoietin binding site at position -144 (Wystub et al., 2004). Mutation of each or all of these sites in BEAS-2B bronchial epithelial cells was found to cause up to a third less or a complete lack of *CYGB* promoter activation by hypoxia exposure, respectively (Guo et al., 2007). Electromobility shift and ChIP analysis within this study also demonstrated these HREs are functional, suggesting *CYGB* can be induced by hypoxic stress signalling. Several studies have reported a time-dependent induction of *CYGB* during hypoxia. For instance, hypoxia treatment led to significant up-regulation of *CYGB* in HN33 murine hippocampus cells, Swiss CD1 mice (Fordel et al., 2004) and also in heart and liver tissue of rodents (Schmidt et al., 2004). *HIF1* dominant-negative knockout mice failed to induce *CYGB* upon hypoxic treatment, further affirming the globin is up-regulated in a HIF1-dependent mechanism (Fordel et al., 2004). Hypoxia treatment of OSC cell lines was shown to significantly increase *HIF1A* expression and this positively correlated with *CYGB* expression (Shaw et al., 2009). However, *CYGB* up-regulation following hypoxia was not as pronounced in rodent brain tissue (Li et al., 2006), with only approximately 20 % induction observed after 3 days of hypoxia. It is worth considering that the severity and duration of hypoxic stress defined by the studies

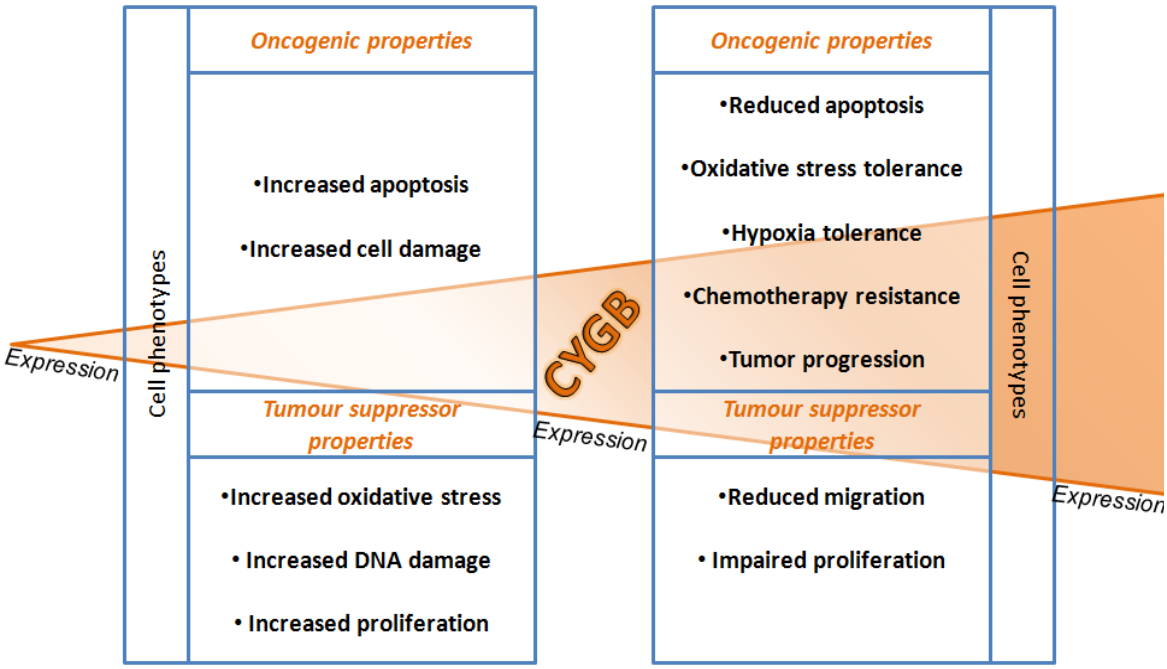

Figure 5 - Currently proposed functions of CYGB.
The tumour suppressor-like and oncogene-like functions that CYGB is shown to be associated with are summarised in the diagram above. The expression level of *CYGB* is associated with which phenotype prevails within the tumour.

investigating hypoxic regulation of *CYGB* varied. For instance, the hypoxia oxygen tension exerted relative to normal was 10 % oxygen in the study by (Li et al., 2006), 1 % in that of (Fordel et al., 2004), 9 % within the studies of (Schmidt et al., 2004) and 0.1 % in the experiments of (Singh et al., 2014), which would have inevitably altered the change in *CYGB* transcript observed in each case. So, the fact Li et al (2006) could not confirm *CYGB* up-regulation following hypoxia may have been due to the oxygen tension not being low enough to permit the augmentation of *CYGB* expression reported after hypoxic stress by many groups.

Interestingly, Singh et al (2009) showed that out of all the tissue types examined, CYGB was most abundant in the heart; a tissue that displays extreme sensitivity to oxygen stress, which is consistent with the hypothesis that CYGB is acting to protect against the potential damage from low oxygen conditions. Immunohistochemical studies have shown CYGB expression is significantly co-localised with carbonic anhydrase IX (CAIX) (a HIF1α target) and PHD2 (a negative regulator of HIF1α, see section 1.5.3.1) in hypoxic breast cancer tissue (Gorr et al., 2011), which further implicates CYGB in the regulation of hypoxia signalling. The correlation between CYGB and CAIX distribution was also found by work in our laboratory in idiopathic pulmonary fibrotic tissue (Carpenter, 2010) and in studies with tissue from normal human stomach, breast, liver and bladder and tissue from human glioblastoma multiforme cells (Emara et al., 2010). Together, these studies show CYGB is expressed in cells that have mounted the hypoxia signalling response. Interestingly, Gorr et al (2011) additionally found that CYGB is expressed in both von Hippel Lindau (vHL) protein-deficient and -proficient RCC4 human renal carcinoma lines during hypoxia, which implies hypoxic stress up-regulation of *CYGB* can

occur independently of HIF1α, as expression can occur with or without HIF1α-degradation by vHL protein (see section 1.5.3.1).

Over-expression of CYGB within rodent pancreatic beta cells (Stagner et al., 2009) and Sprague-Dawley rodent brain tissues (Tian et al., 2013) promoted survival and preserved tissue histology following chronic ischemia, and the latter study showed this was associated with reduced caspase 3 activity. Further evidence of the molecular regulation of *CYGB* under hypoxia was found in hypertrophic C57BL/6 murine cardiac tissue where *CYGB* transcription from the AP1 and nuclear factor of activated T cells (NFAT) promoter sites could be enhanced by hypoxia and this depended on functional calcineurin (Singh et al., 2009), which is a calcium ion-regulated phosphatase that participates in multiple signalling pathways including apoptosis and NF_kB signalling (De Windt et al., 2000; Uchino et al., 2008).

Although there is substantial evidence showing *CYGB* is a hypoxia response gene and its expression is associated with increased protection from hypoxia-mediated damage, little is known about how CYGB may achieve this. CYGB has been hypothesised to shuttle oxygen towards specific oxygen-requiring reactions like PHDs that would mediate a negative feedback mechanism on HIF1α activity and thus reduce the extent of damage caused by activation of pathways by hypoxia, or CYGB may afford protection through the detoxification of ROS that are increased when a cell experiences ischemia-reperfusion (Hodges et al., 2008; Oleksiewicz et al., 2011; Stagner et al., 2005; Tian et al., 2013). It has also been speculated that because hypoxia involves the creation of a reducing cellular environment, the Cys38-Cys83 disulfide bond present in CYGB would be broken and reduce the affinity of the globin to the bound oxygen ligand (see section 1.1), which

would thereby cause release of oxygen into the hypoxic cell (Hamdane et al., 2003; Lechauve et al., 2010). This would implicate CYGB in sensing oxygen tension and mediating oxygen release much like MB in smooth muscle cells, but the low concentration and slow kinetics of ligand dissociation (see section 1.5.1), coupled with the fact that this function would be apparently restricted to fibroblast-like cells (see section 1.4) imply that this general role is unlikely. However, it is reasonable to hypothesise that the oxygen tension changes occurring within hypoxic cells may be transduced by CYGB into a signal to activate the hypoxic response pathway (via conformational changes induced by disulfide bond reduction) and this response is specific to either fibroblast cells or the molecular context of these.

1.6.2. Fibrosis

Fibrosis describes the substantial increase in collagen deposition and accumulation of other extracellular matrix (ECM) components that forms scar tissue. Liver fibrogenesis is characterised by the activation of HSCs into myofibroblasts, which secrete high quantities of ECM that in turn distorts sinusoid tissue architecture and eventually results in compromised liver function and blood perfusion (Bataller and Brenner, 2005). The composition of the ECM during fibrosis is also altered; increased levels of collagen type 1 are observed in addition to raised laminin, chondroitin sulfate proteoglycan and hyaluronan levels (Alcolado et al., 1997) in addition to changes in expression of cell surface integrin receptors (Friedman, 2008). In their inactive state, HSCs function to store vitamin A, but activation induces them to differentiate into myofibroblasts. The activation of HSCs is mediated by cytokines like TGFβ1 (which can be sourced from the catalysis of latent TGFβ1 by matrix metalloprotease 9 (MMP9)), ROS, platelet-derived growth factor (PDGF) and nitric oxide (Friedman, 2008). Biomarkers of active HSCs

include expression of αSMA and myocyte enhancer factor-2 (Bataller and Brenner, 2005).

Several studies have shown *CYGB* expression is induced in response HSC activation during fibrosis. Protein extracts from rodent HSCs after activation were analysed by 2D-PAGE coupled with mass spectrometry and it was found that along with usual biomarkers of activation, a new 21 kDa protein was dramatically up-regulated in a time-dependent manner (Kawada et al., 2001). The researchers named the unknown protein **ST**ellate cell **A**ctivation-associated **P**rotein (STAP) to reflect this. Subsequent investigation by degenerative PCR and comparing the amplicon to the rodent cDNA library revealed it encoded a globin, had a homologous gene in humans (Asahina et al., 2002) and also that it could be detected at high levels in rodent liver following thioacetamide (TAA)-induced fibrosis (He et al., 2011; Kawada et al., 2001). STAP was later renamed CYGB and its up-regulation at both protein and mRNA levels by fibrotic stress was confirmed in rodent (Tateaki et al., 2004) and murine liver (Man et al., 2008), in bone marrow-derived mesenchymal stroma cells from C57BL/6 mice (Cho et al., 2009; Mimura et al., 2010), following carbon tetrachloride-induced fibrosis, in fibrotic regions of chronically inflamed WBN/Kob rodent pancreatic tissue and in Transforming Growth Factor beta 1 (TGFβ1)-activated primary rodent HSCs *in vitro* (Nakatani et al., 2004). A study comparing protein expression profiles of myofibroblasts from HSCs or portal mesenchyme used 2D-PAGE coupled with MALDI-TOF mass spectrometry to show CYGB was among the markers characterising HSC-derived myofibroblasts (Bosselut et al., 2010). Furthermore, up-regulation was noted to be specific to fibrotic

stress and not to others like osmolarity, heat or ultraviolet (Reeder et al., 2011), implying that CYGB elicits a function related to the fibrotic response.

COL1A1 expression was also found inversely correlated with *CYGB* after 12 h of treatment in the liver tissue of carbon tetrachloride-induced Balb/C mice and it was notable that up-regulation of *COL1A1* occurred a full 24 h past the time at which the highest *CYGB* expression was observed (Man et al., 2008), implying that *CYGB* accumulation is a pre-requisite for significant *COL1A1* up-regulation in this context. In agreement with this idea, Shivapurkar et al (2008) reported transient CYGB over-expression in H2228 (lung adenocarcinoma), H2887 (NSCLC cancer) and HCC 1569 (breast cancer) cells resulted in a greater than 2-fold down-regulation of *COL1A1*, indicating that CYGB may modulate levels of transcripts required for collagen 1 production. CYGB is expressed predominantly in fibroblast-like cells such as osteoblasts and HSCs, which are known to secrete higher levels of collagen compared with other cell types (Schmidt et al., 2004), and coupled with the fact *CYGB* expression was simultaneous to enhanced collagen synthesis in the study by Kawada et al (2001), these data suggest CYGB may be involved in collagen synthesis. Indeed, over-expression of CYGB augmented induction of *COL1A1* in TGFβ1-activated HSC (Nakatani et al., 2004).

Inflammation, steatosis and several biomarkers of fibrosis were elevated in *CYGB* knockout compared to wildtype C57BL/6 mice subjected to chronic choline deficiency, and these mice also exhibited greater oxidative stress that was reflected in the down-regulation of a number of anti-oxidant genes such as *GPX6* in HSCs isolated from this *in vivo* model (Le Thi Thanh Thuy et al., 2015). This implies the fibrosis response is in part mediated through enhanced oxidative stress and the absence of CYGB exacerbates this.

CYGB over-expression in HSCs was also shown to prevent differentiation into myofibroblasts and further that it could reduce liver damage caused by chronic carbon tetrachloride treatment in Sprague-Dawley rats when *CYGB* was administered via recombinant adenovirus 2 (rAAV)-mediated carrier injection, before and after damage (Xu et al., 2006). Within these *in vivo* models, CYGB over-expression correlated with reduced pro-collagen 1, TGFβ1 and αSMA as well as to a preserved liver tissue histology and function, suggesting CYGB could inhibit development of the fibrotic phenotype *in vivo*. Furthermore, protection against fibrotic damage was also found in remnant kidney model Wistar rats that showed CYGB over-expression resulted in diminished renal dysfunction (determined by serum creatinine and urine protein concentration), decreased collagen and αSMA immunostaining of kidney tissue, and greater conservation of kidney histology (Mimura et al., 2010), which collectively demonstrates CYGB is anti-fibrotic. This is in agreement with the findings of Xu et al (2006) who showed suppression of HSC differentiation with CYGB over-expression and is further supported by the observation that CYGB is crucial to the inhibition of HSC activation by arundic acid (Cui et al., 2012). CYGB over-expression in TAA-induced fibrotic liver of Sprague Dawley rats caused a reduction in collagen 1 deposition and induced apoptotic cell death in HSC-T6 rodent HSC line in a CYGB concentration-dependent manner (He et al., 2011). The impaired viability identified in this study seems at odds with the findings by other groups showing that CYGB expression is actually able to promote survival following oxidative stress, but this discrepancy may be due to differences in cell type and mechanisms of cell death triggered by fibrosis and oxidative stress.

1.6.3. Cytoglobin and Cancer

1.6.3.1. Tumorigenesis

Tumorigenesis is a complex process characterised in part by the exhibition of uncontrolled cell growth, increased metabolic demand and desensitisation to regulatory signals (Hanahan and Weinberg, 2011). Genetic instability is another key hallmark of the cancer phenotype and is what enables cancer cells to acquire other phenotypes such as increased proliferation and apoptosis evasion (Hanahan and Weinberg, 2011). To facilitate these mutations, cancer cells must compromise DNA detection and repair mechanisms and deregulate epigenetic control, such that during multi-step tumour progression the cancer genome acquires gains and losses of chromosome regions and aberrant gene expression to mediate their survival (Hanahan and Weinberg, 2011). One inducer of mutation is oxidative damage, whereby production of ROS increases levels of 8-oxo-dG bases in the genome that normally triggers protective proteins like p53 to initiate DNA repair mechanisms, but these responses can become overwhelmed or impaired by mutations leading to defective protein function and irreparable DNA damage (Ralph et al., 2010; Vurusaner et al., 2012). This allows propagation of further DNA damage to lead to other oncogenic properties.

1.6.3.2. Cytoglobin Expression in Cancer

Changes in *CYGB* expression have been linked to many cancer types. The first link was made within tylosis with oesophageal (TOC) cancer. Tylosis describes a genetic disorder characterised by hyperkeratosis of the skin of the palms and soles of the feet that is accompanied with oral leukoplakia and a greater risk of oesophageal cancer (Risk et al., 1999). Haplotype analysis identified the *CYGB* gene to be one of two complete genes physically located in the same chromosome region responsible for the TOC phenotype

and the methylated *CYGB* coding sequence did not show any tylosis-associated mutations (Langan et al., 2002). Subsequently, another gene within this region named *RHBDF2* (a transmembrane protein involved in epidermal growth factor signalling (EGF)) was identified to contain missense mutations (that result in a change in an encoded amino acid) and caused promotion of proliferation and down-regulation of EGF receptors within tylotic relative to normal tissue (Blaydon et al., 2012). *CYGB* was significantly down-regulated in TOC patient oesophageal biopsies by almost two thirds that of normal tissue (McRonald et al., 2006) and has also been reported to be within a deleted chromosome region in ovarian cancers, in addition to the *RHBDF2* and *PRCD* (progressive rod-cone degeneration) genes (Wojnarowicz et al., 2012). Together, these studies suggested that loss of *CYGB* expression may be important in tumorigenesis. *CYGB* expression was subsequently found to be significantly down-regulated; primarily by promoter hypermethylation (see section 1.3), in lung (Xinarianos et al., 2006), oral (Shaw et al., 2009), ovarian (Chen et al., 2014; Wojnarowicz et al., 2012), colon, bladder, breast (Shivapurkar et al., 2008) and skin (Fujita et al., 2014) cancers, lending support to the hypothesis made by Shivapurkar et al (2008) and others that CYGB may function as a tumour suppressor.

1.6.3.2.1. Cytoglobin as a Tumour Suppressor

CYGB over-expression has also been reported to impair proliferation in various models, including in *CYGB* knockout C57BL/6 mice (Thuy et al., 2011), H358 human lung adenocarcinoma (Oleksiewicz et al., 2013), ovarian cancer (Chen et al., 2014), G361 and G32TG melanoma cells (Fujita et al., 2014) and U2OS human osteosarcoma (John et al., 2014). Xenografts of G361 human melanomas with stably silenced *CYGB* implanted into nude mice showed greater proliferation rates compared with CYGB expressing

melanoma controls (Fujita et al., 2014), which further demonstrates CYGB is linked to reduced tumor growth. Changes to proliferation rate have also been linked to alterations of the cell cycle. For example, *CYGB*-negative liver tumours had higher cyclin D1 (*CCND1*) levels compared to wildtype (Thuy et al., 2011). Up-regulated CCND1 expression was also reported in CYGB over-expressing SKOV-3 ovarian cancer cell lines that showed reduced proliferation and an increased G1:S cell cycle phase ratio (Chen et al., 2014). Cell cycle arrest and CCND1 expression could be reversed by knockdown of *CYGB*, suggesting regulation of cell cycle advancement is CCND1-dependent. CYGB over-expressing U2OS human osteosarcoma cells were similarly reported to undergo G1 arrest following doxorubicin treatment (John et al., 2014) and the authors suggest this might be one of the functional consequences of CYGB's interaction with p53, also found by this study.

CYGB expression is increased in MCF7 and MDA-MB-468 breast cancer cells after ROS-induced DNA damage triggered by treatment with an aryl hydrocarbon receptor (AhR) agonist, whilst doxorubicin treatment induced a milder increase in *CYGB* expression (McLean et al., 2015). The AhR-mediated up-regulation of *CYGB* was found to involve p38 and JNK signalling pathways. A link between DNA damage response and CYGB was also demonstrated *in vivo* within hepatic tumours of CYGB knockout C57BL/6 mice, where chronic choline deficiency and the lack of CYGB expression was found to significantly raise DNA damage proteins 53BP-1 and γH2AX (Thuy et al., 2011). Doxorubicin treatment of stable CYGB-GFP over-expressing U2OS human osteosarcoma cells resulted in up-regulation of CYGB protein in correlation with expression of p53 (John et al., 2014); a critical regulator of stress responses and initiator of DNA damage

repair (Kruiswijk, et al., 2015, Soussi and Winman, 2015) that is commonly mutated within cancers; including OSC (Leemans et al., 2011; Waridel et al., 1997a). CYGB over-expression decreases oxidative DNA damage after treatment with BSO in TE-8 human oesophageal cancer cells (McRonald et al., 2012) and Ro19-8022 in TE671 human medulloblastoma cells (Hodges et al., 2008), mediated by its ROS scavenger ability. One would surmise from this that CYGB protects the cell from potential oncogenic mutations within an oxidising environment and is therefore a key tumour suppressor. In support of this hypothesis, *CYGB* knockout C57BL/6 mice were more likely to develop hepatic tumours following chronic choline deficiency (Le Thi Thanh Thuy et al., 2015) and this effect was also seen following N,N-diethylnitrosamine (DEN) treatment (Thuy et al., 2011). CYGB loss in these tumours was also shown to be linked to higher V-Akt Murine Thymoma Viral Oncogene Homolog 1 (AKT) phosphorylation, which is an oncogenic protein involved in multiple hallmarks of cancer including proliferation, survival and angiogenesis and is also linked to radiotherapy resistance (Bussink et al., 2008; Hanahan and Weinberg, 2011; Hsieh et al., 2011). A negative correlation between CYGB and phospho-Akt was also seen by Xu et al (2013) in human glioma tumours.

Other phenotypes important to tumour progression are enhanced invasive abilities and motility. Reduced migration associated with CYGB over-expression was demonstrated in murine NIH3T3 fibroblasts and was supported by immunocytochemical staining that showed higher levels of stress fibres and focal adhesions (Nakatani et al., 2004). The rearrangement of the actin cytoskeleton; which includes stress fibres, is necessary to generate intracellular tension for directional cell movement. The expression and re-distribution of focal adhesion complexes is also important for mediating traction and the whole process is regulated by RhoGTPases (Schmitz et al., 2000). CYGB over-expressing

NIH3T3 fibroblasts in the Nakatani et al (2004) study treated with a RhoA RhoGTPase inhibitor could not induce the actin cytoskeletal changes observed in the control or AKT activation, suggesting the Rho signalling pathway may help mediate the effects of CYGB on cell motility. Indeed, a study in WM35 human melanoma cells examining proteome changes induced by over-expression of another RhoGTPase Cdc42; which is responsible for maintaining cell polarity for directional migration, reported significant *CYGB* up-regulation (Kabuyama et al., 2006). Together, these suggest a hypothesis where CYGB may be positioned within a feedback mechanism to allow control of RhoGTPases and this concept is discussed further in section 7.1.

The anti-fibrotic behaviour of CYGB (see section 1.6.2) is also supportive of a role in cell motility and invasion, since this includes CYGB-linked changes to the synthesis and release of collagen 1 and MMPs that promote attachment of cells to the ECM and provide a matrix against which they can move (Rohani et al., 2014), and this is strongly associated with tumour metastasis (Thomas et al., 1999). Over-expression of CYGB was also reported to impair both migration and invasion in H358 and CALU1 lung cancer cells (Oleksiewicz et al., 2013).

1.6.3.2.2. Cytoglobin as an Oncogene

Whilst CYGB has been frequently linked to tumour suppressor-like activities, it has also shown oncogenic properties within certain cellular contexts. For example, there are some tumours that show up-regulation of CYGB. High levels of CYGB expression have been reported in human glioblastoma multiforme cells (Emara et al., 2010), as well as in a subset of OSC (Shaw et al., 2009), lung (Xinarianos et al., 2006), melanoma (Fujita et al., 2014), alveolar soft part sarcoma (ASPS) (Genin et al., 2008), breast (Gorr et al.,

2011) and ovarian (Chen et al., 2014) cancers. Furthermore, CYGB over-expression was associated with increased motility in CALU1 lung cancer cells if they were oxidatively or hypoxically stressed (Oleksiewicz et al., 2013), and with enhanced proliferation in murine myogenic progenitor cells (Singh et al., 2014). Solid tumours commonly experience hypoxia within their centre because of the high proliferation/angiogenesis ratio. CYGB is up-regulated by and affords protection from hypoxia signalling-mediated damage (see section 1.6.1). This would potentially create a situation where tumours showing *CYGB* expression have a growth advantage compared to those without and thus gives rise to oncogenic behaviour of CYGB. Additionally, CYGB's anti-oxidant and anti-fibrotic effects (see sections 1.5.3.2 and 1.6.2) could promote a microenvironment favourable to tumorigenesis by maintaining tumour cell function amidst the development of adverse tumor pathologies.

There are also links between *CYGB* expression and tumour grade. Chen et al (2014) found that low-grade ovarian tumours were more likely to show *CYGB* expression than higher-grade ones, which demonstrates not only do some tumours express *CYGB*, but also indicates they require its silencing for advancement. Similarly, lower grade human glioma exhibited *CYGB* expression and in higher grade tumours the reduction of *CYGB* expression was correlated with an increased blood vessel density and propensity for tumour recurrence (Xu et al., 2013). Shaw et al (2009) reported that OSC tumours with high CYGB expression levels demonstrated characteristics of higher grade tumours such as mandible invasion. A recent *in silico* analysis of lung adenocarcinoma gene expression data by Latina et al (2015) revealed co-expression of tumour suppressor *P63* and *CYGB* was associated with poor prognosis.

Xu et al (2013) found glioma patient survival significantly improved with CYGB (median survival time of 62.5 months compared with just 23.8 months for low expression patients). However, *CYGB* expression does not appear to be a good biomarker of tumour incidence or prognosis. *CYGB* expression in breast cancer tissue did not predict patient survival (Gorr et al., 2011) or correlate with metastasis in the subset of CYGB-expressing lung cancer biopsies (Xinarianos et al., 2006). Examination of historical periodic biopsies from patients with oral epithelial dysplasia (but no history of OSC) did not show a correlation between *CYGB* hypermethylation and the onset of malignancy (Hall et al., 2008).

Although *CYGB* is silenced in many tumours and has shown an ability to protect cells against the emergence of DNA mutations, aberrant signalling and cell damage caused by excessive ROS, there are tumours that show up-regulation of CYGB and these have enhanced tumour pathologies, including invasion and resistance to oxidative stress and hypoxia. CYGB has therefore been hypothesised to exhibit a complex 'bimodal' behaviour (see Figure 5); similar to the growth arrest and proliferation capabilities demonstrated by TGFβ1 (Akhurst and Derynck, 2001; Bachman and Park, 2005; Pardali and Moustakas, 2007). The beneficial or detrimental effects of *CYGB* expression on tumour development seem influenced by the metabolic, environmental and cell type context (Latina et al., 2015; Oleksiewicz et al., 2013).

1.6.3.3. Cytoglobin and Cancer Therapy

1.6.3.3.1 Radiotherapy and Cisplatin

Tumor recurrence in OSC remains a problem, with local tumours arising from the surgical excision margins (the "field carcinogenesis" effect) and metastases due to the

advanced stage at clinical presentation (Braakhuis et al., 2010; Leemans et al., 2011). Cisplatin (*cis*-diamminedichloroplatinum(II)) is an effective genotoxic drug used routinely in the management of solid tumours, including OSC. The mechanism by which cisplatin exerts its cytotoxicity is not completely understood, but it appears to involve a number of pathways. For the drug to elicit its activity, it must first enter the cell and this is mainly accomplished through copper solute transporter CTR1 (Dasari and Tchounwou, 2014). Secondly, the drug must be activated by hydrolysis where *cis*-chloro atoms of the structure are exchanged with water molecules, forming a highly electrophillic product capable of interacting with proteins and DNA (Brozovic et al., 2010; Dasari and Tchounwou, 2014). Activated cisplatin damages DNA through cross-linking strands and forms adducts between protein and DNA, and these distortions trigger the cell to stall replication, arrest the cell cycle, recruit repair machinery and induce apoptosis (Dasari and Tchounwou, 2014; Siddik, 2003a). Cisplatin-damaged DNA is detected by either nucleotide excision repair (NER) or mismatch repair (MMR) machinery which unsuccessfully attempt lesion repair and inevitably triggers the intrinsic apoptosis cascade (Galluzzi et al., 2012). This response involves halting the cell cycle at S-phase before a robust stalling in G2/M, which allows for repair process to take place (Shen et al., 2013). Both cisplatin-induced responses are mediated by the tumour suppressor p53, whose expression and mutational status has been reported to be important in determining responsiveness to cisplatin treatment, for instance in ovarian carcinoma SKOV-3 cells and NSCLC H358 cells (Fujiwara et al., 1994; Kanamori et al., 1998). Cisplatin leads to p53 activation through ataxia-telangiectasia mutated (ATM) and ATM-Rad3-related (ATR) kinase, which in turn results in the transcriptional activation of p53 targets including DNA repair enzymes, cell cycle and apoptosis

regulators that all participate in the protection of the cell against the detrimental effects of cisplatin (Siddik, 2003a). Aside from DNA damage, cisplatin also increases cellular oxidative stress that occurs either by interfering with mitochondrial ETC complex expression (as a consequence of mitochondrial DNA damage) or through depleting antioxidants (such as GSH) that potentiates cisplatin cytotoxicity (Marullo et al., 2013).

Cisplatin is usually provided in the clinic in combination with 5-fluorouracil in the first treatment phase (induction), with radiotherapy treatment (concomitant) or as a second treatment step to either surgery or radiotherapy (adjunct) (Hanna et al., 2013; Vermorken and Specenier, 2010). Most head and neck cancer patients present at an advanced stage (Monnerat et al., 2002) and are normally treated with cisplatin for the drug has shown to significantly improve response to treatment (Forastiere et al., 2003). A major barrier to therapeutic success is cisplatin resistance (Galluzzi et al., 2012; Kelland, 2007) and tumours with this resistance are likely to also be resistant to other platinum-based chemotherapies (Schuler et al., 2010). There are many ways solid tumours can acquire resistance to cisplatin. For example, elevated levels of glutathione, over-expression of γ-glutamylcysteinetene synthetase or the conjugation enzyme GST are associated with reduced sensitivity to cisplatin treatment, due to better cisplatin detoxification (Brozovic et al., 2010). This has been demonstrated in head and neck tumours that display increased GST expression (Nishimura et al., 1996). Other resistance mechanisms include over-expression of drug transporter proteins, increased expression/activity of repair machinery, and aberrant p53 activity resulting in defective apoptosis (Choi and Kim, 2006; Siddik, 2003a) and these resistance mechanisms are discussed by (Kartalou and Essigmann, 2001). Interestingly, cisplatin resistance has been associated with regulation of some proposed downstream transcripts of CYGB.

Reduction in miR29b, for example, desensitised CP70 ovarian carcinoma cells to the cytotoxic effects of cisplatin partially through *COL1A1* suppression that impaired integrin-based activation of survival signalling through Extracellular signal related kinase 1/2 (ERK1/2) activity (Roskoski Jr., 2012; Yu et al., 2014). *UCP2* over-expression in human colon cancer line HCT116 can reduce toxicity of DNA-damaging chemotherapeutic drugs etoposide and doxorubicin (Derdak et al., 2008a). Later work revealed *UCP2* was down-regulated following cisplatin treatment in these cells (Santandreu et al., 2010) and that UCP2 inhibition corresponded to enhanced ROS levels in human acute promyelocytic leukemia (MX2) cells (Mailloux et al., 2010). This relationship was also found in breast cancer cells (Pons et al., 2015).

Radiation therapy is often combined with cisplatin in treatment regimens because it has been shown to enhance relapse-free survival. In a study of 331 NSCLC patients, it was found daily combination of cisplatin with radiotherapy led to 26 % survival after 2 years (compared with 13 % with radiotherapy alone) and 31 % were without recurrence (compared to 19 % with radiotherapy alone) (Schaakekoning et al., 1992). Head and neck cancer trials with 167 late-stage cancer patients showed that combined treatment also improved 5 year survival (53 % compared with 40 %) and recurrence was only prevalent in 18 % of cases (compared with 31 % in the radiation-only group) (Bernier et al., 2004). Radiation therapy is a non-specific method (targeted to the immediate tumour locality) that damages DNA of tumour or normal cells directly or through the generation of ROS from ionisation of cellular water molecules, resulting in caspase 3-mediated apoptosis (Baskar et al., 2012; Cohen–Jonathan et al., 1999). Thus combining these two treatments enhances oxidative stress-induced damage and cell death to the tumour. Radiotherapy resistance is unfortunately another common problem due to the low

oxygen tensions created within solid tumour masses by poor blood perfusion which limits radiation-induced oxidative stress required for toxicity (Koukourakis et al., 2006). HIF1α activation has also been identified as a radio-resistance marker in human embryonic kidney (HEK293) cells (Harada et al., 2012). Together, cisplatin and radiotherapy resistance make it difficult to create a successful treatment regimen for advanced OSC patients, so research into factors affecting cisplatin resistance would be beneficial.

1.6.3.3.2 Cytoglobin and Therapy Resistance

Very little information exists about CYGB expression and sensitivity to chemotherapy and radiotherapy, which are commonly used to treat malignancies. Knockdown of *CYGB* expression in human glioma cells was reported to increase both oxidative stress and efficacy of radiotherapy (Fang et al., 2011). This suggests that CYGB's ROS scavenging (see section 1.5.3.2) and its ability to protect against hypoxia (see section 1.6.1) may be how the sensitisation was achieved in the study by Fang et al (2011). This raises the possibility that CYGB over-expression may contribute to the radio-resistance exhibited by other tumours. In terms of chemotherapeutic agents, the mitochondria uncoupling protein 2 (*UCP2*) transcript that is down-regulated in CYGB over-expressing lung and breast cancer cell lines (Shivapurkar et al., 2008) has been shown to suppress ROS and cell death following treatment with different chemotherapeutic drugs in HCT116 colon cancer cells (Derdak et al., 2008b). CYGB over-expression in C2C12 murine myoblasts was reported decrease apoptosis following etoposide treatment (Singh et al., 2014) and furthermore, knockdown of *CYGB* expression was found to augment oxidative stress induced by doxorubicin in breast cancer cells (Latina et al., 2015). U2OS human osteosarcoma cells that over-express CYGB were found to undergo G1 arrest following

doxorubicin (John et al., 2014). Together, these studies lead to the hypothesis that CYGB over-expression in tumour cells may cause altered sensitivity to radio- and chemo-therapy. Coupled to the cytoprotective roles observed for CYGB so far, this may identify this globin as a potential therapeutic target in cancers that over-express it. It is therefore important to investigate the role CYGB has within the stress response and the tolerance of tumour cells to chemotherapeutic agents, including cisplatin.

1.8. Hypotheses and Objectives

We hypothesised CYGB over-expression affects expression of stress-related transcripts and phenotype of oral squamous carcinoma cells in response to pro-oxidant cisplatin. We aimed to further understand CYGB's mechanism of action in the stress response.

The objectives of this study were:

- Generate and validate a new stable CYGB over-expressing cell model using an oral squamous carcinoma cell line with negligible endogenous CYGB expression.

- Investigate changes to the transcriptome caused by CYGB over-expression, since there have been several indications in the literature that CYGB might function to regulate gene expression to mediate its cytoprotective abilities. To do this, a whole genome cDNA microarray study was conducted.

- Examine the dependence of stress-related genes after cisplatin treatment on CYGB over-expression, since cisplatin resistance is a frequent problem in head and neck cancer and CYGB is reported to determine tumour response to other drugs such as doxorubicin. To achieve this, real time quantitative PCR was used to explore stress-related transcript changes identified by the microarray.

- Investigate the phenotype of CYGB over-expressing cells to deepen understanding of how CYGB functions independently and in response to cisplatin. To address this objective, cell survival, caspase activation, mitochondrial reductase activity, oxidative stress and cell cycle distribution was assessed.

CHAPTER TWO:

Materials and Methods

2.1 Cell Culture

2.1.1 Cell Lines and Media Preparation

Human oral squamous cell carcinoma cells (OSC; cell line identifier PE/CA-PJ41) were a gift from Dr. T. Liloglou (Roy Castle Foundation, University of Liverpool). This cell line derived from the oral squamous epithelium of a female oral cancer patient, has a methylated CYGB (CYGB) promoter and thus expresses the globin at low levels (Shaw et al., 2009). Stable cell line derivatives of PE/CA-PJ41 that over-express CYGB were generated by introducing cDNA encoding the human *CYGB* gene by plasmid transfection and then later selecting for stable expressing clones.

For screening purposes, two cell lines were used to compare CYGB expression levels achieved in PE/CA-PJ41 derived cells. Human Embryonic Kidney 293 (HEK293) CYGB+ cells (previously generated in our laboratory) were used as a highly expressing positive control (Carpenter, 2010). Normal Oesophageal (NE-1) cells were a gift from Dr. Janet Risk (University of Liverpool) and used to represent a cell line with physiological levels of *CYGB* expression, as they previously have been found to express the globin in the same order of magnitude as that observed in several normal tissues (McRonald et al., 2012).

2.1.2 Continual Cell Culture

All cell culture was carried out with aseptic conditions in a class II tissue culture hood (Aura B4, Bio Air, Italy). Cultures were maintained in vented cap T_{75} flasks (Corning, USA) at 37°C in a humidified 5% CO_2 incubator. For transgenic PE/CA-PJ41 cells, cultures were maintained in selective (G418 sulfate; 600 $\mu g ml^{-1}$) media upon revival and the selective pressure removed immediately prior to use in experiments to ensure that this antibiotic did not interfere with the assays. Only cell cultures between passages 7

and 30 were used for experiments. Cultures were checked daily and immediately prior to experiments with an inverted light microscope to check cell general morphology and for any signs of contamination. Splitting regimens for each cell type are described in the following sections. All reagents were pre-warmed to 37°C before use.

2.1.3 Cell Lines

2.1.3.1 PE/CA-PJ41 and Their Transgenic Derivatives

PE/CA-PJ41 cells were maintained in RPMI-1640 media (Sigma) supplemented with 10 % FBS, 1% L-glutamine, 100Uml^{-1} penicillin and 100 µgml^{-1} streptomycin. Cells were passaged 1:6 once attaining approximately 70% confluence. Spent media was removed and cultures washed once with 3 ml of phosphate buffered saline (PBS). Cells were then detached from the tissue culture plastic using 1 ml of Trypsin-EDTA (Life Technologies, UK) that was gently rocked over the culture and incubating at 37°C for 5 min. Once most cells had detached, 2 ml complete media was added to quench trypsin activity and the cell suspension transferred into a 15 ml centrifuge tube (Falcon) and centrifuged at 1500 rpm for 5 min at room temperature. Resulting cell pellets were re-suspended in 6 ml media and 1 ml of this was added to a fresh T_{75} flask along with 10 ml of complete media and returned to the incubator for maintained culture.

2.1.3.2 HEK293 CYGB+

HEK293 CYGB+ (Human Embryonic Kidney over-expressing CYGB) cells previously generated in our laboratory were maintained in DMEM (low glucose, Sigma) supplemented with 10 % FBS, 1% L-glutamine, 100Uml^{-1} penicillin and 100 µgml^{-1} streptomycin. Cells were passaged 1:10 once around 70 % confluence was attained. Spent media was removed and cell detachment was carried out as described in section 2.1.3.1. Cell pellets were re-suspended in 10 ml media and 1 ml of this was added to a

fresh T_{75} flask along with 10 ml of complete media and returned to the incubator for maintained culture.

2.1.3.3 NE-1

NE-1 (Normal Oesophageal) cells were maintained in Keratinocyte Serum-Free Media (Gibco) supplemented with Epidermal Growth Factor 1-53, Bovine Pituitary Extract, 100Uml^{-1} penicillin and 100 µgml^{-1} streptomycin. Cells were passaged 1:4 once approximately 70 % confluence was achieved. Cell detachment was conducted as described in section 2.1.3.1, although trypsin activity was quenched with Soybean Trypsin Inhibitor (Gibco) and suspensions were centrifuged at 700 rpm for 7 min to pellet the cells. Cells were seeded into fresh T_{75} flasks with complete media and returned to the incubator for maintained culture.

2.1.4 Cryopreservation of Cell Lines

To ensure a viable stock of low passage cells were always available for experimentation, cell cultures from a T_{75} flask were detached with trypsin and pelleted as described in section 2.1.3. Cell pellets were re-suspended in 3 ml freezing media (10 % (v/v) sterile-filtered DMSO in FBS) and 1 ml aliquots dispensed into cryovials (Corning), labelled with cell line name and passage number. The vials were transferred to a -80°C freezer overnight before long-term storage in vapour phase liquid nitrogen.

2.1.5 Revival of Cell Lines

To revive cells, cryovials were thawed rapidly in a 37°C water bath to avoid crystal formation. Suspensions were then transferred drop-wise from cryovials to 4 ml of pre-warmed complete media before being centrifuged as described in section 2.1.3, as appropriate for the cell line to spin off the DMSO within the freezing solution. Cell pellets were re-suspended in 2 ml complete media and split 1:2 into fresh T_{75} flasks, before

being moved into a 37°C humidified 5% CO_2 incubator for culture. Media was exchanged for fresh the following day.

2.1.6 *Mycoplasma* Detection

To confirm that the cell cultures being used for experiments were free from *Mycoplasma sp.* contamination, the EZ-PCR *Mycoplasma* Detection Kit was used according to the manufacturer's instructions. Briefly, media samples were taken from each actively growing cell culture and centrifuged twice; firstly at 250 xg for 4 min to remove cell debris and then the resulting supernatant at 16,000 xg for 10 min to pellet any *Mycoplasma*. The pellet was re-suspended in 50 µl of the buffer solution provided and subjected to PCR using primers that target the conserved prokaryotic 16S rRNA gene, producing an amplicon of 270 bp. PCR products from each sample, along with the positive control sample provided within the kit and a 100 bp DNA ladder (NEB) were loaded onto a 2 % (w/v) agarose gel and separated by electrophoresis. All cell cultures were demonstrated to be negative for Mycoplasma before cryostocks were made (see appendix 3).

2.1.7 Viable Cell Counting for Seeding

To ensure reproducible numbers of cells were seeded for each experimental replicate, cell counts were performed using a Neubauer haemocytometer. When cultures were 70 % confluent, cells were detached and trypsin activity quenched as described in section 2.1.3. A 20 µl aliquot from the total trypsin/media volume (3 ml) was taken for counting and added to 20 µl of a 1:10 dilution of 0.4 % trypan blue (Sigma) and mixed gently. Ten microliters of the diluted cells were then added to each chamber of the haemocytometer and drawn under the coverslip by capillary action, before being viewed under the 10 X objective of the microscope (Nikon Eclipse TS100 light microscope). Cells were counted

that were present within the middle 25-square area, along with those on both the left and top border of this central square. Trypan blue is a negatively charged dye that selectively stains cells with compromised membranes (i.e. dead cells). Only cells that were bright and successfully excluded the trypan blue dye were counted to ensure that cell counts obtained reflected the number of live cells in the stock cell suspension being assessed. The viable cell counts from two chambers were averaged and used in Equation 1 to calculate the cell density per millilitre in the cell suspension.

Equation 1 – Cell density calculation.

Cells per ml in suspension =

average cell count x dilution factor (2) x conversion factor (10^4)

2.2 Chemicals and Treatments

All chemicals were purchased from Sigma Aldrich-UK unless otherwise stated. Cisplatin stock solutions were prepared fresh immediately before use as a 2 mM solution, using 25°C PBS as the solvent and then prepared as the working concentrations with pre-warmed complete media. Etoposide stock solutions were similarly prepared, but as a 5 mM stock solution that were stored at 4°C between uses. Hydrogen peroxide stocks were similarly prepared, but immediately before use. Antimycin A was dissolved in DMSO solvent to obtain a 5 mM stock solution and stored in single-use aliquots at -20°C and again working concentrations were made with complete media. All cell treatment studies were started on day 0 with fresh complete media and ended after 48 h in the case of cisplatin and etoposide, 24 h for hydrogen peroxide and 1 h for Antimycin A. All treatments were performed in biological triplicates and a minimum of technical duplicate, with the exact number of technical replicates stated in the figure legends.

Solvent-only controls were included in each treatment set, which contained cells provided with the equivalent solvent volume to the highest concentration of drug treatment.

2.3 Vector Preparation

2.3.1 Acquisition of pCMV6-AC Vector Containing Human CYGB cDNA Sequence

The pCMV6-AC vector (PrecisionShuttle™ mammalian vector with non-tagged expression, PS100020, Origene) containing human CYGB cDNA (TrueClone™ Human Full-Length cDNA clone, SC321813, Origene) was used for transfection (Figure 6).

2.3.2 Transformation of Chemically Competent M182 Bacteria

The plasmid was propagated in chemically competent *E. coli* strain M182. Ice cold bacteria (100 µl) and DNA (100 µg) were mixed and heat shocked at 42°C for 2 min. Cells were recovered in 500 µl LB medium at 37°C with shaking (225 rpm) for 50 min. Cells were then centrifuged briefly (5000 rpm, 3 min) and re-suspended in fresh LB media (500 µl). Bacteria were then spread on selective (Ampicillin 100 $\mu g ml^{-1}$) LB-agar plates that were inverted and incubated at 37°C overnight. The following day, well-isolated colonies were chosen at random and used to inoculate LB selective medium which was incubated at 37°C overnight with shaking before plasmids were extracted.

2.3.3 Plasmid Isolation and Quantification

Plasmids DNA was isolated with the Isolate Mini Kit (Bioline) according to the manufacturers' suggested 'ISOLATE Plasmid Mini Kit (high copy number plasmid DNA)' protocol. Plasmid quality and quantity was determined with a NanoDrop instrument.

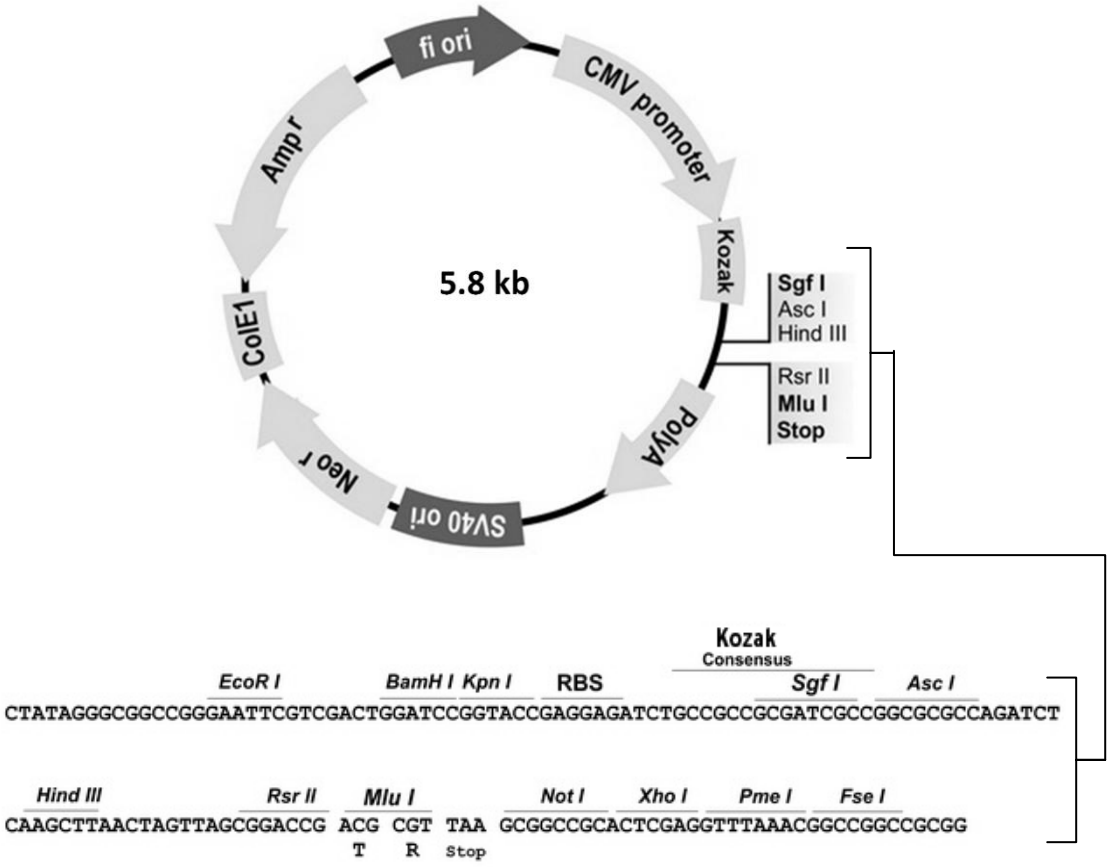

Figure 6 – Precision Shuttle pCMV6-AC Vector Map showing the multiple cloning region EcoRI site into which the human CYGB cDNA sequence had been previously inserted.

The human CYGB cDNA insert is under the regulation of the viral CMV promoter to promote constitutive expression in mammalian cells. The positions of the bacterial (ampicillin; Amp^r) and mammalian selection (G418 sulfate (Geneticin/Neomycin/Neo^r) antibiotic resistance genes are shown, along with the multiple cloning site sequence. Map adapted from TrueClone Vector Guide (Origene).

2.3.4 Human CYGB cDNA Insert Sequencing

The Human CYGB cDNA insert was validated through DNA sequencing (Genomics Facility, University of Birmingham, UK) using VP1.5 (5'-GGA-CTT-TCC-AAA-ATG-TCG-3') and XL39 (5'-ATT-AGG-ACA-AGG-CTG-GTG-GG-3') primers (Alta Biosciences, UK), checking the product against the NCBI BLAST database reference sequence for CYGB mRNA (NM_1342683), which re-confirmed the sequence as wildtype and in frame.

2.4 Cell Transfections

2.4.1 G418 Sulfate Selection and Optimisation

To determine the optimal concentration of G418 sulfate required to select for selection of resistant cell clones, a G418 sulfate cell survival assay was conducted. PE/CA-PJ41 cells were seeded at 55,000 cell per well into a 12-well plate and incubated at 37°C. Spent media was aspirated and replaced with fresh media containing G418 sulfate antibiotic (0, 200, 400, 600, 800 and 1000 $\mu g \mu l^{-1}$, Roche), every 48 h for 10 days. Cell density at each time point was determined through crystal violet staining (see section 2.9.1).

2.4.2 Transfection Methodology

In order to determine the success of the optimised transfection conditions, PE/CA-PJ41 cells were seeded at 35,000 cell per well onto a 12-well plate and incubated at 37°C overnight to achieve 60 % confluence the following day. Cells were transiently transfected according to the manufacturers' instructions with a transfection mixture composed of the pCMV6-AC-CYGB plasmid (1 µg) and Turbofectin 8.0 (Origene) in a 3:1 (v/w) ratio (3 µl) in serum-free RPMI-1640 (100 µl), which was vortexed and left to incubate at room temperature for 25 min before being added to the cells in complete RPMI-1640 (2 ml) in a drop-wise fashion. Plates were tilted gently a few times to ensure

even distribution of the transfection mixture and incubated at 37°C for 48 h. The cultures were then each analysed for transient CYGB expression through RTqPCR and western blotting.

For stable cell lines, PE/CA-PJ41 cells were seeded into 100 mm tissue culture dishes three days before transfection until a density of approximately 60% was reached. Cells were transfected with pCMV6-AC CYGB plasmid (1 µg) and Turbofectin 8.0 in a 3:1 (v/w; Origine) ratio (3 µl) in serum-free RPMI-1640 (100 µl) as per the manufacturer's instructions. Cultures were then incubated for 48 h prior to being split 1:10 and re-seeded into separate 100 mm dishes. Selective media (G418 sulfate 600 $\mu g \mu l^{-1}$; Roche) was applied the following day and exchanged every 2-3 days until there was an absence of cells within the control (un-transfected, 600 $\mu g \mu l^{-1}$ G418 sulfate) cell culture. From this point, 'islands' of transfected cell colonies were monitored and harvested when they reached approximately 100 cells per colony, utilising the cloning ring protocol (Mathupala and Sloan, 2009). Stable clones were propagated in selective medium for further analysis.

2.5 Molecular Biology Techniques

2.5.1 RNA Isolation, Quantification and cDNA Synthesis

Total RNA was isolated from cells using the Absolute RNA MiniPrep Kit (Agilent) with direct lysis of cells on the culture plate according to the manufacturer protocol. Briefly, cells were grown to around 70% confluence on either 6 well plates (or 100 mm dishes in the case of the whole genome microarray samples) before lysis with 350 µl lysis buffer supplemented with 0.01 % (v/v) β-mercaptoethanol (β-ME). Lysate was collected with a cell scraper, transferred to a pre-filter spin column and centrifuged at 13,600 rpm for 5 min in order to homogenise the sample. Filtrate was then mixed with an equal volume of

70 % (v/v) ethanol and vortexed briefly before being transferred to an RNA binding spin column. The membrane-bound RNA in the spin column was then washed with low salt buffer and subjected to on-column DNase I digestion for 15 min at 37°C to remove contaminating DNA. RNA was then washed with a sequence of low and high salt buffers as per the manufacturer's instructions, before elution in 30 µl RNase-free water and storage at -80°C until required. Reverse transcription was carried out with the Tetro cDNA Synthesis Kit (Bioline) in which 500 ng total RNA and oligo dT primers were used. cDNA was stored at -20°C until required.

2.5.2 SYBR Green Real Time Quantitative PCR (RTqPCR)

For RTqPCR, SYBR-Green primers were used and their sequences are listed in Table 1. Primers optimised for RTqPCR were obtained from PrimerDesign (University of Southampton). cDNA samples for singleplex PCR were prepared with cDNA template (25 ng), PrecisionPlus qPCR 2x mastermix (PrimerDesign), Nuclease-free water (Qiagen) and either the gene of interest or housekeeping primer pair in a total reaction volume of 20 µl. A standard 2-step protocol was employed for RTqPCR using a Stratagene Mxp3005 instrument (1 cycle of 10 min at 95°C and 50 cycles of 15 seconds at 95°C and 30 seconds at 60°C). Primer specificity was confirmed in each experiment by the presence of a single peak within the SYBR green dissociation melt curve carried out after the PCR cycling step (see appendix 2). Cycle threshold values for both samples and the standard curve were obtained and used to calculate log fold changes through the Pfaffl ddCt method (see Equation 2) where the reaction efficiency was available (Livak and Schmittgen, 2001; Pfaffl, 2001), using β-actin (ACTB) or the combination of TATA-binding protein (TBP) and β-2-microglobulin (B2M), as indicated in the figure legend for the normalisation factor, and untreated or un-transfected cells as a calibration control.

For the stable clone screen, NE-1 cell CYGB expression was used for calibration controls and HEK293 CYGB+ expression used as a positive control.

Equation 2 - Pfaffl Equation for calculation fold changes in mRNA expression.
Where E is the Efficiency of the reaction, dCt is the difference in cycle thresholds between the control and sample PCR, target is the gene of interest and ref is the house-keeping gene.

$$\text{Fold Change} = \frac{(E_{target})^{dCt\,target\,(control-sample)}}{(E_{ref})^{dCt\,ref\,(control-sample)}}$$

2.5.3 PCR and Agarose Gel Electrophoresis

Routine PCR was carried out with cycling conditions of 1 cycle of 98°C for 30 seconds; 30 cycles of 98°C for 10 seconds, 64°C for 30 seconds and 72°C for 1 minute; 1 cycle of 72°C for 10 min. A Phusion High-Fidelity PCR Kit (NEB) was used as per the manufacturer's instructions. PCR products were separated on a 2 % normal melting point agarose gel (1x TBE agarose supplemented with 5 µl gel red) by electrophoresis for 45 min at 80 V and imaged with UV transillumination.

2.5.4 Protein Isolation and Quantification

Whole cell protein was isolated as follows using ice-cold Radioimmunoprecipitation (RIPA) buffer (1 M Tris HCl pH 7.6, 150 mM NaCl, 1 % Triton X-100, 0.5 M EDTA, 10 % sodium deoxycholate and 200 mM NaF) supplemented with mammalian protease inhibitor cocktail (1:100 dilution; Sigma). Cells were incubated with RIPA buffer for 15 min on ice with occasional vortexing before being centrifuged at 14,000 rpm for 12 min at 4°C. Protein-containing supernatant was stored at -80°C until needed. Concentrations were assayed using Bradford Reagent (BioRad), with absorbance measured at 595 nm against a standard curve of bovine serum albumin (1 $mgml^{-1}$ BSA, 0 to 10 μgml^{-1}; Sigma).

Table 1 – Sequences of oligonucleotide primers.

Gene	*Symbol*	*Forward (Sense)*	*Reverse (Anti-Sense)*
RTqPCR primers (Primer Design, UK)			
CYGB	CYGB	ATCCTCATCCTCATCTTCATCCT	CTGGGTCTGGTTACAAACATCA
Beta-Actin	BACT	(vendor unique assay)	
TATA-Binding Protein	TBP	GTTTGCCAAGAAGAAAGTGAAC	GGGTCAGTCCAGTGCCAT
Beta-2-microglobulin	B2M	(vendor unique assay)	
NAD(P)H Dehydrogenase (Quinone)	NQO1	GCAGACCTTGTGATATTCCAGTT	ATGGCAGCGTAAGTGTAAGC
Cytochrome C Oxidase Subunit 7C (Mitochondrial)	COX7C	CATTTGCTACACCCTTCCTTGT	GAGTTCTAGTTTGATCCACTTCCA
Matrix Metalloprotease 1	MMP1	GCACTGAGAAAGAAGACAAAGG	CTAAGTCCACATCTTGCTCTTG
Integrin Alpha 2	ITGA2	TGAGTAATTTCTTTGGCAACCTTC	ACTTTGGACCGCTGGAGAG
Mitogen-activated protein kinase kinase kinase 5	MAP3K5	CATGAAGGGGTTGACAGAGC	GTACTGGCTAGAACTTGCTTGT
Rho GTPase activating protein 18	ARHGAP18	CTTTCAGGCTGTCCAGAATCT	CAGGTAGGAGGATGACAAGAAG
Cyclin-dependent kinase inhibitor 2A	CDKN2A	ATGTCCTGCCTTTTAACGTAGATA	CTCACTCCAGAAAACTCCAACA
Growth arrest and DNA-damage-inducible, alpha	GADD45A	TACTCCCTACACTGATGCAAG	CATCTGCAAAGTCATCTATCTCC
BCL2/adenovirus E1B 19kDa interacting protein 3-like	BNIP3L	GCTTTGGGGCTAGGCATCTA	TTCACAGGTCACACGCATTTC
gDNA Incorporation PCR primers (Invitrogen, UK)			
Neomycin resistance region	Neo^r	TGGCCACGACGGGCGTTCCTTG	GCAGCCGCCGCATTGCATCAG
Cytoglobin exon 1-exon2 region	CYGB ex1-2	CCACCGCCGCCGCCGAGCAAA	TGGGGGCTCCGCTCCATCTCCA

2.5.5 Western Blotting

Twenty micrograms of protein were heat denatured by mixing with an equal volume of 2 x Laemelli buffer at 95°C for 5 min before loading onto a 12.5 % SDS-polyacrylamide gel (acrylamide:bisacrylamide 12.5 %, Tris-HCl pH 8.8, SDS 0.1 %, TEMED 1.5 $\mu l ml^{-1}$ and 15$\mu l ml^{-1}$ Ammonium persulfate (APS)) and run for 90 min at 120 V. Separated proteins were transferred onto a 0.2 µm PVDF membrane (Millipore) using a mini trans-blot electrophoresis tank (Biorad) at 4°C, 120 V for 90 min and then blocked with 5 % non-fat dry milk (20 ml per membrane, Marvel) in TBST (Tris-buffered saline, 0.05 % Tween-20) on a rocking platform for 1 h at room temperature, to block non-specific binding. After three 5 min washes with TBST (20 ml each), the membrane was incubated with primary antibody (see Table 2) in blocking buffer overnight on a rocking platform at 4°C. After three further 5 min washes with TBST, the membrane was incubated with Goat anti-mouse HRP-conjugated secondary antibody in blocking buffer for 1 h as before. The membrane was washed with TBST twice and TBS once before being visualised with the ECL SuperSignal Chemiluminescent system (ThermoScientific) and Amersham Hyperfilm (GE Healthcare) using an X-ograph machine (AGFA Curix60).

2.5.6 In-Cell Enzyme-Linked Immunosorbent Assay (ELISA)

In-Cell ELISA was used to determine a semi-quantitative measurement for CYGB (Abnova), cyclin D1 (SantaCruz), p21 (SantaCruz), Chk1 (SantaCruz) and p53 (Life Technologies) protein expression in each cell clone. Cells were seeded into 24 well plates in triplicate on three separate days to reach approximately 70% confluence after two days. After treatments, cells were fixed with 300 µl 3.7 % paraformaldehyde (pH 7.4) and incubated for 12 min at room temperature on a rocking platform before being washed three times with 1x PBS (500 µl). Permeabilisation buffer (0.01 % Triton X-100

Table 2 – Antibody Details Used in Western Blotting and In-Cell ELISA Experiments.

Antibody	*Dilution*	*Catalogue Number*	*Company*
	Primary Antibodies		
Anti-CYGB mouse monoclonal M02, clone 1A1	1:500	WH0114757M2	Abnova
Anti-β-actin mouse monoclonal, clone AC-74	1:10,000	A2228	Sigma
Anti-cyclin D1 mouse monoclonal antibody	1:500	Sc-246	SantaCruz
Anti-CHK1 mouse monoclonal antibody	1:500	Sc-8408	SantaCruz
Anti-p21 mouse monoclonal antibody	1:500	Sc-6246	SantaCruz
Anti-p53 mouse monoclonal antibody, clone PAB1801	1:500	13-4000	Life Technologies
	Secondary Antibody		
Goat anti-mouse HRP-conjugated antibody	1:1000	A16066	Life Technologies

in 1x PBS) was added to each well and incubated for 30 min on a rocking platform. Blocking buffer containing 3 % BSA in 1x PBST (0.05 % Tween-20 in 1x PBS) was added in blocking buffer were added as required and left to bind on a rocking platform at room temperature for 1 h. Wells were washed three times with 1x PBST again for 15 min as before. Mouse monoclonal primary antibody was then added in blocking buffer and incubated for 1 h at room temperature again on a rocking platform, before wells were washed three times with 1x PBST again for 15 min as before. Goat anti-mouse HRP-conjugated secondary antibody was then added in blocking buffer and incubated for 1 h at room temperature on a rocking platform. After three washes with 1x PBST, 250 µl of prepared SigmaFAST OPD Substrate (Sigma) was added to each well and developed in the dark for 12 min (the point at which the solution became discriminately yellow compared with the no primary control background wells) and the reaction was stopped by addition of 100 µl of 2 N sulfuric acid. Solutions were transferred from each well to a white-walled 96 well plate and absorbance read at 492 nm using the Infinite 200Pro microplate reader (Tecan Trading AG, Switzerland). Absorbance was corrected for no primary antibody controls and normalised to cell density, as determined by crystal violet staining (see section 2.7.1).

2.5.7 Genomic DNA Isolation

Cells were seeded into 6 well plates at a density in order to achieve a 50 % confluence the following day. To obtain genomic DNA extracts, the DNeasy Blood and Tissue Kit (Qiagen) was used. Cells were washed in warmed PBS before being detached from the tissue culture plastic (see section 2.1.3). Cell pellets were re-suspended in 200 µl PBS supplemented with 20 µl proteinase K (600 $mAUml^{-1}$) and 4 µl RNase A (100 $mgml^{-1}$). Cell suspensions were mixed by gentle vortexing and allowed to incubate at room

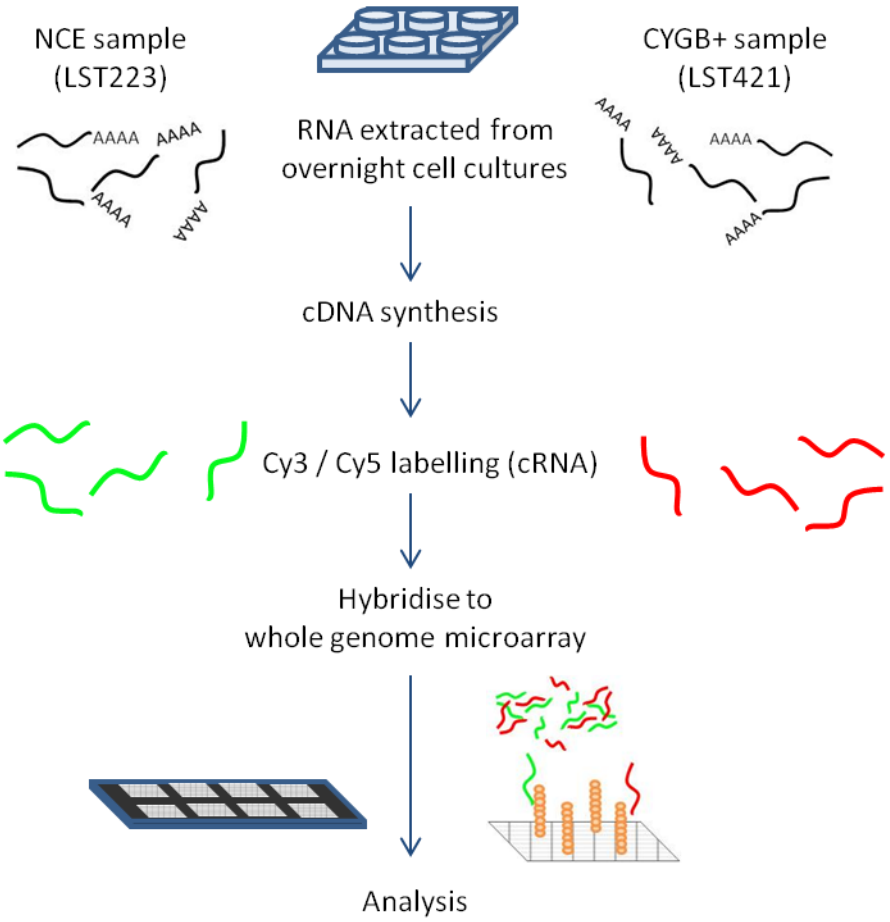

Figure 7 – Whole Genome cDNA Microarray Workflow.
LST421 and LST223 RNA isolates were extracted and checked for integrity before being cyanine-dye labelled ready for hybridisation. The microarray used for hybridisation was the Agilent SurePrint G3 Human Gene Expression 8x 60K v1 Microarray. Transcriptomic differences between LST421 (CYGB+) and LST223 (NCE) OSC clones were analysed in biological triplicate.

temperature for 2 min. Cells were then lysed with 200 µl Buffer AL and incubated at 56°C for 10 min, before undergoing the manufacturer's 'Purification of Total DNA from Animal Tissues (Spin-Column)' protocol. Eluted genomic DNA was quantified for downstream procedures (NanoDrop).

2.6 Whole Genome cDNA Microarray Analysis

To identify downstream transcriptional targets of CYGB, CYGB+ (LST421) and no cytoglobin-expressing (NCE) (LST223) clones were harvested for their RNA on three separate occasions. In the interest of cost, only one representative clone of each model (i.e. one CYGB+ and one NCE) was used for this microarray experiment. The workflow of the experiment is provided in Figure 7. RNA samples were cyanine-labelled and hybridised to an Agilent SurePrint G3 Human Gene Expression 8x 60K v1 Microarray by the Genomics Facility (University of Birmingham) before bioinformatics analysis was carried out using GeneSpring (Dr. Timothy Williams, University of Birmingham) to identify transcripts that are differentially regulated and these are provided in appendix tables 7 and 8. RNA quantity and quality was confirmed with the 2100 Agilent Bioanalyser. RNA samples were assayed by RTqPCR to confirm the expression of CYGB in each cell line prior to microarray preparation. Fifty nanograms of total RNA was used to generate cyanine-labelled cRNA according to the Agilent Two-Colour Microarray-Based Gene Expression Analysis (Low Input Quick Amp Labelling) protocol. NCE samples were cyanine 3 labelled and CYGB+ samples were cyanine 5 labelled. cRNA was quantified (Nanodrop) and added to Agilent SurePrint G3 Human Gene Expression 8x 60K v1 Microarray and 300 ng cRNA was hybridised exactly to the manufacturer's protocol (Genomics Facility, University of Birmingham). The hybridisation recipe for each sample set is provided in appendix 6. Lists of differentially expressed genes

generated by the analysis of Dr. T. Williams were identified through parametric testing and Benjamini and Hochberg correction for multiple testing correction (p value 0.05). Gene Ontology (GO) analysis was performed by myself using PANTHER (v10.0) Gene List Analysis tools; namely the Statistical Over-Representation Test and the Functional Classification Test that are found at http://www.pantherdb.org/tools/genexAnalysis.jsp (Mi et al., 2013; Thomas et al., 2006) . This analysis software uses the binomial statistic to identify under or over represented gene groups with an alpha threshold of 0.05 or lower. Selected transcriptional changes observed in the array samples were further validated by RTqPCR (see section 2.5.2).

2.7 Heme Quantification (Ferrous Hemochromogen Method)

Elevated cellular abundance of ferroporphyrin, containing CYGB, was inferred by measuring total cellular heme proteins, as established by a variation of the pyridine hemochromogen assay (Berry and Trumpower, 1987). This assay relies on the different absorption spectra between oxidised and reduced heme iron. Cells from 70 % confluent 6 well plates were scrape-harvested into RIPA buffer (500 µl) before being added to a solution containing 20% v/v niacin, 200 mM NaOH and 600 µM potassium ferricyanide (500 µl) to fully oxidise the heme iron. Absorbance measurements were taken with a single-beam spectrophotometer at 557 nm and 575 nm wavelengths. A few milligrams of sodium dithionite were then added to each sample to reduce the ferric heme and after 1 minute, absorbances were taken at the aforementioned wavelengths again. Absorption differences between the two wavelengths were then calculated and then also between the oxidised and reduced spectra, which enabled the heme concentration to be calculated using Beers Law (A=ecl) where the length (l) was 1 cm and the extinction

coefficient of iron protoporhyrin (e) was 32.4 $mM^{-1}cm^{-1}$. Concentrations were normalised to total protein determined by the Bradford Assay (see section 2.5.4).

2.8 Confocal Microscopy

Cells were seeded onto 22mm coverslips within 6 well plates and allowed to adhere overnight. The following day, cells were washed once with 500 µl ice-cold PBS and fixed with 300 µl 4% paraformaldehyde (pH 7.4) for 12 min at room temperature on a rocker. Fixative was aspirated and the coverslips washed twice for 5 min with PBS. Cells were permeabilised with 0.1 % Triton X-100 for 10 min at room temperature, before being washed twice for 5 min each with wash buffer (0.05 % Tween-20 in PBS; PBST, 500 µl). Coverslips were then blocked with 2 % BSA in PBST for 1 h at room temperature on a rocker while humidified chambers were prepared. These chambers consist of a petri dish which has a sheet of parafilm atop of distilled water-soaked filter paper and the coverslips are placed cell-side up onto the parafilm for antibody incubations and washes. These humidified chambers have successfully been employed by other labs to reduce the amount of antibody being used for later incubations but ensuring the fixed cells do not dry out (Duke University and Medical Centre, 2015). Once the cells had been blocked, coverslips were washed with PBST twice as before and primary mouse anti-CYGB antibody (1:400 in blocking buffer, Abnova) was added to the coverslips and incubated at 4°C overnight. Coverslips were then washed again in PBST as before and anti-mouse FITC-secondary antibody (1:200 in blocking buffer, DakoCytomation) was added and incubated for 1 h at room temperature in the dark. Coverslips were moved into a dark room to enable the subsequent steps of washing with PBST before the samples were incubated with Hoescht 33342 dye (2 μgml^{-1} stock, 1:8000 (final concentration 0.25 $ngml^{-1}$) for 10 min to counterstain the cell nuclei. Cells were then

washed a final time in PBST before being mounted onto microscope slides with non-fluorescent mounting media (50 µl, Hydromount) and allowed to dry for 1 h at room temperature before being kept in the dark at 4°C until confocal microscopy analysis. Fluorescent images were obtained with the Leica Confocal Microscope (Leica Microsystems) using a 63x oil immersion (NA 1.32) objective (excitation wavelengths were 405 nm for Hoescht 33342 and 488nm for FITC). All images were processed identically and overlaid using the free ImageJ (version 1.47) software.

2.9 Cytotoxicity Analysis

2.9.1 Crystal Violet Method

The crystal violet assay was used for cell survival assessment. Cells (3.8 x 10^4 per well) were seeded in triplicate into 96 well plates to achieve 70% confluence the following day. Media was exchanged for treatment media containing drug for durations stated in the figure legend. Following treatment, cells were then washed once with PBS, air dried and stained with crystal violet (0.05% (w/v) in PBS) for 30 min at room temperature. Cells were washed with PBS before being allowed to air dry at room temperature. A 10 % acetic acid solution (100 µl) was added to solubilise the crystal violet before the solutions were transferred to a fresh 96 well plate and absorbances read at 570 nm using an Infinite 200Pro microplate reader (Tecan Trading AG, Switzerland) against a 10 % acetic acid blank.

2.9.2 Tetrozolium Salt (MTT) Mitochondrial Reduction Method

The 3-(4,5-Dimethyl-2-thiazolyl)-2,5-diphenyl-2H-tetrazolium bromide (MTT) assay was utilised to assess mitochondrial reductive capability as an indicator of cell viability. Cells were seeded in triplicate into 96 well plates at 3.8 x 10^4 cells to achieve 70% confluence the following day. Media was exchanged for treatment media containing drug

for durations stated in the figure legend. Following treatment, cells were washed once with PBS and fresh media containing 0.5 $mgml^{-1}$ MTT was added to each well and incubated for 2 h at 37°C. At the end of this incubation period, the MTT-containing media was removed and fixed with 3.7 % paraformaldehyde (pH 7.4, 12 minutes at room temperature), before being washed with PBS once and the MTT formazan product soluabilised with DMSO (100 µl). The samples were transferred to a 96 well plate and absorbances read at 570 nm using an Infinite 200Pro microplate reader (Tecan Trading AG, Switzerland) against a DMSO blank. The fixed cells were then subjected to the crystal violet assay as described in section 2.9.1.

2.9.3 Sulforhodamine B (SRB) Assay

The Sulforhodamine B (SRB) Assay described by Skehan et al was used as another *in vitro* cytotoxicity assay (Skehan et al., 1990; Vichai and Kirtikara, 2006). The acidic dye has a great affinity for basic amino acids within cellular proteins and binds in a stoichiometric fashion such that the colorimetric absorbance value is directly proportional to the protein content and hence cell number. Cells (2×10^5 per well) were seeded into 24 well plates and allowed to settle overnight in a 37°C incubator. The following day, media was exchanged for treatment media containing drug for durations stated in the figure legend. Following treatment, cells were washed with warm PBS and then fixed with 250 µl ice cold 10 % trichloroacetic acid (TCA) and incubated at 4°C for 30 min. Cells were subsequently washed with 500 µl dH_2O three times and air dried at room temperature for 1 h. Cells were stained with 100 µl 0.4 % (w/v) SRB in 1 % acetic acid for 10 min at room temperature, before the unbound dye was removed by washing three times with 500 µl 1 % acetic acid and plates left to dry once more at room temperature. Two hundred microliters of 10 mM Tris-HCl (pH 10) was used to

soluabilise bound SRB for 30 min on a rocker at room temperature before sample absorbances were read at 510 nm using the Infinite 200Pro microplate reader (Tecan Trading AG, Switzerland). Mean changes in absorbances were compared with untreated controls and corrected with a 10 mM Tris-HCl (pH 10) blank.

2.9.4 Caspase 9 Activation Luminescence Assay

To test for the activity of caspase 9 the Caspase-Glo 9 Assay (Promega) was used. This assay relies on the principle that active caspase 9 will cleave the target substrate; Z-LEHD-aminoluciferin, liberating aminoluciferin to react with ATP and oxygen via luciferase to generate a light signal that is proportional to the amount of active caspase 9 within the culture. Cells (3.8 x 10^4 cells per well) were seeded into a 96 well plate and allowed to settle overnight at 37°C, before being treated to cisplatin at 0 µM, 7.5 µM or 15 µM for 48 h. Following treatment, the plate was allowed to adjust to room temperature, before the Caspase-Glo 9 Assay was carried out according to the manufacturer's instructions (Promega). Briefly, 100 µl Caspase-Glo 9 reagent was added to each sample well and incubated for 45 min in the dark at room temperature, before luminescence was measured using an Infinite 200Pro microplate reader (Tecan Trading AG, Switzerland) and a 1 second integration time with no attenuation. A parallel plate was prepared to use for protein quantification through the Bradford assay (see section 2.5.4) and these protein estimates were used to normalise the luminescence signal. A positive control of 200 µM etoposide to induce apoptosis was also included to confirm the functionality of the assay.

2.10 Proliferation Assay

Cells were seeded in triplicate at 4 x 10^4 cells per well into 24 well plates, to attain ~10% confluence the following day. Fresh media was provided at the end of day 2. On

each day of the five day time course at the same time each day, cells were aspirated of media and washed with PBS before being fixed with 4% paraformaldehyde (500 µl) for 12 min at room temperature. Cells were then washed twice with PBS underwent crystal violet staining as described in section 2.9.1. Absorbance was converted into cell number by interpolating from a crystal violet calibration curve using non-linear regression (see appendix 9).

2.11 Oxidative Stress Analysis

2.11.1 DCFDA Assay

Intracellular ROS levels were assayed by measuring the oxidation of 2',7'-dichlorodihydrofluoroscein-diacetate (H_2DCFDA), which is hydrolysed by esterases in cells to yield H_2DCF which can be oxidised in the presence of ROS to a fluorescent product (Chen et al., 2010). Fluorescence is therefore proportional to the ROS concentration within the cell. Cells were seeded into 6 well plates on three separate days at 3 x 10^5 cells in order to attain 70% confluence the following day, whereupon the cells were treated. After the treatment interval, spent media was removed and 2 ml of fresh media was added to each well with DCF diacetate added to a final concentration of 10 µM and incubated for 3 h at 37°C. Cells were then washed with PBS before being detached as described in section 2.1.3, ensuring a single cell suspension by prolonging trypsin incubation to 15 min. Cell pellets were re-suspended in 1 ml sterile PBS, mixed through pipetting and transferred to a flow cytometry-compatible tube. Samples were vortexed vigorously prior to analysis. Analysis of fluorescence was carried out by flow cytometry with the BD FACS Calibur and CellQuest Pro software (Becton-Dickinson) along with Weasel software (Walter and Eliza Hall Institute of Medical Research, Australia). Cells without DCF diacetate treatment were used for blank controls and

10,000 viable events per sample were analysed for their median fluorescence intensities (excitation 488nm and emission 520 nm). Gating was used to remove dead cells from the analysed population, as determined from their light scattering properties. As a positive control, 48 h H_2O_2 (200 μM) was used.

2.11.2 Mitochondrial Superoxide (O_2^-) MitoSox Red Assay

Mitochondrial superoxide was quantified through measuring oxidation of MitoSox Red dye (a variant of dihydroethidium; Life Technologies). We assessed the blue to red fluorescence shift of the hydroethidine probe that is selectively oxidised by superoxide to become 2-hydroxyethidium that fluoresces (Held, 2015). Fluorescence is proportional to the concentration of superoxide within the mitochondria. Cells were seeded into black-walled, clear-bottom 96 well plates at 3.8 x 10^4 cells in order to attain 70% confluence the following day, whereupon the cells were treated as stated in the figure legend. One hour prior to the end of the time interval, antimycin A was added at a final concentration of 20 μM to positive control cells and incubated at 37°C for the rest of the time course. After the treatment interval, spent media was removed, cells washed once with pre-warmed PBS (100 μl) and 100 μl of fresh media was added to each well with MitoSox Red dye added to a final concentration of 10 μM and incubated for 30 min at 37°C. Fluorescence was determined using an Infinite 200Pro microplate reader (Tecan Trading AG, Switzerland) at the excitation wavelength 510 nm and fluorescence was measured at emission wavelength 580 nm. Cells without MitoSox Red treatment were used for blank controls.

2.11.3 Glutathione (GSH) Assay

To assess total reduced glutathione (GSH) within cells, a fluorescence-based technique was used where ortho-phthalaldehyde (OPT) reacts with reduced glutathione to

generate a fluorescent isoindole product (Hissin and Hilf, 1976). GSH is a primary cellular antioxidant tripeptide that enables redox homeostasis within cells, maintaining oxidising species within certain limits to ensure the appropriate redox-regulation of proteins for a variety of cellular processes (Circu and Aw, 2010). When treated to high levels of ROS (for instance during oxidative stress), GSH becomes oxidised to GSSG (gluathione disulfide) that removes the potentially detrimental reactive oxygen species from the cell. This depletes the GSH pool and raises GSSG levels that have the potential to react with cysteineteine thiols of proteins and modulate their activity, which could disrupt normal signalling and elicit toxicity if aberrantly induced (Circu and Aw, 2012).

Cells were seeded into 6 well plates to achieve 50% confluence the following day before being treated with 0 µM, 7.5 µM or 15 µM cisplatin for 48 h. After treatment, cells were washed in pre-warmed PBS before being scrape harvested into 450 µl of ice-cold lysis buffer (0.1% Triton X100 in PO_4-EDTA buffer (100 mM NaH_2PO_4 and 5 mM Na_2-EDTA, adjusted to pH 8.0). Lysates were transferred into ice-chilled eppendorfs, whilst 2 µl was removed for protein quantification through the Bradford assay (see section 2.5.4). Ice cold protein precipitation buffer (50 µl; 50 % (w/v) trichloroacetic acid in PO_4-EDTA buffer) was added to the lysates prior to centrifugation at 13000 rpm at 4°C for 5 min. A 100 µl sample of each supernatant containing reduced GSH was taken and added to 1.8 ml PO_4-EDTA buffer in a 3 ml polystyrene fluorescence cuvette, along with 100 µl of fresh OPT (1 $mgml^{-1}$ 100% methanol), before being incubated for 15 min at room temperature in the dark on a rocker. A GSH standard curve was made using a 0.1 $mgml^{-1}$ stock solution and were prepared identically to the test samples, but were provided with 5 % (w/v) trichloroacetic acid in PO_4-EDTA buffer. Fluorescence of each prepared sample was subsequently read using a PerkinElmer LS50B luminescence spectrometer

(excitation at 340 nm and emission at 420 nm, slit width set at 12 nm). Glutathione levels in each sample were normalised to total protein content of the sample via the Bradford assay (see section 2.5.4).

2.12 Cell Cycle Analysis

Cells were seeded into a T_{25} flask at 3 x 10^5 cells and allowed to settle overnight at 37°C before being treated with cisplatin (0 µM, 7.5 µM or 15 µM) for 48 h. After treatment, cells were washed in pre-warmed PBS before being detached as described in section 2.1.3. Harvested cell pellets were washed with PBS before being re-suspended in 500 µl PBS whilst ice cold 70 % ethanol (3 ml) was added drop-wise before being stored at 4°C until all samples were obtained for analysis. Fixed samples were centrifuged at 250 xg for 5 min, washed in PBS and then re-suspended in a solution of 500 µl PBS : 50 µl RNase A (1 $mgml^{-1}$ stock) : 5 µl Propidium iodide (PI; 1 $mgml^{-1}$) prior to a 45 minute incubation in the dark at room temperature. PI-stained sample fluorescence was analysed by flow cytometry (excitation 535 nm, emission 617 nm, BD FACS Calibur) and analysed for cell cycle phase proportions using freely available Weasel software (see section 2.11.1). Cells without PI treatment were used for blank controls and 10,000 viable events per sample were analysed. Gating was used to remove dead cells and debris from the analysed population.

2.13 Cell Motility Assessment

Cells were seeded at 4 x 10^4 $cellml^{-1}$ into culture insert chambers (Ibidi, Germany) and each placed into a 24 well plate and cells allowed to adhere overnight at 37°C. These inserts consist of a square silica chamber with a centre wall that allows for two confluent sheets of cells to be separated by a defined gap of ~500 µm (Figure 8). Inserts enable greater reproducibility than conventional scratch assays and also do not damage

the cells or the underlying surface (Ibidi, 2015). The next day, the inserts were carefully removed and the cultures washed briefly with warmed PBS before 1% FBS-containing media was added. The closure of the gap was followed over 6 h, with regular images of the gap taken every 7 min. A similar experiment was carried out again, but with measurements taken every 30 min, and CYGB+ cells treated with either human CYGB siRNA (25 nM CYGB siRNA (Qiagen), 1.25 µl TransIT siQuest (Mirus Biosciences)), or negative siRNA (25 nM Scrambled Sequence Silencer #2 siRNA (Ambion), 1.25 µl TransIT siQuest (Mirus Biosciences)) in order to attempt reversal of any CYGB+ phenotype, according to the manufacturer's protocol (preliminary optimisation experiments with different concentrations of transfection reagent and siRNA were previously carried out by our laboratory). Three biological replicate images (in technical duplicate) were analysed with the Cell IQ software to determine percentage wound closure. Data was exported and analysed with the cell-free area at time zero being defined within the software (conversion factor of 1 pixel = 0.698 µm) and then all subsequent images automatically measured from this to determine the area of the wound that was covered at each time point expressed as a percentage.

2.14 Oxygen Consumption Rate Analysis

The MicroRespiration System (Unisense) was used for assessment of oxygen use within the transgenic clones. The system utilises a Clark-electrode based system that can sensitively monitor oxygen changes within a series of closed glass micro chambers. The 1 ml glass chambers containing cell suspensions of each transgenic clone in fully aerated cell culture media (5 x 10^5 cells ml^{-1}; media was fully aerated by bubbling through air overnight) were submersed in a circulating water bath maintained at 37°C.

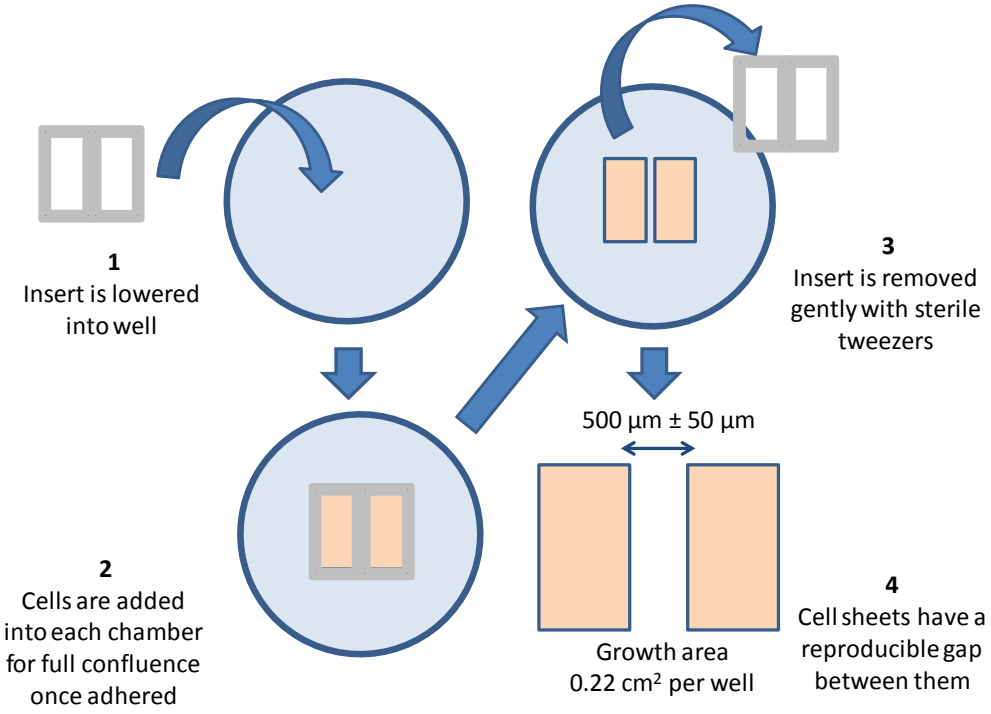

Figure 8 – Ibidi Insert used for the motility assay.

Culture inserts provided a reproducible and sharp cell-free gap that allows for the quantification of cell movement rates (see section 2.13). Briefly, cells are seeded into each chamber of the silica-based template so that full confluence is achieved for the start of the experiment. Once cells have adhered, the insert is gently removed with sterile tweezers and media placed atop of the cells as required for treatment.

Measurements were collected every 30 min over the course of 6 h to follow the depletion of oxygen from the media on four separate occasions and each measurement was averaged from signals detected over a period of 50 seconds. To interpolate oxygen concentrations from the signals detected, two points of calibration were obtained according to the manufacturer's instructions. An aliquot of fully aerated cell culture media was used for the 100 % saturation control (which was equated to a concentration of 210.1 $\mu molL^{-1}$) and the anoxic control was obtained from a solution of sodium hydroxide and sodium ascorbate; each at 0.1 M, prepared freshly for each week of experiments. The microsensor was pre-polarised as per the manufacturer's instructions to ensure the signal stabilised before measurements were taken and was cleaned briefly with distilled water after calibration before use. The accompanying software; SensorTrace, was used to export results for analysis. To determine the rate of oxygen depletion for each transgenic clone, the natural logarithm of the concentrations exported for each time point were calculated and then plotted. Linear regression was then used to calculate their respective gradients that were directly proportional to the rate of oxygen reduction, expressed as $\mu molL^{-1}h^{-1}$ of oxygen.

2.15 Intracellular ATP Determination

To quantify levels of total adenosine triphosphate (ATP) within each cell clone, the Mitochondrial ToxGlo Assay (Promega) was used. This kit relies on the fact that an increase in ATP will increase supply to the luciferase within the ATP Detection Reagent generating a proportional increase in the light signal. Cells (3.8×10^4 per well) were seeded into a white-walled 96 well plate in technical triplicate and allowed to adhere overnight at 37°C. The following day, the amount of intracellular ATP was determined for each transgenic clone and control cell line by using Mitochondrial ToxGlo Assay

(Promega), according to the manufacturer's instructions. A calibration curve of serially diluted ATP standards (Sigma) was prepared in order for the quantity of ATP in the cell extracts to be determined. Luminescence values were obtained using an Infinite 200Pro microplate reader (Tecan Trading AG, Switzerland) and a 1 second integration time with no attenuation.

2.16 p53 Genotyping

Sequencing of p53 was conducted as directed by the relevant IARC protocol (IARC, 2010). Briefly, gDNA isolates from cell clone LST421 (CYGB+) and LST223 (NCE control) were obtained as described in section 2.5.7 and were used as template (25 ng) for a standard PCR reaction provided within section 2.5.3. PCR was carried out for p53 exons 4 to 8 as these are reported to be the most frequently mutated sites (Hollstein et al., 1991) and are the region encoding the DNA binding portion of the gene (Andrews et al., 2004). Primer pairs were used for both PCR and sequencing reactions and their sequences are provided in Table 3 and were obtained from Invitrogen, UK. Amplified PCR products were separated by 2 % normal melting point agarose gel electrophoresis against a 100 base pair ladder (NEB). Expected PCR bands for each exon were located by placing the gel above a UV transilluminator, excised from the gel and transferred into an eppendorf. The PCR product was subsequently separated from the gel and isolated using the QIAquick PCR Purification kit (Qiagen), exactly according to the manufacturer's instructions. Eluted products were sequenced with the ABI 3730 Capillary Sequencer (Applied Biosystems) by the Genomics Department (University of Birmingham) and analysed by myself with freely available Sequence Scanner Software (v1.0, Applied Biosystems). Sequences for each p53 exon assessed were compared to their respective wildtype sequences through using the nucleotide BLAST pair-wise sequence alignment

online database (NLM, 2015). Sequence discrepancies were compared to the chromatogram within the Sequence Scanner software to determine if the base difference was due to software misreads. Forward and reverse sequence reads were compared to determine the bases in the poorly resolved region at the start of the sequence reaction.

Table 3 - p53 exon primers used for both PCR and sequencing reactions

Exon	*Forward (Sense)*	*Reverse (Anti-Sense)*	*Amplicon Size*
4	TGCTCTTTTCACCCATCTAC	ATACGGCCAGGCATGAAGT	353 bp
5	TTCAACTCTGTCTCCTTCCT	CAGCCCTGTCGTCTCTCCAG	248 bp
6	GCCTCTGATTCCTCACTGAT	TTAACCCCTCCTCCCAGAGA	181 bp
7	AGGCGCACTGGCCTCATCTT	TGTGCAGGGTGGCAAGTGGC	177 bp
8	TTCCTTACTGCCTCTTGCTT	AGGCATAACTGCACCCTTGG	231 bp

2.17 Statistics

Microarray data were kindly analysed in-house by Genespring software by Dr. T. Williams (University of Birmingham), with parametric testing where variances were not assumed equal (Welch t-test), p-value cut-off was set at 0.05, and multiple testing correction of Benjamini and Hochberg False Discovery Rate. Differential expression was considered if the gene changed by ≥ 2 fold. All data were assayed for significance using SPSS (v21, IBM) software. Data were assessed for conformity to the normal distribution and for homogeneity of variance. Normally distributed datasets underwent parametric testing; ANOVA with post-hoc Tukey analysis if the variances were equal, and paired student t-test with unequal variances if the variances were unequal. Non-normal data were analysed with Kruskal-Wallis and post-hoc Mann Whitney U tests. All experiments were performed in at least biological triplicate (on three separate occasions), each time in a minimum of technical duplicate (triplicates where expense allowed). Data are expressed as the mean ± standard error of the mean and, statistical significance was accepted when p values were below the alpha threshold of 0.05.

CHAPTER THREE:

Production of the CYGB Over-Expressing (CYGB+) Oral Squamous Carcinoma Model

3.1 Introduction

Transient *CYGB* over-expressing *in vitro* models have been used to explore CYGB function following oxidative, hypoxic or xenobiotic stress, as well as to determine its genetic regulation (Shaw et al., 2009; Xinarianos et al., 2006). However, this method of studying over-expression is not robust since the levels of globin expression will vary between experimental replicates. Furthermore, the long-term effects of CYGB up-regulation on cell signalling and phenotype cannot be examined in such a system due to the restricted time that the over-expression is maintained for (Recillas-Targa, 2006), so a stable cell model with a consistent level of over-expression is a powerful experimental tool to study the biology of CYGB.

Whilst there are three stable *in vitro* models of *CYGB* knockdown in existence within N2a murine neuroblastoma cells (Li et al., 2007), G361 human melanoma cells (Fujita et al., 2014) and NIH-3T3 murine fibroblasts (Halligan et al., 2009), there are four stable CYGB over-expressing *in vitro* models reported to date, within bone osteosarcoma cell line U2OS (John et al., 2014), two non-small cell lung cancer (NSCLC) lines (Oleksiewicz et al., 2013; Shivapurkar et al., 2008) and rodent hepatocytes (Gardner et al., 2010). Currently, three CYGB over-expressing *in vivo* models exist within Wistar rodents (Nishi et al., 2011) and a remnant kidney model of these (Mimura et al., 2010), and AAV-vector-Sprague Dawley rats (Xu et al., 2006). These cell models have been collectively vital in the discovery of phenotypes linked to CYGB expression, such as reduced motility and protection against apoptosis and fibrosis (see sections 1.5 and 1.6). Recently, attention has turned towards employing CYGB over-expressing *in vitro* models for investigating

the mechanism of CYGB function within phenotypes relevant to cancer, such as the DNA damage response (John et al., 2014).

One of the aims of this thesis was to characterise the biological function of CYGB in both cisplatin-stressed and unstressed cells within the context of oral cancer cells that are commonly found resistant to cisplatin (see section 1.6.3.3.1) and do not endogenously express CYGB (Shaw et al., 2006). To achieve this aim, we required a cell line that offered significantly enhanced CYGB expression that would enable its downstream effects to be studied. However, *CYGB* expression is strikingly down-regulated in oral squamous cell carcinoma (OSC) (Shaw et al., 2006).

Therefore, it was necessary to develop a new cell model that stably over-expressed CYGB significantly above background levels and for this the PE/CA-PJ41 cell line was chosen. The PE/CA-PJ41 cell line is an oral epithelial squamous cell carcinoma line that exhibits negligible levels of *CYGB* expression (Shaw et al., 2009) (see section 2.1.3.1) and is therefore suitable for the artificial induction of *CYGB* via plasmid transfection. In this chapter, the development and validation of PE/CA-PJ41 cell clones showing stable CYGB over-expression (CYGB+) is presented. These CYGB+ cell clones (and no CYGB expressing (NCE) cell controls) are used in the following chapters to investigate the mechanism of CYGB function.

3.2 Results

3.2.1 G418 Sulfate Optimisation

Resistance of cells transfected with the pCMV6-AC plasmid to G418 sulfate antibiotic is conferred by the neomycin resistance gene (Neo^r) and this enables selection of successfully transfected clones (i.e. those that have taken up the plasmid). To establish the concentration of the antibiotic to use for this, a survival curve was carried out with PE/CA-PJ41 cells cultured in media with increasing concentrations of G418 sulfate, and cell number measurements were taken every 2 days. The results showed a reduced cell number with increasing concentration of antibiotic; as expected, and higher concentrations of G418 sulfate led to earlier decreases in cell number (Figure 9). The data demonstrated that total cell death was reached within 6 days for all concentrations studied. A treatment of 600 μgml^{-1} (0.6 $mgml^{-1}$) G418 sulfate was chosen for stable cell line selection, as it was the lowest concentration able to cause total cell death within 4 days and would therefore could remove non-transfected cells from the culture population.

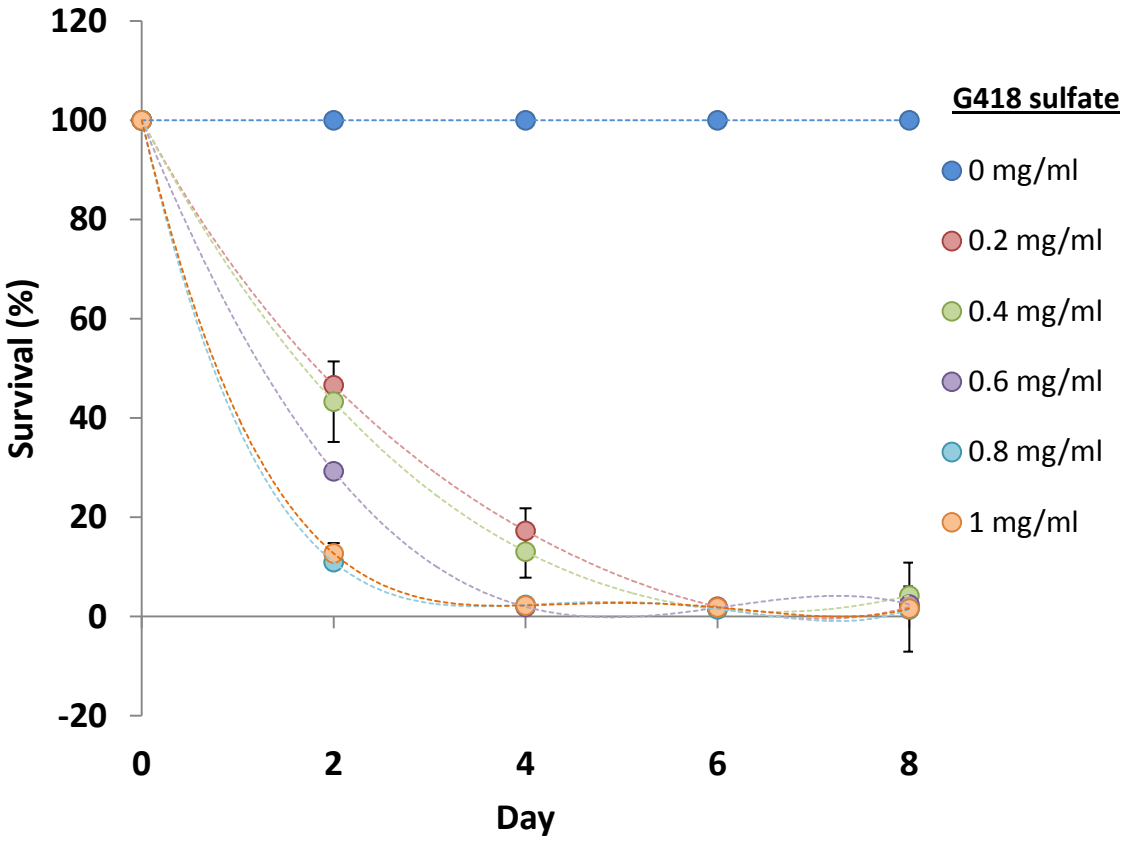

Figure 9 – Determination of the G418 sulfate concentration in complete media to use in stable cell line selection and maintenance.

PE/CA-PJ41 cell survival following treatment to the selection antibiotic; G418 sulfate, was calculated every 48 hs for a total of 10 days. At each time point, cultured were washed with PBS, fixed and stained with 0.05 % crystal violet before being solubilised with 10 % acetic acid and absorbance read at 595 nm in a spectrophotometer. Blank-corrected absorbance was converted into cell number (through a calibration curve before comparison to the day zero untreated control. Survival (%), the number of cells remaining following treatment expressed as a percentage of the untreated control for that time point. Results are the mean of three experiments carried out in triplicate ± standard error.

3.2.2 CYGB Transient Transfection

To confirm the transfection procedure generated cells that had taken up the pCMV6-AC CYGB plasmid and expressed the human *CYGB* cDNA insert successfully, a transient transfection was undertaken with PE/CA-PJ41 cells. Levels of *CYGB* induced in transient clones from this process were determined by RTqPCR and western blotting was used to confirm the presence of translated protein. For RTqPCR, NE-1 cell line cDNA was chosen for a physiological control level of expression as these cells had previously been found to express the globin in the range found within a panel of normal tissue biopsies (McRonald et al., 2012). PE/CA-PJ41 cells were induced to express *CYGB* by approximately 12 fold by the transient transfection, relative to the un-transfected parental cells and this was statistically significant (Figure 10b; t test, p =0.043).

Western blotting confirmed the expression of the CYGB protein (Figure 10a). Unexpectedly, the apparent mass of the band was approximately 70 kDa – much higher than the previously cited 21 kDa monomeric weight of CYGB (Hamdane et al., 2003; Lechauve et al., 2010). However, since the band appeared at the same position in the positive control HEK293 CYGB+ cell line extract (a cell line chosen because it had previously been characterised by our laboratory and found to express the globin abundantly (Carpenter, 2010)), it is highly likely that the antibody used is selectively binding to CYGB and that the transient transfection yielded CYGB expression at the protein level. This CYGB band was also absent from the NCE controls. Furthermore, Tsujino et al (2014) recently reported that separation of purified CYGB protein preparations results in monomeric, dimeric, and even tetrameric (~ 70 to 80 kDa) variants that each displayed differing ligand affinities (which may determine CYGB function). This report of a higher molecular weight band for CYGB strengthens our the

conclusion that the 70 kDa band observed in CYGB+ samples is indeed the intended globin protein. The detection of the β-actin band across all samples demonstrates equal loading of protein between wells. Together, transcript and western blotting data confirm the suitability of the PE/CA-PJ41 cell line to act as a model for CYGB over-expression and also confirms that un-transfected PE/CA-PJ41 cells express negligible levels of CYGB and was a suitable negative control.

To confirm that the plasmid used for the transfection procedure contained the wildtype sequence of human *CYGB* cDNA, the plasmid used for transfection was sequenced to determine the inserted DNA sequence (see section 2.3.4). The sequence obtained for the PCR product using the forward VP1.5 primer covered the entire sequence between the start and stop codons and this could be aligned to the reference *CYGB* mRNA sequence (NM_134268.4) present within the BLAST database. It also matched to the sequence provided by the manufacturer (Origene). BLAST sequence alignment showed a 97 % identity between the sequences (see appendix 4). The reverse primer XL39 unfortunately failed to accurately read the sequence (data not shown).

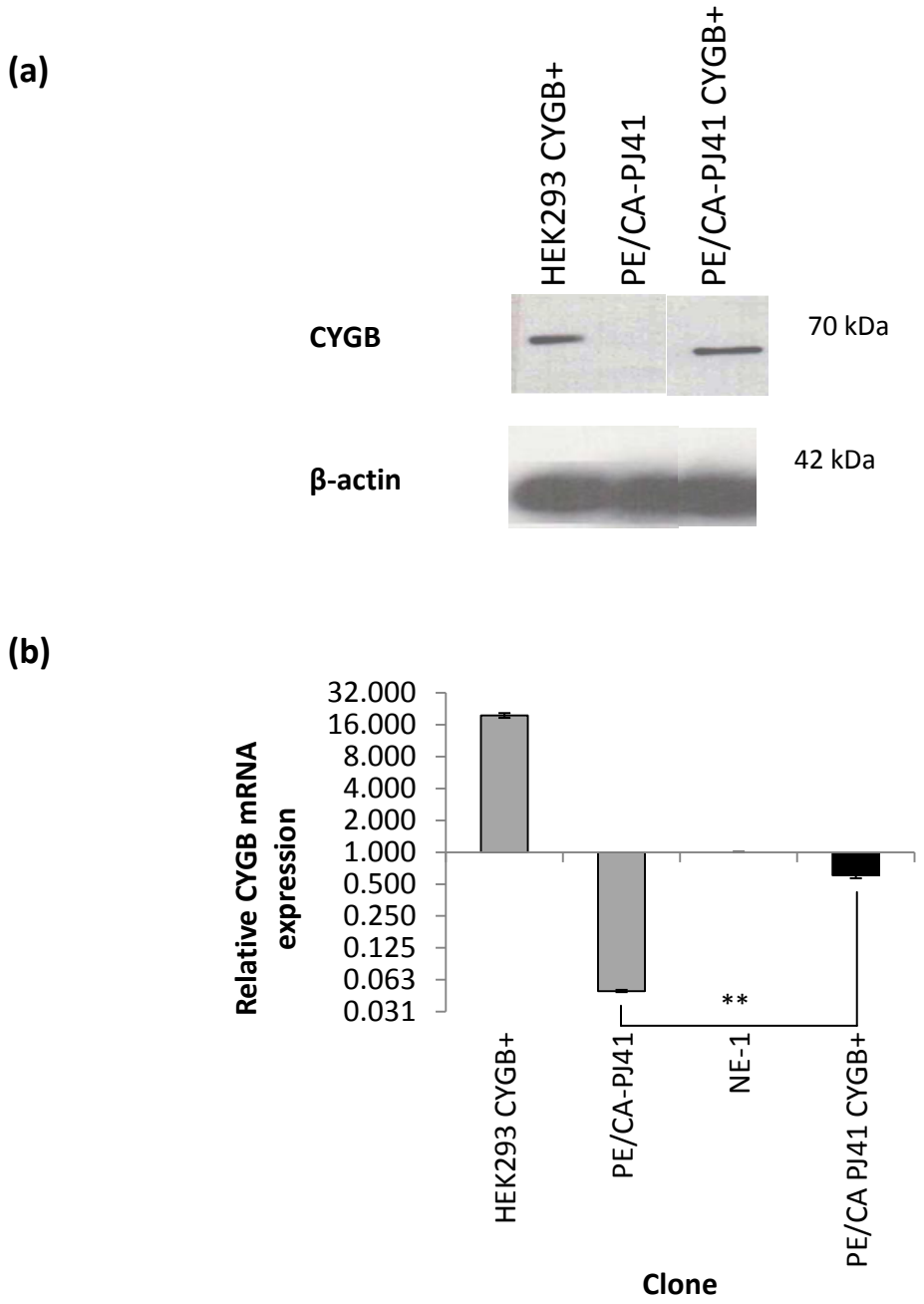

Figure 10 – Transient transfection of PE/CA-PJ41 cells results in induction of CYGB mRNA and protein expression.

(a) Whole cell protein isolates were taken from each transiently transfected PE/CA-PJ41 clone (CYGB+) and control lines after 24 h and then separated by SDS-PAGE before being probed for both CYGB protein and β-actin. **(b)** Expression of *CYGB* was quantified by SYBR Green qRT-PCR on RNA isolated obtained from un-transfected PE/CA-PJ41 cells and PE/CA-PJ41 CYGB+ cells, 24 h post-transfection with the pCMV6-AC vector that included the human *CYGB* cDNA sequence. NE-1 cell (*physiological*) and HEK293 CYGB+ cell (*positive*) RNA isolates were included as controls. Data was normalised to β-actin expression using the Pfaffl ddCt method from Ct values averaged across two biological replicates. Fold change *CYGB* mRNA relative to NE-1 ± standard error. PE/CA-PJ41 induced to express *CYGB* mRNA almost 12 fold by transient transfection. Comparison to PE/CA-PJ41, Student's t test, **p = < 0.01.

3.2.3 CYGB Stable Transfection

Once the conditions for transfection had been optimised and the concentration of G418 sulfate selected (see sections 3.2.1 and 3.2.2), stable transfection could be undertaken of the PE/CA-PJ41 cells with the human *CYGB* cDNA insert-containing pCMV6-AC. The workflow for the generation of the CYGB over-expressing OSC model is shown in Figure 11 and is described in section 2.4. The goal of this was to obtain cell clones that stably over-expressed the *CYGB* transcript and protein at a level that would be sufficient to amplify the downstream effects of the globin and hence enable analysis in future experiments.

Expression of the *CYGB* transcript was significantly induced in several of the clones propagated for screening in comparison to the un-transfected PE/CA-PJ41 parental control cell line (Figure 12, as assessed with t-test, non-equal variances, p value = < 0.05 in all cases). The HEK293 CYGB+ and NE-1 *CYGB* transcript expression values were included as a positive and physiological control, respectively. Expression of CYGB protein within stable clones was determined by western blotting and further quantified with in-cell ELISA (Figure 13). The western blot indicated that those clones identified to have *CYGB* transcript over-expression similarly expressed the CYGB protein (Figure 13a), and the in-cell ELISA experiment confirmed this (Figure 13b). The difference between CYGB protein expression in LST32 and the average of all three NCE controls was statistically significant (t-test (unequal variance), $p = 0.001$).

Stable clones exhibited a range of *CYGB* transcript over-expression including some that were close to physiological values. Therefore, a series of transfected cell clones were identified that represented low, medium and high CYGB over-expression compared to

the physiological-equivalent level found in NE-1 cells. Hence, all subsequent verification of stable CYGB expression was conducted within the following cell clones: LST421, LST54 and LST32 (that were all CYGB+ and exhibited high, medium and low over-expression, respectively) and LST223, LST42 and LST82A (that were all equivalent to the expression found within the un-transfected parental cell line and are collectively referred to as no CYGB expressing or NCE control clones). The NCE controls had undergone the exact same transfection procedure and culture as the CYGB+ clones, but remained comparable with the parent, un-transfected PE/CA-PJ41 cell line in terms of *CYGB* transcript and protein expression, hence it is reasonable to suggest that these would be an appropriate control against which changes in the CYGB+ clones could be compared.

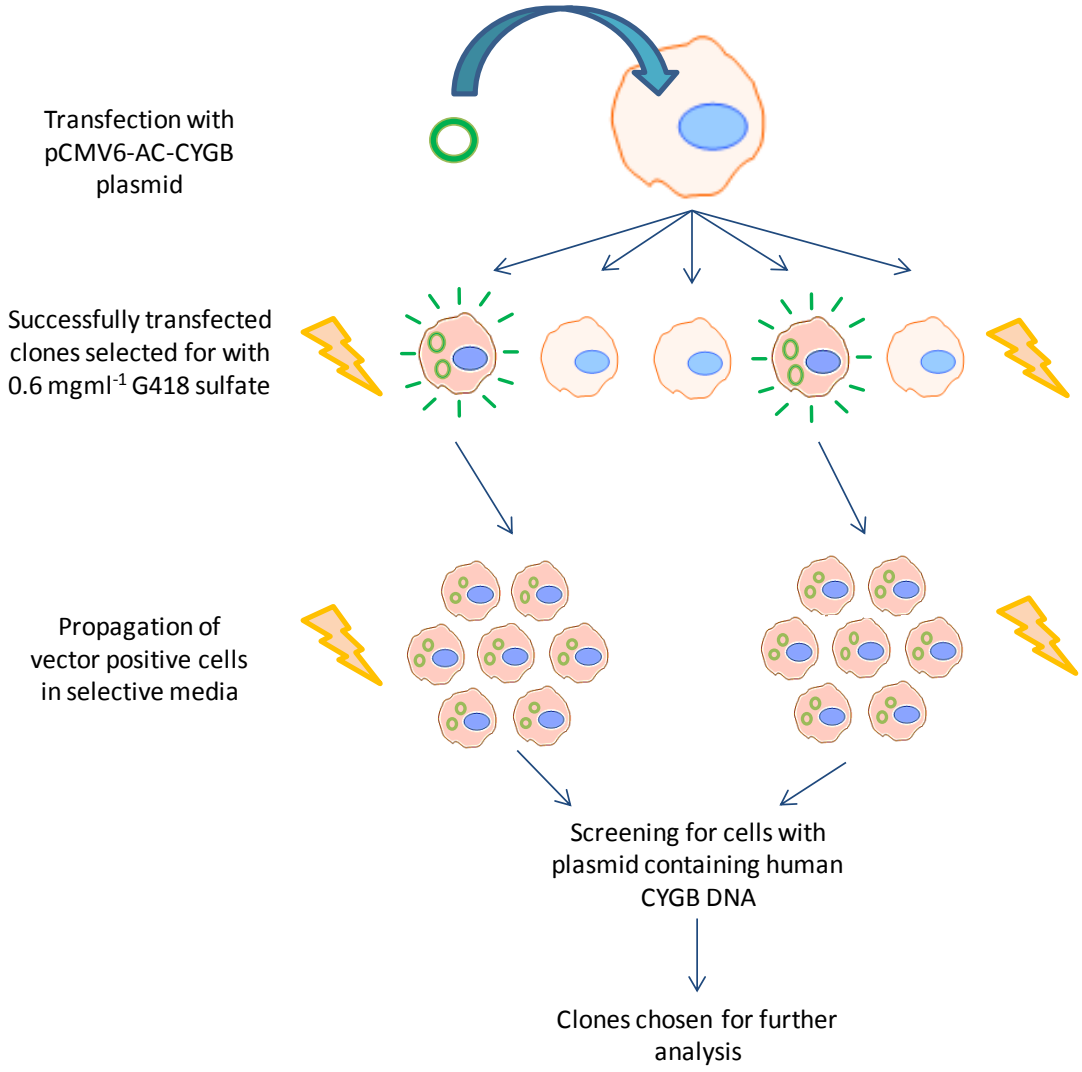

Figure 11 – Workflow for the generation of stably over-expressing CYGB positive PE/CA-PJ41 (OSC) cell clone models.

Production of stable cell clones that exhibited stable CYGB over-expression was carried out as shown. Successful transfection of the pCMV6-AC CYGB plasmid was selected for using G418 sulfate antibiotic selection at a concentration (0.6 $mgml^{-1}$) that had been optimised. Selective media was exchanged every 2-3 days until cell populations were confluent enough for screening and cryostocks were made of those that displayed CYGB expression. Stable cell clones expressing the inserted human *CYGB* cDNA sequence were confirmed to be mycoplasma negative prior to cryopreservation and to maintain a robust system, clones were only used between passages 7 and 30.

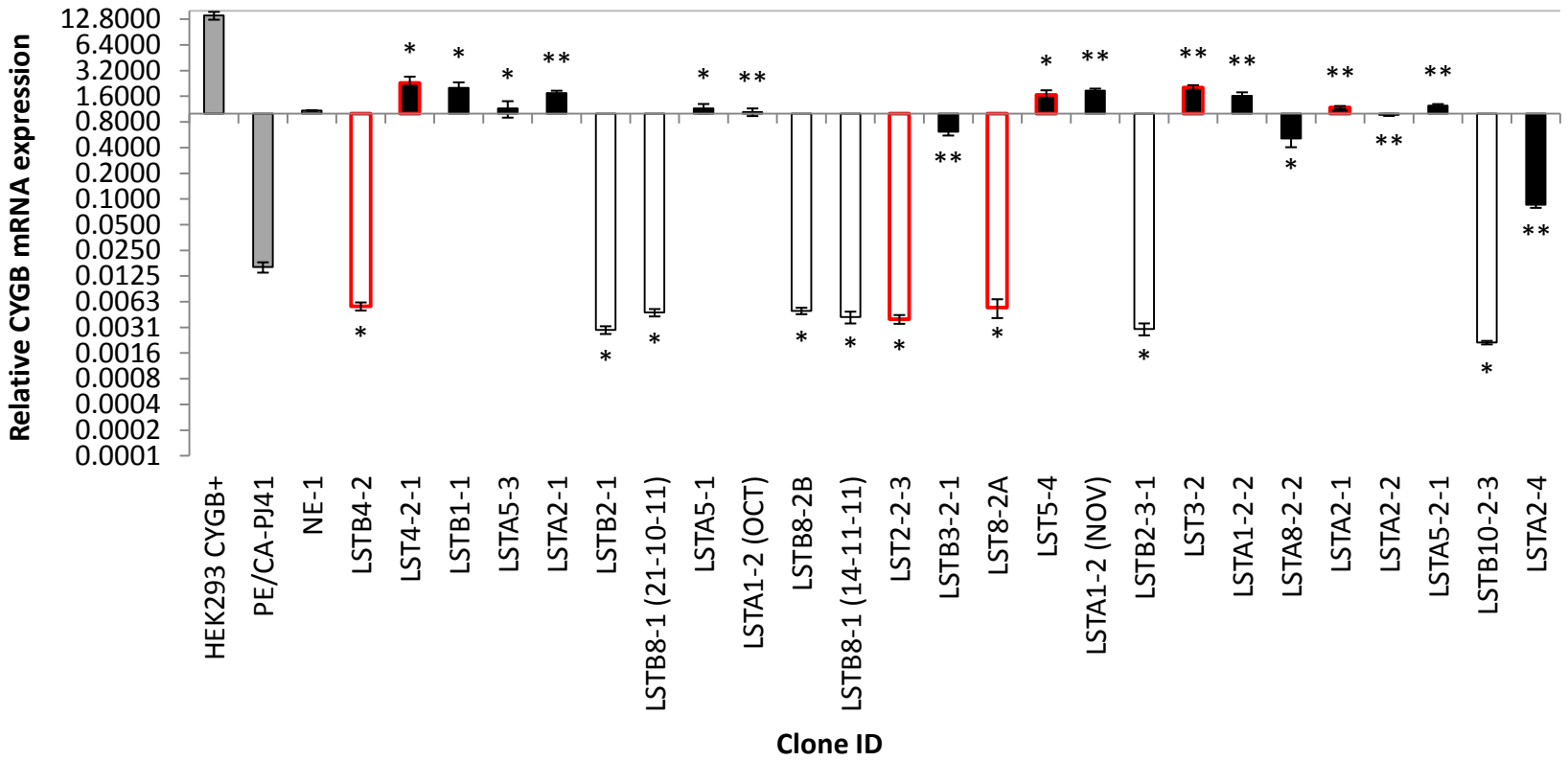

Figure 12 – Stable transfection of PE/CA-PJ41 cells results in cell lines that showed markedly induced CYGB mRNA expression (*black bars*) and a selection that showed comparable expression to the un-transfected parental population (*open bars*).

Expression of *CYGB* mRNA was measured by SYBR Green qRT-PCR on RNA isolated obtained from un-transfected PE/CA-PJ41 cells and PE/CA-PJ41 cells that were transfected with the pCMV6-AC vector that included the human *CYGB* cDNA sequence. After 48 h of incubation with the vector, cells were split 1:10 and underwent selection with 600 $\mu g ml^{-1}$ G418 sulfate in complete media until 'islands' of a hundred or so cells emerged that were harvested and cultured. RNA isolates were obtained once these cultures reached a cell density of 70 % in a 6-well plate. Data was normalised to β-actin expression using the Pfaffl ddCt method from Ct values averaged across three biological replicates. Fold change of *CYGB* mRNA relative to NE-1 ± standard error. Clones chosen for further analysis are highlighted in red. Comparison to PE/CA-PJ41, t test (unequal variances) * $p < 0.05$, ** p value = < 0.01.

(a)

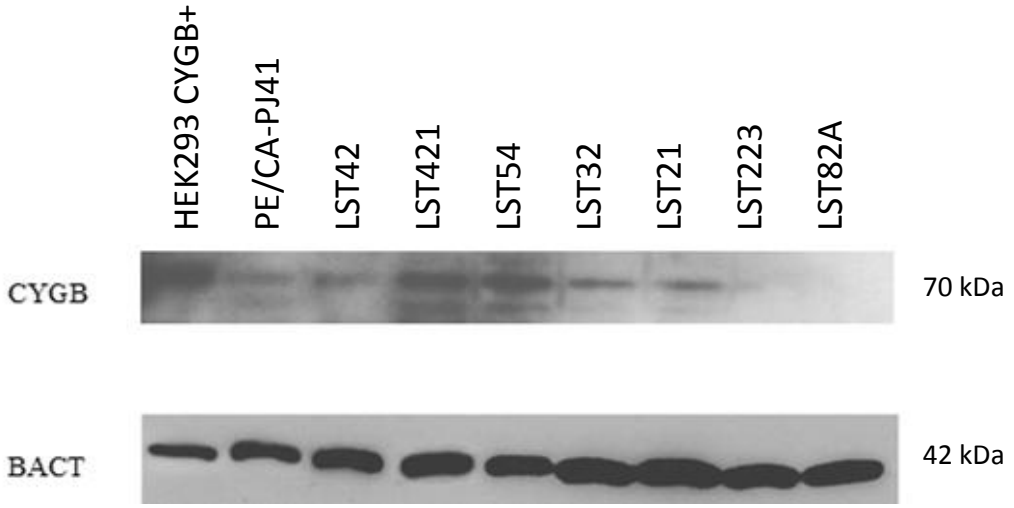

(b)

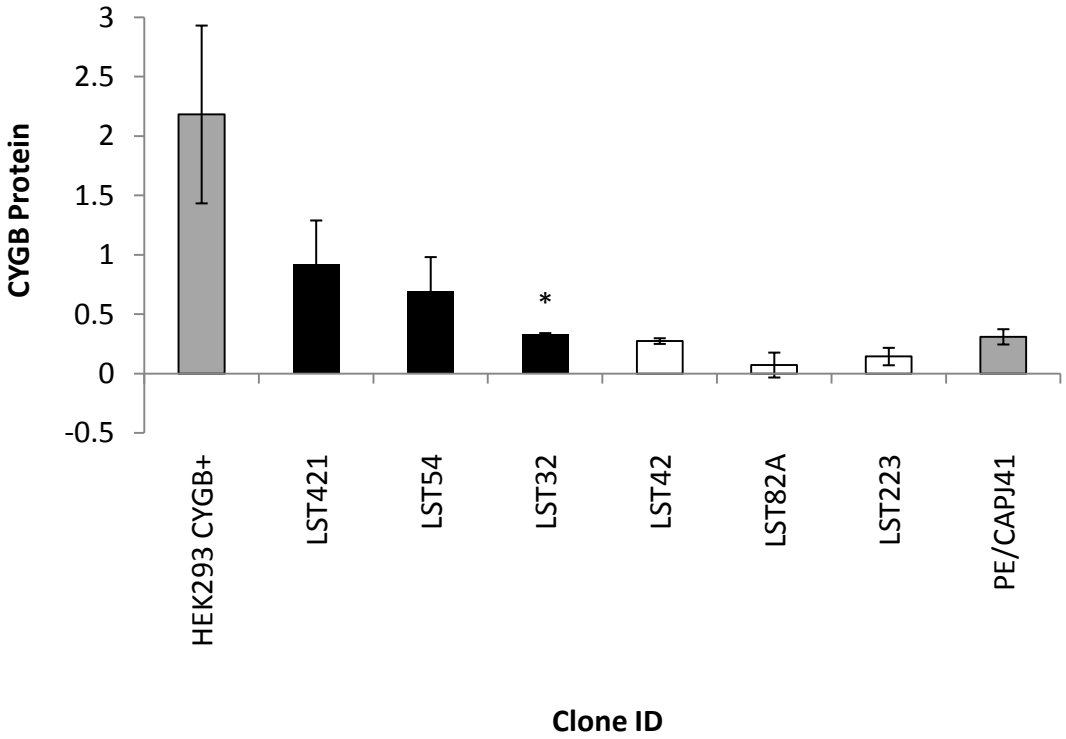

Figure 13 – Stable transfection of PE/CA-PJ41 cells results in clones that express high levels of the CYGB protein and a selection of clones that showed expression equivalent to the un-transfected parental population.

Clones were screened for CYGB protein expression by (a) western blotting and (b) In-Cell ELISA. Compared to NCE average (t-test (unequal variances), *$p < 0.01$).

3.2.4 CYGB cDNA Genomic Incorporation

To ensure the human *CYGB* cDNA sequence carried into the successfully transfected clones by the pCMV6-AC CYGB plasmid was incorporated stably within the genome, total gDNA was extracted from the clones and subjected to standard PCR to amplify a region of the G418 sulfate resistance gene and also a region of the human *CYGB* cDNA sequence.

The TrueClone™ human full-length *CYGB* sequence is provided in its cDNA format, hence primers were designed to amplify a sequence at the junction between exon 1 and 2 to detect the sequence's insertion into the genome. These primers enabled amplification of the artificially inserted cDNA sequence but not endogenous *CYGB* genomic sequences that contains introns. Primer sequences for both Neo^r and CYGBex1-2 sequences are given in Table 1.

Integration of the Neo^r gene was confirmed in all transfected clones by the presence of a 162 bp Neo-specific product and that was not present in the un-transfected parental PE/CA-PJ41 cell line (Figure 14). Insertion of the *CYGB* cDNA sequence was verified in the successfully transfected clones by the existence of an additional 275 bp CYGB-specific band (Figure 14).

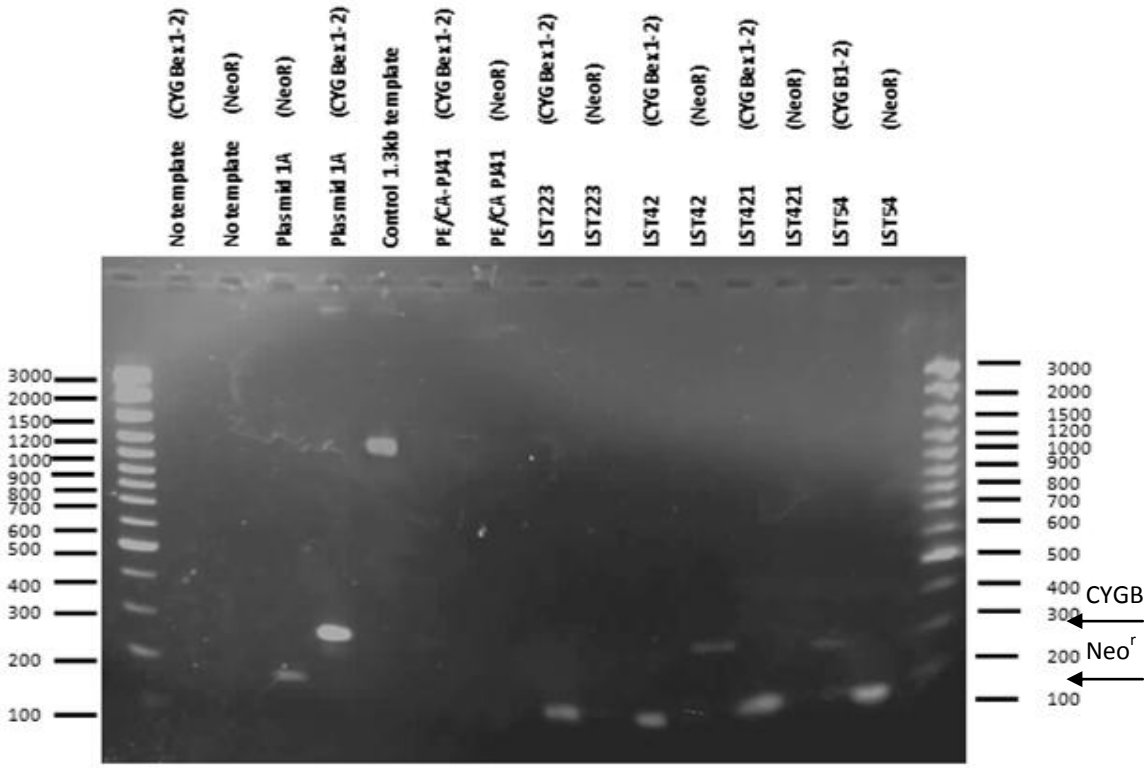

Figure 14 – PCR analysis of genomic DNA shows CYGB cDNA recombination within stably transfected PE/CA-PJ41 clones, but not in the NCE negative transfected clones.

Isolated genomic DNA from the G418 sulfate resistant clones subjected to standard PCR with primers designed to amplify either a sequence within the *CYGB* cDNA (a 275 bp region overlapping the junction between exons 1 and 2) or a 162 bp region within the Neomycin/G418 sulfate (Neo^r) gene. An aliquot of the plasmid preparation used for the transfection process; Plasmid 1a, was used for a positive control, whilst PE/CA-PJ41 gDNA isolates (that underwent the PCR as per the other samples) were included as a negative control. As technical controls, a control 1.3kb fragment, along with no templates controls for each primer set were amplified of which the latter showed no reagent contamination.

3.2.5 Heme Quantification

CYGB as a heme protein requires the inclusion of the heme moiety for normal biological function and hence it was important to characterise the CYGB+ transgenic clones for the presence of the ferroporphyrin (heme) group. To do this, the ferrous hemochromogen assay was employed, the basis of which is that protein containing a heme group, when reduced by sodium dithionite, undergoes a spectral shift from 557 to 575 nm (see section 2.7). The total absorption difference between oxidised and reduced spectra peaks enables calculation of the total heme content of the sample. Analysis by this method demonstrated that medium and high expression CYGB+ cell clones (LST421 and LST54, respectively) had greater quantities of heme, whilst the low expression clone (LST32) was within the range of the mean values of the three NCE clones (Figure 15). LST421 and LST54 clones were found to have a higher heme content (0.735 nM heme ngµl^{-1} protein ± 0.34 and 0.987 nM heme per ngµl^{-1} protein ± 0.37, respectively), relative to that quantified across the three NCE clones (0.41 nM heme ngµl^{-1} protein ± 0.037) but these differences were not statistically significant (Kruskal-Wallis, $p = 0.643$).

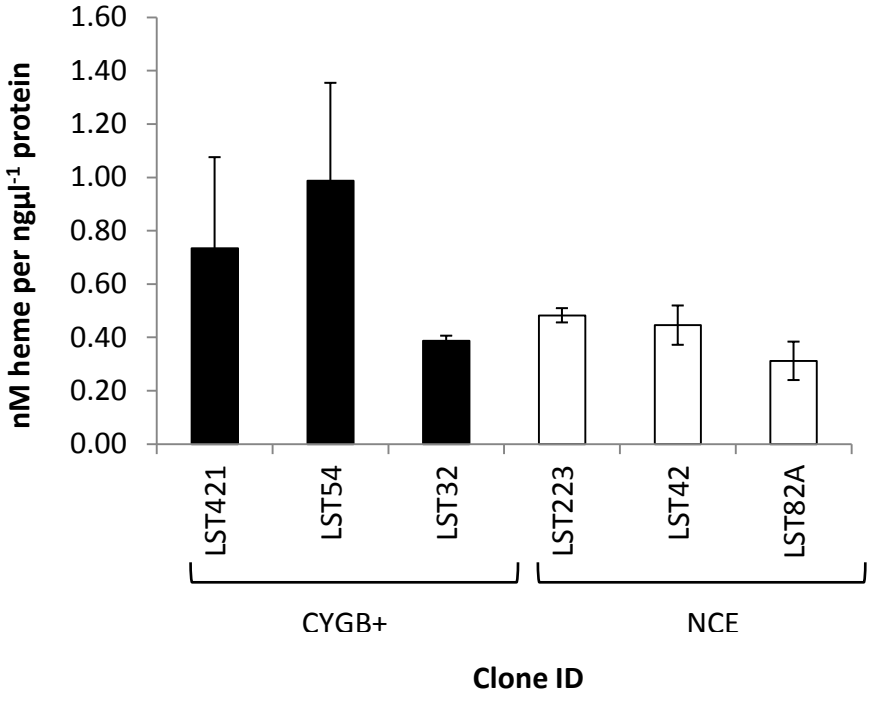

Figure 15 – Heme content is high in the stably transfected PE/CA-PJ41 cells expressing CYGB, but not in the NCE negative transfected controls.
Ferroporphyrin (heme) in each cell clone was quantified through the ferrous hemochromogen assay. There was an observed trend for greater heme levels in CYGB+ relative to NCE control clones. Whole cell protein isolates were obtained and added to an oxidising solution containing niacin. The absorbance difference between 557 nm and 575 nm was obtained, before the heme was reduced by dithionite addition and the absorption difference measured again. The total absorption difference between oxidised and reduced spectra was then calculated that enabled the calculation of total heme content through Beer's Law. Concentrations were normalised to total protein content (in $ng\mu l^{-1}$) determined by the Bradford Assay. Measurements were the average of biological triplicates ± standard error. No statistically significant differences were found between means of each CYGB+ to the average of three NCE controls (Kruskal-Wallis, $p = 0.643$).

3.2.6 Intracellular Distribution of CYGB Protein

As a further assessment of the expression of the transfected CYGB protein, as well as determining where within the cell CYGB is localised, transfected clones were examined by immunocytochemistry and confocal microscopy. To confirm the specificity of the secondary FITC-conjugated antibody for the primary target antibody, cultures were incubated with just the secondary antibody, but otherwise underwent an identical protocol to the test samples. These controls showed no green fluorescence (see appendix 1), which confirmed the fluorescence detected in the test samples was specific to the presence of the target primary antibody.

Successfully transfected CYGB+ clone cultures exhibited substantially greater fluorescence (Figure 16) compared to the NCE clones (Figure 17). The CYGB+ clones analysed by this method showed comparable levels of staining to that observed for the HEK293 CYGB+ positive control, whilst the NCE controls each demonstrated little or no fluorescence and were visibly similar to the un-transfected PE/CA-PJ41 parental cells. In terms of protein localisation, fluorescence indicated that CYGB was located diffusely mainly within the cytoplasmic region of the cell, although there was some overlap with the nuclear compartment, as indicated by the concurrent staining of the Hoechst dye and FITC-conjugated secondary antibody (Figure 16).

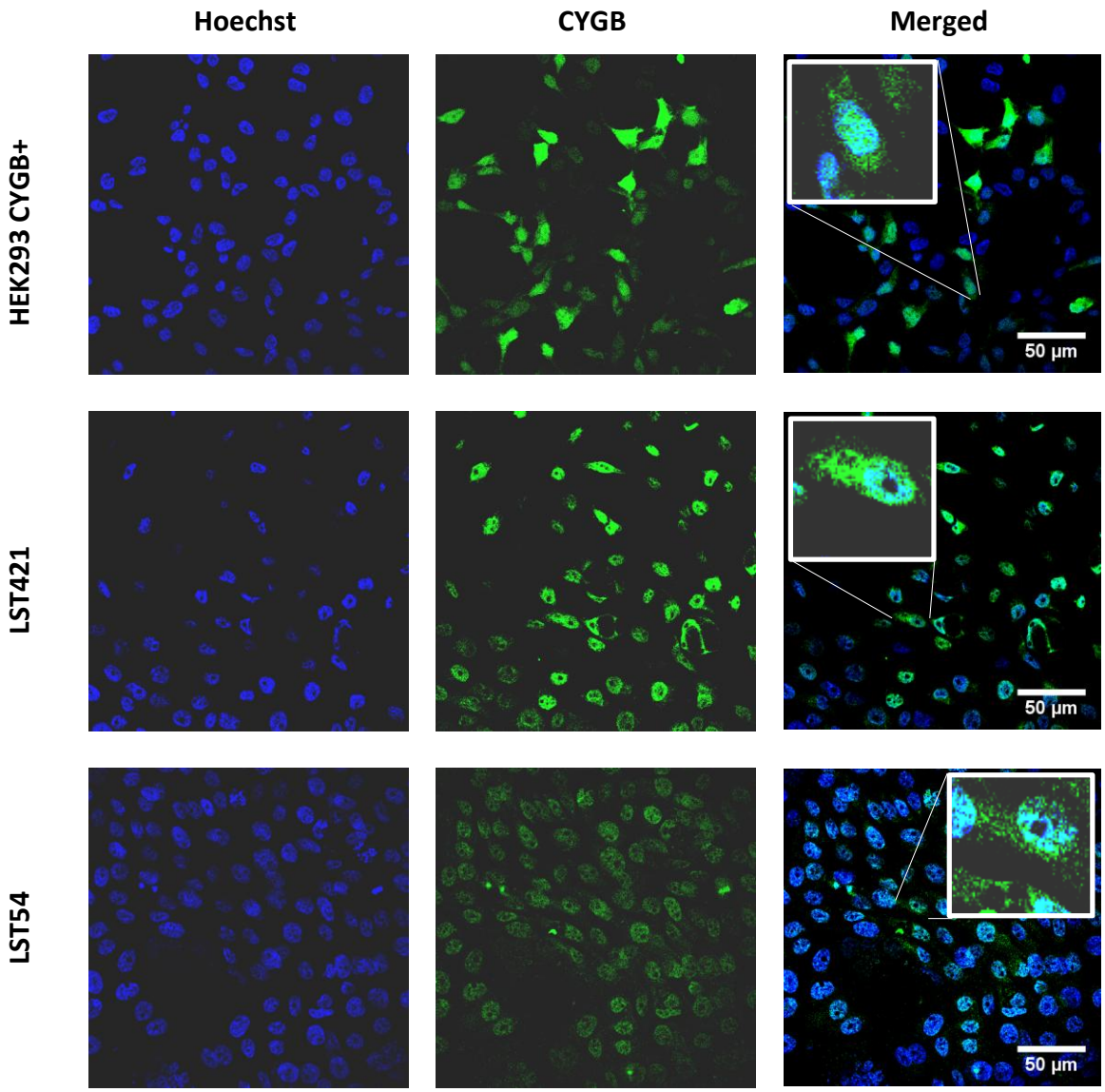

Figure 16 – The transfected CYGB protein is localised mainly to the cytosol in CYGB expressing cells.

Fixed cell cultures were immunostained for CYGB protein (Monoclonal murine anti-human CYGB antibody, 1:500) using a FITC-conjugated secondary antibody (1:200) and counterstained with the nuclear stain, Hoechst (1:8000). Inserts show a magnified cell within the image. Secondary-only stained cultures were devoid of green fluorescence, suggesting the specificity of the antibody for the primary target (appendix 1). Representative confocal images are shown. Stably transfected PE/CA-PJ41 cells expressing CYGB show green fluorescence and hence the presence of the CYGB protein in these cells. Scale bar 50 µm.

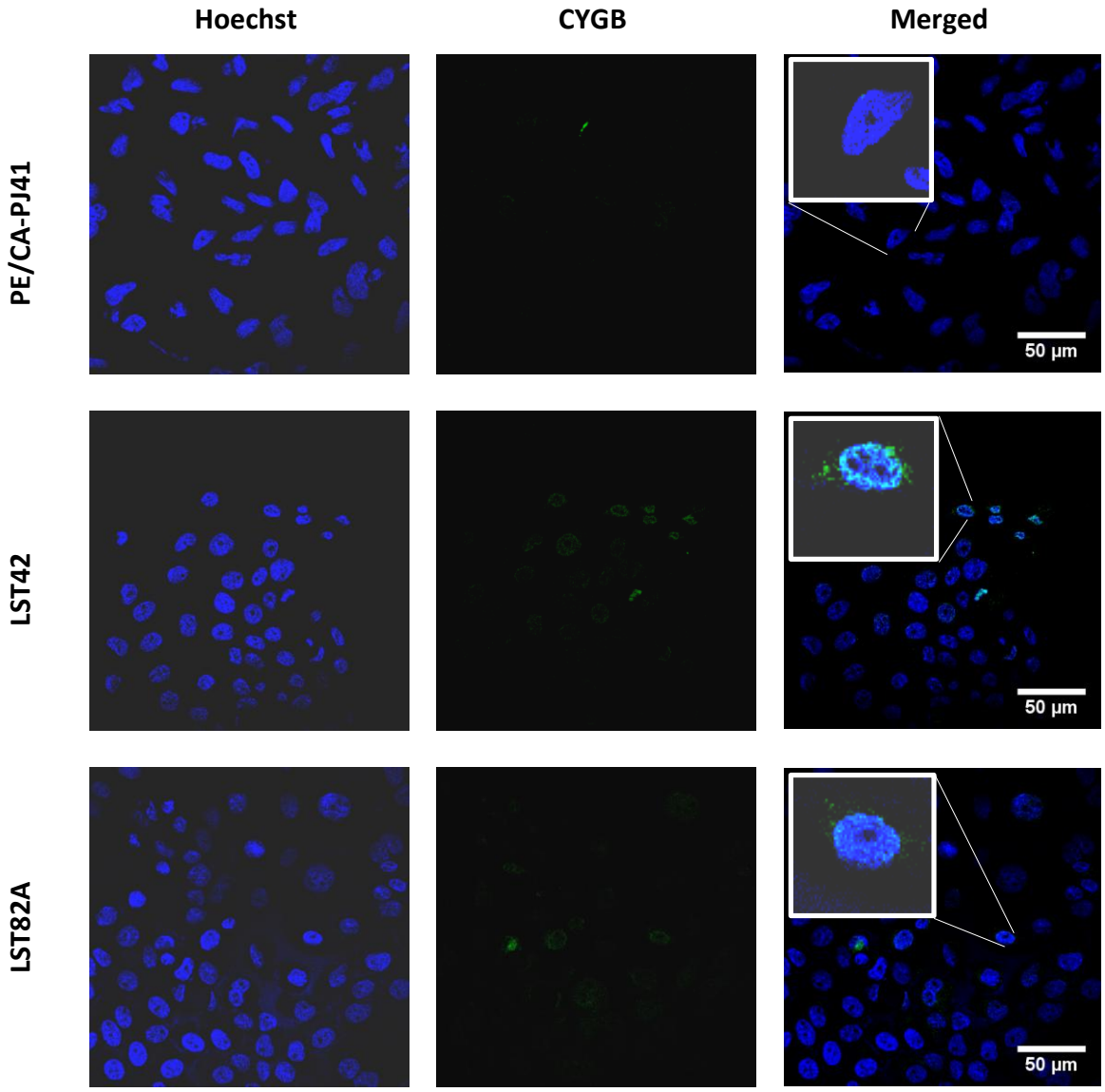

Figure 17 – CYGB protein is negligible in negative transfected, NCE cell clones.
Fixed cell cultures were immunostained for CYGB protein (Monoclonal murine anti-human CYGB antibody, 1:500) using a FITC-conjugated secondary antibody (1:200) and counterstained with the nuclear stain, Hoechst (0.25 $ngml^{-1}$). Inserts show a magnified cell within the image. Secondary-only stained cultures were devoid of green fluorescence, suggesting the specificity of the antibody for the primary target (appendix 1). Representative confocal images are shown. Negative transfected PE/CA-PJ41 cells show no green fluorescence and hence a lack of CYGB protein expression. Scale bar 50 µm.

3.2.7 Respiratory Function

Since there have been hypotheses in the literature that suggest CYGB may influence cellular respiration (Halligan et al., 2009; Stagner et al., 2009), and oxygen use is an important indicator of the energy requirements of a cell that could influence some assays that would employed in future experiments, we also assessed oxygen consumption rates along with levels of ATP within the transfected clones.

No collective trends related to CYGB over-expression were identified in either oxygen consumption rates (Figure 18) or ATP levels (Figure 19). There was a gradual increase in mean oxygen consumption rate from low (LST32) to high (LST421) CYGB expression but none are significantly different from the NCE clone average (t-test (unequal variances), $p = > 0.05$). LST32 clones showed higher ATP concentrations of 10.58 μM ± 0.06 compared to NCE controls (8.68 μM ± 0.03). LST421 clones showed slightly higher ATP concentrations of 9.29 μM ± 0.45 than the NCE controls, whilst LST54 showed similar concentrations to NCE controls. None of these differences were statistically significant (one way ANOVA, $p = 0.721$). Although no association with CYGB expression could be established, ATP production did show some variability between CYGB+ clones, with concentrations varying in total by approximately 1.3 μM within CYGB+ clones and by negligible amounts within NCE clones.

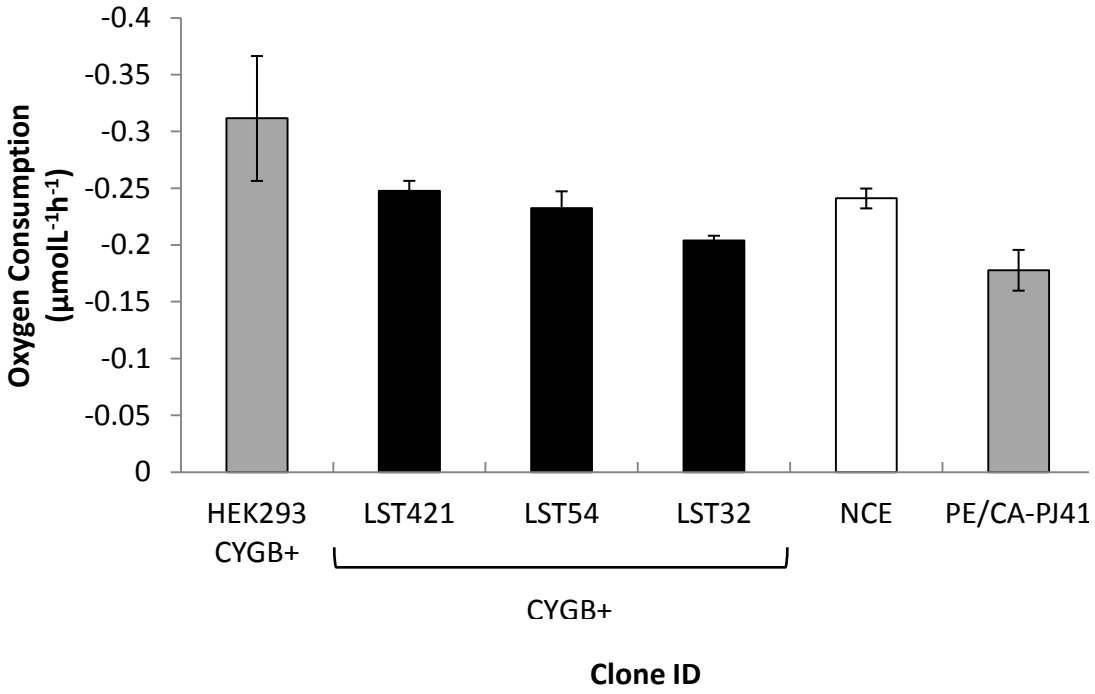

Figure 18 – No differences were observed in the basal oxygen consumption rates of CYGB+ clones when compared to NCE clones.

Oxygen consumption rates were assessed through a Clark electrode-based system. Measurements were taken every 30 min (an average was taken from signals recorded over a 50 second duration) across a 6 h period to determine the oxygen decline within the culture media. The experiment was repeated on four separate occasions. Calibration controls of 100 % saturation media (aerated overnight) and 0 % anoxic control solution (0.1 M sodium hydroxide/sodium acsorbate) were employed to enable interpolation of oxygen concentrations. To determine the rate of oxygen depletion for each transgenic clone, the natural logarithm of the concentrations exported for each time point were calculated and then plotted. Linear regression was then used to calculate their respective gradients that were directly proportional to the rate of oxygen reduction, expressed as $\mu molL^{-1}h^{-1}$ of oxygen. There were no statistically significant differences when compared to NCE controls (t-test (unequal variances), $p > 0.05$).

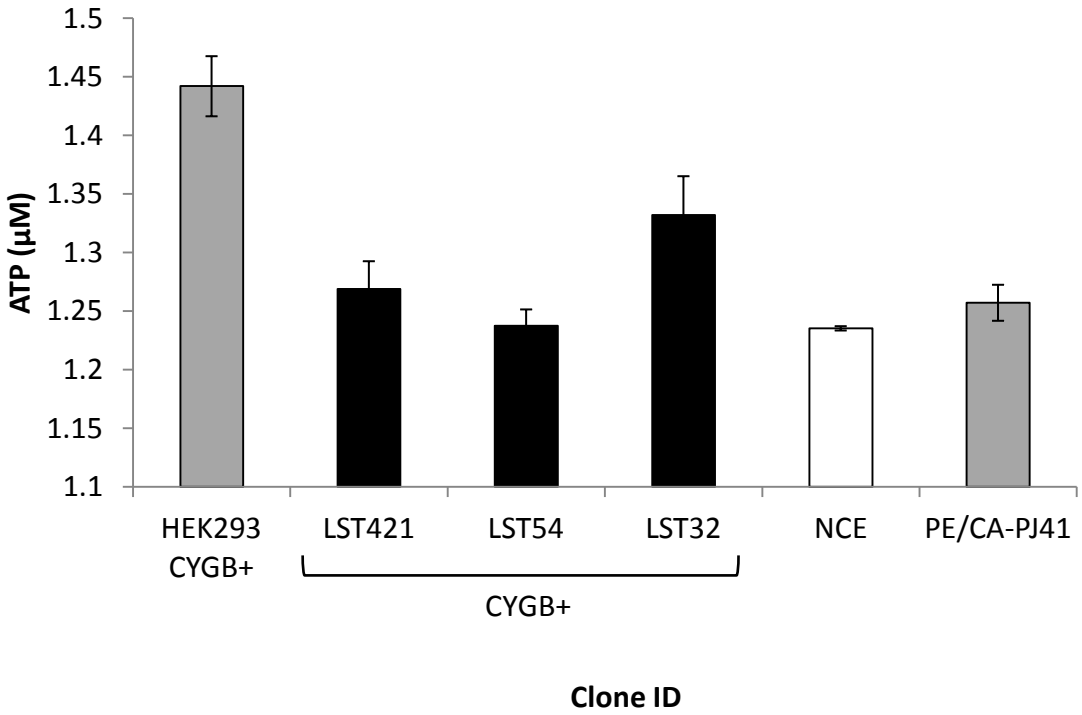

Figure 19 – Basal ATP concentrations in CYGB+ clones and NCE controls.
ATP production by the transfected clones was determined through a luciferase-based assay where the light signal generated is proportional to the quantity of intracellular ATP. There were no statistically significant differences between NCE controls and CYGB+ clones (one-way ANOVA, p = 0.721).

3.2.8 p53 Genotype

An important genetic alteration within many cancers is mutation of the *p53* gene (Leemans et al., 2011) and this is an early inactivation event in 40 to 60 % of HNSCC tumours (Waridel et al., 1997b), leading to disruption of its central stress-responsive functions of cell cycle regulation, apoptosis and DNA repair. Mutations within *p53* have been linked to radio and chemotherapeutic resistance (Hoffmann et al., 2008), which makes it an important target to explore for its mechanism of action and regulation. Additionally, there have been recent reports connecting CYGB to members of the p53 protein family, such as p53 itself (John et al., 2014) and ΔNp63 (Latina et al., 2015), which increases the importance for the mutational status of *p53* to be established in the CYGB+ clones used in future experiments. We sequenced the *p53* gene within the CYGB+ clone LST421 to determine whether the gene was wildtype in our cell model.

Exons 4 to 8 of *p53* that encode the DNA binding domain region were chosen for analysis since they are where most (> 85 %) mutations have been cited to occur (Hollstein et al., 1991; Leroy et al., 2013). All analysed exons between 4 and 8 showed no nucleotide differences to the reference sequence that could not be attributed to software error or poor resolution at the start of the sequence reaction (Figure 20 to Figure 24, see *p53* sequencing chromatograms file on the supplementary CD-ROM). Any discrepancies resulting from the latter were investigated by examining the sequence obtained from the opposing read direction for the region. Thus, the *p53* gene appears to be wildtype within the parent PE/CA-PJ41 cell line and CYGB+ clones.

Figure 20 – p53 Exon 4 Forward Read in CYGB+ clone LST421.

PCR products were sequenced by direct sequencing and the basecalls obtained were used to conduct a pairwise BLASTn search against the FASTA sequence for exon 4 (GenBank Accession Number JF923569.1). Discrepancies resulting from software errors are shown with a red star, whilst bases circled were checked in the corresponding opposite read sequence and confirmed to match the *p53* exon 4 reference sequence. No mutations were found within the regions sequenced, suggesting that this *p53* exon is wildtype in CYGB+ clones.

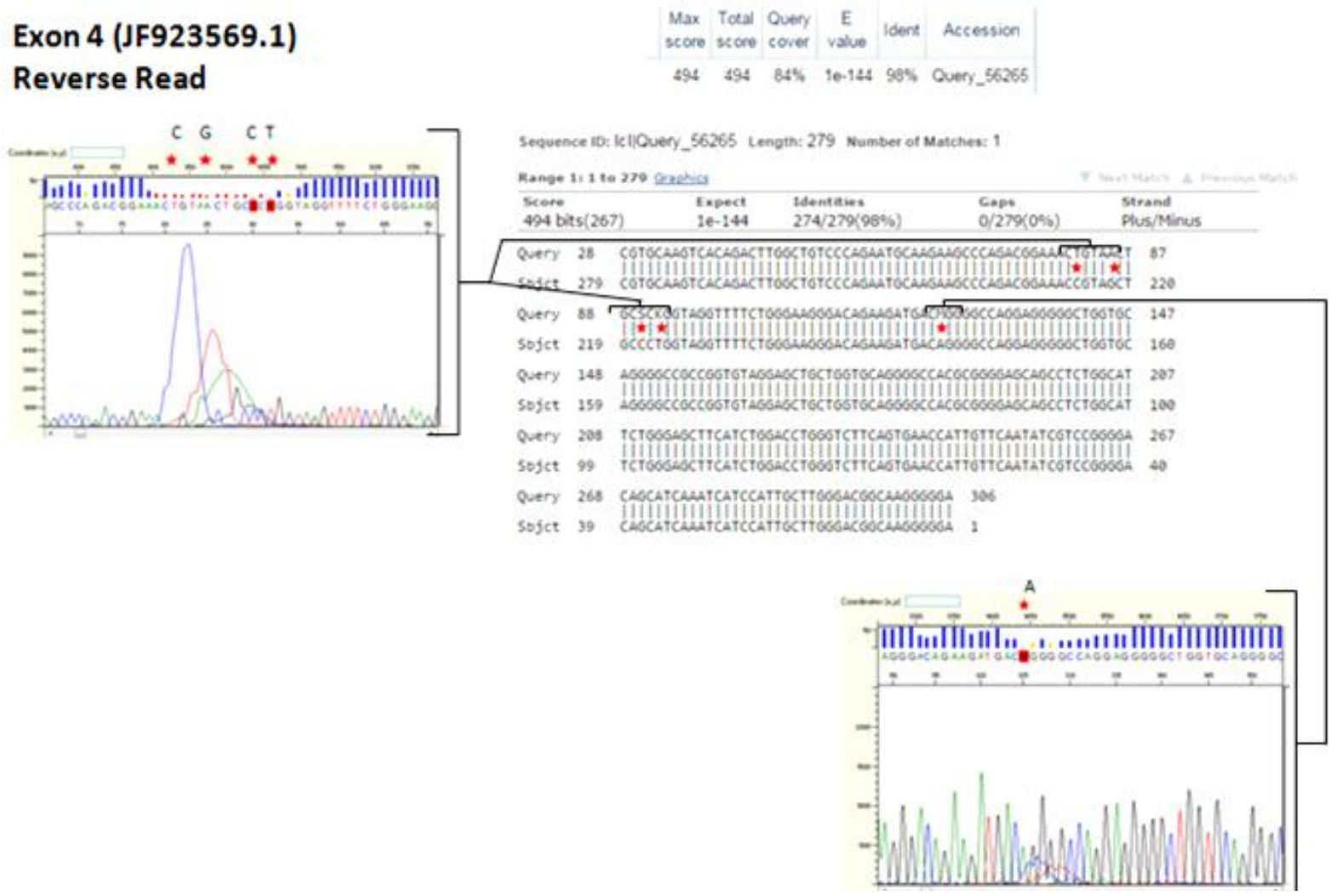

Figure 20 (continued) – p53 Exon 4 Reverse Read in CYGB+ clone LST421.

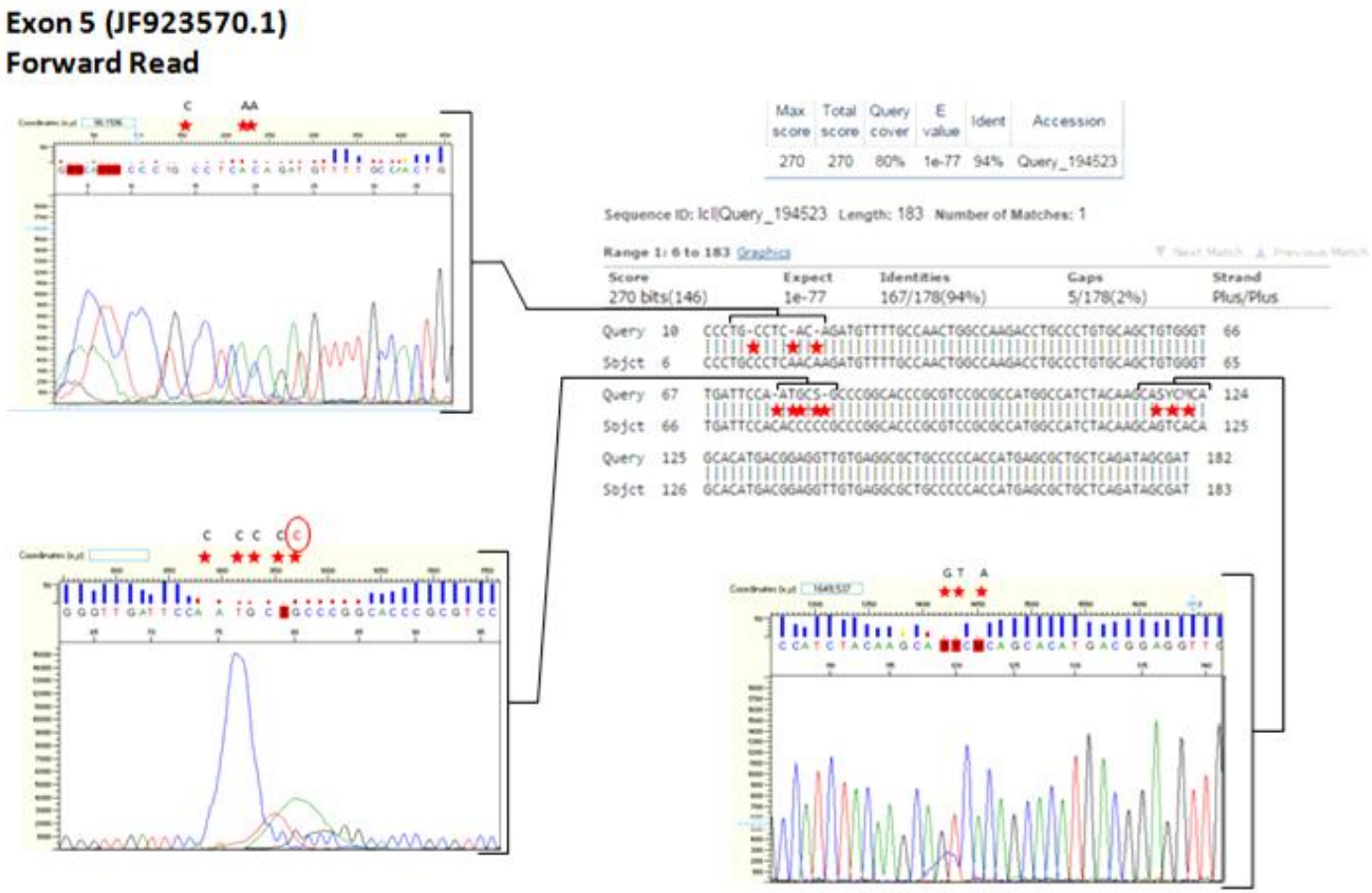

Figure 21– p53 Exon 5 Forward Read in CYGB+ clone LST421.

PCR products were sequenced by direct sequencing and the basecalls obtained were used to conduct a pairwise BLASTn search against the FASTA sequence for exon 5 (GenBank Accession Number JF923570.1). Discrepancies resulting from software errors are shown with a red star, whilst bases circled were checked in the corresponding opposite read sequence and confirmed to match the *p53* exon 5 reference sequence. No mutations were found within the regions sequenced, suggesting that this *p53* exon is wildtype in CYGB+ clones.

Exon 5 (JF923570.1)
Reverse Read

Max score	Total score	Query cover	E value	Ident	Accession
329	329	81%	2e-95	99%	Query_60071

Sequence ID: lcl|Query_60071 Length: 183 Number of Matches: 1

Range 1: 1 to 183 Graphics

Score	Expect	Identities	Gaps	Strand
329 bits(178)	2e-95	183/185(99%)	2/185(1%)	Plus/Minus

```
Query  11   ATCGCTTATCTGGAGCAGCGCTCATGGTGGGGGCAGCGCCTCACAACCTCCGTCATGTGC  70
            ||||| |||| ||||||||||||||||||||||||||||||||||||||||||||||||
Sbjct  183  ATCGC-TATCT-GAGCAGCGCTCATGGTGGGGGCAGCGCCTCACAACCTCCGTCATGTGC  126

Query  71   TGTGACTGCTTGTAGATGGCCATGGCGCGGACGCGGGTGCCGGGCGGGGGTGTGGAATCA  130
            ||||||||||||||||||||||||||||||||||||||||||||||||||||||||||||
Sbjct  125  TGTGACTGCTTGTAGATGGCCATGGCGCGGACGCGGGTGCCGGGCGGGGGTGTGGAATCA  66

Query  131  ACCCACAGCTGCACAGGGCAGGTCTTGGCCAGTTGGCAAAACATCTTGTTGAGGGCAGGG  190
            ||||||||||||||||||||||||||||||||||||||||||||||||||||||||||||
Sbjct  65   ACCCACAGCTGCACAGGGCAGGTCTTGGCCAGTTGGCAAAACATCTTGTTGAGGGCAGGG  6

Query  191  GAGTA  195
            |||||
Sbjct  5    GAGTA  1
```

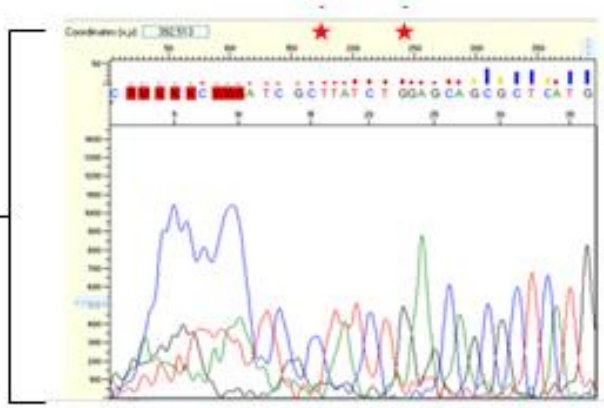

Figure 21 (continued) – p53 Exon 5 Reverse Read in CYGB+ clone LST421.

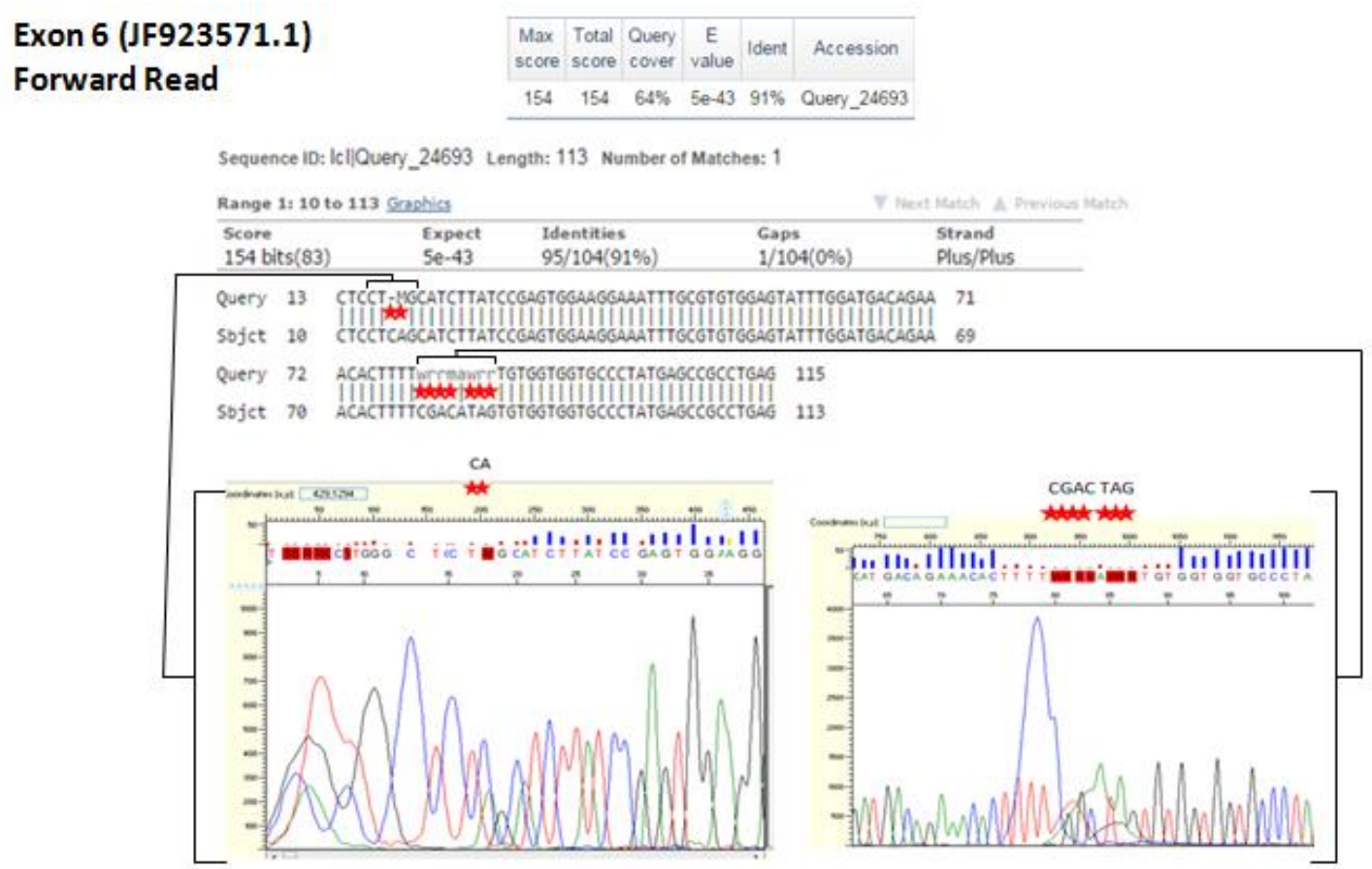

Figure 22 – p53 Exon 6 Forward Read in CYGB+ clone LST421.

PCR products were sequenced by direct sequencing and the basecalls obtained were used to conduct a pairwise BLASTn search against the FASTA sequence for exon 6 (GenBank Accession Number JF923571.1). Discrepancies resulting from software errors are shown with a red star, whilst bases circled were checked in the corresponding opposite read sequence and confirmed to match the *p53* exon 6 reference sequence. No mutations were found within the regions sequenced, suggesting that this *p53* exon is wildtype in CYGB+ clones.

Exon 6 (JF923571.1)
Reverse Read

Max score	Total score	Query cover	E value	Ident	Accession
182	182	69%	2e-51	97%	Query_5189

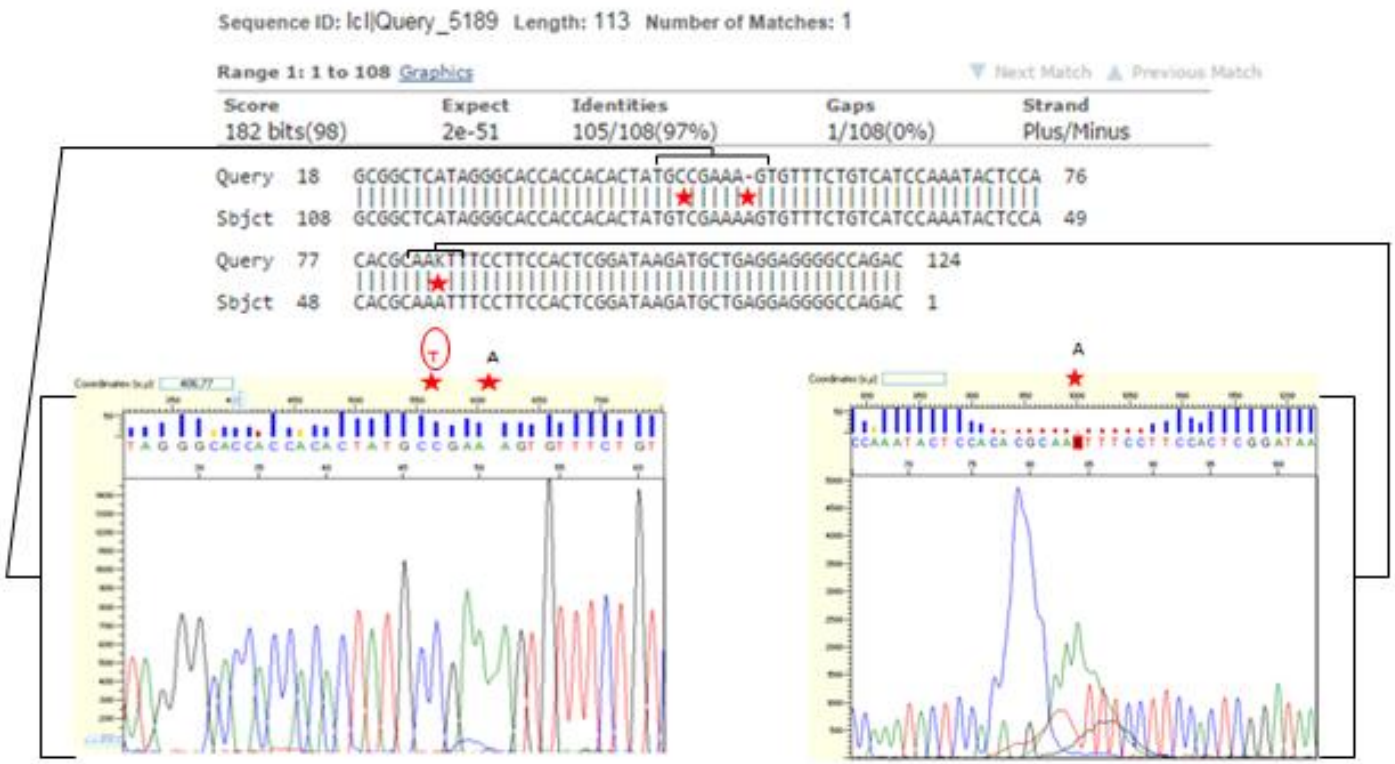

Figure 22 (continued) – p53 Exon 6 Reverse Read in CYGB+ clone LST421.

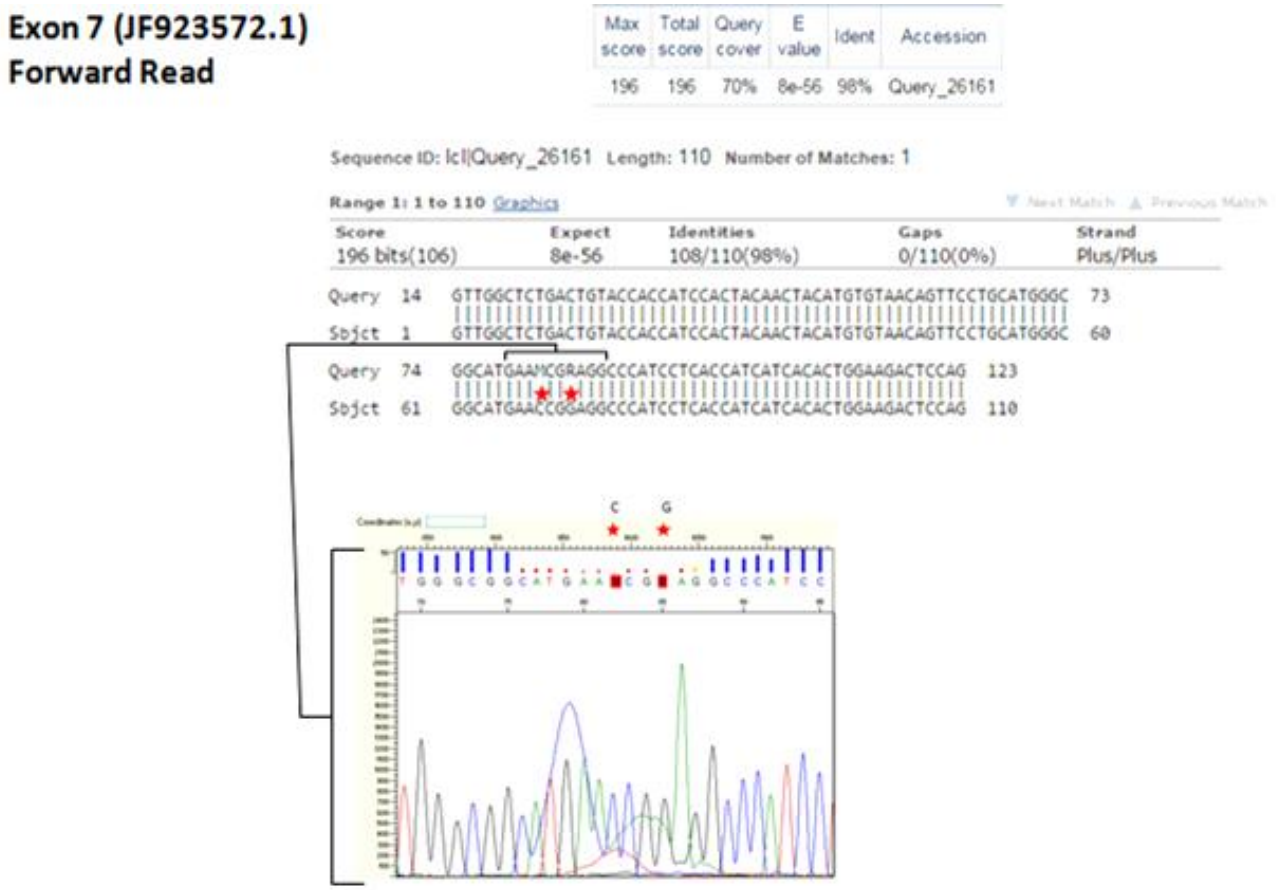

Figure 23– p53 Exon 7 Forward Read in CYGB+ clone LST421.

PCR products were sequenced by direct sequencing and the basecalls obtained were used to conduct a pairwise BLASTn search against the FASTA sequence for exon 7 (GenBank Accession Number JF923572.1). Discrepancies resulting from software errors are shown with a red star, whilst bases circled were checked in the corresponding opposite read sequence and confirmed to match the *p53* exon 7 reference sequence. No mutations were found within the regions sequenced, suggesting that this *p53* exon is wildtype in CYGB+ clones.

Exon 7 (JF923572.1)
Reverse Read

Max score	Total score	Query cover	E value	Ident	Accession
183	183	36%	1e-51	100%	Query_62203

Sequence ID: lcl|Query_62203 Length: 110 Number of Matches: 1

Range 1: 1 to 99 Graphics ▼ Next Match ▲ Previous Match

Score	Expect	Identities	Gaps	Strand
183 bits(99)	1e-51	99/99(100%)	0/99(0%)	Plus/Minus

```
Query  13   CAGTGTGATGATGGTGAGGATGGGCCTCCGGTTCATGCCGCCCATGCAGGAACTGTTACA  72
            ||||||||||||||||||||||||||||||||||||||||||||||||||||||||||||
Sbjct  99   CAGTGTGATGATGGTGAGGATGGGCCTCCGGTTCATGCCGCCCATGCAGGAACTGTTACA  40

Query  73   CATGTAGTTGTAGTGGATGGTGGTACAGTCAGAGCCAAC  111
            |||||||||||||||||||||||||||||||||||||||
Sbjct  39   CATGTAGTTGTAGTGGATGGTGGTACAGTCAGAGCCAAC  1
```

Figure 23 (continued) – p53 Exon 7 Reverse Read in CYGB+ clone LST421.

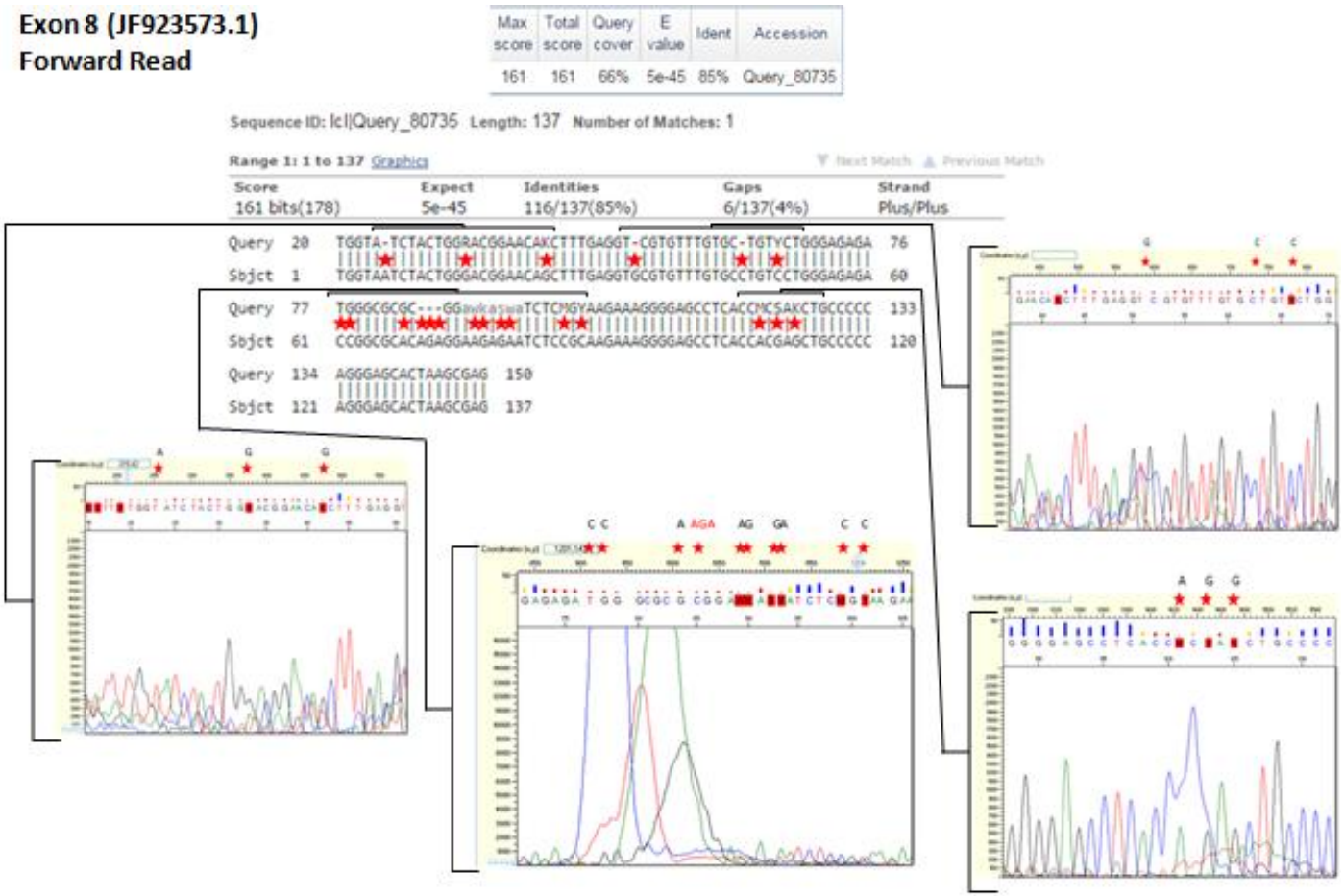

Figure 24– p53 Exon 8 Forward Read in CYGB+ clone LST421.

PCR products were sequenced by direct sequencing and the basecalls obtained were used to conduct a pairwise BLASTn search against the FASTA sequence for exon 8 (GenBank Accession Number JF923573.1). Discrepancies resulting from software errors are shown with a red star, whilst bases circled were checked in the corresponding opposite read sequence and confirmed to match the *p53* exon 8 reference sequence. No mutations were found within the regions sequenced, suggesting that this *p53* exon is wildtype in CYGB+ clones.

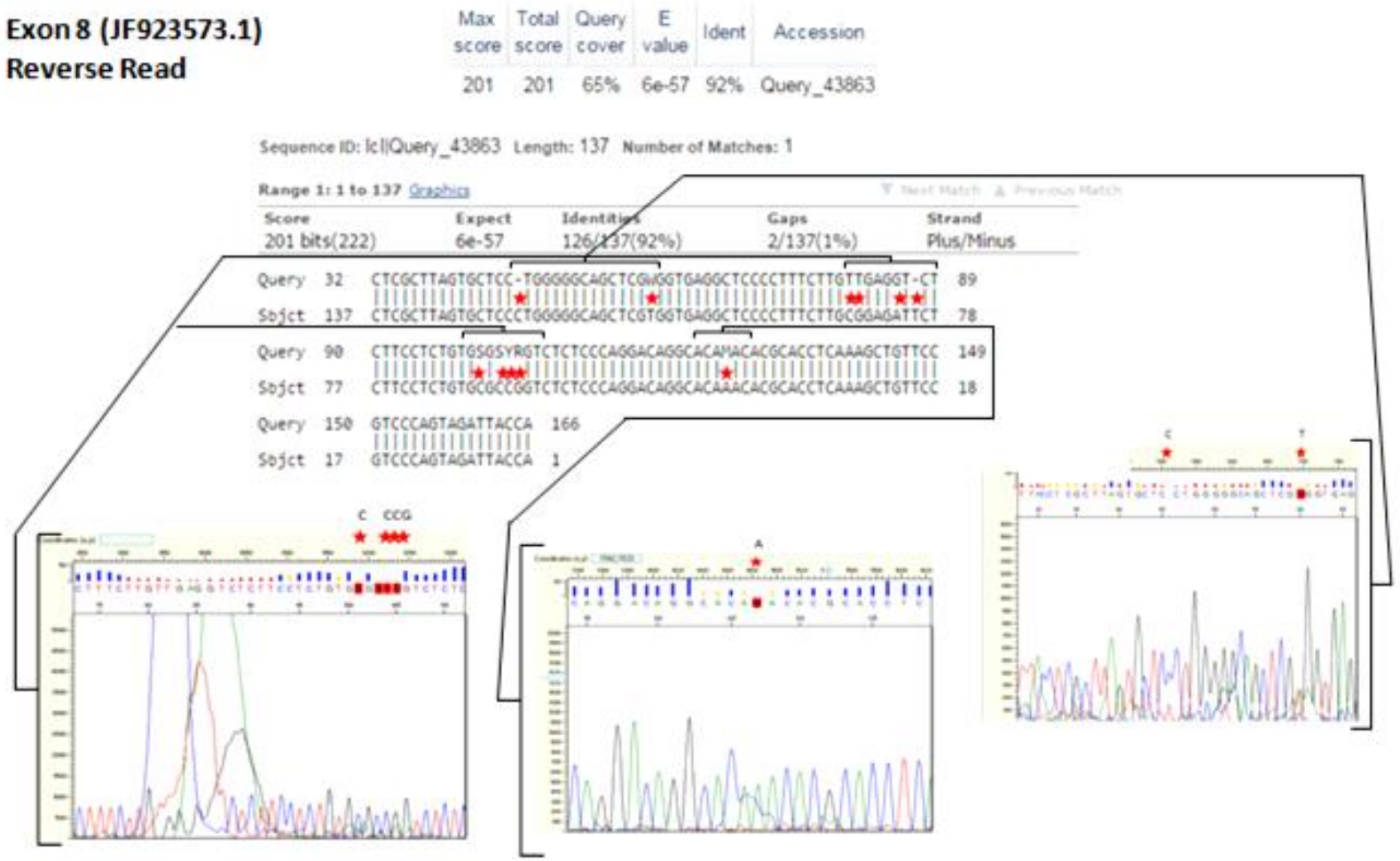

Figure 24 (continued) – p53 Exon 8 Reverse Read in CYGB+ clone LST421.

3.3 Discussion

The use of stable CYGB over-expressing transgenic cell lines has been previously instrumental in extending understanding of CYGB function. In this chapter, stably transfected PE/CA-PJ41 cells that over-express CYGB to a low, medium or high level were generated and validated. This is a unique OSC *in vitro* cell model that was subsequently used to examine the impact of CYGB over-expression on the transcriptome (see chapter 4) and also on cellular phenotypes both before and after treatment to the chemotherapy drug cisplatin (see chapters 5 and 6).

CYGB gene silencing in the PE/CA-PJ41 cell line is strongly epigenetically regulated, with the promoter exhibiting in excess of 96 % methylation and culture in media containing 5-aza-2-deoxycitidine induced *CYGB* mRNA > 350 fold, highlighting the importance of methylation in regulating its expression (Shaw et al., 2009). The PE/CA-PJ41 cell line provided an ideal system for over-expression as it does not endogenously express *CYGB*. Additionally, > 60 % of OSC tumours, and the PE/CA-PJ41 cell line, contain a methylated *CYGB* promoter, suggesting it may function as a tumour suppressor (Shaw et al., 2013, Shaw et al., 2009).

Although *CYGB* is down-regulated in a number of tumours (Oleksiewicz et al., 2011), around 15 % of NSCLC samples within one study were found with *CYGB* up-regulation (Xinarianos et al., 2006) (see section 1.6.3.2.2). Five in seven head and neck tumour cell lines displayed a concurrent increase in both hypoxia inducible factor 1A (*HIF1A*) and *CYGB* transcripts following hypoxic treatment (see section 1.6.1, Shaw et al., 2009). Most recently, three melanoma cell lines were shown to have strikingly increased *CYGB* expression above that observed for other tumours screened in the study, which the

authors propose is due to a pre-existing high ROS level in pre-malignant cells of this type (Fujita et al., 2014). These reports show *CYGB* expression is cell-specific and regulated by cellular environment, which complicates the perception of CYGB as a simple tumour suppressor gene and implies that re-expression of *CYGB* has a role in tumorigenesis. Thus, the OSC cell model presented in this chapter that aimed to stably induce CYGB over-expression to study its function should also improve understanding of its activity in relation to cancer-related phenotypes.

The main objective of this chapter was to genetically modify PE/CA-PJ41 cells so CYGB was stably over-expressed to enable further investigation into its function in subsequent chapters. Transfection of PE/CA-PJ41 cells was achieved with the pCMV6-AC plasmid containing the human *CYGB* cDNA sequence regulated by the cyclomegalovirus (CMV) promoter. This vector also contains the G418 sulfate resistance gene that enabled positive selection of successfully transfected clones. A 97 % identity of the insert with the reference *CYGB* sequence was confirmed and the remaining sequence difference could mainly be attributed to the poor resolution towards the end of the sequence read.

The heme quantification attempted in Figure 15 was not as conclusive as hoped. The assay demonstrated medium and high expression CYGB+ clones exhibited greater total heme levels, but the third; lowest, CYGB+ clone showed similar levels to the NCE controls. Although this assay can give an indication as to whether the total heme content is increased in CYGB+ clones (which can be assumed to be due to the increased abundance of heme-containing CYGB due to the transfection process), it is limited in its sensitivity as it does not directly quantify the CYGB-specific heme; rather, it quantifies the total heme content of cells. As CYGB only represent a small fraction of the total

cellular heme content, the difference attributed to CYGB expression is likely to be quite small and difficult to quantify. Our data, however, supports the conclusion that induced CYGB over-expression from the transfection has resulted in more heme-containing; rather than apoprotein, proteins, that can be assumed to be due to the induced over-expression of CYGB.

Twenty five transgenic clones that had G418 sulfate resistance were selected and propagated for further screening, of which 16 exhibited significant levels of *CYGB* expression above background parental cell PE/CA-PJ41 levels. The remaining 9 transfected clones were resistant to G418 sulfate but did not express the CYGB gene any differently to the parent cell line.

Of the 16 CYGB over-expressing clones, three were chosen for further analysis; LST421, LST54 and LST32 that exhibited high, medium and low over-expression respectively, and all displayed *CYGB* mRNA levels above NE-1 cells that were used as a physiological reference level of expression (see section 3.2.2). These three CYGB over-expressing clones are herein collectively referred to as CYGB positive clones (or CYGB+ clones). The CYGB+ clones exhibit different extents of expression because of the random integration of the *CYGB* cDNA sequence from the vector into the genome. The insertion site may, by chance, occur within a heterochromatic region that could diminish transcription of the neighbouring transgenic sequence and result in differences in expression between otherwise genetically identical clones with the same inserted gene (Kleinjan and van Heyningen, 1998).

Of the 9 transgenic clones not expressing *CYGB* mRNA, three were selected for further analysis (LST223, LST42 and LST82A) and were used as transgenic controls for

subsequent experiments since they had undergone the same selection pressures as CYGB+ clones but did not successfully express the *CYGB* transcript or protein any differently to the parental PE/CA-PJ41 cell line. These clones are herein collectively referred to as NCE control cells. The inclusion of three CYGB+ and three NCE clones in all experiments described in the following chapters is important to determining CYGB-specific responses, since changes observed in one CYGB+ clone should be reproducible in a further, set of independent CYGB+ clones and also reveal evidence of any gene-dose effects observed between high, medium and low expression clones. These 3 CYGB+ transgenic clones were verified to over-express CYGB at the protein level by western blotting and in-cell ELISA, and contained greater mean heme concentrations indicating that the assembly of the over-expressed globin protein included the heme group that makes its functional.

All three clones demonstrated genomic incorporation of the human *CYGB* cDNA sequence as well as a mostly cytoplasmic localisation of the CYGB protein, as assessed by confocal microscopy. Our finding that the transgenically expressed CYGB was also in this cellular compartment is in agreement with others who report as such in epithelial cells (Gorr et al., 2011), hepatocytes (Shigematsu et al., 2008), hepatic stellate cells (Kawada et al., 2001) and fibroblast-like cells (Schmidt et al., 2004) (see section 1.4). This also suggests that clones have physiologically relevant levels and location of CYGB. Partial nuclear staining of the CYGB primary antibody was also detected in the CYGB+ cells, which has similarly been reported in hepatocytes (Shigematsu et al., 2008), myoblasts (Ye et al., 2006) and neuronal cells (Geuens et al., 2003).

It has been reported by Halligan et al that over-expression of CYGB within fibroblasts is correlated with an increase in oxygen metabolism, compared to cells with the *CYGB* transcript depleted through short-hairpin RNA (shRNA)-mediated knockdown (Halligan et al., 2009). A link between CYGB and oxygen metabolism was also suggested by Stagner et al (2009). As far as we are aware, these are the only reported instances of such a finding, but these necessitated that transgenic clone respiratory function should be assessed because many of the assays planned in this thesis to investigate CYGB function (for example, cell death analysis) have chemistries that depend upon oxidative metabolism (for instance, reductase-mediated MTT assay and ATP-dependant Caspase-Glo assay) so it is important to characterise this in the cell model.

Although not significantly different to average NCE oxygen consumption rates, CYGB+ clones exhibited a similar trend to that reported by Halligan et al (2009), where increasing CYGB expression is correlated to a corresponding slight rise in basal oxygen metabolism and a rise in ATP within the lowest over-expressing CYGB+ clone (LST32) compared to the NCE control. However, as neither ATP nor oxygen consumption is different collectively between NCE and CYGB+ clones, it seems unlikely that this will strongly interfere with the experiments described in later chapters.

ATP levels in NCE clones showed the least variability and did not show a difference when compared to CYGB+ clones. Within CYGB+ clones, there was a difference within a range of approximately 1.3 μM, which suggested that there are clone-specific differences in ATP concentration but these are small, not statistically significant, and unlikely to influence results presented in the following chapters. The phenomenon of some inter-CYGB+ clone heterogeneity in these assays is expected, as it is known that variation in

expression within transgenic clones generally may arise due to stochastic cell-inherent events (Stockholm et al., 2007). The stable transfection procedure can also contribute to deviation of responses between genetically identical clones because of the lack of control over where the cDNA sequence inserts into the genome. Non-specific insertion within a clone may occur in a gene site that causes its mutation or disrupts its regulation that would affect related signalling cascades just within that one clone (Wurtele et al., 2003).

We also characterised the mutational status of *p53* gene in CYGB+ clones by sequencing exons 4 to 8; regions known to contain most of the reported mutations (Hollstein et al., 1991) and discovered that these regions do not harbour any mutations, suggesting wildtype p53. This is in agreement with the findings in chapter 4 that show significantly regulated p53 targets in cisplatin-treated CYGB+ clones and also chapter 5 that shows CYGB+ clones display greater resistance to cisplatin whose response is primarily mediated through p53 signalling (see section 4.1).

In an attempt to overcome the inter-clone variability caveat and make stronger conclusions of how CYGB over-expression influences phenotype, methodologies that work on different principles for each endpoint measure were employed in following chapters. For instance, cytotoxicity assessments following cisplatin treatments utilised MTT in addition to crystal violet and sulforhodamine B assays that measured cell survival by quantifying reductase activity, nuclear DNA, and protein, respectively. Secondly, the experiments were conducted within three independent CYGB+ and NCE clones to reduce the possibility of observing clone-specific phenotypes.

The successful generation and authentication of three stable CYGB+ clones reported in this chapter provided a new cell model system to evaluate the transcriptomic and phenotypic alterations that occur before and after cisplatin treatment in an OSC cell context (see chapters 4, 5 and 6). These studies importantly furthered understanding of previously reported findings associated with CYGB function such as impaired proliferation and resistance to oxidative and chemical stressors.

CHAPTER FOUR:

Transcriptomic Changes Associated with CYGB Over-Expression

4.1 Introduction

CYGB up-regulation has been observed following hypoxia (Burmester et al., 2007; Fordel et al., 2004; Guo et al., 2007), fibrotic (Man et al., 2008; Tateaki et al., 2004) and oxidative stressors (Chua et al., 2009; Li et al., 2007). These findings have enabled researchers to begin to identify regulatory sites for the *CYGB* gene (see section 1.3). There is emerging evidence that part of CYGB's function involves mediating change to the transcriptome as part of the cellular response to hypoxic and oxidative stresses. For example, *CYGB* expression was found to be co-induced with *HIF1A* transcripts in hypoxic head and neck cancer cells (Shaw et al., 2009). Lung cancer (NCI-H2228 and NCI-2887) and breast cancer (HCC 1569) cells that transiently over-expressed *CYGB* were found to reduce mRNA expression of collagen (*COL1A1*), PRP40 pre-mRNA (*PRPF40*) and Uncoupling protein 2 (*UCP2*) (Shivapurkar et al., 2008). It has also been found CYGB over-expression is associated with down-regulation of *COL1A1* (Man et al., 2008; Shivapurkar et al., 2008) and *CNND1* (Chen et al., 2014). A brief summary of their functions are provided in Table 4.

Liver tissue from mice injected with carbon tetrachloride to induce fibrosis also showed a change in the ratio of *CYGB:COL1A1* mRNA; increasing at 24 h and decreasing at 48 h post-treatment (Man et al., 2008). There is also evidence from a transiently CYGB over-expressing BEAS2B (transformed normal bronchial epithelial cell) model treated with oestrogen-like compound ZEA, where CYGB reduced the time-dependent increase in ROS (in association with decreased apoptotic cell death), which in their subsequent microarray of wildtype ZEA treated versus untreated samples involved changes in genes

Table 4 – Transcripts Putatively Down-Regulated with CYGB Over-Expression.

Gene Name	*Symbol*	*Description*	*References*
Pre-mRNA processing factor 40	*PRPF40*	Critical ribonuclear factor of the spliceosome involved in processing precursor mRNA sequences newly transcribed by RNA polymerase II into mature mRNA, through the removal of non-coding introns and ligation of exons. Up-regulated in in pancreatic tumours. Found to negatively regulate Neural Wiskott-Aldrich Syndrome Protein (N-WASP) that normally activates Cdc42 RhoGTPase for assembly of filopodial actin chains.	Ritchie et al., 2009 Thakur et al., 2008 Mizutani et al., 2004
DNA Methyltransferase 1	*DNMT1*	Plays an important role in epigenetic regulation of gene expression by methylating cytosine bases primarily at promoter sites (that have a high proportion of GC dinucleotides) and interacting with histone deacetylases that together suppress transcription. Thus it is key for modulating tumour suppressor gene expression.	Robertson et al., 2000
Uncoupling Protein 2	*UCP2*	This is an inner mitochondria membrane carrier protein whose activity involves ROS-induced transport of H+ ions from the intermembrane space to the matrix and this acts to detoxify superoxide radicals that result from uncoupled electron transfer between complexes of the electron transport chain. Over-expression has been associated with chemoresistance in breast cancer, in part because of its ability to counter the oxidative stress caused by drugs like cisplatin.	Brand and Esteves, 2005 Pons et al., 2015
Collagen, Type I, Alpha 1	*COL1A1*	This gene encodes the alpha chain of collagen fibrils that are present within the extracellular matrix and act as ligands for specific integrins (such as integrin α2) and activate downstream signalling that includes promoting migration. It can be over-expressed in tumours and linked to the promotion of tumour development such as the transition to metastasis through altering ECM composition and outside-in signalling from integrins and discoidin receptors.	Plant et al., 2009 Vazquez-Villa et al., 2015 Moser et al., 1996
Cyclin D1	*CCND1*	Encodes a growth phase one (G1) cell cycle regulator that binds to and promotes the activity of cyclin dependent kinase 4 and 6 (CDK4/6) to trigger entry into the DNA synthesis 'S' phase of the cell cycle. This is achieved by the CCND1-CDK4/6 complex-mediated phosphorylation of retinoblastoma protein, which in turn liberates the transcription factor E2F to enable the transcription of S-phase genes. It is found over-expressed in breast cancer and has also been reported to participate in the expression of genes related to DNA damage repair, but this is independent from CDK activity.	Burhans and Heintz, 2009b Yu et al., 2001 Musgrove et al., 2011

associated with DNA damage, repair and replication (So et al., 2014), so it is feasible that CYGB over-expression may also elicit changes to these gene groups.

Little is known about how CYGB may be linked to these changes. CYGB could operate directly as a transcription factor, associate with other factors that alter gene expression, or affect cellular functions (e.g. levels of ROS, GSH etc.) that in turn elicit transcriptional changes. Rather than a direct interaction with transcription factors, CYGB may influence the activity of other factors that cause transcriptional changes. More recent studies report that p53 could be stabilised by CYGB (John et al., 2014). A detailed discussion of p53 function and regulation is beyond the scope of this thesis, but in summary it is a critical tumour suppressor gene that encodes a transcription factor that, upon activation by cellular stress, controls expression of a variety of genes involved in the signalling cascades of cell survival and apoptosis. The reader is directed towards two good reviews on p53 function and its ability to act as a protective protein and signal for cell death (Kruiswijk et al., 2015; Soussi and Wiman, 2015).

DNA strand breaks are known to trigger p53 activation in part through inducing ATM kinase-mediated phosphorylation of both p53 and its inhibitory protein mouse-double minute 2 (MDM2), which subsequently promotes p53 activity to signal DNA repair machinery to attempt repair of the damage (Meek, 2004) (see section 1.6.3.3.1). Oxidative DNA damage has been found significantly reduced in neuronal cells transiently transfected with GFP-labelled CYGB (Hodges et al., 2008) but this effect may be linked to non-physiological levels of the globin (McRonald et al., 2012). CYGB has shown an ability to impair p53 degradation (John et al., 2014). This interaction raised expression of p21 (a known p53 transcriptional target) and mediated activation of the

G1/S checkpoint upon doxorubicin treatment, increasing evidence in favour of a p53-promoting function for CYGB. Other research groups have also reported results that suggest p53 may be activated by CYGB (Latina et al, 2015).

It is known that cisplatin; a commonly used cancer chemotherapeutic agent, activates p53 signalling to promote cell cycle arrest and the DNA damage response (see section 1.6.3.3.1). Thus investigating the changes in transcriptional targets of p53 following cisplatin in CYGB+ clones generated by our study in chapter 3 may further explore the hypothesis that CYGB is able to regulate p53 activity and afford the cell an enhanced ability to respond to cisplatin. In chapter 3, the *p53* was found to be wildtype in the CYGB+ clones used in this study, so this indicates the cells would be capable of p53 signalling.

The discovery of CYGB-associated transcriptional changes has already permitted greater insight into its role in protection against oxidative, hypoxic and fibrotic stressors (see section 1.5). It is as yet unknown if CYGB over-expression affects other transcripts. Investigation into this would help further interpret the phenotypes that manifest following induced CYGB expression in cancer cells. We aimed to examine the transcriptomic changes that occurred in response to CYGB over-expression and then identify how a subset of these changes were altered following cisplatin treatment. In this chapter, results are presented for a whole human genome cDNA microarray study in the new CYGB+ OSC model. Because of microarray cost constraints, only four selected transcripts were assessed in CYGB+ clones following 48 h cisplatin treatment and these results are also presented.

The microarray data presented in this chapter identified numerous changes connected to CYGB over-expression in our OSC cancer cell model that could be grouped into gene ontological groups relating to stress responses, biological regulation and migration. From the array findings, several transcripts were selected that were representative of the biological categories and were validated in other CYGB+ and NCE control clones. An enhanced response of p53 target transcripts was found in CYGB+ controls following cisplatin treatment, suggesting that promotion of p53 activity is part of CYGB's stress response function.

4.2 Results

4.2.1 Microarray Design and Validation of CYGB Status

Prior to microarray analysis, RNA was first assessed using a Agilent 2100 Bioanalyser, which confirmed the samples to be of sufficient quality to generate cyanine-labelled cRNA for the hybridisation step (Figure 25). 28S/18S rRNA ratios were all above 2 (see appendix 5) indicating the nucleic acid was of good quality and all approached the theoretical ratio for human 28S/18S rRNA of 2.7 (5034 bp / 1870 bp) (Schroeder et al., 2006). The RNA Integrity Number (RIN) is a classification system developed by Agilent to categorise how degraded or intact RNA samples are on a scale between 1 and 10; higher numbers indicating more intact RNA (Schroeder et al., 2006). It is suggested for microarray experiments RINs above 9 are preferred and above 5.2 are recommended; the samples obtained for the current study all provided RINs of 10 demonstrating that the RNA was of the highest quality possible and suitable for hybridisation (Diaz and Barisone, 2011).

Expression levels of the *CYGB* transcript in each clone line were confirmed by RTqPCR within each RNA sample prior to microarray hybridisation. As expected, *CYGB* expression was detected in LST421 (CYGB+) samples while lack of expression was confirmed in LST223 (NCE) samples (Figure 26). The *CYGB* transcript was significantly induced within the CYGB+ clone by approximately 16 fold, relative to the NCE clone (t-test (unequal variance), $p = < 0.001$). Together, these results confirmed the suitability and authenticity of CYGB+ and NCE RNA samples for the subsequent microarray experiment.

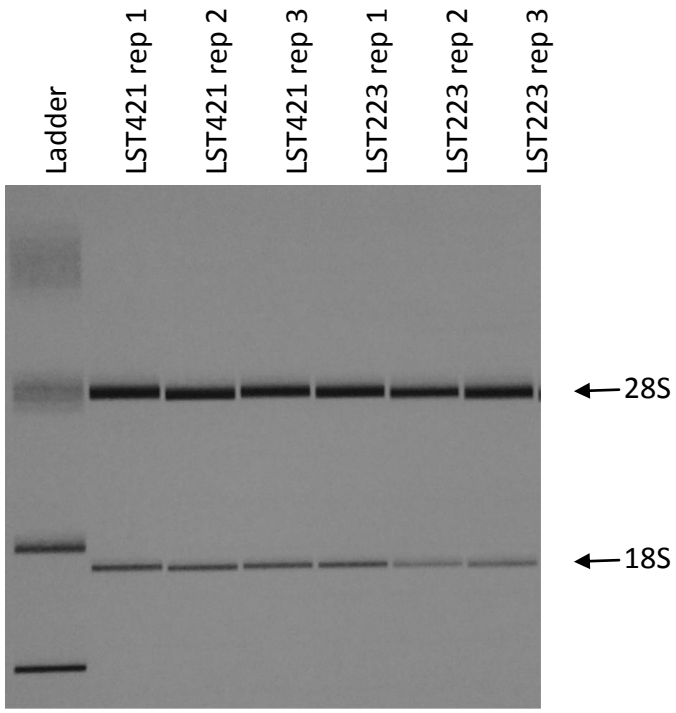

Figure 25 – Agarose Gel Image of RNA samples used for microarray experiment.
LST421 (CYGB+) and LST223 (NCE) clones were each cultured in 10 cm dishes to attain 70 % confluence the following day, before RNA was isolated. Samples were quantified and checked for integrity using an Agilent Bioanalyser. The 28S and 18S rRNA bands are shown for each sample. Sample electropherograms, RNA Integrity Numbers (RINs), along with concentrations are provided in appendix 5. RNA Samples from each clone were extracted from three independent cultures.

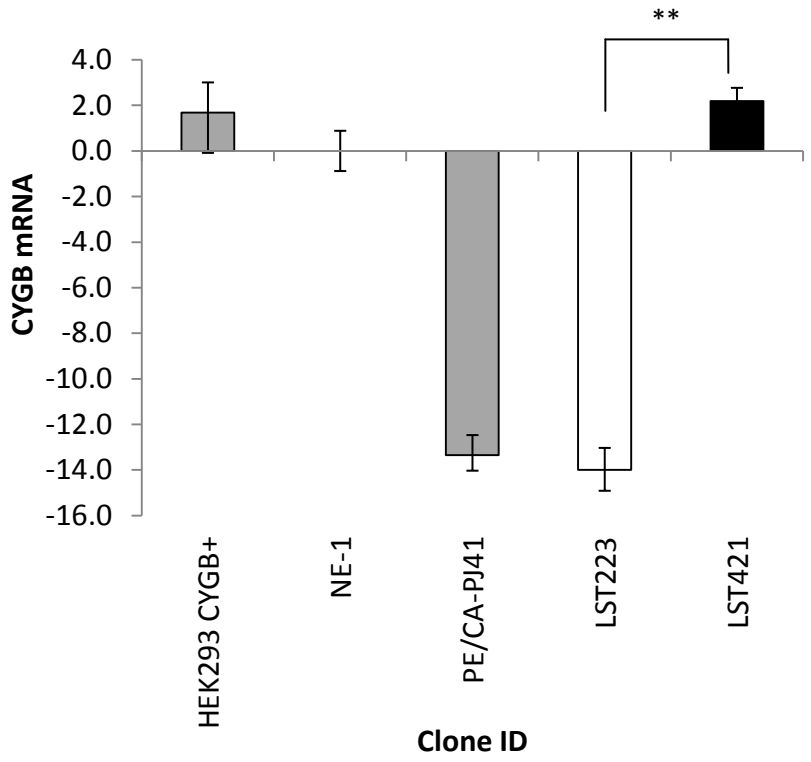

Figure 26 – Confirmation of CYGB expression in CYGB+ and NCE cell lines by RTqPCR.

LST421 (CYGB+) and LST223 (NCE) clones were each cultured in 10 cm dishes to attain 70 % confluence the following day, before RNA was isolated. Expression of *CYGB* mRNA was measured by SYBR Green qRT-PCR on RNA isolates. NE-1 and HEK293 CYGB+ RNA isolates were included as physiological and positive controls, respectively. Data was normalised to β-actin expression using the Pfaffl ddCt method from Ct values averaged across three biological replicates. Average mRNA fold change ± standard error. CYGB+ clones exhibited 16 fold greater expression of *CYGB* relative to the NCE clone controls. Compared to NCE control, t-test (unequal variance), ** $p = < 0.01$.

4.2.2 Transcriptome Changes in CYGB Positive OSC Cells

Differences in expression were considered statistically significant between CYGB+ and NCE clone samples if they were 2 fold or greater (i.e. they showed either a ≥ 2 fold increase or ≤ 0.5 fold decrease). Biological triplicates of each clone were analysed. To identify the GO annotations for the array results, the PANTHER (v10.0; **P**rotein **AN**alysis **TH**rough **E**volutionary **R**elationships) Gene List Analysis Tool was used (see section 2.6). A full summary of the biological processes the altered transcripts grouped into is shown in appendix 7 and 8, whilst a chart showing the distribution of genes altered in each process is provided in Figure 27. Table 7 lists example transcripts for each of the biological processes, with those investigated further and used to validate the microarray that were representative of each of these groups are italicised. All microarray data, along with PANTHER Gene Lists are also provided in on the supplementary CD-ROM.

Gene ontological analysis with PANTHER showed that up-regulated transcripts in CYGB+ clones included major changes in groups for cell processing (GO:0009987), metabolic process (GO:0008152) and response to stimulus (GO:0050896). For the down-regulated targets, groups altered included genes involved in adhesion (GO:0022610), biological regulation (GO:0065007), cell processing (GO:0009987), localisation (GO:0051179) and response to stimulus (GO:0050896) (Figure 27, Table 5 and Table 6). Selection of genes for microarray validation was made on the criteria of them being representative of particular gene groups identified by the PANTHER Gene List Analysis Tool and/or had been previously reported to be linked to CYGB in the literature. These included genes related to cellular adhesion and locomotion (*ITGA2*), stress-induced apoptosis (*BNIP3L*, *MAP3K5*, *GADD45A* and *NQO1*) and metabolic

processes (*COX7C, ARHGAP18* and *CDKN2A*). The majority of genes represented on the microarray did not show significant change - a total of only 529 transcripts (0.88 % of the transcript probes on the array) were affected by CYGB over-expression relative to the NCE control sample. In total, 328 genes were significantly down-regulated and 201 genes were up-regulated. A comprehensive list of the fold changes and other information for each transcript is provided in Appendix 7 and 8, whilst the gene ontological categories regulated (with associated genes shown) is provided in Table 7.

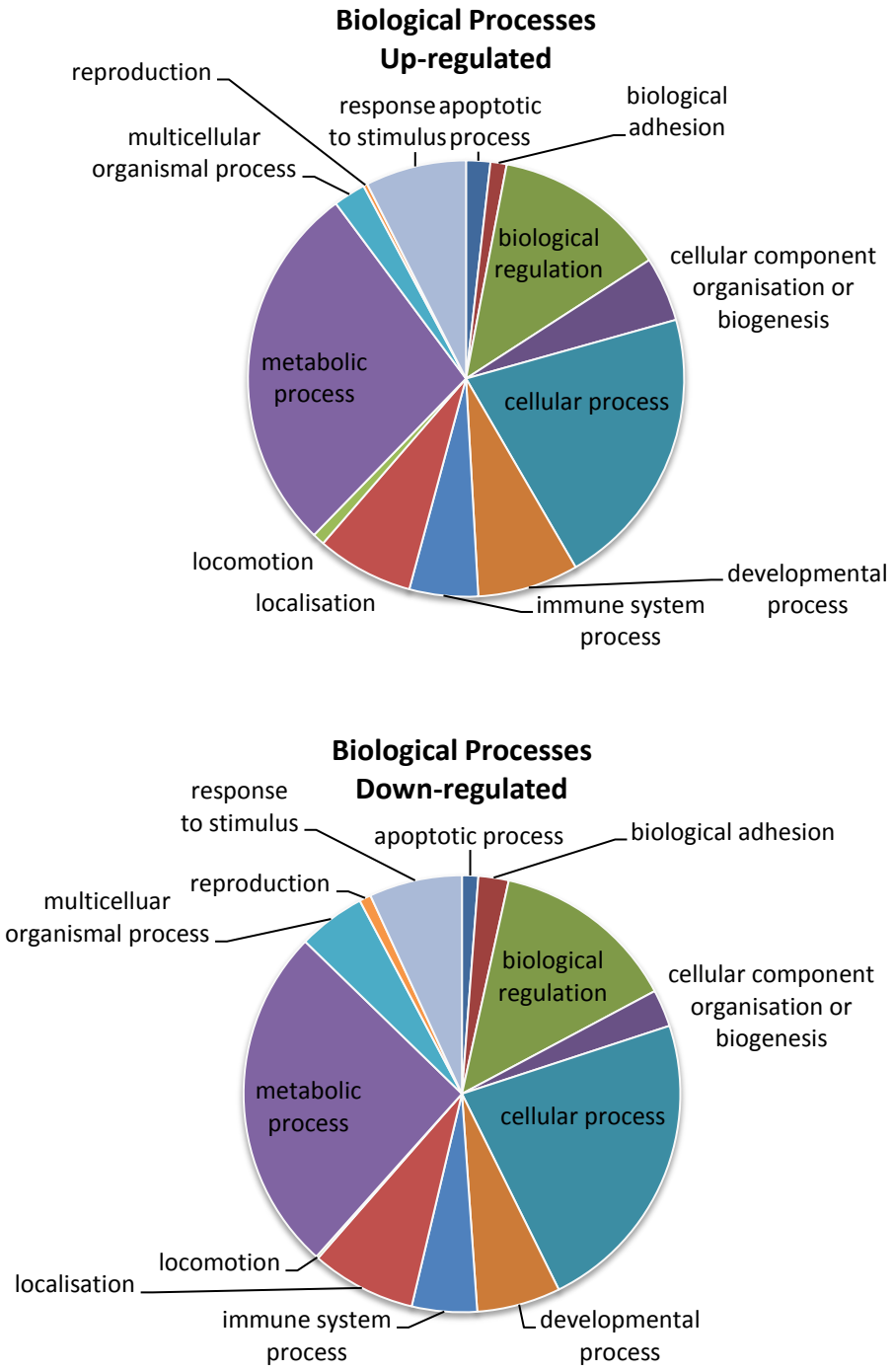

Figure 27 – Charts showing the distribution of transcript changes to occur grouped by biological process.

Genes that were changed by 2 fold or more in LST421 (CYGB+) relative to LST223 (NCE) clones were uploaded to the PANTHER Gene Analysis Tool that enabled classification of the gene transcripts into ontological groups, summarised as percentages of the total number of changed transcripts. A full gene list within each category for down-regulated and up-regulated transcripts is provided in tables 5 and 6, respectively.

Table 5 – Summary of transcripts that were significantly down-regulated within LST421 (CYGB+) clones.

Genes that were changed by 2 fold or more in LST421 (CYGB+) relative to LST223 (NCE) clones were uploaded to the PANTHER Gene Analysis Tool that enabled classification of the gene transcripts into ontological groups.

GO Code	*Description*	*Genes ID Down-regulated*				
0006915	Apoptotic process	BNIP3L CD40	CRYZL1 DSCAM	STAT2 TNFSF14	TRAF6	
0022610	Biological adhesion	ADAMTS1 AGAP3 ARVCF	CFH DSCAM FLT3	HAS3 ITGA2 ITGB6	ITGB8 JAG1 NRP1	PAPLN TSPAN1
0065007	Biological regulation	ADAMTS1 ADPRH AGAP3 ANGEL1 ARHGAP18 ARHGAP27 ARHGEF40 ATP11C BDKRB1 BNIP3L BRWD1 CAV3 CBFA2T2 CD40 CHD8 CSTB	DCAF5 DCBLD2 E2F8 EREG FLRT3 FNBP1 FOXB1 FOXL1 FZD4 FZD7 GABPA GRHL1 GZF1 HES2 HIF1A HKR1	HMGA2 HOMEZ HOXA9 IFNAR2 IFNGR2 IRS1 ITSN1 KCNJ15 LHX6 NKX3-1 NPAS2 NRP1 NUCB2 OXTR PAPLN PDK1	PKIB PLAGL2 PLCB2 PPARG PRMT5 PTK6 RAVER1 RIN2 RPRD1B RUNX1 SLC4A11 SOX7 SSH2 STAT2 SUPT16H SYTL1	SYTL4 TCF7L1 TEP1 TIMP3 TNFRSR14 UNCX WFDC2 ZNF138 ZNF217 ZNF219 ZNF329 ZNF512B ZNF573 ZNF626 ZSCAN2
0071840	Cellular component organisation or biogenesis	ADPRH ATP11C BNIP3L BRWD1	CHD8 FANCC HAS3	HSPA13 HSPA2 NGDN	PRMT5 SNX5 SSH2	SYT16 SYTL1 SYTL4
0009987	Cellular process (continued overleaf)	ADAMTS1 ADPRH AGAP3 ANKRD1 APEX1 ARHGAP27 ARHGEF40 ARVCF ASPH ATP11C AVP B3GNT3 BCAR3	BDKRB1 BNIP3L BRWD1 BTG3 CALML4 CAP2 CAV3 CBFA2T2 CD163L1 CD40 CD82 CDH3	CEP250 CFH CHD8 CNTRL CPVL CXADR DCAF5 DCBLD2 DEPDC7 DIAPH2 DPY19L4 DSCAM	DSCR3 E2F8 EMP1 EPS8L2 EREG ESCO2 FAM179B FANCC FGF7 FLRT3 FMNL3 FNBP1	FOXB1 FOXL1 FZD4 FZD7 GABPA GADD45A GINS1 GNB4 GPR68 GPR88 GRHL1 HAS3

Table 5 (continued).

GO Code	*Description*	*Genes ID Down-regulated*				
0009987	Cellular process (continued)	HMGA2	LGR4	OXTR	PTK6	TCF7L1
		HOMEZ	LMCD1	PAPLN	RUNX1	TIMP3
		IFNAR2	LRIG3	PARD6B	S100A4	TNFRSF14
		IFNGR2	LRRCC1	PDK1	SEMA3A	TNS4
		IL12RB2	MAP1B	PEX3	SEMA6C	TRAF6
		IL1RAP	MAP3K5	PKIB	SGK494	TRAPPC10
		IRS1	MAP3K5	PLAGL2	SLC4A11	TSPAN1
		ITCH	MCM8	PLCB2	SNX21	TSPAN4
		ITGB6	MLH3	PLEKHF2	SNX5	UGT1A6
		ITGB8	MYLK2	POLE2	SRD5A1	VAPB
		ITSN1	NEK11	PPARG	SSH2	WEE1
		JAG1	NEK9	PRKCE	STAT2	WRB
		KCNJ15	NGDN	PRMT5	SUPT16H	ZNF573
		KIF16B	NRP1	PROCR	SYTL1	
		LGALS8	OSGEP	PTGER4	SYTL4	
0032502	Developmental process	ADAMTS1	CD40	GABPA	MYL9	RUNX1
		ADPRH	CDH3	HES2	NFE2L3	SEMA6C
		ANKRD1	CRYZL1	HIF1A	NKX3-1	SGK494
		B3GNT3	DSCAM	HOXA9	NRP1	SSH2
		BACH1	EMP1	IL12RB2	PBX4	STAT2
		BNIP3L	FGF7	JAG1	PTK6	TNFRSF14
		BRWD1	FLRT3	LMCD1	RBMS2	TRAF6
0002376	Immune system process	ACSS2	DSCAM	IL12RB2	RUNX1	TNFRSF14
		ALOX12	GBP1	JAG1	S100A4	TRAF6
		ARHGEF40	GPR88	NRP1	SEMA3A	TSPAN1
		BNIP3L	GPX2	PPARG	SEMA6C	WEE1
		CD40	HSPA13	PROCR	SH2D2A	
		CFH	HSPA2	PTK6	STAT2	
0051179	Localisation	ADPRH	CMTM8	NRP1	SBF2	SLC7A2
		ALG10B	CPNE1	PARD6B	SLC13A3	SLC7A8
		AP1G2	DCBLD2	PEX3	SLC19A1	SNX5
		AP4S1	DSCR3	PIGU	SLC35A3	SYTL1
		ATP11C	FNBP1	PLEKHF2	SLC37A1	SYTL4
		BNIP3L	ITSN1	PROM2	SLC37A2	TEP1
		CAV3	KCNJ15	PTGER4	SLC39A8	TRAPPC10
		CD163L1	KIF16B	PTK6	SLC4A11	TRPM4
		CFH	MYLK2	RIN2	SLC5A3	VAPB
0008152	Metabolic process	ARHGEF40	CBR3	FER1L4	LRIG3	SEMA3A
		AVP	CDH3	GPR88	MYL9	SSH2
		B3GNT3	DHRS4	HES2	MYLK2	SYTL1
		BACH1	DHRS4L1	HOXA9	NRP1	SYTL4
		BDKRB1	DHRS4L2	ITSN1	OXTR	TSPAN1
		CBR1	DSCAM	LGR4	RUNX1	

Table 5 (continued).

GO Code	*Description*	*Genes ID Down-regulated*				
0032501	Multicellular organismal process	ARHGEF40 AVP B3GNT3 BACH1 BDKRB1 CBR1 CBR3 CDH3	DHRS4 DHRS4L1 DHRS4L2 DSCAM FER1L4 GPR88 HES2 HOXA9	ITSN1 LGR4 LRIG3 MYL9 MYLK2 NRP1 OXTR	RUNX1 SEMA3A SSH2 SYTL1 SYTL4 TSPAN1	
0050896	Response to stimulus	APEX1 ARHGEF40 BNIP3L CD40 CD82 CFH DCBLD2 EREG FZD4	FZD7 GBP1 GPR88 GPX2 HMGA2 HSPA13 HSPA2 IFNAR2 IFNGR2	IL12RB2 IRS1 ITGB6 ITGB8 LHX6 MLH3 NFE2L3 NRP1 OXTR	POLE2 PPARG PROCR PTK6 SH2D2A STAT2 TCF7L1 TIMP3 TNFRSF14	TSPAN1 TSPAN4 UGT1A6 WEE1

Table 6 – Summary of transcripts that were significantly up-regulated within LST421 (CYGB+) clones.

Genes that were changed by 2 fold or more in LST421 (CYGB+) relative to LST223 (NCE) clones were uploaded to the PANTHER Gene Analysis Tool that enabled classification of the gene transcripts into ontological groups.

GO code	*Description*	*Genes ID Up-regulated*				
0006915	Apoptotic process	GADD45G GDF11	GDF15 IL6	LIF TGFB1		
0022610	Biological adhesion	ANGPTL4	CFB	CTNNA1	FER	
0065007	Biological regulation	APBB3 CAST CDC42EP1 CHD1 CXCL1 FER	GDF15 GNAZ IL6 JUNB LIF MAF1	MAP4K4 MLXIP MYO10 PITX1 SEL1L3 SERPINA3	SGSM3 SMAD7 SQSTM1 SYTL3 TBC1D1 TGFB1	UIMC1 YAF2 ZFPM1 ZMYND15 ZNF13
0071840	Cellular component organisation or biogenesis	ATG12 CDC42EP1 CHD1	CTNNA1 FLNC HSPA6	IQSEC2 KRT80 MAF1	MYO10 SGSM3 SYNPO	SYTL3 TBC1D1 TUBA3C UIMC1
0009987	Cellular process	ADRBK2 ADSSL1 ANGPTL4 AOX1 APBB3 ATG12 BAIAP2L2 BCR BSG CARD11 CDC23 CDC42EP1 CDC42SE2 CDK11B	CDKN2A CFB CHD1 CLEC11A CSF2 CTNNA1 CXCL1 CXCL2 DPM3 ELL2 FER FLNC FOXP4 GADD45G	GAS6 GDF11 GDF15 GNAZ GRB14 GRK6 HTRA1 IL6 IMPA2 IQSEC2 JUNB KRT80 LCN2 LIF	LRSAM1 MAF1 MAP4K4 MFSD3 MLXIP MSH3 MYO10 NEURL1B PRICKLE1 PTPRM RALBP1 RARG S100A9 S1PR3	SGSM3 SLC36A1 SMAD7 SPIRE1 SPRY4 SQSTM1 STK10 SYNPO SYTL3 TBC1D1 TGFB1 TUBA3C UIMC1 ZFPM1
0032502	Developmental process	CDC42EP1 CLEC11A CTNNA1 FER FLNC	GADD45G GDF11 KRT80 LIF LMO4	MAML1 MYO10 PRICKLE SPRY4 SYNPO	TBC1D1 TGFB1	
0002376	Immune system process	ABCC3 CFB CSF2 CXCL1	CXCL2 FER GADD45G HSPA6	IL6 KLK5 LIF LRSAM1	PXDNL S100A9 SMAD7 TXNRD1	ZFPM1

Table 6 (continued).

GO Code	*Description*	*Genes ID Up-regulated*				
0051179	Localisation	ABCC3 AKR1C3 AP3B1 CFB CXCL1	CXCL2 FER ISCA1 KLK5 LCN2	MFSD3 MYO10 RAMP1 REEP2 REEP5	SEC31B SGSM3 SLC35E2B SLC36A1 SLMO1	SPIRE1 SYTL3 TBC1D1 TUBA3C
0040011	Locomotion	CXCL1	CXCL2	FER	MMP1	
0008152	Metabolic process	ABCC3 ACRC ADRBK2 ADSSL1 AOX1 APBB3 ARSI ATG12 BCR CAST CDC42EP1 CDK11B CES1 CFB CHD1 CHPF2 CLU COX7C CYB5R4	CYB5RL CYP27B1 CYP4F11 CYP4F12 DHFR DHRS11 DPM3 ELL2 FER FOXP4 GALNT14 GDA GDF11 GDF15 GNAZ GRK6 HES5 HMOX1 HSPA6	HTRA1 HYI IDS IMPA2 IP6K1 ISCA1 JUNB KLK5 LCN2 LMO4 LNPEP MAF1 MAP4K4 MLXIP MSH3 MYO10 NADK NQO1 PHGDH	PTPRM PXDNL RALBP1 RARG REEP2 REEP5 RPL28 S100A9 SCLY SEL1L3 SERPINA3 SGSM3 SLC35E2B SLC3A2 SMAD7 SPIRE1 SQSTM1 STK10 TAF8	TBC1D1 TGFB1 THOC3 TRIM37 TRMU TXNRD1 UIMC1 UPP1 YAF2 ZFPM1 ZMAT2 ZMYND15 ZNF513
0032501	Multicellular organismal process	GRK6 HES5	LIF MYO10	PRICKLE1 SYTL3	TAGLN3 ZFPM1	
0050896	Response to stimulus	ABCC3 ATG12 BCR CDC42EP1 CDC42SE2	CFB CSF2 CXCL1 CXCL2 FER	GADD45G GDF11 GDF15 GNAZ HSPA6	KLK5 LIF LMO4 MAP4K4 MSH3	SMAD7 SQSTM1 STK10 TGFB1 UIMC1

Table 7 – Fold changes of significantly changed transcripts in CYGB+ cells.
Only transcripts with ≥ 2-fold change (i.e. 0.5 = 2 fold down-regulated and 2.0 = 2 fold up-regulated) were considered significant. For ease of interpretation, an arrow next to the gene symbol is provided to indicate significant up (▲) or down (▼) regulations in CYGB positive cells relative to NCE control. Transcripts used for array validation are in bold and italicised.

Gene name	*Gene symbol*	*Accession number*	*Fold change (u = up; d = down)*	*P value*
		Biological Adhesion and Locomotion		
Matrix metalloprotease 1, interstitial collagenase	MMP1 ▲	NM_002421	u 4.70	1.44 E-07
Integrin alpha 2 subunit	***ITGA2* ▼**	***NM_002203***	**d *2.17***	***4.83 E-03***
Angiopoietin-like 4	ANGPTL4 ▲	NM_139314	u 2.26	7.84 E-03
Integrin beta 6	ITGB6 ▼	NM_000888	d 2.01	5.81 E-04
Integrin beta 8	ITGB8 ▼	NM_002214	d 2.70	7.76 E-05
Matrix metalloprotease 14	MMP14 ▼	NM_004995	d 2.52	3.26 E-08
Tissue inhibitor metalloprotease 3	TIMP3 ▼	NM_000362	d 2.27	1.87 E-05
		Response to Stress		
Mitogen-activated protein kinase kinase kinase 5	***MAP3K5* ▼**	***NM_005923***	**d *2.87***	***6.38 E-06***
BCL2/adenovirus E1B 19kDa interacting protein 3-like	***BNIP3L***	***NM_004331***	**d *1.91***	***1.72 E-03***
Glutathione peroxidase 2 (gastrointestinal)	GPX2 ▼	NM_002083	**d** 2.43	8.79 E-06
Growth arrest and DNA-damage inducible alpha	***GADD45A***	***NM_001924***	***d 1.93***	***9.86 E-05***
NAD(P)H dehydrogenase quinone 1	***NQO1* ▲**	***NM_000903***	***U 2.28***	***8.53 E-07***
BTB and CNC homology 1, basic leucine zipper transcription factor 1	BACH1 ▼	NM_206866	d 2.22	6.69 E-04
CD40 TNF receptor superfamily member 5	CD40 ▼	NM_001250	d 2.40	6.30 E-06
Peroxisome proliferator-activated receptor gamma variant 3	PPARG ▼	NM_138711	d 2.79	9.28 E-06
Heat shock 70kDa protein 2	HSPA2 ▼	NM_021979	d 2.33	9.44 E-05

Table 7 (continued).

Gene name	*Gene symbol*	*Accession number*	*Fold change (u = up; d = down)*	*P value*
		Metabolic Process		
Cytochrome c oxidase subunit VIIc	***COX7C ▲***	***NM_001867***	***u 2.36***	***2.44 E-04***
Cyclin-dependent kinase inhibitor 2A	***CDKN2A ▲***	***NM_058197***	***u 2.17***	***6.17 E-04***
Rho GTPase activating protein 18	***ARHGAP18 ▼***	***NM_033515***	***d 2.14***	***6.69 E-04***
Tumour growth factor beta 1	TGFB1 ▲	NM_000660	u 2.20	3.49 E-03
Autophagy related 12 homolog (S. cerevisiase)	ATG12 ▲	NM_004707	u 2.38	2.67 E-04
HtrA serine peptidase 1	HTRA1 ▲	NM_002775	u 6.75	4.05 E-10
Myosin 10	MYO10 ▲	NM_012334	u 3.21	0.126
SMAD family member 7	SMAD7 ▲	NM_005904	u 2.18	3.01 E-04
CDC42 effector protein Rho GTPase binding 1	CDC42EP1 ▲	NM_152243	u 2.10	4.56 E-07
Jun B protooncogene	JUNB ▲	NM_002229	u 2.01	6.77 E-04
Heme oxygenase (decycling) 1	HMOX1 ▲	NM_002133	u 2.60	1.36 E-05
Retinoic acid receptor gamma	RARG ▲	NM_000966	u 2.06	3.35 E-03
Cytochrome P450 family 27 subfamily B polypeptide 1	CYP27B1 ▲	NM_000785	u 2.39	2.43 E-03
Cytochrome P450 family 4 subfamily F polypeptide 11	CYP4F11 ▲	NM_021187	u 3.46	3.44 E-05

4.2.3 Validation of Transcriptome Changes

RTqPCR was used to assess whether selected targets were altered in a similar manner to those found by the array and across a panel of independent CYGB+ clones. Transcripts found to be similarly regulated would then be more likely to be related to up-regulation of CYGB expression and not a clone-specific effect.

All gene targets analysed by RTqPCR in the LST421 (CYGB+) clone followed the same trend as the microarray data (Figure 28), demonstrating array integrity. Furthermore, agreement between the microarray data and gene expression in other CYGB+ clones was found. *NQO1* mRNA was found up-regulated in CYGB+ clones with medium and high over-expression of the globin (LST54 and LST421, and Figure 28e). *ITGA2, MAP3K5, ARHGAP18* and *CDKN2A* transcripts were demonstrated to be down-regulated in the same CYGB+ clones (Figure 28). *NQO1* up-regulation correlated with levels of CYGB expression in the different clones and with 2.31 fold (± 0.29) in LST421 and 1.32 fold (± 0.05) in LST54, relative to the NCE control and both of these were statistically significant changes, as determined by Kruskal-Wallis, post-hoc Mann Whitney U testing (both $p = 0.05$, Figure 28e). *ITGA2* mRNA identified to be 1.33 fold (± 0.14) down-regulated in LST421 clones was found similarly repressed in LST54 clones (1.33 fold ± 0.15) relative to NCE controls (Figure 28b), although no statistical significance was found within this dataset (one-way ANOVA, $p = 0.455$). *MAP3K5* was reduced by 1.54 fold (± 0.06) in LST421 clones, whilst the target was repressed less so in LST54 clones (1.05 fold ± 0.19) (Figure 28c) compared with NCE controls, but these changes were not statistically significant (one-way ANOVA, $p = 0.463$). *ARHGAP18* was also found to be down-regulated by approximately the same extent in LST421, LST54 and LST32 CYGB+ clones (1.22 fold ± 0.13, 1.25 fold ± 0.10 and 1.14 fold ± 0.10, respectively, Figure 28d)

compared to NCE controls, but this was not statistically significant (one-way ANOVA, p = 0.833). *BNIP3L* mRNA expression exhibited a titrated repression in CYGB+ clones, with the lowest CYGB over-expressing clone showing the strongest repression (2.70 fold ± 0.12), and collectively CYGB+ clones showed a down-regulation of *BNIP3L* compared to NCE controls (Figure 28g) and no statistical significance was found in this dataset (one-way ANOVA, p = 0.081). *CDKN2A* was reduced by 1.75 fold (± 0.07) in LST54 clones, whilst the target was repressed more so in LST32 clones (by 2.27 fold ± 0.38) and was up-regulated strongly by 5.86 fold (± 1.98) in LST421 compared with NCE controls (Figure 28a), but none showed statistical significance by t-test (unequal variances) (LST421, p= 0.238; LST54, p = 0.340; LST32, p = 0.276). *COX7C* and *GADD45A* genes did not show regulation with CYGB expression, with low and medium CYGB over-expressing clones showing approximately equal levels to that of the NCE controls (Figure 28f and h). The increases in *COX7C* and *GADD45A* expression in LST421 clones relative to the NCE controls were not statistically significant (one-way ANOVA, p = 0.068 and t-test (unequal variances), p = 0.238, respectively).

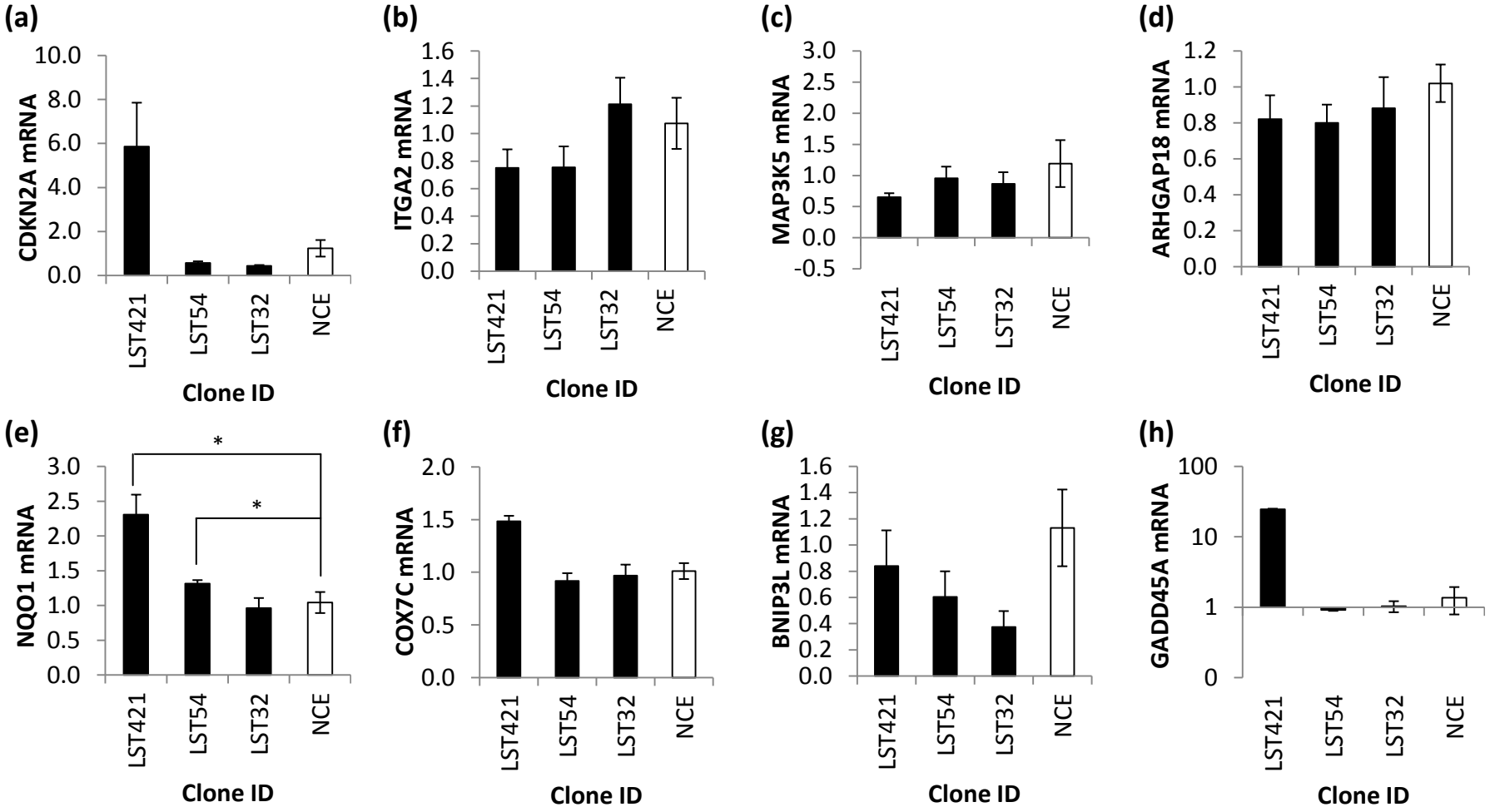

Figure 28 – Transcript changes that occur within LST421 (CYGB+) clones also occur within other CYGB+ clone derivatives of PE/CA-PJ41. Expression of **(a)** *CDKN2A* **(b)** *ITGA2* **(c)** *MAP3K5* **(d)** *ARHGAP18* **(e)** *NQO1* **(f)** *COX7C* **(g)** *BNIP3L* and **(h)** *GADD45A* were all quantified by RTqPCR using RNA that was isolated from other PE/CA-PJ41 CYGB+ clones and compared to expression within the NCE controls. Data was normalised to the average of *TBP* and *B2M* expression using the Pfaffl ddCt method from Ct values averaged across three biological replicates. Fold change in mRNA expression ± standard error is shown for each target. Compared with NCE controls, Kruskal-Wallis, post-hoc Mann Whitney U, * p = 0.05.

4.2.4 Transcriptional Changes Following Cisplatin Treatment

Some of the transcripts identified from the microarray study in CYGB+ clones are known to be stress response targets, including *CDKN2A*, *GADD45A*, *NQO1* and *MAP3K5*. To investigate the role of these differentially expressed transcripts under conditions of cellular stress, cells were treated with 7.5 μM 48 h cisplatin (this concentration and time was chosen from concentration-response studies in section 5.2.3 that showed this was approximately the IC_{40}) and the levels quantified before and after treatment by RTqPCR.

CDKN2A was greatly up-regulated in all three CYGB+ clones following 48 h of 7.5 μM cisplatin treatment, with a trend towards increased expression at lower CYGB over-expression (LST421 (17.38 fold ± 3.90), LST54 (20.99 fold ± 2.71) and LST32 (32.32 fold ± 17.73) compared to the NCE control (3.55 fold ± 1.90) (Figure 29). The difference between LST421 or LST32 clones and NCE controls for *CDKN2A* expression was not significant in either case (t-test (unequal variances), p = 0.102 and p = 0.347, respectively), but the LST54 fold change was significant (t-test (unequal variances), p = 0.025). *GADD45A* conversely exhibited a decline in expression with increasing CYGB over-expression (Figure 29), and CYGB over-expressing clones showed lower expression than NCE control, exhibiting 2.04 fold ± 0.01 (LST421), 1.11 fold ± 0.06 (LST54), and 0.51 fold ± 0.53 (LST32) expression, respectively. The difference between LST421 and NCE was significant (t-test (unequal variances), p = 0.044). *NQO1* showed a positive correlation between *NQO1* expression and increasing CYGB over-expression following 7.5 μM cisplatin treatment (LST421 (220.53 fold ± 42.24), LST54 (23.73 fold ± 6.60) and LST32 (23.44 fold ± 12.61) relative to the NCE controls (16.05 fold ± 5.81) (Figure 29). The difference between LST421, LST54 or LST32 and NCE controls was not statistically significant (t-test (unequal variances), p = 0.119, p = 0.571 and p= 0.733, respectively).

Additionally, *MAP3K5* transcripts were induced in all three CYGB+ clones (LST421 (3.71 fold ± 1.81), LST54 (2.86 fold ± 0.95) and LST32 (14.65 fold ± 4.24) above the expression exhibited by the NCE clones (1.03 fold ± 0.19) and the increase was statistically significant in LST421 and LST54 clones (Kruskal-Wallis test with Mann-Whitney U post-hoc test, $p = 0.05$ for both) (Figure 29).

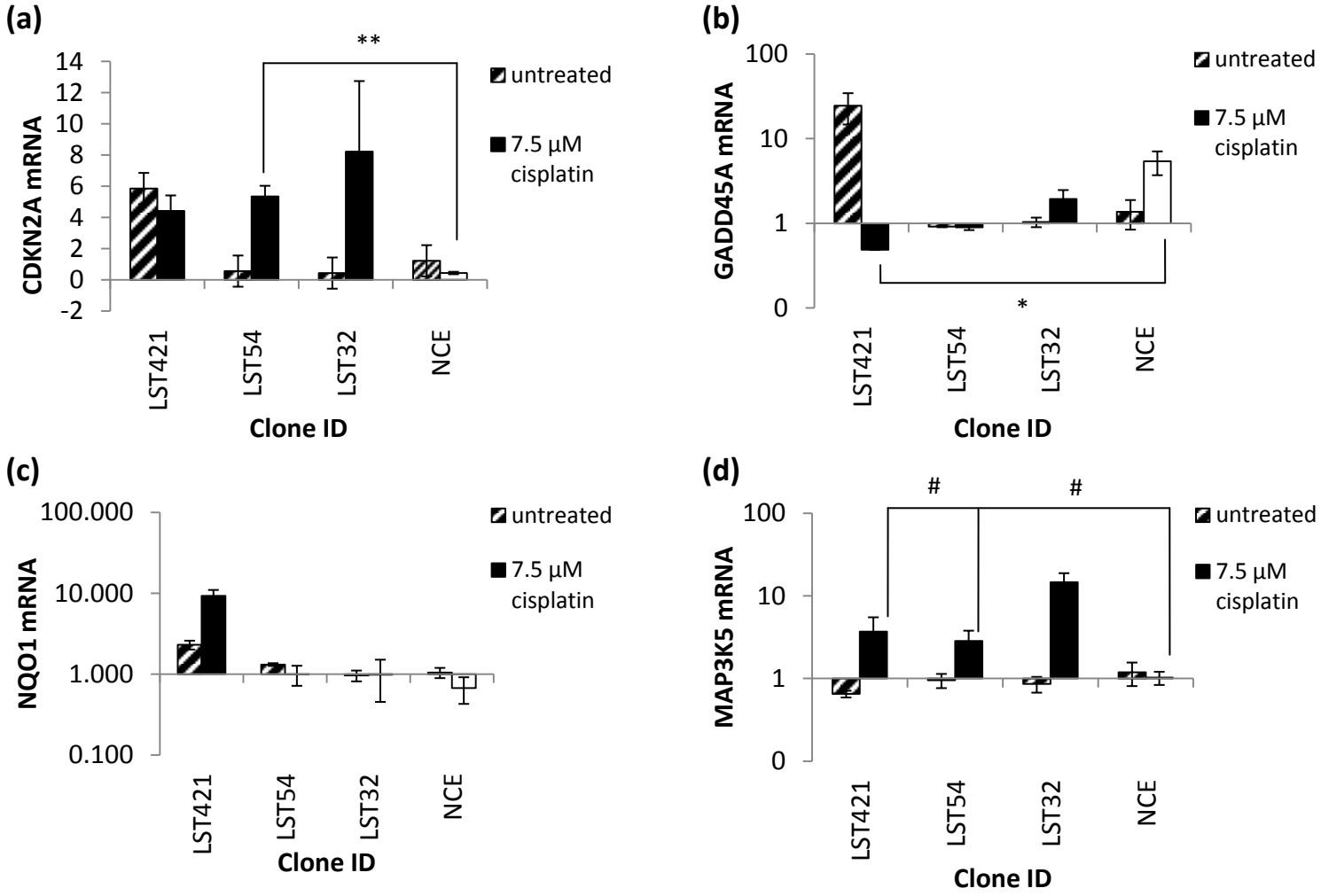

Figure 29 – Selected transcript changes in CYGB+ clones in response to 48 h 7.5 µM cisplatin treatment.

Expression of **(a)** *CDKN2A* **(b)** *GADD45A* **(c)** *NQO1* and **(d)** *MAP3K5* were all measured by qRTPCR on RNA that was isolated from other PE/CA-PJ41 CYGB+ clones after 48 h treatment to 7.5 µM cisplatin and compared to expression within the respective NCE control. NCE control expression after cisplatin treatment is shown relative to NCE untreated control. Data was normalised to the average of *TBP* and *B2M* expression using the Pfaffl ddCt method from Ct values averaged across three biological replicates. Fold change in mRNA expression ± standard error is shown for each target. Compared with respective NCE controls, t-test (unequal variances), * p = < 0.05 and ** p = < 0.01, Kruskal-Wallis with Mann Whitney U test, # p = < 0.05.

4.3 Discussion

In this chapter, we hypothesised that CYGB over-expression may be able to alter stress response transcripts within the transcriptome since it has previously been linked to stress-response phenotypes (see section 1.5). We present evidence for CYGB over-expression significantly influencing the transcription of genes within several ontological categories and to our knowledge this is the first study to identify these transcript groups differentially regulated in CYGB over-expressing OSC cancer cells. We show in this chapter a new set of transcriptional changes associated with CYGB over-expression that relate to migration and cell survival following stress. We also identified p53 targets; *NQO1*, *MAP3K5*, *GADD45A* and *CDKN2A*, to respond more greatly to cisplatin treatment in CYGB over-expressing clones, suggesting CYGB may elicit its protective function against cisplatin cytotoxicity (see chapter 5) in a p53-dependent manner.

It is important to validate the array results with RTqPCR because of the potential for clone specific effects on the transcriptome not directly related to CYGB expression. We used RTqPCR to validate the array with eight selected transcripts within three independent CYGB+ clones. All 8 transcripts in the RTqPCR study using samples from LST421 were found to match the changes in the array and were also consistent in all three CYGB+ clones for 5/8 of the transcripts validated. The 3 targets that did not show similar trends in expression across the three untreated CYGB+ clones did however show significant induction following treatment with cisplatin. Interestingly, significant regulation of these three stress-response (and p53-regulated) transcripts - *MAP3K5, CDKN2A* and *GADD45A* - was only evident in CYGB+ clones that over-expressed higher CYGB levels (LST421) before treatment.

It was only after cisplatin treatment that the expression of these transcripts could be observed in medium and low over-expressing CYGB+ clones. This could either be just a clone-specific effect or more likely indicate a threshold effect where significant regulation of these transcripts will occur in the context of high, but not low over-expression of CYGB, as has been previously observed for ROS depletion by CYGB after oxidant stress (McRonald et al., 2012). Regulation of stress-response transcripts within cisplatin-treated CYGB+ clones (that appears dependent on the expression level of CYGB) suggests higher levels of the globin could lead to a greater response in these stress transcripts and that cells with lower levels of CYGB over-expression require the cisplatin stress for the effect to manifest.

To date, there has been only one other study to examine gene expression following transgenic CYGB expression, which identified four down-regulated transcripts; *UCP2*, *PRPF40A, DNMT1* and *COL1A1*, in transiently transfected CYGB over-expressing NSCLC lines all related to the response to hypoxic stress (Shivapurkar et al., 2008). Although we did not find corroborating down-regulations for *UCP2, DNMT1* or *COL1A1* in our array study, we did find significantly reduced expression of the paralogous transcript to *PRPF40A*; *PRPF40B* (2.48 fold down-regulated, $p = 0.005$), in CYGB+ clones.

In this chapter, we identified 201 genes that were significantly up-regulated by CYGB over-expression and 328 genes that were down-regulated relative to NCE controls. For up-regulated transcripts in CYGB+ clones, major changes occurred in groups for cell processing (GO:0009987), metabolic process (GO:0008152) and response to stimulus (GO:0050896). For the down-regulated targets in CYGB clones, groups altered included genes involved in adhesion (GO:0022610), biological regulation (GO:0065007), cell

processing (GO:0009987), localisation (GO:0051179) and response to stimulus (GO:0050896). By examining the differentially altered genes in these ontological groups more closely, it became clear that there were genes being regulated in the CYGB+ clone relating to migration signalling (such as *MMP1, ITGA2, ARHGAP18, MMP14, TIMP3, CDC42EP1* and *CTNNA1*), cell survival following oxidative stress (such as *NQO1, MAP3K5, BNIP3L*, *GADD45A, PRDX5, GPX2, BACH1, UIMC1* and *ATG12*) and cell cycle regulation (such as *CDKN2A, CDK11B, GADD45G*, *SMAD7*, *E2F8* and *STK10*). Transcripts to validate the microarray findings were chosen from each ontological group to be representative of them - migration (*ITGA2* and *ARHGAP18*), oxidative stress survival (*NQO1*, *MAP3K5*, *GADD45A* and *BNIP3L*) and cell cycle regulation (*CDKN2A*) - and most of these changes could be confirmed in three independent untreated CYGB+ clones, confirming that they were directly related to CYGB and not just clone-specific artefacts. Overall, the ontological groups that were identified by the array as being significantly altered in CYGB+ over-expressing clones were consistent with phenotypic changes already reported in the literature.

CYGB over-expression has been previously linked to reduced motility and invasive properties in NSCLC and ovarian cancer cell lines, although the molecular basis of this effect is unknown (Chen et al., 2014; Oleksiewicz et al., 2013) (see section 1.6.3.2). In chapter 5, we present data showing medium and high expression CYGB+ clones show increased migration compared with NCE controls (see section 5.3.1), and this is consistent with regulation of transcripts related to motility signalling seen in the microarray data presented here and also by the down-regulation of cell migration-related *PRPF40* transcript observed by Shivapurkar et al (2008) (Table 4). There is evidence that CYGB may elicit motility changes by signalling through the cytoskeleton

regulator Rho GTPase (Nakatani et al., 2004), and further that the globin is a target of Cdc42 (Kabuyama et al., 2006). Interestingly, our microarray identified an effector protein of Cdc42; *CDC42EP1*, to be significantly up-regulated in CYGB over-expressing cells. We also saw significant down-regulation of *ARHGAP18*, a positive regulator of RhoA GTPase activity, in the panel of CYGB+ clones. It is also of note to mention RhoA GTPase can be activated directly through oxidation (Aghajanian et al., 2009). As we also found CYGB+ clones showed suppression of oxidative stress (see section 6.3.3) it may be possible CYGB activity may indirectly regulate RhoA signalling by interfering with control of its redox status (discussed further in section 7.1).

Rho GTPases co-ordinate cell movement in a complex signalling pathway by establishing polarity (through Cdc42 GTPase), membrane protrusion (through Rac1 GTPase) and actin cytoskeletal reorganisation (through RhoA GTPase) (Karlsson et al., 2009). Our array found CYGB+ clones down-regulated Rho-Type GTPase-Activating Protein 18 (*ARHGAP18*), which encodes a protein that suppresses stress fibre and focal adhesion formation at the leading edge of motile cells through inhibition of RhoA GTPase activity (Maeda et al., 2011) and *ARHGAP18* loss has been associated with a greater propensity for melanoma growth and vascularisation *in vivo* (Chang et al., 2014b). We also found *ITGA2* was significantly reduced in CYGB+ clones. The product of this gene forms part of an integrin receptor - α2β1 - that has an important role in initiating Rho signalling, whereby collagen 1 activation of the receptor signals for FAK-mediated Rho family GTPase activation to trigger directional migration (Rohani et al., 2014). This integrin has also been implicated in epithelial to mesenchymal transition that is required for tumour metastasis, as inhibition of this receptor reduces hepatocarcinoma cell invasion (Yang et al., 2003) and liver metastasis of melanoma cells (Yoshimura et al., 2009). Our

laboratory has recently demonstrated that HSC-T6 (rodent hepatic stellate) and LX2 (human hepatic stellate) cells cultured upon a collagen 1-coated substratum down-regulate *CYGB* and its protein in a time and collagen 1 concentration-dependent manner (Stone et al., 2015). Of particular note, integrin α2 (*ITGA2*) transcripts were elevated following attachment to collagen 1 (Stone et al., 2015). Interestingly, the results of this chapter found that highly over-expressing CYGB+ clones markedly repressed *ITGA2* expression relative to NCE controls, which is consistent with the relationship between these transcripts previously reported.

Our array revealed several biomarkers of the antioxidant response were appreciably altered in CYGB+ clones. These included down-regulation of *BACH1* (a negative regulator of Nrf2 and thus antioxidant gene transcription), *GPX2* (a glutathione-dependent enzyme involved in H_2O_2 detoxification), *MAP3K5* (a regulator of both JNK/p38 and *GADD45A* signalling, that promotes oxidative stress-induced apoptosis) (Ray et al., 2012b). The antioxidant response signalling pathway and its importance in maintaining cellular redox homeostasis is described in section 1.5.3.1. Induction of antioxidant gene transcription in CYGB+ clones suggests that CYGB-expressing cells will have reduced levels of oxidative stress and this was confirmed by the reduction in total cellular ROS and mitochondrial superoxide and higher reduced glutathione levels in CYGB+ clones (see section 6.3.3). NAD(P)H dehydrogenase (*NQO1*) transcripts encode a NADH-dependent reductase found within the mitochondrial electron transport pathway that limits oxidative stress by reducing quinones and their reactive derivatives, thereby preventing these molecules from generating ROS by reacting with diatomic oxygen (Vasiliou et al., 2006). As a result, NQO1 has potential to reduce the toxicity of pro-oxidant anti-cancer drugs and this has been demonstrated for doxorubicin in hepatic

cholangiocarcinoma (KKU-M214) cells, where knockdown of *NQO1* increases sensitivity (Zeekpudsa et al., 2014). Supporting these observations, CYGB+ clones showed higher *NQO1* expression compared to NCE controls that was maintained following 48 h 7.5 μM cisplatin, whilst CYGB+ clones also had greater resistance to cisplatin (see section 5.3.3). Untreated CYGB+ clones significantly up-regulate *NQO1* compared to NCE controls, which suggests that CYGB-expressing cells are better adapted for minimising oxidative stress and this is consistent with other research groups identifying CYGB as an antioxidant (see section 1.5.3.2). Indeed, we found in chapter 6 (see section 6.2.3) that CYGB+ over-expression was associated with lower mitochondrial superoxide levels which is consistent with evidence by other groups showing *NQO1* over-expression linked to superoxide depletion (Dinkova-Kostova and Talalay, 2010).

Another stress-response gene identified by our array, BCL2/Adenovirus E1B 19kDa Interacting Protein 3-Like (*BNIP3L*), was down-regulated in CYGB+ clones. *BNIP3L* encodes a mitochondria-targeted factor of the Bcl2-homology domain 3 (BH3) family that exerts a pro-apoptotic function by associating with and inhibiting Bcl-2 and Bcl-xL (Imazu et al., 1999), which normally prevent mitochondria outer membrane permeabilisation and release of cytochrome c (Czabotar et al., 2014). A correlation between *in vivo BNIP3L* knockdown and increased resistance to radiotherapy-induced cell death has been reported (Fei et al., 2004), supporting a role in tumour suppression. The reduced expression of *BNIP3L* within CYGB+ clones may partly explain other research groups' findings that *CYGB* knockdown in glioma cells leads to sensitisation to radiotherapy (Fang et al., 2011), potentially by promoting expression of factors like *BNIP3L* that trigger intrinsic cell death. p53 is a critical regulator of the response to stress-inducing agents including genotoxins, inducing *NQO1, GADD45A*, *CDKN2A,* and

MAP3K5 targets that were all found differentially regulated in CYGB+ clones treated with cisplatin. This suggests that CYGB over-expression causes an enhanced p53 response following cisplatin stress. This was further supported in CYGB over-expressing clones relative to NCE controls by the greater induction of p53 protein following cisplatin treatment and this trend was reversed in untreated clones (see section 5.2.5). Interestingly, the protein product of *NQO1*; whose transcript is increased in CYGB+ clones, has been found to directly stabilise p53 independently of MDM2 regulation and is most effective following oxidative stress (Asher et al., 2002). Additionally, the $p14^{ARF}$ product of the *CDKN2A* locus up-regulated in CYGB+ clones has been reported to increase stability of p53 by inhibiting MDM2 activity (Zhang et al., 1998) and its binding to retinoblastoma protein (Brown et al., 2004). The other *CDKN2A* product $p16^{INK4a}$ is able to prevent CDK4/6 activity and thus blocks progression past the G1 phase of the cell cycle (Brown et al., 2004). These data are consistent with recent reports by other research groups that CYGB interacts with p53 and modulates transcriptional activity (John et al., 2014) and the transcriptional up-regulation of *NQO1* and *CDKN2A* we find in CYGB+ clones may indicate a p53 regulatory mechanism being activated upon cisplatin treatment.

Some of the transcripts that did not show an association with *CYGB* expression in untreated cells except for the highest CYGB over-expressing clone were further investigated following cisplatin treatment. Cisplatin-treated CYGB+ clones with the two highest levels of over-expression demonstrated higher levels of *NQO1*, *MAP3K5*, *CDKN2A* and lower levels of *GADD45A* transcripts than NCE controls, where the latter two mRNAs depended on the level of CYGB expression (Figure 29d, a and b). To our knowledge, this is the first time these transcripts have been linked to CYGB following cisplatin stress.

Evidence that four of the p53 targets identified on the microarray were also significantly preferentially regulated in other CYGB+ clones in this chapter is, to our knowledge, the first evidence for a causal link between the reported CYGB-p53 association and a downstream p53 transcriptional response following cisplatin stress.

The discovery that DNA damage stress response targets (such as the DNA damage recognition gene *GADD45A* and MMR genes *MSH3* and *MLH3*) were significantly regulated in CYGB+ clones, is in agreement with previous reports showing CYGB expression can protect against ROS-induced DNA damage (Hodges et al., 2008; McRonald et al., 2012) and also with reports that CYGB is up-regulated by stress (John et al., 2014; Latina et al., 2015; Li et al., 2007; Nishi et al., 2011). *GADD45A* is down-regulated in all clones following cisplatin treatment (in association with increasing CYGB over-expression) than in NCE controls, which is expected with an improved DNA damage response. It is interesting that *GADD45A* expression also shows a dependence on CYGB over-expression level. Genotoxins stimulate *GADD45A* expression; in part through p53-dependent mechanisms (Xiao et al., 2000), which promotes synthesis of a protein that interacts with factors involved in DNA repair and cell cycle regulation (such as proliferating cell nuclear antigen (PCNA) and CDK2/cyclinB1) (Liebermann and Hoffman, 2008). The interaction with PCNA occurs as part of the NER DNA damage repair response involving blockade of replication and promotion of repair machinery (Hildesheim and Fornace, 2002). GADD45A also promotes G2/M checkpoint activation through inhibiting the kinase activity of CDK2/cyclinB1 complex and thus mitosis (Kastan and Bartek, 2004) and has also been found to protect cells against aneuploidy and tumour formation (Hollander et al., 1999). GADD45A also activates the p38/JNK

signalling pathway that regulates p53 activity and apoptosis (Gupta et al., 2006; Hildesheim et al., 2002).

Another transcript in the stress response category that is significantly up-regulated in CYGB+ clones is Mitogen-activated protein kinase (*MAP3K5*); also known as apoptosis signal-regulating kinase 1 (*ASK1*). *MAP3K5* transcripts are enhanced in all CYGB+ clones after cisplatin treatment compared to their modest down-regulation in NCE controls. This a serine/threonine protein kinase that activates the p38 /JNK signalling cascades upon detection of oxidative stress through the dissociation of thioredoxin (Matsukawa et al., 2004; Tobiume et al., 2001) and it has been reported that ASK1 triggers inflammatory responses that in turn generates ROS for promotion of tumour progression (Kinoshita et al., 2013). *ASK1* has been found up-regulated in gastric cancer and linked to tumour proliferation (Hayakawa et al., 2012).

It was interesting to observe that cell cycle regulators were differently expressed in CYGB+ clones, with a number being up-regulated like *CDKN2A, GADD45G* and *CDK11B*. There is increasing evidence that indicates a role for CYGB in cell cycle regulation and this is discussed in section 1.6.3.2. Treatment of breast cancer MDA cells with hydrogen peroxide showed up-regulation of a number of antioxidant transcripts, including *CYGB* that occurred with cell cycle arrest at G1/S-phase (Chua et al., 2010). A more direct link that implies cell cycle regulation may be a downstream effect of CYGB was reported in a study of ovarian SKOV-3 cancer cells transfected with CYGB that showed greatly reduced CCDN1 levels and increased G1 arrest (Chen et al., 2014). It is certainly logical to expect cell cycle genes to be affected by CYGB over-expression, given the protection that CYGB offers cells against DNA damage since it would allow a greater opportunity for repair to

be attempted. *CDKN2A* encodes the cell cycle regulator $p16^{ARF}$, which inhibits CDK4 to prevent its interaction with CCDN1 that normally promotes S-phase entry (Giono and Manfredi, 2006; Kastan and Bartek, 2004). The fact *CDKN2A* levels are enhanced more so in CYGB+ clones indicates that these cells would be better equipped to activate the G1/S checkpoint after cisplatin treatment.

In this chapter, we identified and validated novel transcripts that are differentially regulated by CYGB in OSC cancer cells, with some showing a dependence on cisplatin treatment for their association with CYGB over-expression to be revealed. These transcripts were related to migration (*ITGA2* and *ARHGAP18*) and protection against stress-induced damage (*MAP3K5*, *NQO1*, *GADD45A*, *CDKN2A* and *BNIP3L*).

As the CYGB protein is cytoplasmic and does not contain any known nuclear-targeting motifs (Kawada et al., 2001), it would be necessary for the protein to associate with or regulate activation of a transcription factor to specifically alter the transcriptome. It must also be noted that associations between CYGB over-expression and a gene target may be due to indirect regulation. Recently, CYGB has been shown capable of entering the nuclear compartment by splicing a nuclear localisation sequence to its N terminus (Itoh et al., 2013) that suggests it is at least small enough to move across the nuclear membrane and its inherent nuclear expression within neurones has also been reported (Geuens et al., 2003) suggests a possible nuclear function in these cell types. There is also a recent report showing evidence for an interaction between CYGB and p53, where CYGB can promote stabilisation of p53 (John et al., 2014). Thus, it is possible for CYGB to be acting by some as yet unidentified mechanism to specifically regulate the expression

of gene categories identified in this chapter and by Shivapurkar et al (2008) and hence deserves further investigation.

Also in this chapter, it is shown that CYGB+ clones exhibit an enhanced response of a number of known p53 targets, namely *GADD45A*, *MAP3K5*, *CDKN2A* and *NQO1*, which supports the idea that CYGB may indeed be increasing p53 signalling in this cell model. These could be validated in three independent CYGB+ clones. Although this chapter cannot show how the CYGB protein modifies transcription, it is clear that over-expression of CYGB results in a number of significantly altered mRNAs and furthermore, part of the transcriptional response to CYGB over-expression is control of p53-target expression following cisplatin stress. A summary of this is shown in Figure 30. These changes have importance in predicting CYGB function, such as the protection afforded to cancer cells against genotoxin cytotoxicity. The phenotypic alterations resulting from CYGB over-expression predicted from the findings of this chapter is the focus of chapter 5.

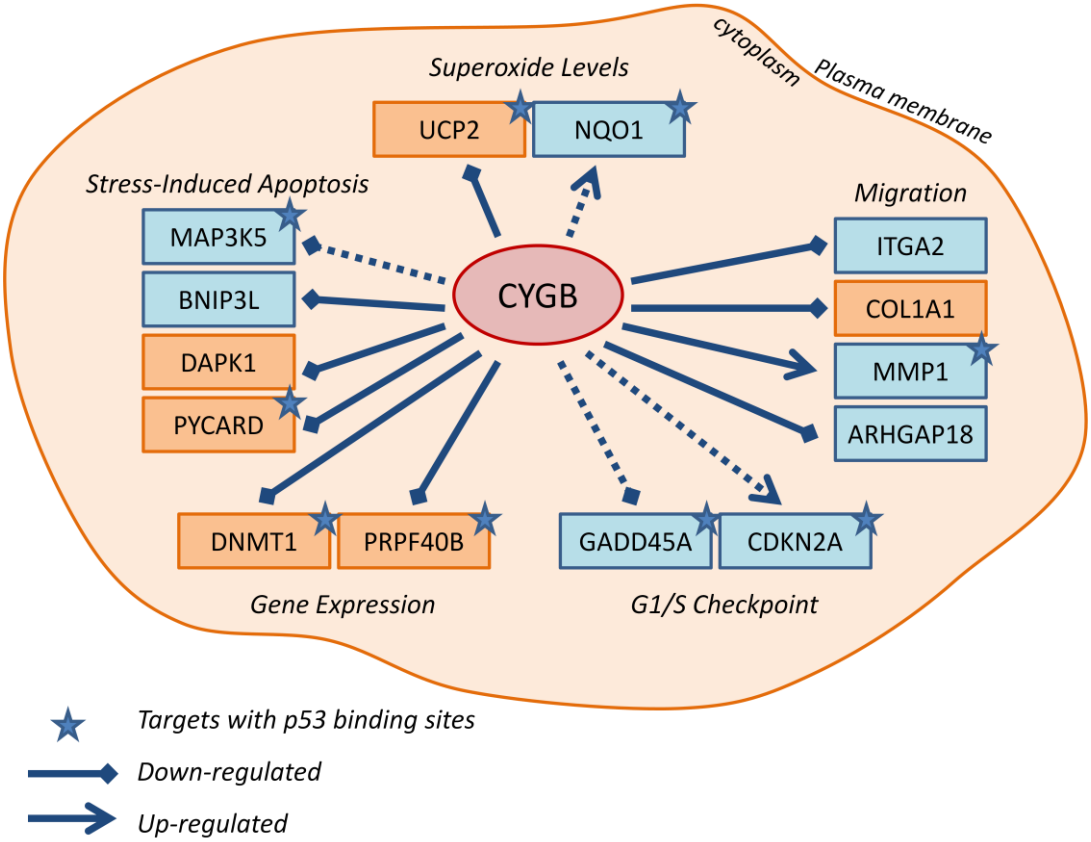

Figure 30 – Summary of downstream targets related to CYGB over-expression.
Transcripts that showed a change in expression within the CYGB+ clones found by the experiments in chapter four (in blue); along with those reported by Shivapurkar et al (2009) and Oleksiewicz et al (2011) (in orange), are shown. Transcripts have been grouped into broad categories for ease of interpretation, but some may have an involvement in more than one phenotype, as described in the discussion of chapter four. Transcripts are shown with blunted arrows if down-regulated and a complete arrow with transcripts up-regulated by CYGB over-expression. Transcripts regulated by 48 h 7.5 µM cisplatin treatment are shown with dotted lines. Targets of with p53 binding sites in the promoter are labelled with a star (information for this was obtained from the GeneCards Human Genes Database).

CHAPTER FIVE:

Cisplatin Resistance and the Phenotypic Changes Associated with CYGB Over-Expression.

5.1 Introduction

Limited evidence exists that examines the role of CYGB in the response to chemo- and radio- therapy (see section 1.6.3.3.2). Response to radiotherapy in human glioma cells has been demonstrated to improve with *CYGB* knockdown (Fang et al., 2011). Doxorubicin treatment of U2OS cells stably expressing GFP-CYGB was found to induce the conjugate's expression levels and this occurred in parallel with p53 accumulation, which also could be demonstrated in these cells after etoposide treatment (John et al., 2014). C2C12 murine myoblasts also showed reduced apoptotic cell death in response to etoposide if CYGB is stably over-expressed (Singh et al., 2014). Most recently, breast cancer cells were shown increase ROS levels when *CYGB* was knocked down with doxorubicin treatment (Latina et al., 2015). Together, these studies suggest CYGB has an important function in determining tumour cell response to chemotherapeutic agents and suggests further that CYGB might participate within therapy resistance mechanisms.

The results presented in chapter 4 showed CYGB over-expression could differentially regulate of a number of genes and a subset of these were validated in multiple CYGB over-expressing clones. Transcripts were related to migration (*ITGA2* and *ARHGAP18*), cell cycle regulation (*CDKN2A*), and cellular response to stress-induced damage (*MAP3K5*, *NQO1*, *GADD45A*, and *BNIP3L*), which added to the growing list of transcripts that are potentially downstream of CYGB (Figure 30). Four of these transcripts; *NQO1*, *CDKN2A*, *GADD45A* and *MAP3K5*, are known to be regulated by p53 as discussed in section 4.3 and these targets were significantly regulated in CYGB+ clones after cells were treated for 48 h with 7.5 μM cisplatin. In combination with our data, there is emerging evidence that CYGB associates with p53 function (John et al., 2014; Singh et al.,

2010). This suggests over-expression of CYGB influences p53 function and ultimately the response of cells to cytotoxic agents such as cisplatin, which activates the p53 signalling pathway (see section 1.6.3.3.1). As CYGB over-expression was linked to the significant alteration of transcripts involved in migration and stress response from our study in chapter 4, we hypothesised that CYGB may alter the phenotypes associated with these transcriptional changes. We further postulated that changes in p53-related functions such as apoptosis activation and cell cycle regulation in CYGB+ clones treated with cisplatin should be observed, since there were significantly regulated p53 targets following treatment.

In the current chapter, we present data for the effect that CYGB over-expression had on phenotypes related to tumorigenesis in our OSC cancer cell model. We show CYGB+ clones have altered migratory and mitochondrial reductive abilities, as well as a reduced cytotoxicity response to cisplatin. Significant gene expression changes observed in CYGB+ clones (presented in chapter 4) were consistent with these phenotypes. To our knowledge, we also show for the first time evidence for CYGB's ability to alter cell cycle distribution both prior to and following cisplatin treatment and that factors associated with the DNA damage detection response including CHK1 and p21 were significantly increased with CYGB over-expression.

5.2 Results

5.2.1 Effect of CYGB on Cell Motility

Motility of CYGB+ clones was examined with a wound healing assay, where a cell-free gap between two opposing cell sheets was created (see section 2.13) and the closure of the gap was quantified. Medium (LST54) and high (LST421) over-expressing CYGB+ clones were significantly more mobile than NCE controls (Figure 31). At 3 h, for instance, NCE controls had left 30.2 % (± 8.03) of the gap, whilst LST421 and LST54 clones left only 19.7 % (± 6.33) and 7.3 % (± 3.79), respectively. A representative image from one experiment is shown in Figure 32 and also provided in movie format on the Supplementary CD-ROM.

This suggests there was a CYGB "dose" dependent effect on cell migration where levels closer to normal physiological CYGB levels (such as in LST32 clones) give a slower migration rate, whilst higher levels of CYGB expression (as demonstrated by LST421 and LST54 clones) leads to faster migration rates. The difference between the NCE measurements and the CYGB+ clones was not found to be statistically significant (one-way ANOVA, $p > 0.05$ for all time points).

If the effect on migration rate were related directly to CYGB expression, then siRNA-mediated knockdown of *CYGB* expression would be expected to reverse the phenotypes observed in the CYGB+ clones. The highest CYGB over-expressing clone, LST421, was chosen for this RNA interference (RNAi) study and it was indeed observed that CYGB siRNA treated cultures had impaired ability to close the cell-free gap by 3 h (55.3 % ± 3.13), compared with wildtype CYGB+ clones (67.5 % ± 4.50, Figure 33a), but this was not statistically significant (Kruskal-Wallis, $p= 0.276$). Surprisingly, experiments using a

scramble RNAi sequence also caused knockdown of *CYGB* expression and this was also associated with reduced cell motility (Figure 33). Further experiments are required with another negative siRNA control to fully validate this experiment.

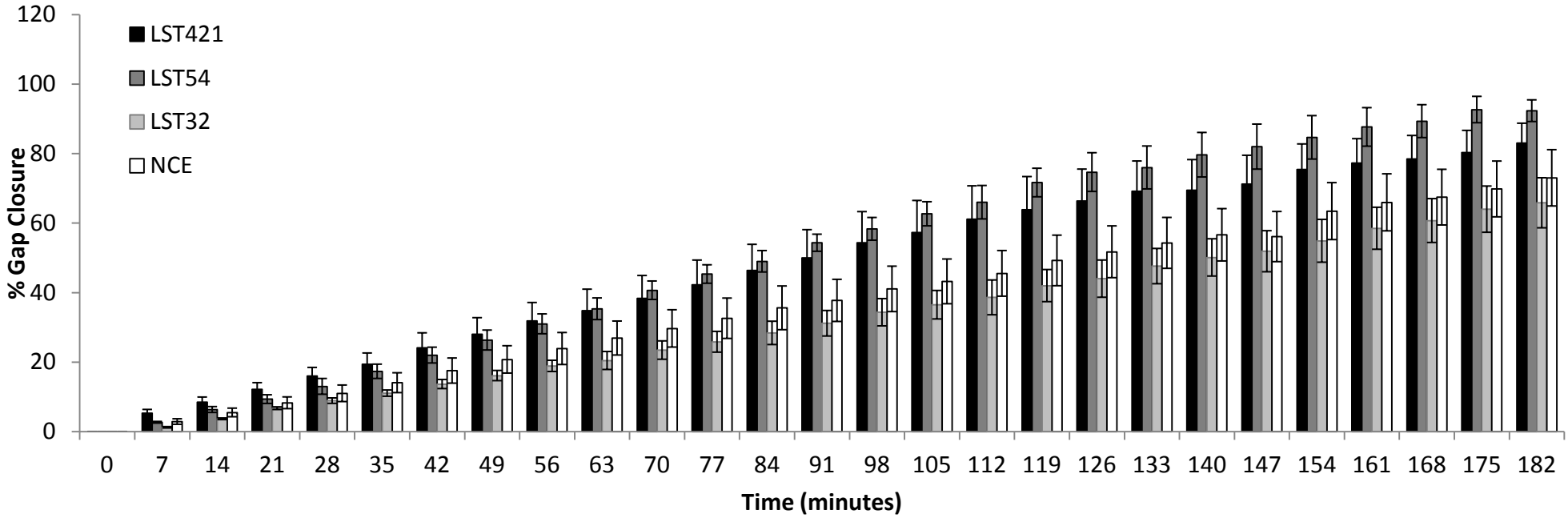

Figure 31 – CYGB+ clones close a cell-free gap faster than NCE control clones.
CYGB+ and NCE clones were seeded into silica culture templates in a 24 well plate to reach full confluence the next day. The templates were removed immediately prior to the experiment, leaving a 500 µm ± 50 µm cell-free region between two confluent cell sheets. Cells were then left to migrate towards each other in low serum (1% FBS) media to limit any proliferation that would otherwise confound the results. The closure of the gap was monitored over 6 h using the Cell IQ microscope to record both bright field images and gap measurements every 7 min across three biological replicates (technical duplicate). Data was analysed with the cell-free area at time zero being defined within the software (conversion factor of 1 pixel = 0.698 µm) and then all subsequent images automatically measured from this to determine the area of the wound that was covered at each time point expressed as a percentage. % gap closure relative to time zero control ± standard error.
No significant differences were found between CYGB+ and NCE clones at any time (one-way ANOVA, $p = > 0.08$).

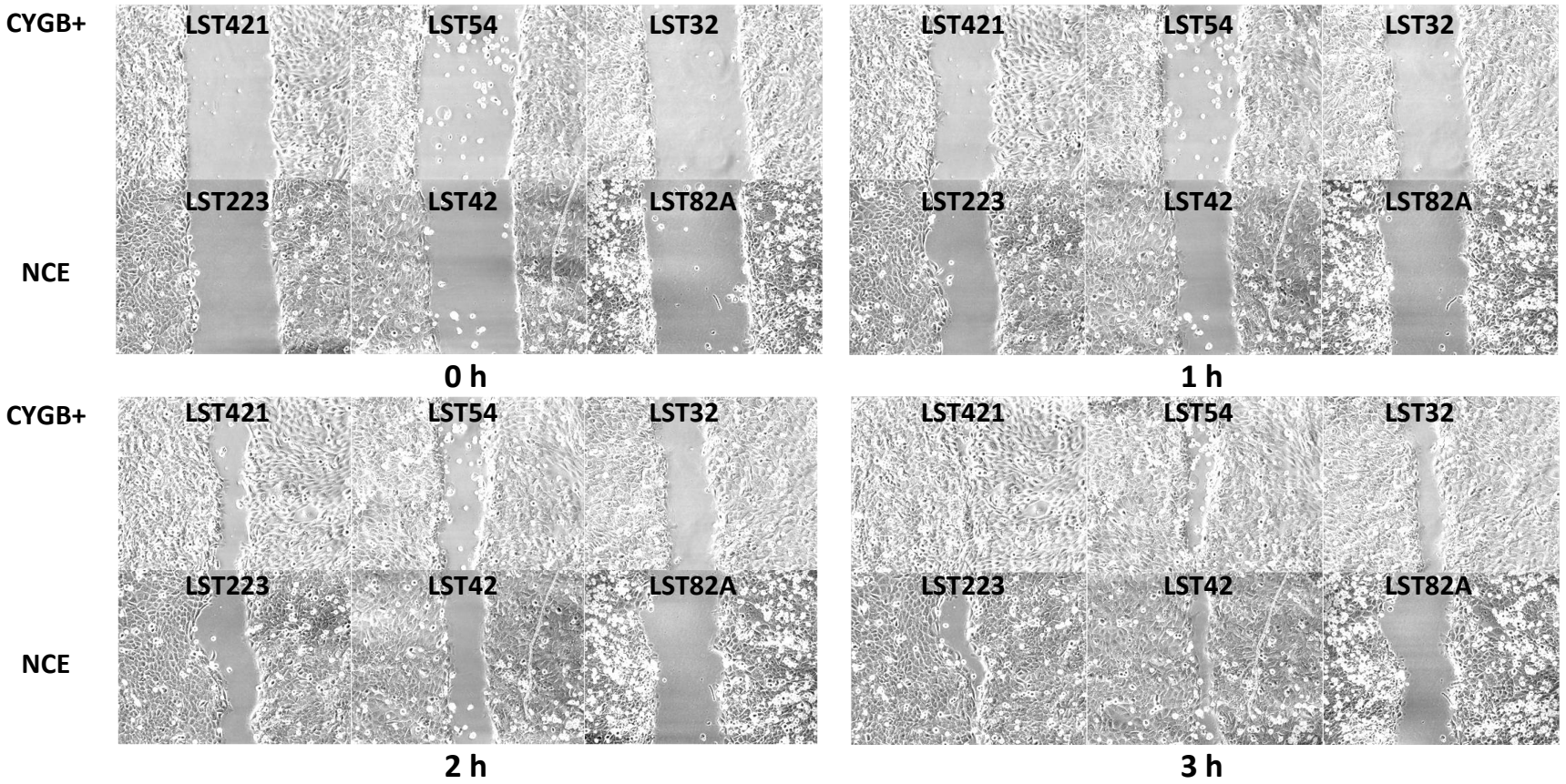

Figure 32 – Representative Bright field images of CYGB+ and NCE clones show CYGB+ clones close the cell-free gap more quickly.
CYGB+ and NCE clones were seeded into silica culture templates in a 24 well plate to reach full confluence the next day. The templates were removed immediately prior to the experiment, leaving a 500 µm ± 50 µm cell-free region between two confluent cell sheets. Cells were then left to migrate towards each other in low serum (1% FBS) media to limit any proliferation. The closure of the gap was monitored over 6 h using the Cell IQ microscope to record both bright field images and gap measurements every 30 min across three biological replicates (technical duplicate). Representative images from 0, 1, 2 and 3 h are shown for each clone.

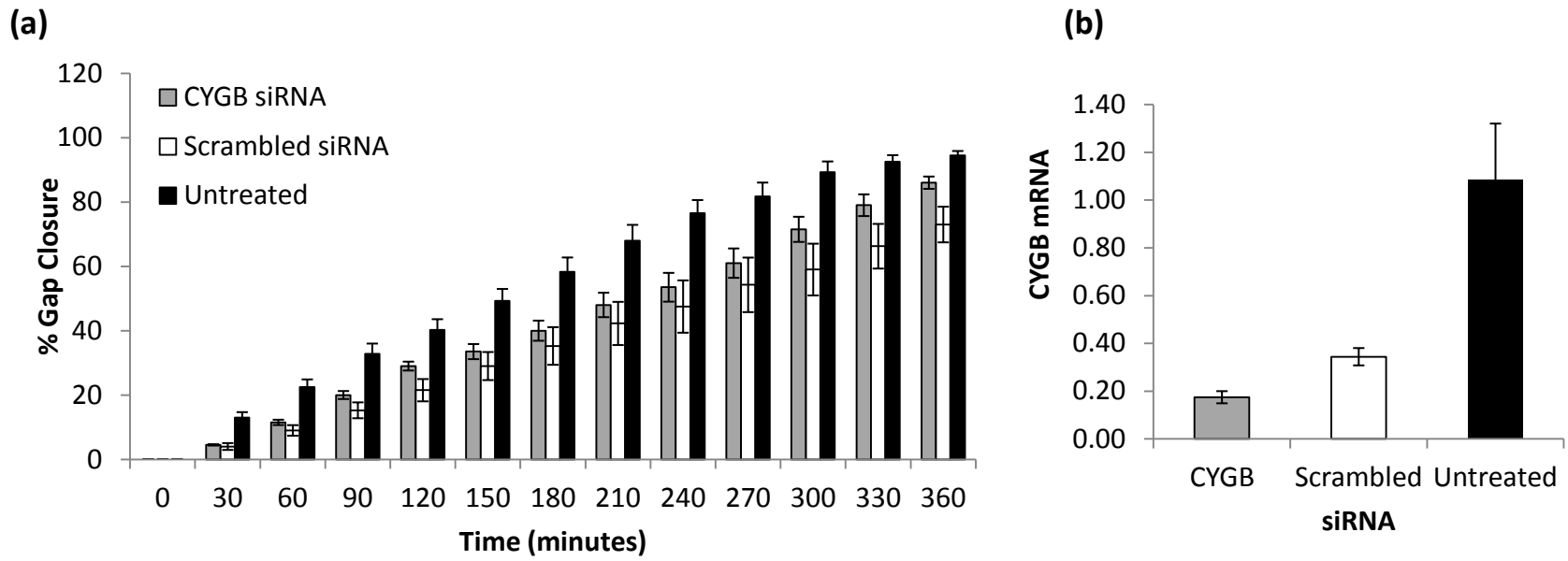

Figure 33 – siRNA-mediated knockdown of CYGB expression on motility of LST421 (CYGB+) clones.
(a) Following 24 h of CYGB or negative siRNA transfection, LST421 CYGB+ clones were seeded into silica culture templates in a 24 well plate to reach full confluence the next day. The templates were removed immediately prior to the experiment, leaving a 500 µm ± 50 µm cell-free region between two confluent cell sheets. Cells were then left to migrate towards each other in low serum (1% FBS) media to limit any proliferation that would otherwise confound the results. The closure of the gap was monitored over 6 h using the Cell IQ microscope to record both bright field images and gap measurements every 30 min across two biological replicates (technical duplicate). **(b)** RTqPCR of RNA isolated from siRNA-transfected cultures. Data was normalised to the TBP expression using the Pfaffl ddCt method from Ct values averaged across three biological replicates. Average mRNA expression ± standard error. No significant differences compared to untreated control, Kruskal-Wallis, p = > 0.05.

5.2.2 Proliferation of Cells with CYGB Over-Expression

The influence of CYGB expression on cellular proliferation was assessed using the crystal violet assay, taking measurements every day for a 4 day duration as described in section 2.10, to develop a growth curve profile. There was no statistically significant difference in proliferation between CYGB+ clones and NCE controls (Figure 34). Reduced cell numbers were observed at the start of the time course in LST421 and LST54 clones on day one (1425 cells ± 489 for LST421 and 1829 cells ± 825 for LST54; not statistically significant (one-way ANOVA, p=0.055)) and day three (10800 cells ± 1474 for LST421 and 14104 cells ± 398 for LST54; not statistically significant (one-way ANOVA, p=0.293)), relative to NCE controls on these days (3176 cells ± 512 on day 1 and 16375 cells ± 914 on day 3). On day 4, LST421 and LST32 clones also has reduced cell densities than NCE controls (17644 cells ± 1275 for LST421 and 15202 cells ± 1149 for LST32 (not significant, Kruskal-Wallis, p = 0.408) compared to 20071 cells ± 1474 for NCE controls), whilst the LST54 clone gave surprisingly higher densities compared with the NCE controls. LST421 and LST54 cells were higher than NCE controls at day two (15171 cells ± 2338 for LST421 and 14827 cells ± 1477 for LST54 compared to 9118 cells ± 1107 for NCE controls, but this was not significant (Kruskal-Wallis, p = 0.099)). Overall, there is an indication that CYGB over-expression can impact on proliferation but the results from this assay are inconclusive.

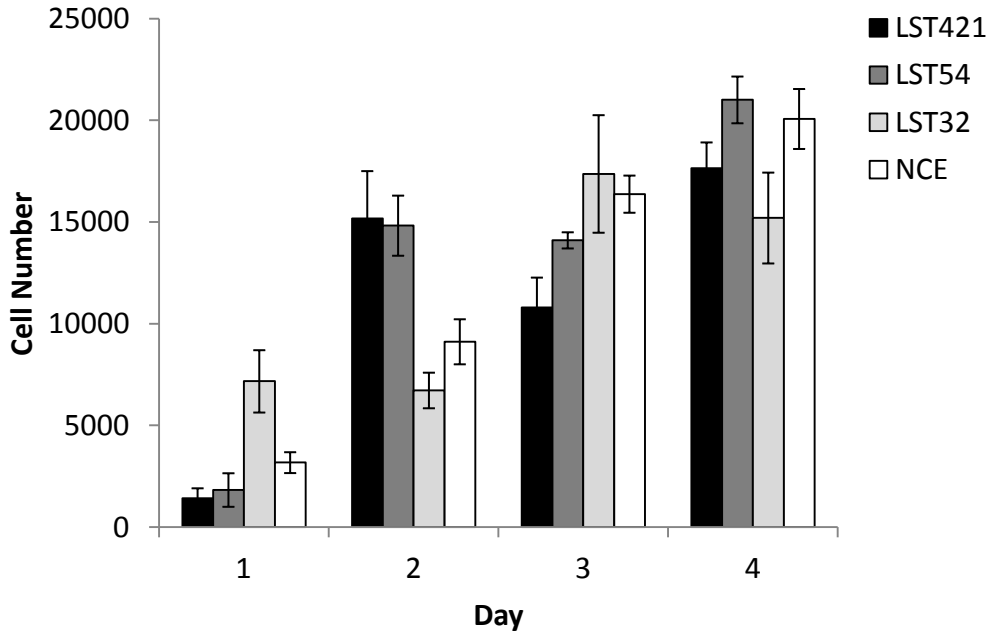

Figure 34 – Effect of CYGB expression on cell proliferation.
Cells were seeded at equal numbers as described in section 2.10 in complete media for four days and cell densities were measured daily using the crystal violet method and interpolated as cell number using a crystal violet calibration curve. Measurements for each day were normalised to their respective day zero seeding densities. Results for three NCE clones were averaged. Data points are the average of three biological replicates. Mean normalised absorbance ± standard error. There were no statistically significant differences between CYGB+ clones and NCE controls at any day (all $p > 0.05$, see text).

5.2.3 Effect of CYGB on Cisplatin Survival

Viability of CYGB+ and NCE clones following 48 h of cisplatin treatment was examined by three cytotoxicity endpoint assays (MTT, Crystal Violet and SRB) as described in section 2.9. The crystal violet assay enables staining of cell nuclei that gives an indirect way to determine cell number, the MTT assay provides a measure of mitochondrial reductase function and hence cell viability, and the SRB assay quantifies total cellular protein.

As expected, all three assays showed a concentration-dependent reduction in cell number with increasing cisplatin concentration. The IC_{50} (the 50 % inhibitory concentration) was estimated to be 10 μM cisplatin, thus the concentrations either side of this (the IC_{40} (7.5 μM) and IC_{60} (15 μM)) were selected for use in subsequent experiments to investigate the responses of CYGB+ clones to cisplatin. Overall, CYGB+ clones treated with 7.5 μM cisplatin for 48 h showed a trend towards increased viability compared with NCE controls, as determined by all three cytotoxicity assays, and this effect was maintained in the two highest-expressing CYGB+ clones until the IC60 concentration (Figure 35).

As assessed by the MTT assay, LST421 clones exhibited greater survival (46.7 % survival ± 3.00) than NCE clones (42.5 % ± 1.33) following treatment with 7.5 μM cisplatin, but this was statistically insignificant (one-way ANOVA, $p = 0.336$, Figure 35a). The LST54 clone also exhibited a non-statistically significant trend towards increased viability to NCE controls (49.9 % ± 1.99) at this concentration. Likewise, the crystal violet assay indicated survival was enhanced in CYGB+ clones (LST421 (65.4 % ± 1.76), LST54 (53.9 % ± 1.41) and LST32 (53.01 % ± 1.61)) compared with NCE clones (45.5 % ± 1.78) at 7.5

μM cisplatin (one-way ANOVA, p = 0.709), which was a trend maintained for all concentrations of cisplatin studied (excluding 15 μM and 20 μM cisplatin) (Figure 35b).

Results from the SRB assay support this trend in LST421 and LST32 clones between 2.5 μM and 10 μM cisplatin, with 7.5 μM cisplatin exhibiting 140.1 % (± 4.79) and 90.5 % (± 6.16), respectively, of the cell population remaining relative to NCE clones (89.3 % ± 4.81) (statistically insignificant, as assessed by the Kruskal-Wallis test, p = 0.055, Figure 35c). LST54 cells were determined to have similar levels of SRB staining to NCE controls for most of the intermediate cisplatin concentrations.

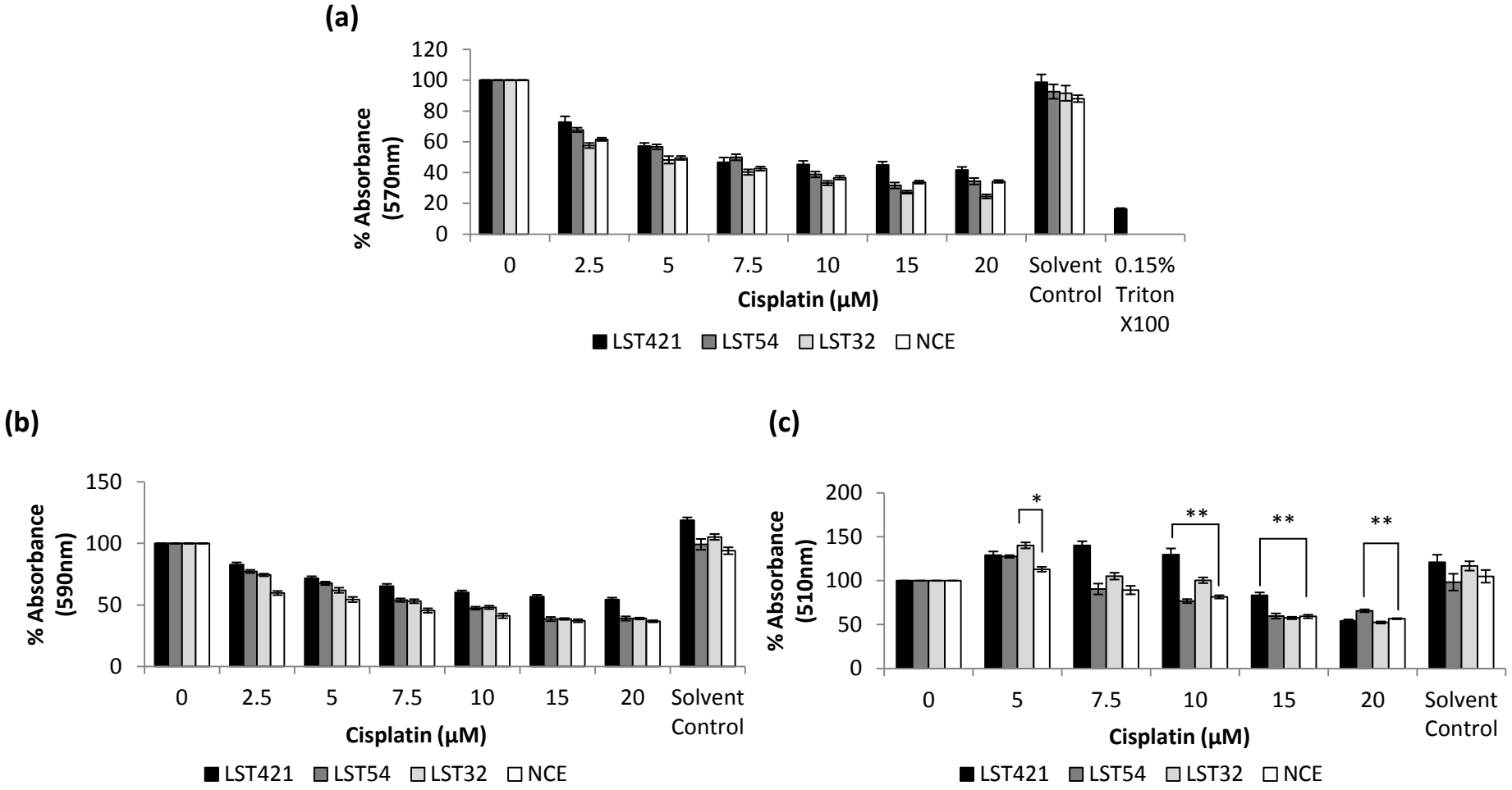

Figure 35 – Effect of CYGB expression on clone survival following cisplatin treatment.
Cells were treated with cisplatin for 48 h, before undergoing **(a)** the (MTT) assay, **(b)** Crystal Violet (CV) assay and **(c)** Sulforhodamine B (SRB) assay (see section 2.9) to assess the response of CYGB+ clones to cisplatin-induced cell death. Data are the average of three biological replicates (in technical triplicate) ± standard error. For the MTT assay positive control, a quadruplicate set of readings were taken in the LST421 clone. One-way ANOVA with post-hoc Tukey * $p < 0.05$ and ** $p < 0.01$.

5.2.4 Effects of CYGB on Cell Cycle Distribution

We hypothesised that we would also be able to detect CYGB-dependent cell cycle changes following cisplatin treatment as we observed increased survival following cisplatin treatment in CYGB+ clones (see section 5.2.3). Cell cycle distributions are shown in Figure 36 and Figure 38, whilst representative cell cycle histograms and dot blots to show the singlet gate are shown in Figure 37 and Figure 39. Secondly, expression of four proteins related to cycle regulation; cyclin D1, p21, p53 and CHK1, were quantified using in-cell ELISA assays to determine if the findings of the cell cycle analysis could be validated further, as well as provide insight into the mechanism of CYGB action (see section 5.2.5).

In the absence of treatment, CYGB over-expressing clones were marginally more likely to be in S-phase compared to NCE controls, although this was statistically insignificant (one-way ANOVA, $p = 0.143$, Figure 36a and Figure 38a). There was a also a trend towards greater S-phase accumulation with increasing CYGB over-expression (LST421 (high, 29.8 % ± 2.07) > LST54 (medium, 28.3 % ± 1.74) > LST32 (low, 22.2 % ± 1.67)) relative to the NCE controls where only 24.0 % ± 1.51 cells were in S-phase.

Treatment with cisplatin (7.5 μM) for 24 h caused an accumulation of cells in S-phase that was followed by G1 accumulation of cells at 48 h and 72 h (Figure 36). After 72 h, 50.3 % (± 7.93) of LST421 and 43.2 % (± 5.59) LST54 CYGB+ clones were in G1, compared to just 34.9 % (± 3.15) of NCE controls, although this difference was statistically insignificant (Kruskal-Wallis test, $p = 0.333$). At 15 μM, there were clear differences between CYGB+ and NCE clones in S-phase distribution at 24 h and persisting across the later time points (Figure 38). At 24 h of 15 μM cisplatin, 62 % (±

10.51), 42.2 % (± 1.934) and 32.3 % (± 5.69) of LST421, LST54 and LST32, respectively, were within S-phase, compared with just 35.6 % (± 2.60) of NCE clones (insignificant, one-way ANOVA, p=0.958). By 72 h, this increased further to 67.3 % (± 12.72), 39.1 % (± 3.42) and 36.9 % (± 7.12) of LST421, LST54 and LST32, respectively, whilst NCE samples only had 29.3 % (± 3.65) within this cycle phase, although none of these differences were found to exhibit statistical significance with the Kruskal-Wallis test (p = 0.292).

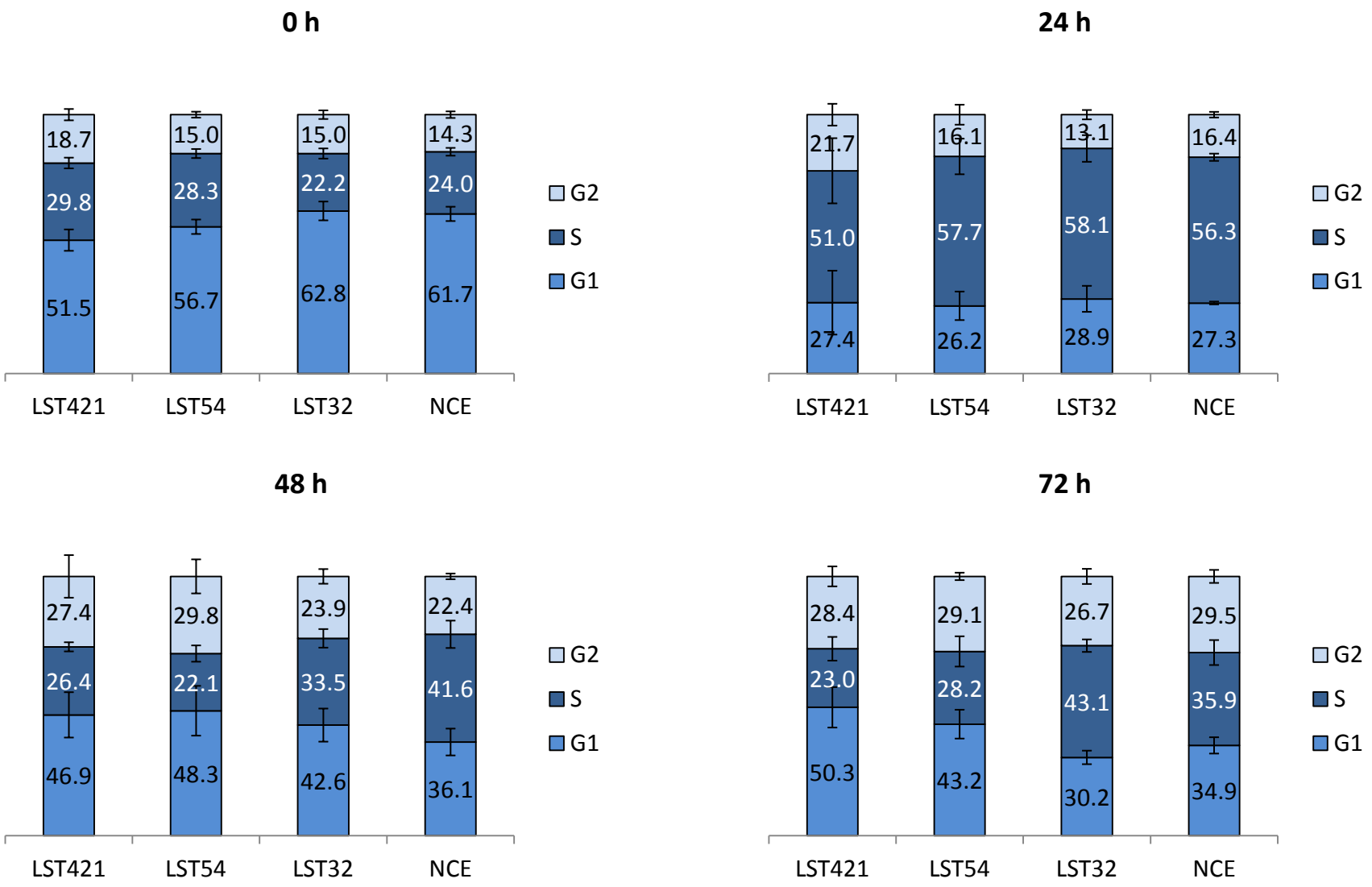

Figure 36 – Effect of CYGB and 7.5 µM Cisplatin on Cell Cycle Distribution.

Cells were seeded into T25 flask prior to being treated or not with 7.5 µM cisplatin for 24 h, 48 h or 72 h. After these durations, cells were harvested, fixed and stained with propidium iodide (PI) and analysed by flow cytometry, as described in section 2.13. Proportions of cells in each stage of the cell cycle were assessed and expressed as percentages across three biological replicates and corrected for the unstained cell control. There were no statistically significant differences between group means (all p values > 0.05, see text).

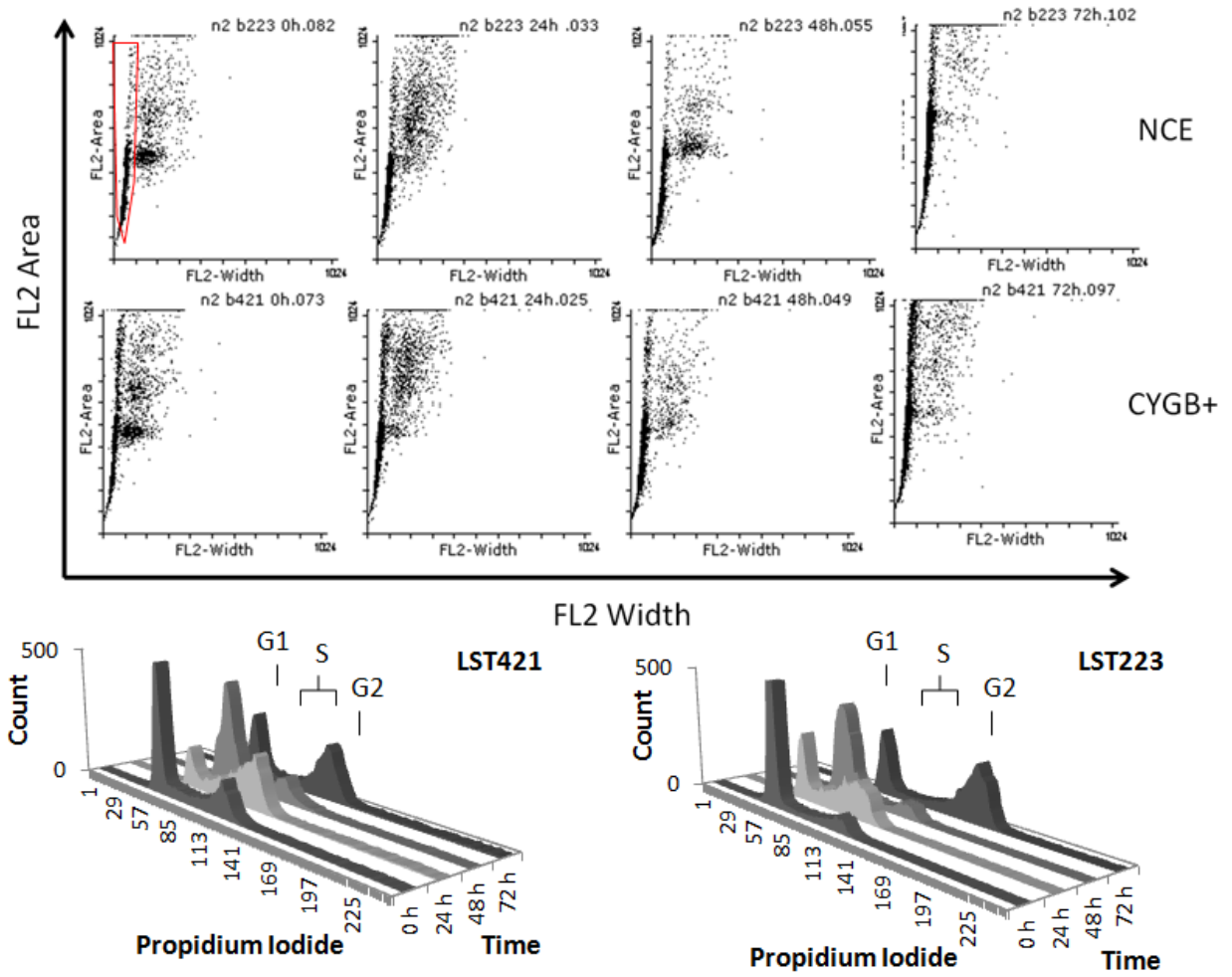

Figure 37 – Representative Cell Cycle Distributions for LST421 (CYGB+) and LST223 (NCE) clones following 7.5 µM cisplatin treatment.
Cells were seeded into T25 flask prior to being treated with cisplatin for 24 h, 48 h or 72 h. After these durations, asynchronous cells were harvested, fixed and stained with propidium iodide (PI) and analysed by flow cytometry, as described in section 2.13. Gating was carried out for viable cells across three biological replicates and corrected for the unstained cell control for cell cycle analysis. Example dot blots and histograms of viable cells are also shown, along with the singlet population gate (red outline).

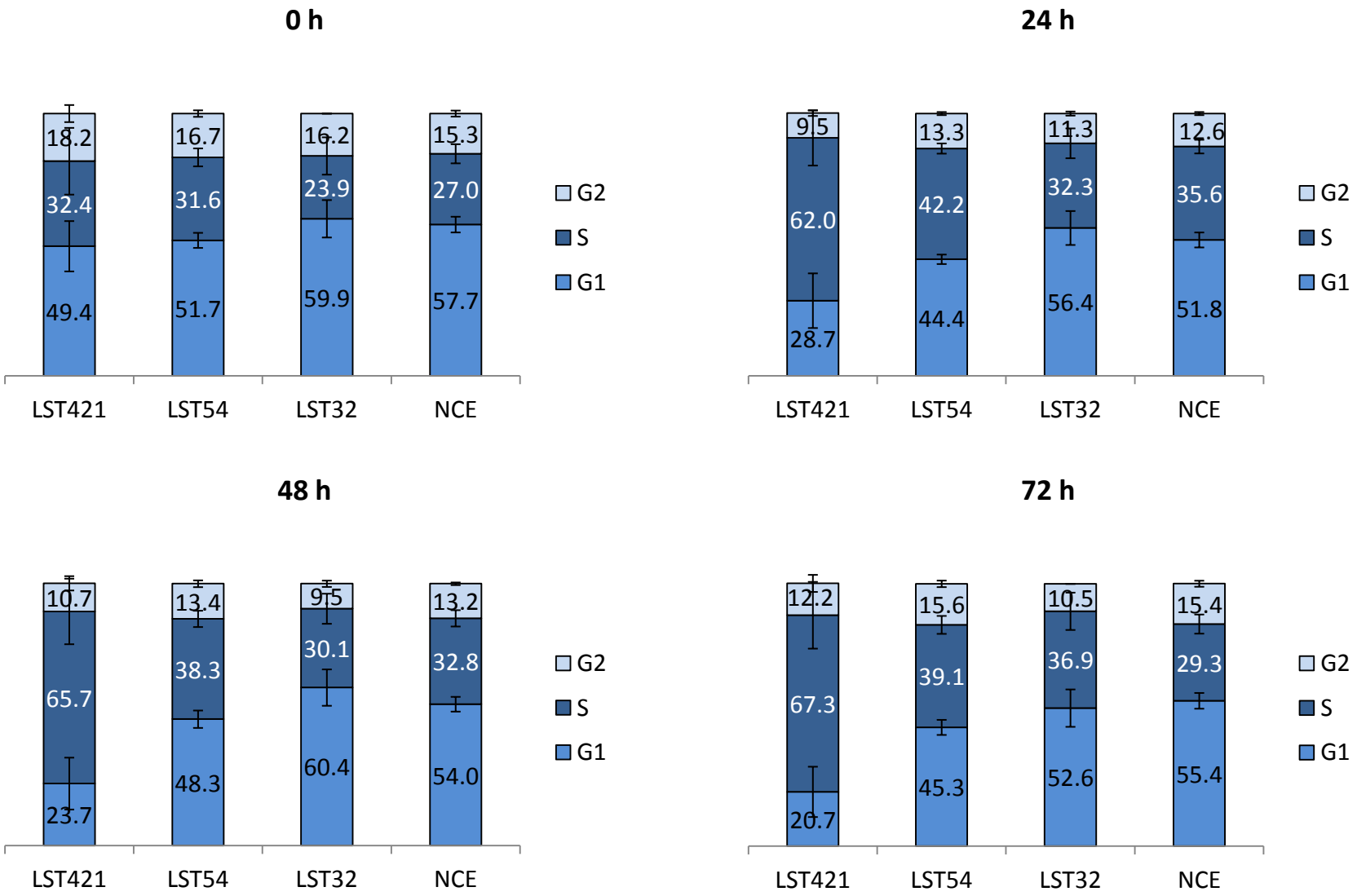

Figure 38 – Effect of CYGB and 15 µM Cisplatin on Cell Cycle Distribution.

Cells were seeded into T25 flask prior to being treated or not with 15 µM cisplatin for 24 h, 48 h or 72 h. After these durations, asynchronous cells were harvested, fixed and stained with propidium iodide (PI) and analysed by flow cytometry (see section 2.13). Proportions of cells in each stage of the cell cycle were assessed and expressed as percentages across three biological replicates and corrected for the unstained cell control. There were no statistically significant differences between group means (all p values > 0.05, see text).

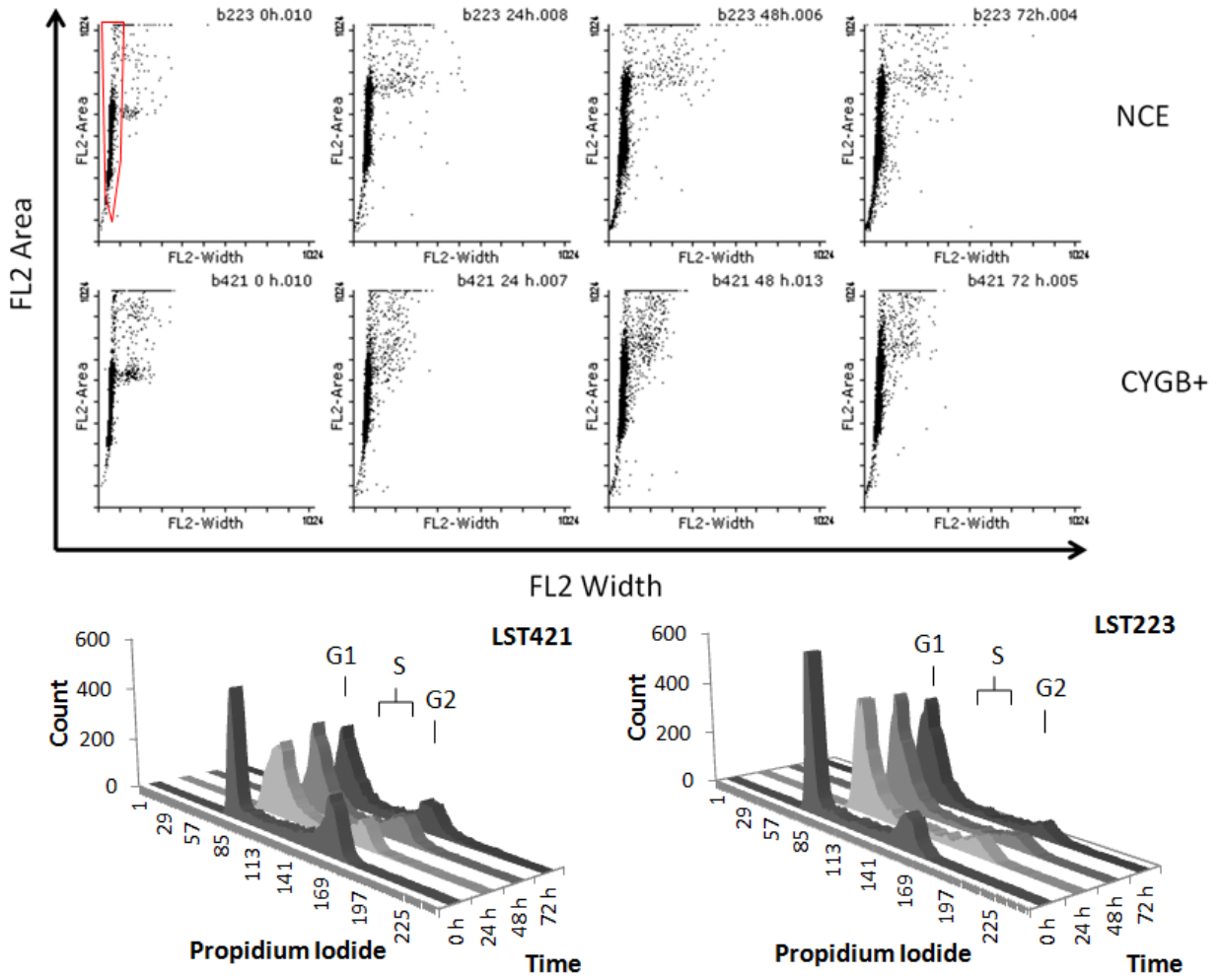

Figure 39 – Representative Cell Cycle Distributions for LST421 (CYGB+) and LST223 (NCE) clones following 15 µM cisplatin treatment.
Cells were seeded into T25 flask prior to being treated or not with 15 µM cisplatin for 0, 24 h, 48 h or 72 h. After these durations, cells were harvested, fixed and stained with propidium iodide (PI) and analysed by flow cytometry, as described in section 2.13. Gating was carried out for viable cells across three biological replicates and corrected for the unstained cell control for cell cycle analysis. Example dot blots and histograms of viable cells are also shown, along with the singlet population gate (red outline).

5.2.5 Expression of Proteins Related to Cisplatin-Induced Cell Cycle Change

Cisplatin causes DNA adduct formation that leads to DNA strand breaks (see section 1.6.3.3.1) and these are detected by ATR kinases that transduce the DNA damage signal into activation of CHK1 that via CDC25 contributes to cycle arrest (Patil et al., 2013; Wagner and Karnitz, 2009), and phosphorylation of p53 by CHK1 aids its stabilisation for recruitment of DNA repair machinery to the cisplatin-damaged site (Ali et al., 2012; Pabla et al., 2008). Quantification of cell cycle associated proteins following treatment of cells with cisplatin levels for 48 h demonstrated that as expected, p21, p53 and CHK1 proteins were all up-regulated in all cell clones (Figure 40).

p21 expression in high and medium expressing CYGB+ clones was higher compared to NCE controls after cisplatin treatment. In untreated LST421 and LST54 clones, there was an increase of p21 expression by 1.08 fold (± 0.15), 1.69 fold (± 0.39), respectively, compared with NCE controls. After treatment with cisplatin (7.5 μM for 48 h), LST421, LST54 and LST32 increased p21 expression by 2.72 fold (± 0.67), 2.52 fold (± 0.65) and 2.33 fold (± 0.62), respectively, compared with untreated NCE controls (LST54 and LST32, $p = 0.021$ and $p = 0.04$, respectively, t-test (paired)). After treatment with cisplatin (15 μM for 48 h), LST421, LST54 and LST32 increased p21 expression by 4.39 fold (± 1.08), 4.89 fold (± 0.75) and 4.61 fold (± 0.49), respectively, compared with untreated NCE controls, and at 15 μM, the expression in LST32 was statistically significant (t-test (paired), $p = 0.027$).

Cyclin D1 levels were higher in CYGB+ clones than NCE controls across cisplatin concentrations. After 7.5 μM cisplatin treatment, LST54 and LST32 over-expressing clones had higher cyclin D1 expression (8.83 fold (± 1.21), and 11.49 fold (± 1.38),

respectively) above the NCE controls (non-significant, t-test (paired), $p > 0.05$). At 15 μM, LST421 and LST32 over-expressing clones had higher cyclin D1 expression (12.34 fold (± 5.39) and 14.63 fold (± 5.46), respectively) above the NCE controls. None of the differences at 15 μM were significant (one-way ANOVA, $p = 0.865$).

p53 expression was lower in untreated high and medium expressing CYGB+ clones (0.75 fold (± 0.01) and 0.80 fold (± 0.09), respectively) compared to NCE controls. The difference between LST421 clones and NCE controls was statistically significant (t-test (paired), $p = 0.003$). After 7.5 μM cisplatin, LST54 and LST32 increased p53 expression by 2.54 fold (± 0.65) and 2.63 fold (± 0.66), respectively, above the untreated NCE control. After 15 μM cisplatin for 48 h, LST54 and LST32 increased p53 expression by 2.42 fold (± 0.17) and 2.72 fold (± 0.14), respectively, above the untreated NCE control. At 15 μM, the expression in LST54 and LST32 were significant (t-test (unpaired), $p = 0.04$ and 0.021, respectively).

CYGB+ clones all increased CHK1 expression following cisplatin treatment. Before and after 7.5 μM cisplatin, there was a trend towards increased CHK1 expression with increasing CYGB expression. At 7.5 μM, LST421, LST54 and LST32 increased CHK1 expression by 2.11 fold (± 0.59), 2.50 fold (± 0.65), and 3.50 fold (± 0.76), respectively compared to the NCE control (significant, t-test (paired), $p = 0.00$, 0.044 and 0.009, respectively). At 15 μM the effect was more pronounced with LST421, LST54 and LST32 increasing CHK1 expression by 4.50 fold (± 0.34), 5.84 fold (± 0.16), and 6.00 fold (± 0.74), respectively, to NCE untreated control. The expression at 15 μM in LST32 was significant (t-test (paired), $p = 0.027$).

Interestingly, p53, cyclin D1 and CHK1 protein expression in CYGB+ was dependent on the level of CYGB over-expression, with a trend towards higher expression of these proteins with lower CYGB over-expression.

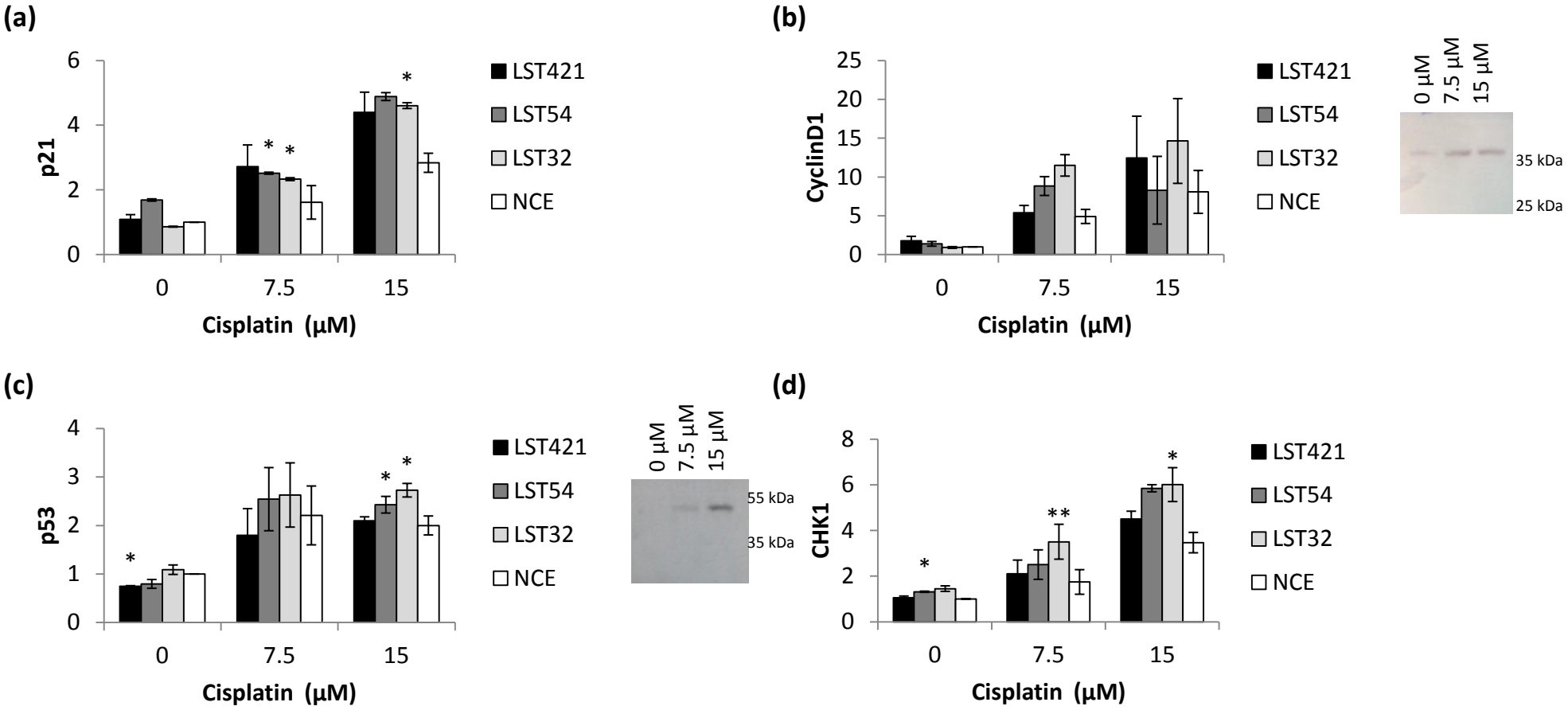

Figure 40 – CYGB+ clones exhibit differential expression of cell cycle associated factors following cisplatin treatment.

Cells were seeded into 24 well plates before treatment to 0µM, 7.5 µM or 15 µM cisplatin for 48 h. Cell cycle associated factors **(a)** p21 **(b)** cyclin D1 **(c)** p53 and **(d)** CHK1 were semi-quantified in CYGB+ and NCE clones, using indirect In-Cell ELISA. Representative western blots are provided that show antibody binding specificity in LST421 clone samples for (left to right) 0µM, 7.5 µM and 15 µM cisplatin (excluding p21 and CHK1 due to western blot development technical issues). Luminescent signals were corrected with no primary antibody labelled controls and normalised to cell number, as determined by crystal violet staining following the ELISA assay. Data are in normalised relative luminescence units (RLU) relative to the untreated NCE control to show the relative induction of the protein. They are the average of three biological replicates ± standard error.

Compared to NCE, t-test (paired),*p<0.05, **p<0.01.

5.3 Discussion

The previous chapter showed how stable over-expression of CYGB altered transcripts associated with migration and the stress response, including changes in four known p53 targets following cisplatin treatment. This current chapter characterised the effects of CYGB on cell phenotype, with particular focus on migration, proliferation, cell cycle distribution, and survival following cisplatin treatment. We found that high CYGB over-expression caused both tumour suppressor-like and oncogenic phenotypes in our OSC cell model and as far as we are aware, presents the first evidence of these in a oral cancer and cisplatin-treated context.

This study found medium and high expressing CYGB+ clones showed increased cell migration. In contrast, low over-expression of CYGB reduced migration relative to NCE controls. All CYGB+ clones also showed resistance to cisplatin-induced apoptosis, which we show in chapter 6 is associated with reduced caspase 9 activation. Finally, this study demonstrated changes in cell cycle parameters with CYGB+ clones following treatment with cisplatin that included more pronounced accumulation of cells in G1-phase and differences in average induction of CHK1, p53 and p21 proteins. These changes are discussed in more detail in the following sections.

5.3.1 Effect of CYGB Expression on Migratory Behaviour

In the current study, medium and high expression CYGB+ clones could close a cell-free area significantly faster than NCE controls. Previous studies in other cell lines (NSCLC) have shown that CYGB impairs migration before stress but migratory potential could be enhanced following peroxide-induced oxidative stress (Oleksiewicz et al., 2013). Furthermore, reduced invasiveness by CYGB over-expression was reported in ovarian SKOV-3 cells (Chen et al., 2014) and NIH3T3 fibroblasts (Nakatani et al., 2004).

Interestingly, in the current study, the low expression CYGB+ clone showed a trend towards migration inhibition. Together, these suggest CYGB's effect on migration is dependent on cell type as well external factors like stress.

Based on the fact we saw different migratory responses with different CYGB over-expression levels, one explanation is that cell migration outcome is sensitive to the level of CYGB expressed. A similar concentration-dependent effect on migration has been previously reported in human vascular smooth muscle cells in relation to PDGF-β receptor signalling where high concentrations of PDGF-β is inhibitory whilst lower amounts is stimulatory (Clunn et al., 1997), and this was dependent on FAK phosphorylation (Hauck et al., 2000). FAK signalling has been linked to activation of Rac1 GTPase that generates ROS to oxidise low molecular weight protein tyrosine phosphatases (LMW-PTP) and subsequently activate RhoA, so it is possible that as an antioxidant, CYGB might intervene directly or indirectly in this (see section 7.1 for more detail). Alternatively, the difference between migratory behaviour in CYGB+ clones observed in this study and that observed by other groups may also be simply due to cell type-specific properties that would influence migration, such as differences in cell surface ECM receptors.

To confirm the migratory phenotype exhibited by high expressing CYGB+ clone could be reversed, CYGB siRNA was transfected in order to knockdown expression of the globin. Whilst *CYGB* knockdown did cause a reversion in phenotype in high CYGB+ clones, there were problems with the negative control siRNA and further knockdown experiments are required to fully confirm the data. Nevertheless, the fact we observe the same migratory response in two independent CYGB+ cell clones relative to three independent NCE

controls strengthens the likelihood of the conclusion that medium to high CYGB over-expression causes an enhanced migratory response.

Antioxidants have been mostly associated with cell motility inhibition, such as the case of catalase over-expressing breast cancer cells (Glorieux et al., 2011). However, higher levels of CYGB could reduce total cellular ROS allowing modulation of redox-controlled RhoA GTPase signalling and this might be cell or context specific. Certainly, *CYGB* over-expression in fibroblasts has been linked to increased actin stress fibre formation and focal adhesion complex assembly (Nakatani et al., 2004) and these are known consequences of Rho GTPase activity (Arthur and Burridge, 2001; Parri and Chiarugi, 2010).

5.3.2 The Effect of CYGB on Proliferation

The influence of CYGB over-expression on proliferation was determined on a daily basis with the crystal violet assay, which found CYGB over-expression was mildly associated with a reduced cell number compared to the NCE control; aside from day two where the growth of the two highest over-expressing CYGB+ clones exceeded the NCE controls. The CYGB+ clones showed reduced proliferation one day, 3 days and 4 days (excluding LST54) after seeding. This is in agreement with other research groups who found CYGB to significantly influence the proliferation capacity of cells. Liquid colony formation assays showed breast cancer NCI-HCC1569 cells stably over-expressing CYGB had impaired growth relative to the control that lacked CYGB (Shivapurkar et al., 2008) and this effect was also seen in osteosarcoma U2OS cells (John et al., 2014) and melanoma G361 cells (Fujita et al., 2014). However quite whether CYGB promotes or inhibits proliferation is still under debate and the data we obtained in this study was not

conclusive, as a consistent trend between CYGB+ and NCE controls was not observed across the time course. *CYGB* knockdown could significantly reduce proliferation in fibroblast cells (Halligan et al., 2009), whilst CYGB over-expression in pulmonary H358 adenocarcinoma cells (Oleksiewicz et al., 2013) and ovarian SKOV-3 cells (Chen et al., 2014) was reported to increase cell growth. Therefore, it is likely that cancer cell proliferation in association with CYGB expression involves a more complex regulation mechanism that is cell type dependent.

5.3.3 CYGB Expression and Cisplatin Resistance

CYGB+ clones demonstrated enhanced survival following treatment with cisplatin for 48 h compared to NCE controls, and this correlated with reduced oxidative stress and intrinsic apoptosis pathway activation (see section 6.3.1). This confirms many previous reports showing CYGB to protect the cells against cell death induced by oxidants (see section 1.5.3.2), but this is the first to demonstrate an anti-apoptotic function for CYGB against cisplatin-induced cell death. Cisplatin exerts its cytotoxicity by triggering cellular responses to DNA damage and oxidative stress (see section 1.6.3.3.1), which are both processes protected by CYGB (see section 1.6.3.2.1 and 1.5.3), so it is unsurprising to observe greater survival after cisplatin treatment in CYGB+ clones. Tian et al (2013) demonstrated lower caspase 3 activity (the downstream executer caspase activated by caspase 9) in hypoxic brain tissue isolated from CYGB over-expressing rodents compared with controls. Other groups have similarly reported lower caspase-mediated cell death following oxidant stress when CYGB is over-expressed (Fujita et al., 2014; Jourd'heuil et al., 2012; Singh et al., 2014). We also find caspase 9 activity is reduced within CYGB+ clones in chapter 6 (see section 6.3.1), which is supportive of the observed cisplatin resistance in this chapter.

5.3.4 CYGB Expression Alters Cell Cycle Response to Cisplatin

The slightly greater S:G1 ratio of CYGB+ clones we found before cisplatin treatment is consistent with reports of CYGB over-expression impairing proliferation in untreated cells (see section 1.6.3.2.1). Our study also found asynchronised medium and high over-expression CYGB+ clones underwent initial cisplatin-induced S-phase arrest at 24 h of 7.5 μM treatment and from 48 h showed an increase in the ratio of G1:S-phase cells relative to NCE controls that largely remained in S-phase arrest (with a low G1:S-phase ratio). Furthermore we found the increase in G1:S ratio depended on the level of CYGB over-expression, with a greater G1:S-phase ratio being observed with increasing CYGB over-expression. In agreement with our data, Chen et al (2014) found CYGB over-expressing ovarian SKOV-3 cells showed greater accumulation of cells in G1-phase compared to S-phase and also that *CYGB* knockdown reversed this ratio, which the authors' attributed to CYGB arresting cells at G1. Their study contrasts with the findings of Latina et al (2015) who found no change in cycle distribution with *CYGB* knockdown. However, cisplatin-resistant NSCLC cells are known to increase the distribution of cells into G1 (Barr et al., 2013), and U2OS human osteosarcoma cells over-expressing CYGB and treated with doxorubicin (John et al., 2014) also demonstrate this. The increased G1:S ratio we found associated with CYGB over-expression is therefore consistent with other groups' findings and also with our other observations that CYGB+ clones have resistance to cytotoxicity (see sections 5.2.3) and higher cell numbers in G1-phase after cisplatin exposure.

The higher G1:S-phase ratio seen with increasing CYGB over-expression at 48 h and 72 h following cisplatin treatment, suggests these cells are either more able to promote cell cycle progression or that they are more arrested in G1 than NCE controls. Cyclin D1

levels in CYGB+ clones were higher than NCE controls at this concentration and thus supports the cell cycle changes observed, suggesting the increased G1-phase distribution in cisplatin-treated CYGB+ clones is likely to be related to increased cell cycle progression. To our knowledge, there is little pre-existing evidence for CYGB's effect on the cell cycle in response to genotoxins, so here we discuss the possible mechanisms by which CYGB may be eliciting its effect on the cell cycle we see in this study.

Cisplatin DNA damage is detected by ATR kinase that activates CHK1 to stimulate p53-p21 signalling downstream and triggers the G2 checkpoint of the cell cycle (He et al., 2011) (see section 1.6.3.3.1, Figure 41). The fact we observed altered expression of p53-regulated transcripts after cisplatin in CYGB+ clones (see section 4.2.4) and found this was associated with higher expression of CHK1, p21 and p53 in at least two of the three CYGB+ clones here, suggests the CHK1-p53-p21 signalling route may be slightly more active in CYGB+ clones and, by consequence, DNA damage repair signalling at the G2 checkpoint (Figure 42). This is consistent with previous reports that CYGB is protective against oxidative DNA damage (see section 1.5.3.2 and 1.6.3.2.1) as greater activity of repair machinery would presumably increase a cells' ability to overcome damage. This theory is consistent with the down-regulation of cell cycle and DNA repair response transcript *GADD45A* that we observed in CYGB+ clones in section 4.2.4. The increase in expressed p21 in CYGB+ clones is in agreement with the observations of John et al (2014) in CYGB over-expressing U2OS osteosarcoma cells treated with etoposide and also with those of Thuy et al (2011). Cisplatin was found to cause S-phase accumulation within all clones at 7.5 μM cisplatin, showing treatment may have acted to semi-synchronise the cells, which subsequently allowed for the cycle differences between CYGB+ and NCE clones to become visible. Cisplatin negatively affected cycle progression

by activating the G2 checkpoint, which is shown by higher numbers of S-phase cells at 24 h and G2 cells at 48 h in all clones relative to their untreated controls. The increasing G1:S ratio in CYGB+ clones from 48 h implies these clones are able to overcome the cisplatin-induced G2 checkpoint arrest and re-enter G1, where they continue cycling. Meanwhile, NCE controls continue to block progression at G2, with far fewer cells re-entering at G1. If we had examined distributions at an intermediate time of 60 h, it would be anticipated a lower number of CYGB+ clones in G2 would be seen. The increased transit through G1 in CYGB+ clones is supported by higher levels of cyclin D1 expression, which is one of the E2F-regulated genes required for S-phase entry (Figure 41). Cyclin D1 has also been reported to have potential for ROS regulation, since its transcription promoter contains regulatory sites for redox-regulated proteins including NFκB (Menon and Goswami, 2007).

The CYGB expression-dependent increase in G1:S-phase ratio implies these cells can evade cisplatin-induced cytotoxicity more effectively than NCE controls, which is in agreement with the reduction in cisplatin-induced cell death (see section 5.2.3) and oxidative stress (see section 6.3.3) in CYGB+ clones. This trend may be due to an increased ability to enter G1, decreased ability to leave S-phase or increased ability to overcome the G2 checkpoint block for re-entry to the cycle. More detailed studies are needed to investigate this. CYGB over-expression may act to 'prime' the cells to respond more quickly and effectively to cisplatin stress enabling cells to pass the G2 checkpoint, divide in M phase and re-enter the cell cycle at G1. This 'priming' may be mediated either by the direct control of cell cycle signalling or modulation of redox homeostasis that influences cell cycle progression.

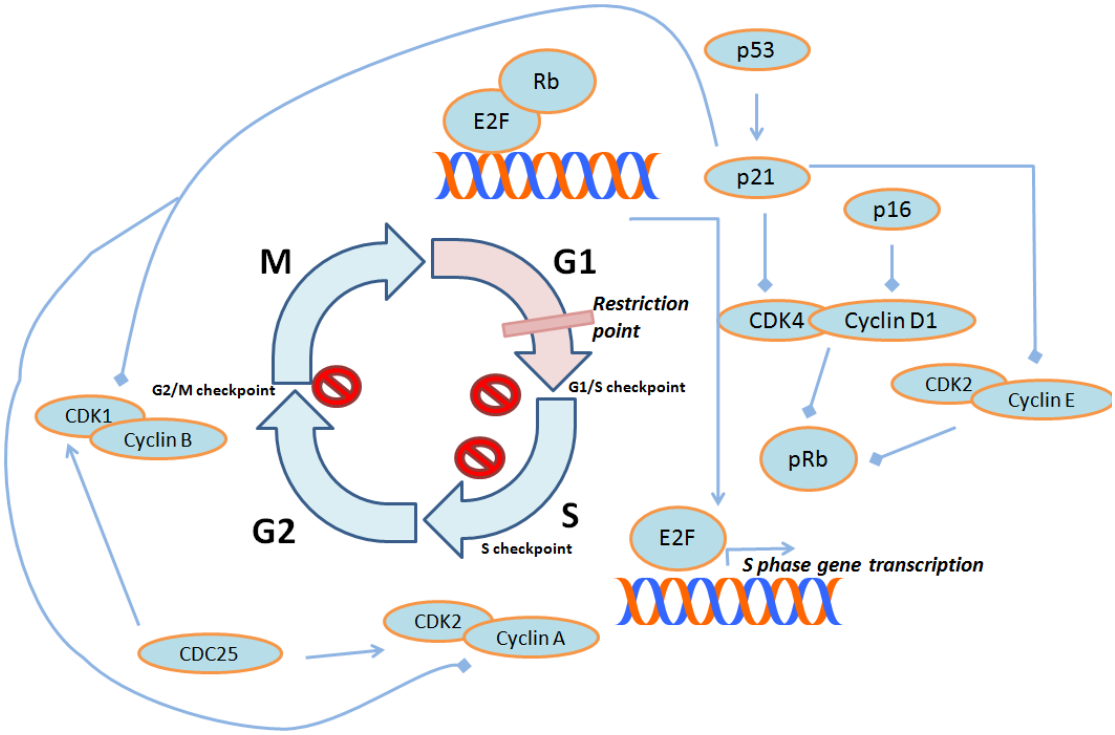

Figure 41 – Cell Cycle Regulation and Checkpoints

The cell cycle is separated into four major phases - growth phase 1 (G1), synthesis phase (S), growth phase 2 (G2) and mitosis (M). Levels of oxidants are highest in G1 (shown by the pink arrow), whilst the rest of the cycle has a more reducing environment. The S-phase is the point wherein DNA is replicated ready for packaging into the two daughter cells created by M phase. The first gap phase (G1) contains a crucial "restriction point" that enables the cell to respond to environmental cues to orchestrate signalling for the advancement or cessation of the cell cycle. The progression from G1 into S-phase begins with cyclin D1 association with CDK4 or CDK6, which triggers the hyper-phosphorylation of retinoblastoma protein (RB) to liberate the transcription factor E2F for it to activate S-phase gene transcription of genes such as cyclin D1 and components of the DNA replication machinery (Menon et al., 2007). p21 (a transcriptional target of p53) is a key cycle regulator that hyper-phosphorylates and inactivates retinoblastoma protein, and inhibits CDK/cyclin activity (Dutto et al.,2015). CDC25 is a redox sensitive protein that can control the activities of CDK2 cyclin complexes. There are three major checkpoints that need to be overcome by cells for them to progress successfully through the cell cycle - G1/S, intra-S and G2/M. The G1/S checkpoint prevents replication happening in the presence of damaged DNA. The intra-S checkpoint triggers repair of replication and DNA damage errors before allowing cycle progression. The G2/M checkpoint prevents entry of cells to M phase if they have unrepaired damage from the two earlier checkpoints or damage from G2. Figure adapted from Chiu et al., (2012).

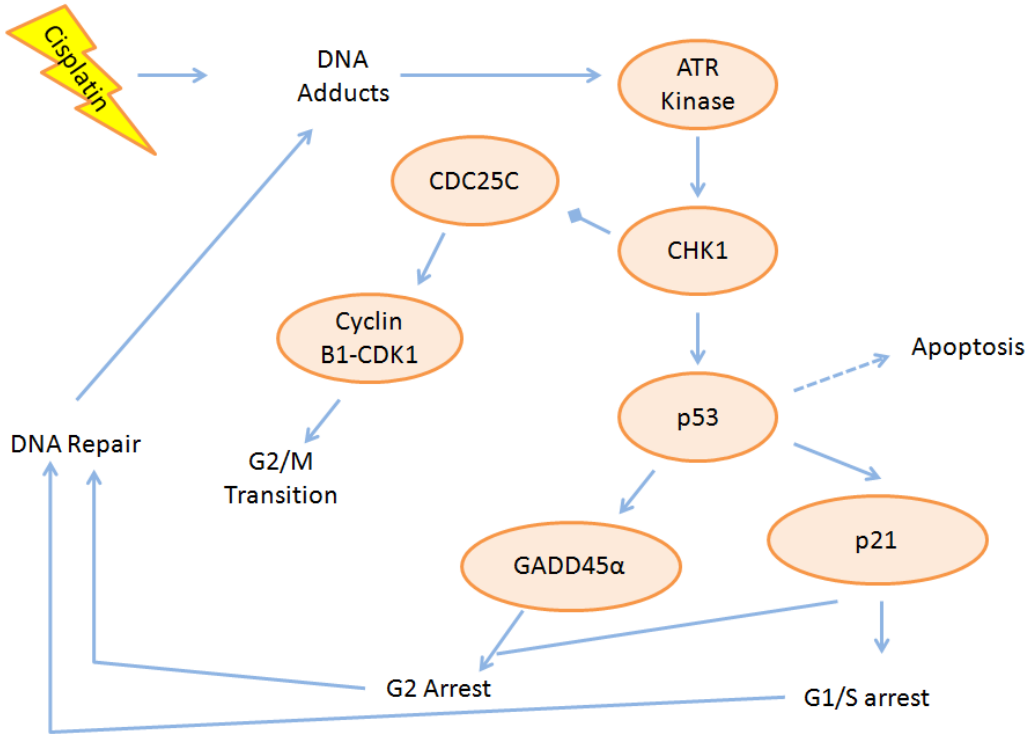

Figure 42 – The G2 Checkpoint in response to cisplatin.
To ensure integrity of the genome from one generation of cells to another, there are checkpoints between each pair of phases in the cell cycle. Cisplatin causes DNA adduct formation. During the DNA damage response at G2/M phase, cell cycle progression is halted whilst repair is attempted and, if successful, the cycle is re-started. The G2/M checkpoint prevents entry of cells to M phase if they have unrepaired damage from the two earlier checkpoints or damage from G2. ATR kinase is activated upon the detection of DNA damage and promotes the phophorylation and activation of CHK1, which in turn activates CDC25 that negatively regulates the cyclinB/CDK1 complex that manages the progression of G2 to M phase. CHK1 also activates p53 signalling that activates transcription of factors like GADD45α and p21 that inhibit the cell cycle and stimulate DNA damage repair pathways for less problematic damage, whilst more irreparable damage promotes the activation of apoptotic signalling. Adapted from Bucher and Britten (2008) and Kastan et al. (2004).

There have been previous reports suggesting CYGB can stabilise and activate p53 (John et al., 2014) and also that the globin is a transcriptional target of another member of the p53 family, ΔNp63 (Latina et al., 2015). The link between CYGB over-expression and higher p53 levels is also implied by our in-cell ELISA data in this chapter. Although we did not observe a reproducible difference between all CYGB+ clones and NCE controls, we observed that medium and high over-expressing clones showed lower p53 expression before treatment, whilst low and medium expressing clones showed higher p53 induction following 7.5 μM cisplatin. We are assured p53 is highly likely to be wildtype in these cells since direct sequencing of the most commonly mutated exons did not show any evidence of polymorphisms (see section 3.2.8). Together with the observed p53-related transcript regulation in section 4.2.4, the data of this chapter implies p53 could be important in mediating the CYGB+ clone response to cisplatin.

Aside from increasing p53 signalling at the G2 checkpoint, CYGB may also be increasing cell cycling through its ability to decrease cellular ROS. There is increasing evidence linking cell cycle control to redox state, with ROS being higher in G1-phase than elsewhere in the cycle and oxidative stress reported to inhibit cycle progression and trigger apoptosis (Burhans and Heintz, 2009; Chiu and Dawes, 2012; Menon and Goswami, 2007). It was shown in murine embryonic fibroblasts (Menon et al., 2003), CH72-T4 carcinoma cells (Ibanez et al., 2011) and murine aorta endothelial cells (Onumah et al., 2009) that stalling in G1-phase can be triggered by the presence of antioxidants, demonstrating the importance of endogenous ROS for G1 entry. There are also factors within the G2 checkpoint that are redox-controlled and CYGB may be able to modulate these through its antioxidant ability (for more detail, see section 7.1).

CYGB over-expression has been reported to protect against lipid peroxidation (see section 1.5.3.2 and 1.6.2) and G2-phase is the stage where membrane lipids are synthesised along with ATP ready for mitosis (Moreira et al., 2015). So it is feasible that CYGB over-expression might even protect against extensive damage to membranes and mitochondria metabolism during this phase caused by cisplatin treatment that would normally lead to cell death, and instead favour survival and repair signalling rather than signalling for death and apoptosis. Therefore, the ability of CYGB+ clones to re-enter the cell cycle more readily than NCE clones suggests promotion of the G2 checkpoint for DNA repair and then of re-entry into the cell cycle.

At 15 μM cisplatin, the effect of CYGB over-expression seems more complex. The protective effect of CYGB over-expression at this concentration appears to be lost, with a lower G1:S ratio being evident in medium and high over-expressing CYGB+ clones, indicating the cells are unable to escape from cisplatin-induced cycle arrest, unlike the NCE controls that appear to gradually reach similar cycle distributions by 72 h post-treatment to those shown before cisplatin treatment. This is the opposite of the trend observed at 7.5 μM cisplatin and may be related to the more extensive damage caused by doubling the cisplatin concentration. This would imply that whatever the protective survival mechanism is that CYGB employed against 7.5 μM cisplatin stress becomes detrimental at the higher concentration and seems to facilitate persistence of the cisplatin-induced cycle arrest rather than overcome it, but as we show in section 6.2.1, this does not result in caspase 9-mediated apoptosis. Further and more detailed cell cycle studies are certainly necessary to determine why CYGB over-expression can lead to two distinct cell cycle regulations depending on the cisplatin concentration.

CHAPTER SIX:

Investigating the Mechanism of Phenotypic Change

6.1 Introduction

The previous chapter showed CYGB over-expression was associated with changes to migration and proliferation, and also with increased survival and altered cell cycle distributions following cisplatin treatment. Furthermore, we revealed cisplatin tolerance in CYGB+ clones may involve CYGB-based modulation of the p53 signalling network because of increased induction of factors of the CHK1-p53-p21 signalling cascade (chapter 5) and regulation of p53-controlled stress response transcripts (chapter 4). This chapter focuses upon investigating the underlying mechanisms of these changes.

Recently, studies have started to look beyond a simple anti-oxidant ROS scavenging role for CYGB, and have instead commenced investigation into whether CYGB can re-locate intracellularly to organelles or interact with other proteins to mediate its effects. For instance, CYGB over-expression in U2OS osteosarcoma cells was found to reduce the ubiquitin-mediated degradation of p53 (John et al., 2014) and also alter both cell cycle distributions and associated regulatory proteins without treatment (Chen et al., 2014) or after genotoxins (John et al., 2014) (see section 5.3.4). Moreover, CYGB has been reported to react with lipid peroxides and this was proposed to be the basis of a potential intracellular second messenger system (Reeder et al., 2011). There has also been a report to suggest that low oxygen stress may re-locate CYGB towards the mitochondria (Ye et al., 2006).

There have also been studies that show CYGB participates in apoptosis as brain tissue from rodents over-expressing CYGB and injured by hypoxia-ischemia have reduced caspase 3 activity (Tian et al., 2013), and this was similarly reported in murine

myoblasts with *CYGB* knockdown in association with reduced *Bcl-2* and increased pro-apoptotic *Trp73* transcripts (p73, a p53-related protein) (Singh et al., 2014). Similarly, He et al (2011) demonstrated in HSC-T6 rodent fibroblasts with thioacetamide (TAA)-induced fibrosis that if CYGB was added to cells extracellularly, there was a decrease in Bcl-2 expression, which is a suppressor of Bax-mediated mitochondrial permeability transition pore (mPTP) opening for the release of apoptosome assembly factors (Siddiqui et al., 2015). This is of note because phosphorylated Bcl-2 has also been reported to reduce complex 4-generated mitochondrial ROS, and also bind Rac1 GTPase, p53 and other proteins (Chong et al., 2014).

To begin exploration of the mechanisms by which CYGB over-expression elicits the phenotypes found in chapter five, we examined ROS and reduced glutathione levels, mitochondrial reductase activity, and caspase 9 activation. We found that with cisplatin treatment, CYGB-expressing cells showed diminished caspase 9 and mitochondrial reductase activity, a reduction in both total cellular and mitochondrial ROS and higher reduced glutathione (GSH) levels when compared with NCE controls. These are in agreement with the cisplatin resistance of CYGB+ clones demonstrated in chapter 5.

6.2 Results

6.2.1 Caspase 9 Activity

To further investigate the mechanism by which CYGB over-expression could improve survival after cisplatin treatment, activation of caspase 9 was determined. A positive control (200 μM etoposide, 48 h) was included to demonstrate the functionality of the assay (caspase 9 induction reached 687.25 ± 120.8 RLU $\mu g^{-1}ml^{-1}$).

Caspase 9 is an initiator caspase of the intrinsic apoptotic pathway and is a key mediator of cisplatin-induced cell death in ovarian and head and neck cancer cell lines (Kuwahara et al., 2000; Singh et al., 2013). As expected, caspase 9 activity increased following 48 h cisplatin treatment (Figure 43). Mean caspase 9 activity within high (LST421) and medium (LST54) over-expressing CYGB+ clones was consistently lower after cisplatin treatment.

Whilst caspase 9 induction reached 640.25 RLU $\mu g^{-1}ml^{-1}$ (± 57.01) in NCE clones following 48 h treatment with 7.5 μM cisplatin, caspase 9 activity in LST421 and LST54 clones was only induced to 575.90 RLU $\mu g^{-1}ml^{-1}$ (± 79.63) and 544.51 RLU $\mu g^{-1}ml^{-1}$ (± 95.57), respectively. At 15 μM cisplatin, there was a the trend towards reduced caspase 9 activation in CYGB+ clones relative to NCE clones, where there was a CYGB expression-dependent reduction in caspase activity (Figure 43). The smallest induction of caspase 9 at 15 μM cisplatin was observed in LST421 clones (605.99 RLU $\mu g^{-1}ml^{-1}$ ± 74.59), with the largest response observed in LST32 clones (754.656 RLU $\mu g^{-1}ml^{-1}$ ± 44.04). These results suggest CYGB+ clones exhibit a trend toward lower caspase 9 activity following cisplatin treatment in this cell model. The difference in caspase 9 activity in LST421 at 0 μM ($p = 0.045$) and 15 μM ($p = 0.005$), was significant, as assessed by t-test (paired).

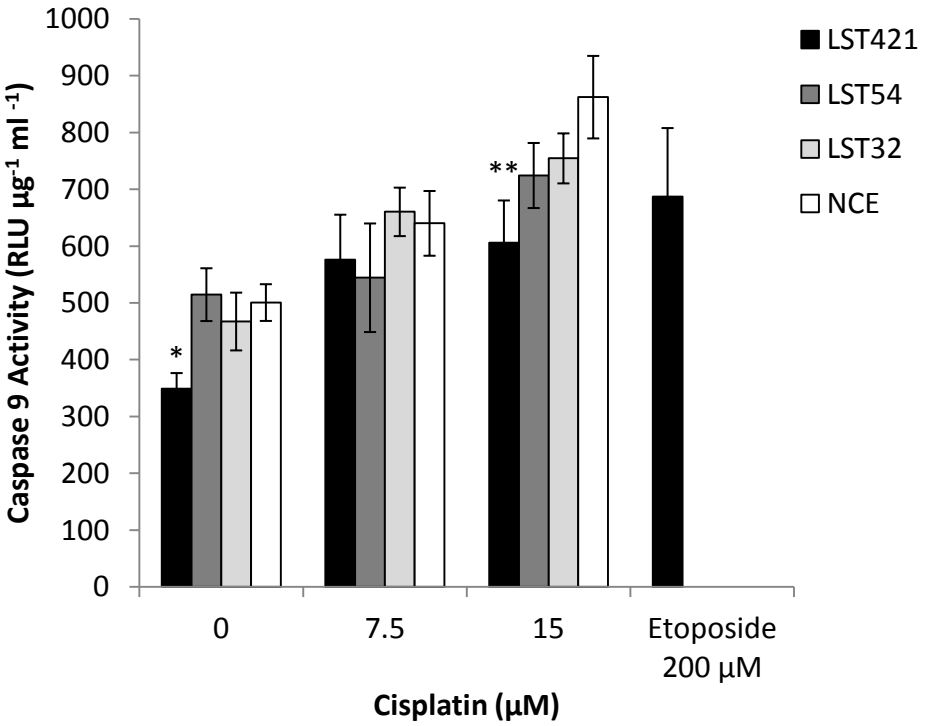

Figure 43 – Effect of CYGB on cisplatin-induced caspase 9 activation.
Cells were treated with 0 µM, 7.5 µM or 15 µM cisplatin for 48 h, after which the luminescent caspase 9 activity assay was carried out. Luminescent measurements were taken after 45 min and corrected for protein content through the Bradford assay. Data are the mean of 4 biological replicates (in technical duplicate) ± standard error. A positive control for caspase activation was included using the LST421 clone treated with 200 µM etoposide for 48 h. * $p < 0.05$, ** $p = 0.01$ (t-test (paired)).

6.2.2 Mitochondrial Reductase Activity

Mitochondrial reductase activity was assessed using the MTT assay. Cells were cultured in the presence or absence of 7.5 μM cisplatin for 48 h before the MTT assay was carried out as described in section 2.9.2. MTT absorbance values were corrected for cell density as described in section 2.9.1. CYGB+ clones showed reduced mitochondrial activity compared to NCE controls both before and after cisplatin treatment, although the greatest difference occurred prior to treatment (Figure 44). Untreated CYGB+ clones LST421, LST54 and LST32 clones exhibited a trend of decreased MTT reduction (0.78 a.u. ± 0.06, 0.63 a.u. ± 0.03 and 0.63 a.u. ± 0.06, respectively) when compared with NCE controls (0.90 a.u. ± 0.10). However, there were no statistically significant differences between any of the untreated CYGB+ and NCE clones (one-way ANOVA, post-hoc Tukey, $p = 0.216$). Following cisplatin treatment, CYGB+ clones LST421, LST54 and LST32 clones exhibited a less pronounced decrease in MTT reduction (0.62 a.u. ± 0.08, 0.59 a.u. ± 0.04 and 0.51 a.u. ± 0.04, respectively) relative to NCE controls (0.67 a.u. ± 0.07). There were no statistically significant differences between any of the cisplatin treated CYGB+ clones and NCE control (one-way ANOVA, post-hoc Tukey, $p=0.690$).

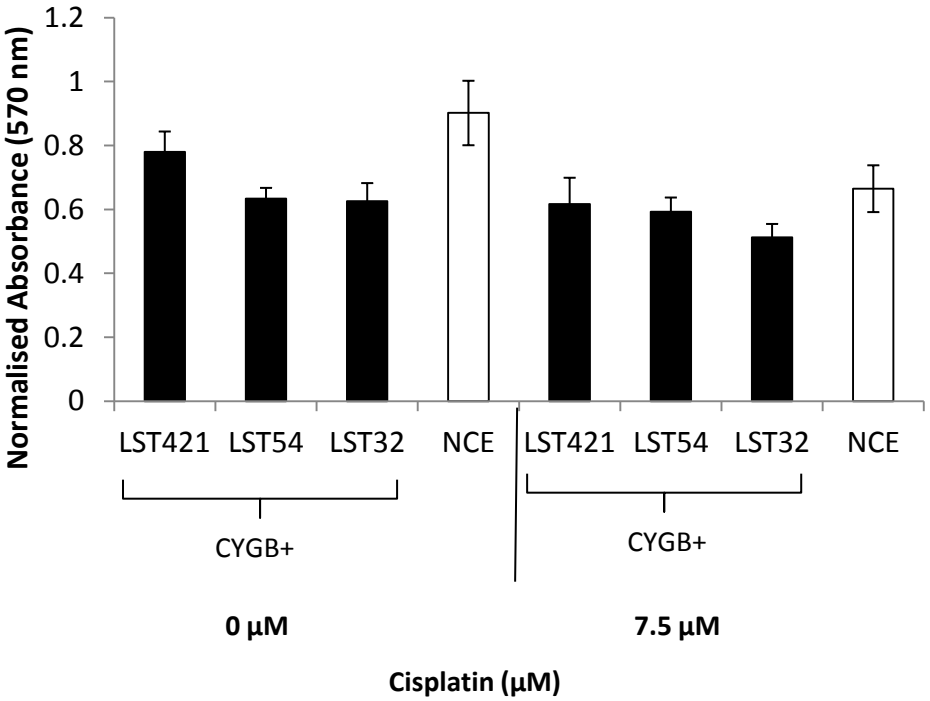

Figure 44 – Effect of CYGB expression on mitochondrial reductive capacity.
Cells were cultured in the presence of absence of 7.5 µM cisplatin for 48 h prior to MTT assay, followed by the crystal violet assay to enable normalisation to cell number. Blank-corrected MTT absorbance was normalised to the blank-corrected crystal violet absorbance to correct the MTT measurement for cell number. Results for three NCE clones were averaged. Data points are the average of three biological replicates. Mean blank-corrected absorbance values were calculated for each clone ± standard error. There were no statistically significant differences compared to NCE control, one-way ANOVA with post-hoc Tukey, $p > 0.05$.

6.2.3 Total and Mitochondrial Levels of ROS

The mode of action for cisplatin involves oxidative stress and this is dependent on mitochondria-generated ROS (Santos et al., 2007). Indeed, cisplatin-resistant cancer cells are less susceptible to oxidative stressors and research is underway to identify antioxidants specific to the mitochondria (such as MitoQ) that might help minimise the detrimental oxidant-induced side effects *in vivo*, such as impaired renal function (Mukhopadhyay et al., 2012). Knowing that CYGB is an antioxidant and we herein found its over-expression is associated with modulation of cisplatin-induced gene expression changes (see section 4.2.4) and cell survival following increasing cisplatin treatment (see section 5.2.3), we investigated whether cisplatin resistance in CYGB+ clones could correspond to reduced levels of either total or mitochondrial ROS.

As expected, treatment of all clones with cisplatin (48 h) resulted in an increase in total cellular ROS (Figure 45). Interestingly, prior to treatment, CYGB+ clones exhibited lower levels of ROS compared to NCE clones; especially within medium (LST54, 26.5 RFU ± 5.15) and high (LST421, 27.3 RFU ± 2.21) expressing CYGB+ clones (not significant, Kruskal-wallis test, $p = 0.833$). CYGB+ clones also had reduced total ROS after treatment with 7.5 μM cisplatin, but this was not significant (one-way ANOVA, $p = 0.412$, Figure 45). At this concentration, high CYGB over-expressing clone LST421 showed the strongest suppression of ROS (25.0 RFU ± 7.44), whilst LST54 (medium CYGB over-expression) gave milder suppression (47.2 RFU ± 12.75) when compared with NCE controls (57.4 RFU ± 15.97). At 15 μM cisplatin, high CYGB over-expressing clone LST421 shared the strongest suppression of ROS (28.70 RFU ± 2.24, (non-significant, Kruskal-wallis test, $p = 0.332$)), whilst LST54 (medium CYGB over-expression) gave milder suppression (64.75 RFU ± 21.75) when compared with NCE controls (68.70 RFU

± 5.63). Clones were also treated with 100 μM hydrogen peroxide for 2 h as a positive control and in line with previous reports that CYGB is a peroxidase, high and medium over-expressing CYGB+ clones had lower total ROS levels (Li et al., 2007; Nishi et al., 2011), but neither were statistically significant changes (t-test (unequal variances), $p = 0.451$, and $p = 0.646$, respectively).

Quantification of mitochondrial superoxide revealed a substantial increase following both cisplatin concentrations in all clones, whilst a smaller increase was observed following 100 μM hydrogen peroxide (Figure 45). At all cisplatin concentrations, there was a trend towards reduced mitochondrial superoxide in CYGB+ clones, that was dependent on CYGB expression; with superoxide being increasingly diminished with increasing CYGB over-expression. At 7.5 μM cisplatin, LST421 and LST54 clones demonstrated the largest (but non-significant) reduction in superoxide levels (8887 RFU (± 1760.5) and 10488 RFU (± 2384.1), respectively) from the NCE control (12781 RFU ± 3592.1) (not significant, one-way ANOVA, $p = 0.832$). This trend was also observed following 15 μM cisplatin treatment (LST421, 9965.7 RFU ± 961.5 and LST54, 13734 RFU ± 373.9) compared to NCE controls (16424 RFU ± 2020.5), and this was statistically significant between LST421 and NCE (one-way ANOVA, post-hoc Tukey, $p = 0.038$). Differences in superoxide between clones treated with 200 μM hydrogen peroxide were also apparent, with all CYGB+ clones showing approximately half the level of superoxide of the NCE controls (Figure 45).

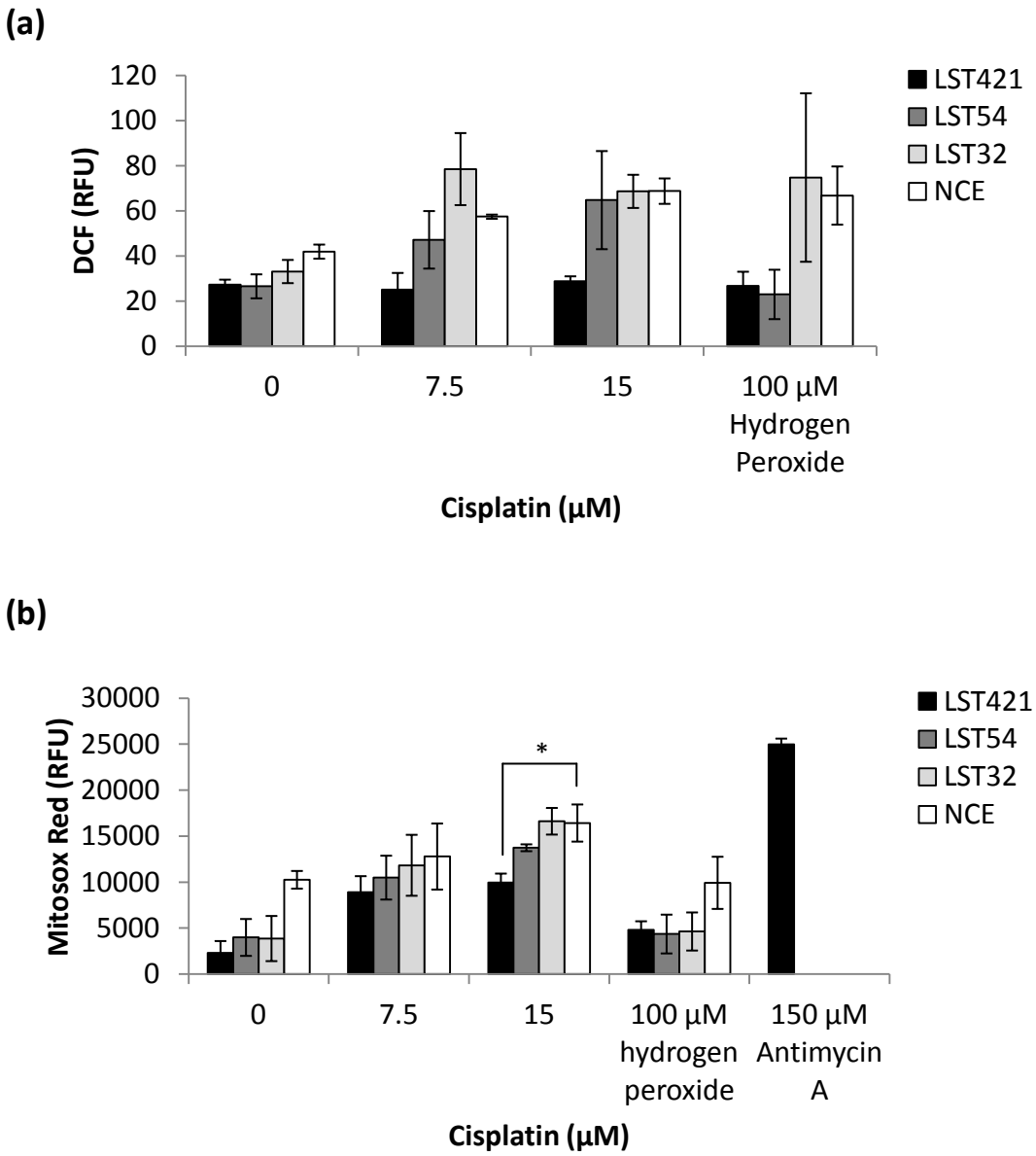

Figure 45 – Effect of CYGB expression on ROS.

(a) Cells were seeded into 6 well plates and treated with cisplatin for 48 h (7.5 µM and 15 µM), before cells were incubated for with $DCFH_2DA$ dye and assessed for fluorescence by flow cytometry, as described in section 2.11.1. Cells were also incubated with 200 µM hydrogen peroxide (H_2O_2) for 2 hs to induce cellular oxidative stress as a positive control. Results were corrected for a no dye control for each cell clone. Data are the average of biological triplicates ± standard error. **(b)** For the Mitosox Red assay, cells were seeded and treated as before but after treatment, cells were incubated for 45 min with MitoSox Red dye and assessed for fluorescence with a plate reader, as described in section 2.11.2. LST421 cells were also incubated with 150 µM antimycin A for 1 h as a positive control to induce mitochondrial oxidative stress (via inhibition of complex 3 of the electron transport chain, leading to uncoupling of electron transfer and superoxide production). Results were corrected for a no dye control for each cell clone. Data are the average of biological triplicates ± standard error. Compared to NCE control (one-way ANOVA with post-hoc Tukey, * $p < 0.05$).

6.2.4 Glutathione Levels

Concentrations of GSH can be utilised as a biomarker of oxidative stress. Additionally, nucleophillic GSH is an inhibitor of cisplatin cytotoxicity by inhibiting its activation reactions with water, and elevated cellular GSH has been linked to cisplatin resistance both clinically and *in vitro* (Godwin et al., 1992; Kasherman et al., 2009; Siddik, 2003b). It would therefore be beneficial to establish whether modulation of GSH levels is involved in the mechanism of CYGB protection against cisplatin-induced cell death (Figure 35, Figure 43) and oxidative stress (Figure 45).

As expected, all clones showed decreasing GSH levels following cisplatin treatment, although no statistically significant differences were found between CYGB+ and NCE controls (Kruskal-Wallis test, $p = 0.585$, Figure 46). High over-expressing CYGB+ clones exhibited higher GSH levels than NCE controls before and after 15 μM cisplatin treatment, although this was not statistically significant (Kruskal-Wallis test, $p = 0.343$). Untreated LST421 and LST54 CYGB+ clones had GSH concentrations of 17.13 nmoles per μg protein (± 3.48) and 11.75 nmoles per μg protein (± 4.73), whilst NCE clones had a GSH concentration of 8.50 nmoles per μg protein (± 2.06). Following treatment with 15 μM cisplatin, the trend for elevated intracellular GSH concentrations within CYGB+ samples persisted, with LST421 having 14.82 nmoles GSH per μg protein (± 4.32) and LST54 having 6.98 nmoles per μg protein (± 2.38), relative to NCE controls where GSH levels reduced by approximately half that of their respective untreated control (4.79 nmoles μg protein ± 0.95).

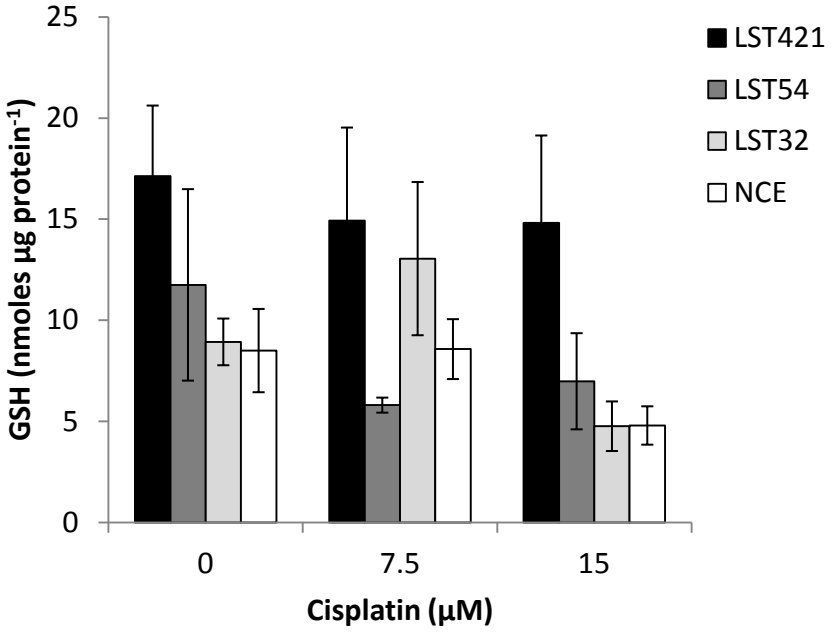

Figure 46 – Effect of CYGB expression on cellular levels of GSH.
Cells were seeded into 6 well plates and treated with cisplatin for 48 h, before total reduced glutathione was quantified as described in section 2.11.3. A glutathione calibration curve was utilised to calculate the total quantity of reduced glutathione within the samples, expressed in nmoles. This was subsequently normalised to the total protein content of the sample ($\mu g ml^{-1}$), as assessed by the Bradford assay. Data are the average of biological quadruplicates ± standard error. A positive control of 48 h 100 µM hydrogen peroxide was included and 623.80 GSH nmole µg protein (± 7.78) was observed in NCE clones (data not shown). There were no statistically significant differences between group means (Kruskal-Wallis, $p > 0.05$).

6.3 Discussion

The previous chapter revealed CYGB+ clones exhibited greater cell survival following treatment with cisplatin at 7.5 μM and 15 μM, as well as altered cell cycle profiles and enhanced expression of p53, CHK1 and p21. To begin investigating the mechanistic basis of these effects, we assessed total and mitochondria ROS, total reduced glutathione concentrations, mitochondria reductase activity and caspase 9 activation in CYGB+ clones. In this chapter, we found all CYGB+ clones reduced mitochondrial reductase activity before and after cisplatin treatment compared to NCE controls. CYGB over-expression also associated with reduced caspase 9 activation, which is in agreement with the increased resistance to cisplatin-induced cell death found in chapter 5. Total and mitochondrial ROS levels were observed lower in CYGB-expressing cells before and after cisplatin treatment. This ROS reduction was mirrored by enhanced concentrations of reduced cellular GSH in CYGB+ clones compared to NCE controls. These findings are discussed in more detail in the following sections.

6.3.1 Caspase 9 Activity

The mechanism by which CYGB mediates survival is still not fully understood, but the finding that caspase 9-mediated cell death is impaired, supports the involvement of CYGB upstream of the intrinsic apoptotic cascade. Caspase 9 is the initiator caspase of the intrinsic apoptotic pathway, activated by the release of cytochrome c from the mitochondrial cardiolipin tether for assembly of the apoptosome that subsequently promotes caspase 3 activity for apoptosis to ensue. Reduced caspase 9 activity has been linked to cisplatin resistance in head and neck cancer cells (Kuwahara et al., 2003). CYGB has been shown to bind to cardiolipin (Reeder et al., 2011), so it is feasible that CYGB may reduce caspase 9 activity through binding to and protecting cardiolipin from

oxidation, or even through redox-control of mPTP that normally facilitates cytochrome c influx into the cytosol. These hypotheses are discussed in greater detail in section 7.1.

6.3.2 Mitochondrial Reductase Activity

We investigated the ability of CYGB+ cells to reduce MTT into its formazan precipitate with or without 48 h 7.5 μM cisplatin treatment. MTT reduction was noticeably impaired in CYGB-expressing cells compared to NCE clones, and this trend was also seen following 7.5 μM cisplatin, although the difference was less pronounced.

There are almost no studies investigating a metabolic role for CYGB, but Oleksiewicz et al (2013) reported NSCLC cells over-expressing CYGB reduced MTT more greatly than controls and this trend could be inverted with *CYGB* knockdown. This is different to our observation, suggesting this effect may be cell type-specific. The reduction of mitochondrial reductase activity we observe in CYGB+ clones is supported by depletion of mitochondrial superoxide, which together suggest that CYGB might impair mitochondria function. We found that although there were no tangible differences in ATP production in untreated cells with CYGB over-expression, oxygen consumption rates were slightly raised in a CYGB dose-dependent manner; albeit insignificantly to NCE controls (see section 3.2.7). This is in contrast to the study by Stagner et al (2009), but consistent with the study in CYGB over-expressing fibroblasts (Halligan et al., 2009).

MTT reduction depends on the availability of reduced cofactors like succinate, GSH or NAD(P)H (Kim et al., 2009) and mitochondrial succinate dehydrogenase and NAD(P)H are important in mediating the reaction (Berridge and Tan, 1993). CYGB detoxifies cellular ROS (see section 1.5.3.2), which would facilitate higher GSH concentrations prior to and following cisplatin stress (as seen in this chapter), which may theoretically

permit increased MTT reduction by maintaining a supply of reduced NAD(P) for the reaction. However, this is at odds with the observation that collectively CYGB+ clones show attenuated MTT turnover that persists under cisplatin treatment. Superoxide has been reported to promote MTT conversion into its formazan precipitate by providing electrons to the tetrazolium salt to mediate its reduction (Wang et al., 2011), so the observation of diminished reductive capacity in CYGB+ clones may simply be the indirect result of depleted superoxide, mediated by CYGB. It remains to be established whether CYGB can be actively involved in regulating metabolism. However, the changes we see in mitochondrial MTT turnover and superoxide generation independently of cisplatin treatment suggest CYGB can affect mitochondrial activity.

6.3.2 Oxidative Stress

As expected, cisplatin treatment led to increased oxidative stress across all clones. Both before and after cisplatin treatment, medium and high expressing CYGB+ showed lower total cellular ROS and superoxide compared with NCE controls and this was also true in the positive control treatment, hydrogen peroxide. This was supported by enhanced concentrations of GSH in medium and high expression CYGB+ clones, which is in agreement with CYGB over-expressing H_2O_2-treated lung cancer cells (Oleksiewicz et al., 2013). Together, these data corroborate with numerous studies showing that CYGB acts as an antioxidant to reduce oxidative stress. Although we could not produce statistically significant data for the Mitosox Red study aside from at 15 μM between the highest expressing CYGB+ clone and NCE controls, there is a clear trend of lower mean superoxide levels in CYGB+ clones independent of cisplatin treatment and this is a new discovery.

Superoxide dismutase activity has been suggested for CYGB (see section 1.5.2). In our experiments, we measured superoxide levels within a cellular system so it avoided the confounding factor of limited cofactor availability in the *in vitro* Trandafir et al (2007) study. There is potential for the probe to become oxidised in the cytoplasm on its way to the mitochondria (Mukhopadhyay et al., 2007). Nevertheless, the lower signal we obtained for this probe in CYGB+ clones is suggestive that CYGB may preferentially decrease free radical species from the mitochondria. Although CYGB has been found to be cytoplasmic by ourselves (see section 3.2.6) and others (see section 1.4), there are reports suggesting CYGB relocates to the mitochondria following hypoxic stress in C2C12 myoblast cells (Ye et al., 2006). If this is proved under cisplatin treatment, then it is feasible that following exposure to the pro-oxidant, CYGB localises to the mitochondria to rapidly quench excess superoxide leakage resulting from uncoupled electron transfer between complexes and thus protect the cell from cisplatin-induced oxidative damage. The same may also be true following hydrogen peroxide treatment, as we observed similar trends (see section 6.2.3). Using fluorescence microscopy to examine whether CYGB in our over-expressing clones localises to the mitochondria after cisplatin treatment would be beneficial in exploring this hypothesis.

Cisplatin has been reported to preferentially form adducts with mitochondrial DNA (Cullen et al., 2007; Olivero et al., 1997), in part because mitochondria DNA is close to the ROS-generating electron transport chain and lacks protective nucleic acid-associated histone proteins and nucleotide excision repair machinery (Cullen et al., 2007; Indran et al., 2011). Over-expression of manganese SOD (but not catalase) is able to reduce renal injury induced by cisplatin (Davis et al., 2001), and RNAi mediated knockdown of *SOD1*

impairs cisplatin resistance of ovarian cancer cells (Kim et al., 2010), which together implicates superoxide as a mediator of cisplatin toxicity.

Cisplatin has a greater tendency to form adducts mitochondrial proteins and particularly with voltage-dependent anion channels (VDAC) (Yang et al., 2006). VDACs are in the outer mitochondrial membrane to enable exchange of solutes between the cytoplasmic compartment and mitochondria (McCommis and Baines, 2012) and are regulated by many stimuli including lipids, ROS and calcium ions (Martel et al., 2014). Use of mitochondrial VDAC-inhibitors could stop the superoxide-triggered release of cytochrome c (Madesh and Hajnoczky, 2001) and reduce efflux of mitochondria complex 1-produced superoxide through VDAC (Lustgarten et al., 2012). The fact CYGB+ clones showed increased cell survival after cisplatin treatment (see section 5.2.3) and this corresponded to a decrease in both mitochondrial superoxide (see section 6.2.3) and caspase 9 activity (see section 6.2.1), suggests a hypothesis where during cisplatin treatment, CYGB scavenges superoxide locally at the mitochondria; theoretically involving control of VDAC, and depletes active caspase 9. Interestingly, when Singh et al (2014) found *CYGB* knockdown in C2C12 murine myoblasts could increase cytoplasmic cytochrome c concentrations, their mitochondrial protein marker VDAC was significantly increased. Assuming equal protein loading, this may important for our hypothesis. Indeed, *VDAC1* knockdown in NSCLC cells reduces cisplatin-induced apoptosis without superoxide depletion (Tajeddine et al., 2008).

Whilst high and medium levels of CYGB over-expression reduced cellular ROS and mitochondrial superoxide and this coincided with an increase in GSH concentration, the protective effect was lost in the lowest CYGB over-expressing clones. This implies high,

but not near-physiological levels of CYGB can protect against cisplatin-induced oxidative stress, and as we discussed in section 5.3.1, CYGB expression may require a threshold concentration to be reached to enable effective protection. Additionally, the fact we observed medium and high over-expression CYGB+ clones show better ROS scavenging and survival (see section 5.2.3) under cisplatin stress is particularly interesting, given the up-regulation of CYGB in subpopulations of oral cancers and other tumours (see section 1.6.3.2) and the resistance to chemotherapy reported for a subpopulation of cells within head and neck cancer that have lower ROS levels (Chang et al., 2014a), which future investigation might reveal to be one of the same.

CHAPTER SEVEN:

General Discussion

7.1 Summary

It had previously been reported that CYGB has a complex dual ability to act as both an oncogene or tumour suppressor that is likely to be context and cell type dependent (Oleksiewicz et al., 2013). Few mechanistic details exist to date for how CYGB actively elicits these changes, but it seems that its anti-oxidant and anti-apoptotic abilities are critical components of its activity, as shown within pathologies of cancer, fibrosis and oxygen stress (see sections 1.6 and 1.5.3.2). Although *CYGB* is silenced in many cancers, subsets of some tumour types such as head and neck cancer, display enhanced expression (see section 1.6.3.2.2), but *CYGB* expression *per se* was not a biomarker for predicting tumour occurrence. Solid tumours like OSC are successfully initially treated with a combination of radiation therapy and chemotherapeutic agents like cisplatin, but success rates of these are hampered by the emergence of drug and radiation resistance within the treated tumour (see section 1.6.3.3.1). Therefore, investigations into cisplatin resistance mechanisms are important.

As CYGB has been previously shown to be cytoprotective against oxidative stress and its expression appears conditionally modulated in head and neck cancer, the primary objective of this thesis was to investigate the mechanism of CYGB action in response to stress within a head and neck cancer context. Acquired cisplatin resistance has been found to be a barrier to successful treatment of head and neck cancer, and its mechanism of cytotoxicity in part involves oxidative stress damage, so cisplatin was chosen as a relevant stressor for the experiments within this thesis. As the model for head and neck cancer, we chose to use PE/CA-PJ41 oral squamous cell carcinoma cells that had negligible endogenous CYGB expression. The results of chapter 3 show the

generation of the stable CYGB over-expression oral cancer *in vitro* model (CYGB+) and its validation. We then used this new model to study how CYGB expression influenced the cancer cell phenotype in response to cisplatin, with the aim of developing a greater understanding of CYGB function. To our knowledge, this is the first study to investigate how CYGB over-expression can influence cisplatin-induced cytotoxicity in oral cancer cells. Furthermore, we confirmed previous reports that CYGB could diminish total cellular ROS as previously reported by other groups (see section 1.5.3.2), but the work of chapter 6 has revealed for the first time that CYGB over-expression was linked to depletion of mitochondrial superoxide in particular, and this was further associated with higher cellular levels of GSH.

The data presented in chapter 4 showed CYGB over-expression was associated with significant changes to transcriptional targets related to the stress response, motility, and cell cycle regulation. These transcripts add to the possible downstream effectors of CYGB function already identified (Table 4 and Figure 30) and show these changes to the transcriptome by CYGB over-expression may facilitate its affects on phenotype. Further investigation also showed for the first time that CYGB over-expression enhances the response of p53-regulated target genes following cisplatin treatment. The transcriptional changes associated with CYGB over-expression identified by the microarray study could also support the phenotypic findings of chapters 5 and 6.

Subsequently, we explored whether CYGB over-expression could cause an altered response to cisplatin at the phenotype level, and the results for this are presented in chapter 5. We showed CYGB over-expression was associated with resistance to cisplatin-induced cell death, involving reduced caspase 9 activation. We also observed CYGB over-

expression was associated with decreased superoxide and total cellular ROS, and higher GSH concentrations following cisplatin treatment. This indicated the resistance to cisplatin-induced cell death was in part facilitated by reducing oxidative stress. Our finding that caspase 9 activity is reduced in CYGB-expressing cells is consistent with the lower caspase 3 activity found by Tian et al (2013) in hypoxic brain sections of CYGB over-expressing mice and with the reduced apoptosis observed in by others in the context of CYGB over-expression (Jourd'heuil et al., 2012; Singh et al., 2014). Recent developments in the field of another hexaco-ordinate globin, neuroglobin has shown it mediates protection from apoptosis by direct inhibition of cytochrome c (Fago et al., 2008; Raychaudhuri et al., 2010), buffering the intrinsic apoptosis cascade by reducing the heme iron in cytochrome c into its ferrous, anti-apoptotic state (Brown and Borutaite, 2008). Although not proven here, a similar function of CYGB cannot be excluded.

It was recently reported that CYGB over-expressing U2OS osteosarcoma cells increased expression of p53 and p21 following etoposide-induced DNA damage, and evidence was also provided to suggest this was linked to diminished p53 ubiquitination (John et al., 2014). This does not, however, exclude other mechanisms by which CYGB may promote p53 activity. We found CYGB-expressing cells increased CHK1 induction following cisplatin treatment (see section 5.2.5) and this factor responds to DNA damage by phosphorylating p53 to promote its stabilisation (Ou et al., 2005), so this observation might be important in interpreting the results of John et al (2014). Additionally, *CYGB* expression was down-regulated 18-fold by *ΔNp63* knockdown (a p53-related protein with similar transcriptional targets), and knocking down *CYGB* expression resulted in

depletion of p63, but only because of an increase in ROS (Latina et al., 2015). Together, these data support the theory that CYGB modulates p53 family function. Similarly to the John et al (2014) study, we showed augmentation of p53 and p21 in CYGB-expressing cells in response to cisplatin treatment and further demonstrated this was associated with an enhanced transcriptional response of p53-regulated genes.

Cellular p53 is increased in response to stress and can elicit a multitude of downstream effects that primarily involve the mitochondria to regulate the survival-death balance at the transcriptional level (Wang et al., 2014) (Figure 47). Cytochrome c is normally tethered to the inner mitochondrion membrane by the lipid cardiolipin that when oxidised causes cleaved Bid to localise to the mitochondria to provoke the release of cytochrome c for caspase 9 activation (Ott et al., 2007; Shidoji et al., 1999). CYGB also has shown potential to interact with cardiolipin (Reeder et al., 2011), and thus suggests a possible mechanism of apoptosis regulation. However, this would require the cytosolic CYGB protein be associated with inner mitochondria membrane-bound cardiolipin and currently there is limited evidence in support of mitochondrial localisation of the CYGB protein (see section 1.4). Reeder et al (2011) also reported CYGB increases peroxidation of lecithin liposomes, which at first appears to suggest a pro-apoptotic role; especially if cardiolipin was oxidised upon being bound by the globin. Theoretically, this conflict could be resolved if the binding of CYGB acts covers the oxidisable sites of cardiolipin, for instance, or detoxifies ROS before they can reach cardiolipin.

Aside from transcriptional control of apoptosis, there is evidence that p53 re-locates to the mitochondria following DNA damage or hypoxia stress, where it interacts directly with apoptotic proteins to enable mPTP for cytochrome c release, and this process does

not occur if p53 initiates cell cycle arrest (Marchenko et al., 2000). We observed similar phenotypes with CYGB over-expression in chapters 5 and 6, where cisplatin-treated CYGB+ clones were associated with decreased caspase 9-mediated cell death, altered cell cycle distributions, increased p21, and increased response of p53-controlled transcription, which all suggest a p53 is involved in CYGB-associated cisplatin resistance. Similar to the Marchenko et al (2000) study with p53, hypoxia stress has been reported to re-distribute CYGB to the mitochondria in murine cardiac C2C12 myoblasts (Ye et al., 2006). Hence, it is tempting to propose CYGB may intervene in the control of the p53-mitochondria interaction and disrupt apoptosis induction.

Alternatively CYGB may act independently of p53, suppressing intrinsic apoptotic signalling through its ROS scavenging capacity. Superoxide generated by the mitochondrial ETC can activate mPTP (Madesh and Hajnoczky, 2001). CYGB over-expression in the current study has been linked to substantially reduced superoxide levels before and after cisplatin stress (see section 6.2.3). Therefore, it may be CYGB reduces caspase 9 activity through redox-controlling mitochondrial mPTP opening. We also found the ability to metabolise MTT was reduced with CYGB over-expression before and after cisplatin treatment, with the implication that this may lower superoxide production by the mitochondria at complexes 1 and 3 (see section 1.5.3.1). Therefore, the reduction in superoxide levels we observe in CYGB+ clones in conjunction with impaired mitochondrial reductase activity may be linked, but further investigation is necessary to determine if this is the case.

We did not find conclusive evidence that CYGB over-expression altered cellular proliferation. We found cell densities were slightly reduced in medium and high over-

expressing CYGB+ clones compared to NCE controls on two days of the study, which is consistent with the findings of others (Chen et al., 2014; Fujita et al., 2014; Halligan et al., 2009; John et al., 2014; Oleksiewicz et al., 2013; Shivapurkar et al., 2008). However, we did not observe a consistent difference between CYGB+ and NCE controls during the study. The crystal violet assay used correlated well with cell number (see appendix 9), but studies carried out elsewhere in the literature utilised different methods including haemocytometer cell counts or MTT assays. Turnover of MTT (in section 6.2.2) was lower in CYGB+ clones compared to NCE controls, so using this method to assess proliferation might underestimate cell numbers. More sensitive techniques could be used in future proliferation analysis in CYGB-expressing cells, such as 5-bromo-2'-deoxyuridine (BrdU) staining that involves substituting thymidine bases during DNA replication with BrdU that can be detected with a specific anti-BrdU antibody to quantify proliferating cells.

However, we did find the cell cycle response to cisplatin treatment was altered with CYGB expression, with a higher distribution of cells in G1-phase than S-phase following 48 h of 7.5 μM cisplatin, supported by slightly higher cyclin D1 induction compared to NCE controls. Accumulation of CYGB-expressing cells in G1-phase was previously reported in ovarian cancer cells without treatment (Chen et al., 2014) and also in osteosarcoma cells responding to doxorubicin (John et al., 2014), but ours is the first study to show CYGB-expressing oral cancer cells increase the proportion of G1-phase cells in response to cisplatin. This suggests CYGB-expressing cells can evade cisplatin-induced arrest more effectively, which is in line with our findings in chapters 5 and 6 that CYGB over-expression reduced cell death and oxidative stress induced by cisplatin.

Without more detailed studies focussed on CYGB-associated changes to the cisplatin-altered cell cycle distribution, we can only speculate how CYGB is involved. Certainly, the higher G1:S-phase ratio after cisplatin treatment implies a greater ability to enter G1-phase, an impaired ability to leave S-phase or an enhanced ability to overcome the G2 checkpoint initiated by cisplatin. p53 has a critical role in controlling cell cycle checkpoints (see sections 1.6.3.3.2 and 5.3.4). The duration of the G2 checkpoint is modulated by p53, partly through p21 and GADD45α that each inhibit the function of the cyclinB-CDK2 complex (Giono and Manfredi, 2006; Taylor and Stark, 2001). We found *GADD45A* and other p53 target transcripts were substantially regulated in CYGB+ cells following cisplatin treatment (see section 4.2.4) which is in support of increased p53-dependent G2 checkpoint response in CYGB+ clones. We found *GADD45A* was down-regulated in CYGB-expressing cells treated with cisplatin, which suggests the negative regulation of cyclinB-CDK2 is impaired. We also found CYGB over-expressing cells were wildtype for p53 (see section 3.2.8) and p53 induction was higher than NCE controls in CYGB+ clones following cisplatin treatment, again in support of the hypothesis that CYGB affects wildtype p53 signalling in response to cisplatin. Alternatively, the altered cell cycle response to cisplatin with CYGB over-expression may be related to its ability to scavenge ROS rather than its ability to promote p53 signalling. At the G2 checkpoint, CHK1 target, CDC25c, contains redox sensitive cysteine residues that are reversibly oxidised by H_2O_2, to inactivate the phosphatase and delay G2 to M transition (Savitsky and Finkel, 2002).

Theoretically, as an antioxidant able to deplete ROS, CYGB may reduce the oxidation of CDC25c that would maintain its pro-cycling capacity and hence result in more cells distributing into G1 after cisplatin treatment. Re-entry into the cell cycle from a

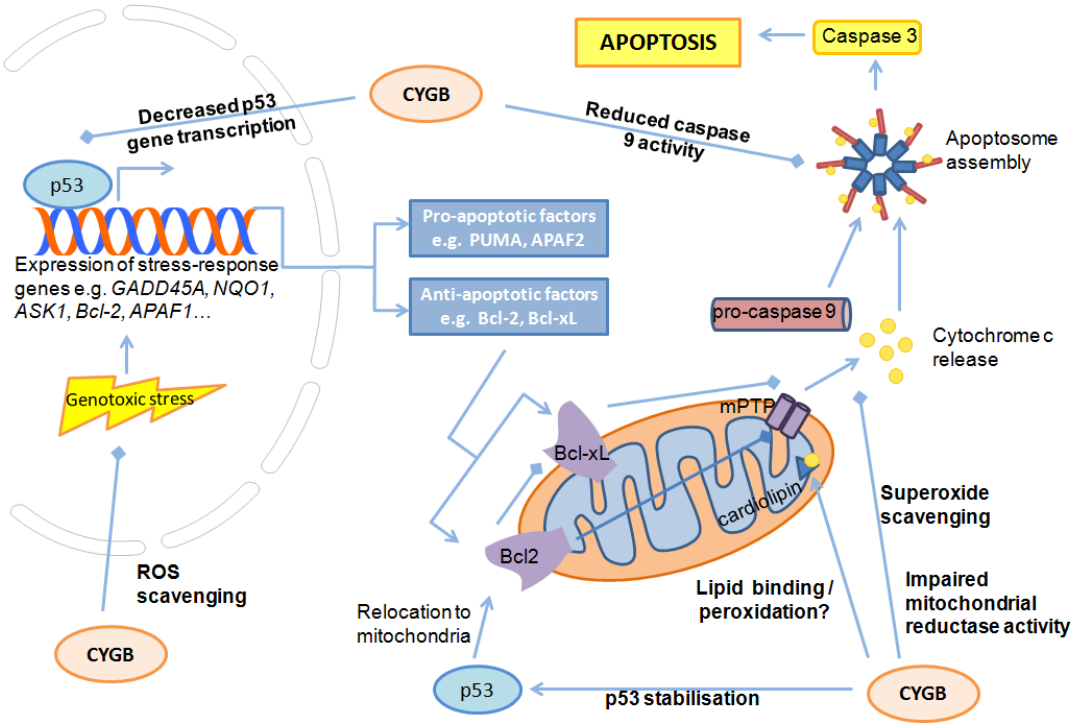

Figure 47 – Possible points of CYGB intervention within the intrinsic apoptosis signalling pathway.

In the classical mechanism of p53-induced intrinsic cell death, p53 enhances the transcript expression ratio of pro-apoptotic factors (like PUMA and APAF1) to anti-apoptotic factors (like Bcl-2 and Bcl-xL) that act to release cytochrome c and other factors from the mitochondria to stimulate the intrinsic apoptotic cascade downstream that includes sequential activation of caspase 9 and executioner caspase 3 to mediate degradation of the cell (Andersen and Kornbluth, 2013). There is also evidence to show p53 re-localises to the mitochondria to physically interact with apoptosis-related proteins (Marchenko et al., 2000). Points where CYGB may intervene in apoptosis activation are shown (text in bold indicates supportive evidence from the existing literature or from this thesis). These hypothesised interactions are discussed in greater detail in the text of section 6.1 and in companion Figure 48.

quiescent sub G1-phase (G0) is dependent upon transcription factors rather than CDK regulators, and a number of these including c-Jun and NFκB can be oxidised or conjugated to glutathione to control their activity (Chiu and Dawes, 2012). CYGB was found to protect against GSH depletion and enhanced ROS scavenging (see sections 6.2.3 and 6.2.4), so this may possibly protect the transcription factors responsible for G1-phase entry from becoming inactivated.

As the cisplatin response normally involves activation of the CHK1-p53-p21 signalling pathway because of DNA damage (see section 1.6.3.3.1), in chapter 5 we investigated the expression of these and found CYGB-expressing cells showed greater induction of all three proteins after cisplatin treatment. This implies the CHK1 signalling pathway leading to DNA repair is more active when CYGB is over-expressed. This agrees with previous reports from our laboratory that *CYGB* over-expression reduces the incidence of DNA damage in response to pro-oxidant treatments (Hodges et al., 2008; McRonald et al., 2012) and also with other groups showing CYGB loss in choline deficiency stressed C57BL/6 mice is correlated with higher levels of double strand DNA break markers, 53BP-1 and γH2AX (Thuy et al., 2011) that are important in promoting the activation of the G2/M checkpoint (Fernandez-Capetillo et al., 2002).

It was also shown that medium and high over-expression of CYGB was associated with increased migratory behaviour, but the opposite was true at lower levels of CYGB over-expression, suggesting the possibility of a 'threshold rheostat' effect on migration. The fact we observed greater motility following high CYGB over-expression is contrary to previous reports that show CYGB expression is related to reduced migration (see section

1.6.3.2.1), but intriguingly is consistent with reports in CALU1 lung cancer cells treated with oxidative and hypoxic stress (Oleksiewicz et al., 2013).

However, we can speculate that as CYGB demonstrates antioxidant functions, this may enable modulation of redox-sensitive RhoA GTPase activation. ROS are found at high levels at the leading edge of a motile cell sheet and oxidise low molecular weight protein tyrosine phosphatases (LMW-PTP) through Rac1-dependent ROS (Van Slambrouck et al., 2009). This relieves the inhibition of p190Rho-GAP (Nimnual et al., 2003) so it can prevent RhoA GTPase from altering actin fibres and focal adhesions to promote migration at the leading edge, but p190Rho-GAP still remains active in the reducing environment at the rear of the cell (Chiarugi et al., 2003; Hurd et al., 2012). Therefore it could be hypothesised that high CYGB expression would significantly deplete Rac1-ROS, disabling LMW-PTP to direct RhoA GTPase-mediated changes to the cytoskeleton at the rear of the cell, and thus promote migration. Although classically considered to act at the rear of a motile cell, there is recent evidence of RhoA GTPase activation at both leading and trailing edges of HeLa cells (Kurokawa and Matsuda, 2005), indicating a regulatory mechanism is in place to permit necessary cytoskeletal rearrangements for migration. Interestingly, Cdc42 RhoGTPase over-expression was found to increase *CYGB* (Kabuyama et al., 2006) and this RhoGTPase is important for cell polarity (Etienne-Manneville, 2004) and considered to co-ordinate with Rac1 and RhoA to enable membrane protrusion (Kurokawa and Matsuda, 2005), so this may be one avenue of further investigation in establishing the link between CYGB, ROS and motility.

Collectively, the data presented in this thesis suggest a hypothesis where CYGB over-expression can, in response to cisplatin treatment, promote activation of the p53

signalling pathway for an enhanced DNA damage response (as evidenced by p53, CHK1, and p21 levels (see section 5.2.5) and regulation of p53-regulated transcripts (see section 4.2.4)) that does not culminate in apoptotic cell death (see section 6.2.1). Additionally, these data suggest CYGB over-expression permits improved cell cycle advancement in the presence of cisplatin (see section 5.3.4) that may be controlled through reduced mitochondrial activity (see section 6.2.2) that, in turn, may decrease cellular superoxide availability for the redox-regulation of factors for cell cycle and transcriptional change (see sections 1.6.3.2.2 and 6.2.3). This hypothesis is summarised in Figure 48. The most pronounced effect for each phenotypic change studied was always observed in medium and high over-expressing CYGB+ clones, whilst the lowest over-expressing clone; LST32, tended to consistently be similar in response to NCE controls, or give an opposite response to other CYGB+ clones. We showed LST32 exhibited the closest *CYGB* expression to NE-1 cells that we used as a control for normal cell expression level (see section 2.4), so it may be argued that the responses we observed in this clone are more physiologically relevant changes.

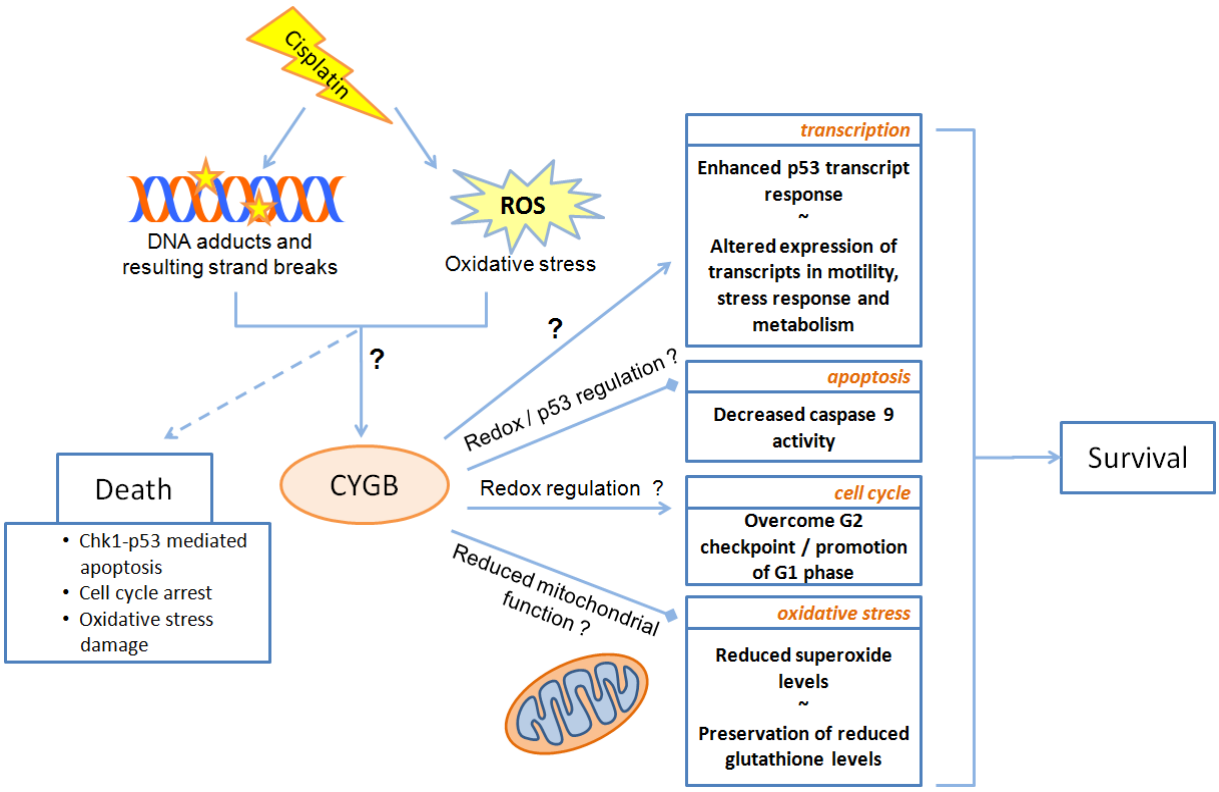

Figure 48 – Possible Mechanisms of Cisplatin Survival by CYGB Over-expression.
Shown here is a summary of how CYGB may be mediating the survival of cells in response to cisplatin treatment, through suppression of oxidative stress and caspase-mediated apoptosis, circumvention of cell cycle arrest and changes to the transcriptome. Further detail of these hypothesised pathways is given in the preceding results chapter discussions and summarised within the text of section 7.1.

7.2 Future Work

A major new observation from this thesis was that CYGB-expressing oral squamous carcinoma cells exhibited a higher induction of p53 and p53-related transcriptional changes following cisplatin stress. It would be beneficial to conduct a whole genome cDNA microarray upon cisplatin-treated CYGB+ clones to determine whether other p53-regulated transcripts are as significantly regulated to more fully characterise the transcriptional response to the combination of CYGB over-expression and cisplatin treatment. We also found CYGB over-expression protected cells from cisplatin-induced apoptosis and oxidative stress. To find out whether this protection also involves diminished DNA damage, comet assays could be conducted. There is already evidence from our laboratory (Hodges et al., 2008; McRonald et al., 2012) and others (Le Thi Thanh Thuy et al., 2015) that suggest this is likely. Furthermore, we found the cisplatin response in CYGB+ clones was associated with higher levels of CHK1 protein, which suggested the DNA damage response pathway was more active in CYGB+ clones. Thus it would be logical to see if the activities of proteins within this pathway were increased with CYGB over-expression. This would also help define where in the CHK1-p53 signalling route (if at all) CYGB might be eliciting its effects, and whether a direct interaction with p53 activity is a possibility. Another important study for this would be to use immunoprecipitation and mass spectrometry to identify novel protein partners of CYGB. Intriguingly, we found in section 5.2.1 that CYGB was linked to altered migratory behaviour that was dependent on the extent of CYGB over-expression. Unfortunately, technical issues confounded efforts to reverse the observed phenotypes, so it is necessary to repeat the *CYGB* knockdown experiments to see if this can be achieved. This would strengthen the hypothesis that CYGB is able to affect migration in the cell model,

but also that its level of over-expression determines whether the response is positive or negative.

Recent work in our laboratory revealed HSC-T6 cells cultured on collagen 1 lowered CYGB protein expression when FAK was inactivated, and also found the expression of *ITGA2* (known to bind collagen 1 in the α2β1 complex) was increased in these cells. The microarray study presented in chapter 4 showed there was a marked down-regulation of *ITGA2* with CYGB over-expression. Notably, in section 4.2.3, we showed the lowest over-expressing CYGB+ clone (LST32) up-regulated *ITGA2* expression compared to NCE controls, whereas medium and high expressing CYGB+ clones showed down-regulated expression. This differential response to high and low CYGB over-expression was curiously mirrored with the different migratory responses (see section 5.2.1). It would be very interesting to look firstly at whether ITGA2 protein expression is different with increasing CYGB over-expression and further if there is different (and perhaps even titrated) inactivation of FAK signalling, including an assessment of whether ROS from the downstream mediator of FAK, Rac1GTPase, is reduced. This is especially important when considering directional cell migration involves higher ROS levels at the leading edge of cells. These proposed studies would deepen understanding of CYGB's mechanism of action in the migratory response.

Other important experiments to consider would be to further investigate the reductions of superoxide and mitochondria MTT turnover associated with CYGB over-expression. This implied that CYGB might be involved in suppressing mitochondrial activity. More detailed subcellular localisation studies would be useful to see if the predominately cytoplasmic CYGB we observed in CYGB+ clones (see section 3.2.6) can relocate to the

mitochondria following cisplatin treatment. This hypothesis is currently the subject of investigation within our laboratory. Other methods to assess markers of mitochondrial activity would also be beneficial, including cellular ATP concentrations, oxygen consumption rates, and superoxide production by particular complexes within the ETC.

The observation that CYGB-expressing cells alters the cell cycle distribution response to cisplatin is also worthy of further investigation, because it leaves the open question of whether CYGB can directly or indirectly elicit these changes. Follow-up experiments could look at CYGB expression at different stages of the cell cycle to see if it can be related to the ROS fluctuations that characterise different stages of the cell cycle. Additionally, redox-controlled cell cycle factors like CDC25 may also be good targets to explore in relation to CYGB's anti-oxidant properties to see if this is part of its effect on the cell cycle response to cisplatin. Combined with our other results that CYGB-expressing cell have increased resistance to cisplatin-mediated cell death, it would be nice to confirm these observations *in vivo,* where the CYGB+ clones generated in this thesis are xenografted into mouse models and treated with cisplatin. The *in vitro* results presented in this thesis are currently being included within a grant application for this objective.

7.3 Final Conclusion

We have successfully generated a new *in vitro* model that stably over-expresses human CYGB in oral squamous cell carcinoma cells as a model to investigate CYGB function. The data presented in this thesis supports previous evidence showing CYGB over-expression can afford protection against oxidative stress, and also shows for the first time that CYGB over-expression is associated with oral cancer cell protection against cisplatin cytotoxicity. We also revealed this protection may involve CYGB-dependent modulation of the p53 signalling network, because of increased induction of factors of the CHK1-p53-p21 signalling cascade and greater regulation of p53-controlled transcripts in CYGB+ clones. The implications of this thesis' findings are that over-expression of CYGB might be partly the reason for cisplatin resistance exhibited by some head and neck tumours, since it is known that although most tumours silence CYGB expression, subsets of solid tumours have been reported to exhibit CYGB expression.

In terms of meeting this thesis' overall objective to increase understanding of CYGB function, the results presented herein have provided additional new evidence for how CYGB may elicit its cytoprotective capabilities. They suggest over-expression of CYGB may enable cells to respond more rapidly and effectively to oxidative stressors, and further suggest that this may be achieved by reducing mitochondria function, depleting mitochondrial superoxide and potentially triggering a switch from p53-induced apoptosis to p53-induced DNA repair signalling. These new findings could have a considerable impact on understanding CYGB function and also demonstrate that CYGB may prove useful clinically in the future for the treatment of cisplatin-resistant tumours.

To conclude, we hypothesise that some cancer cells may re-activate CYGB expression to hijack and exploit its cytoprotective tumour suppressor properties to increase tolerance to the harsh environmental conditions of tumorigenesis, and those caused by clinical management. This may account for the apparent "bimodal" activity of CYGB in displaying both tumour suppressor and oncogene -like properties that have been reported in the existing literature, as well as why CYGB shows a context and cell type specificity in its behaviour. However, there is a need for the molecular mechanism of CYGB to be more fully understood before it could be considered as a clinical target, but the findings of this study have shown this use to be a strong possibility.

Appendix

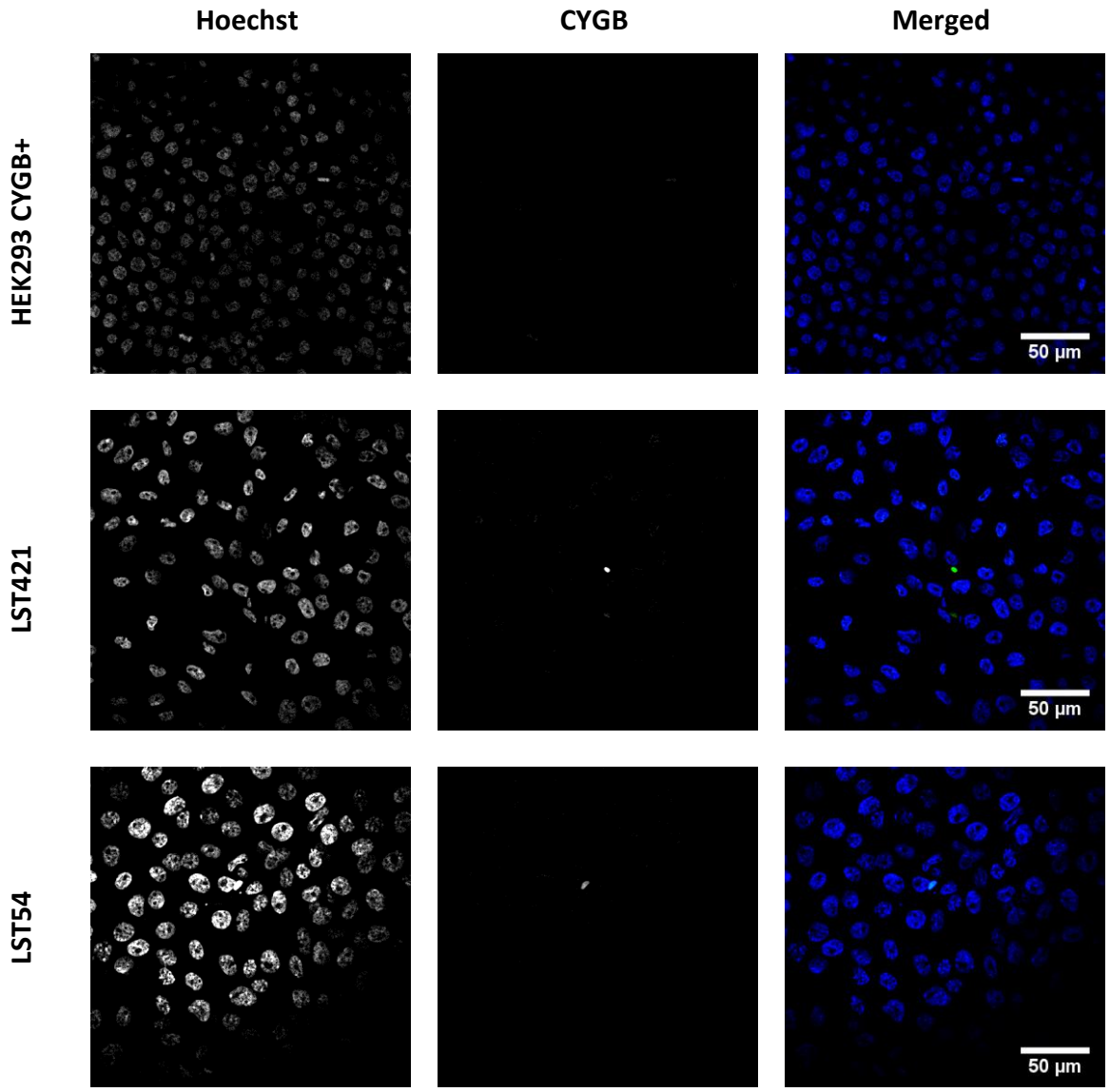

Appendix 1 – Secondary Antibody Staining Controls.
Fixed cell cultures were immunostained using a FITC-conjugated secondary antibody (1:200) only (no primary antibody) and counterstained with the nuclear stain, Hoechst (1:8000). Secondary-only stained cultures were devoid of green fluorescence, suggesting the specificity of the antibody for the primary target. Representative confocal images are shown. Scale bar 50 µm.

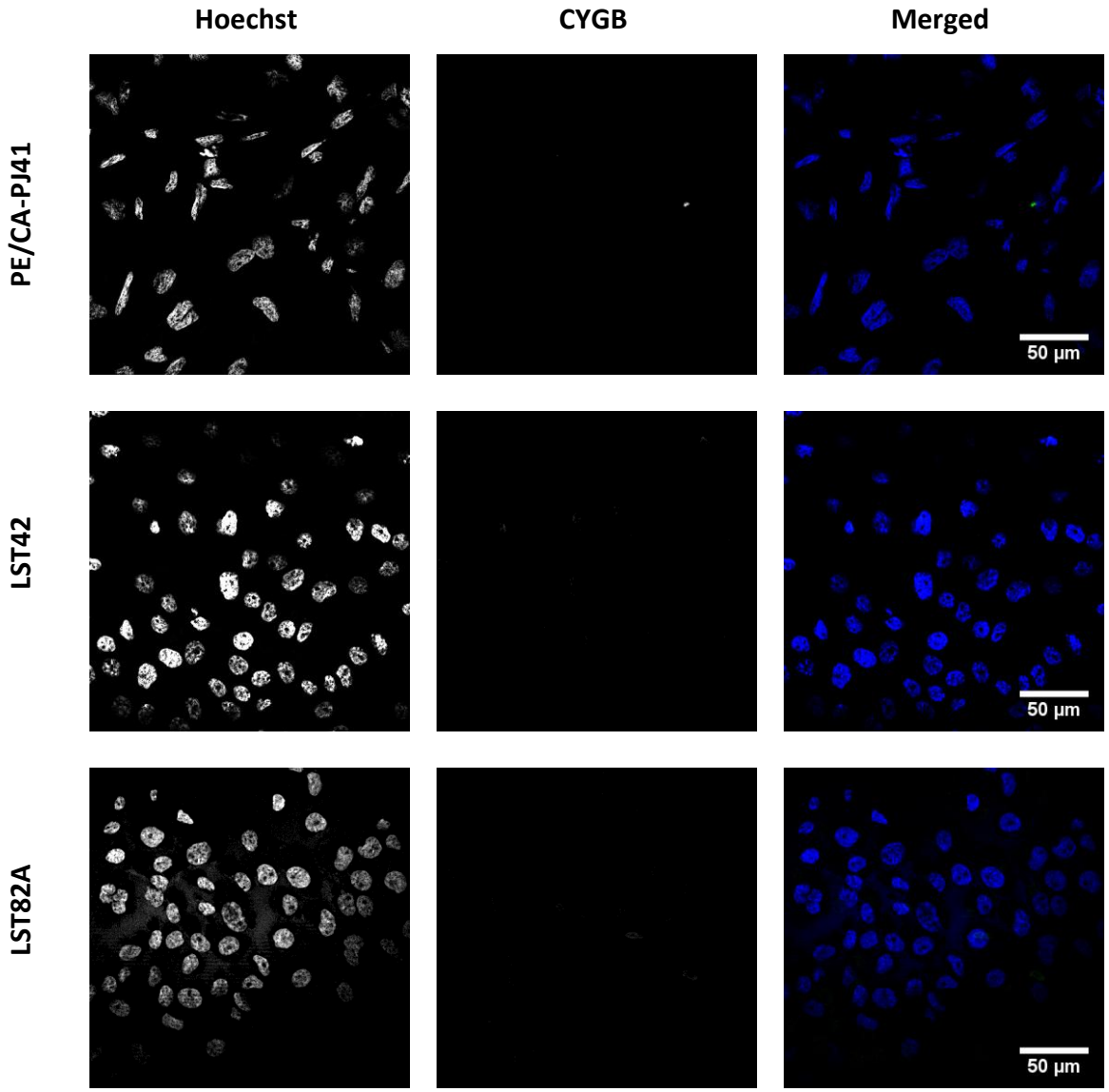

Appendix 1 (continued).

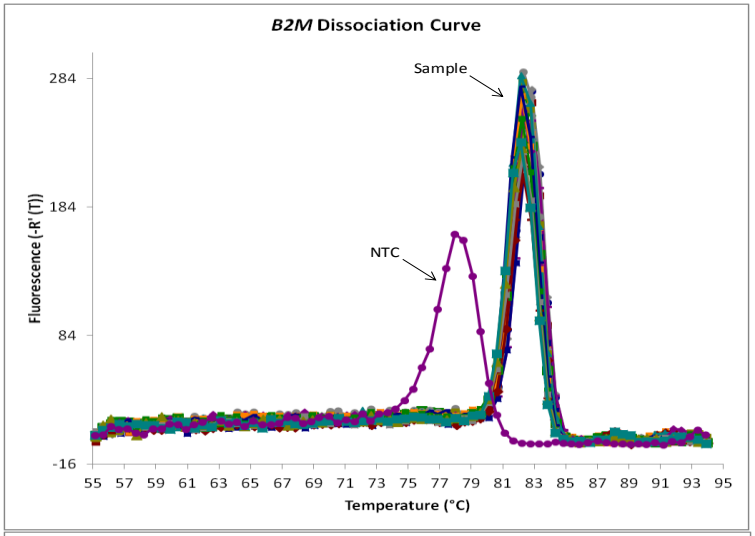

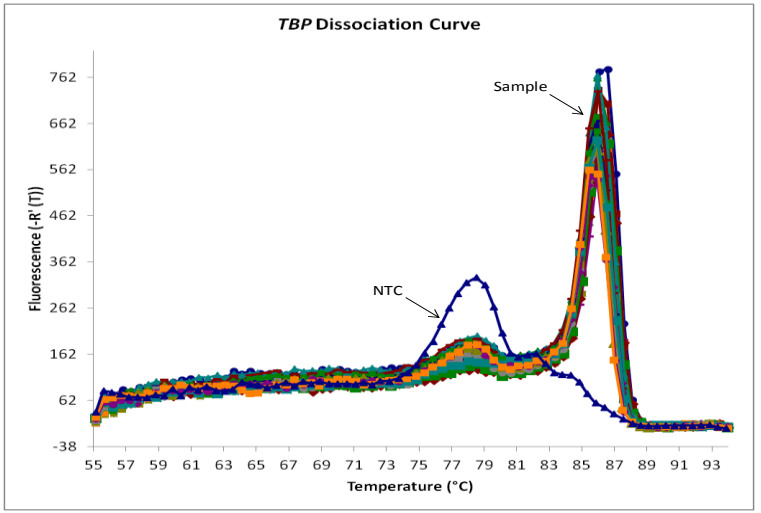

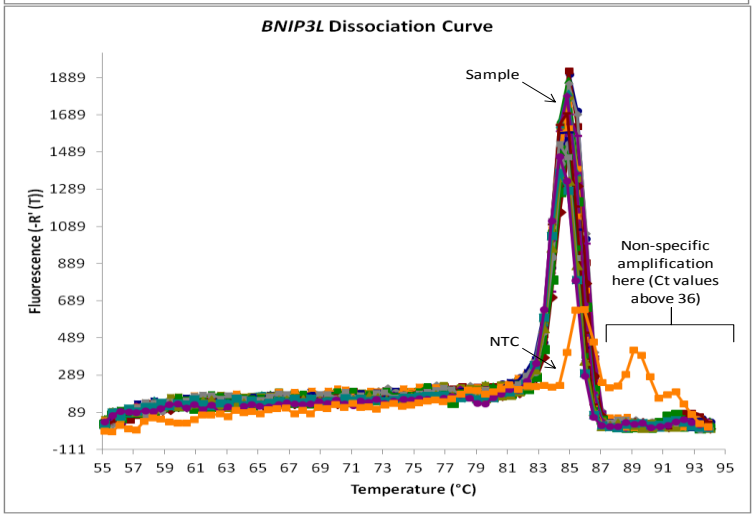

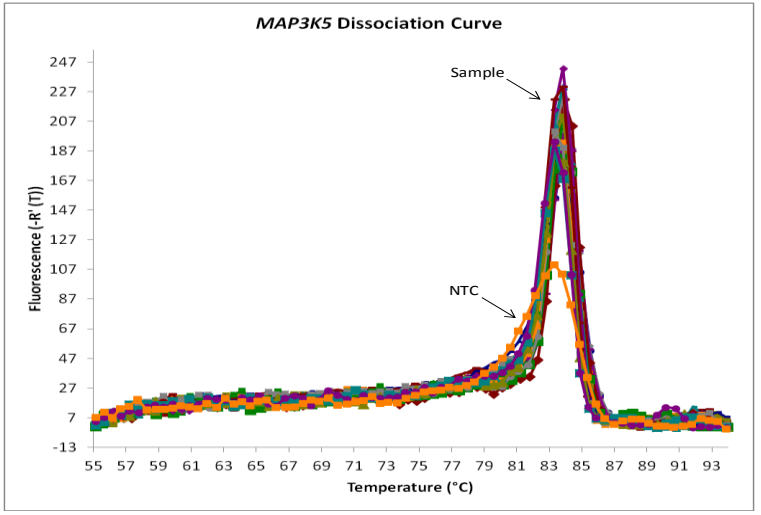

Appendix 2 – SYBR Green Dissociation Curves.

After each RTqPCR reaction, melt curve analysis was carried out to confirm the specificity of the SYBR green probe to the target being quantified. The presence of a single peak within sample curves is at the melting temperature of the amplicon and also shows the presence of primer dimer peaks shifted to the left of the sample peak within the no template (NTC) controls. All NTC samples gave a Ct value of 36 or more, whilst samples amplified at a maximum Ct of 30.

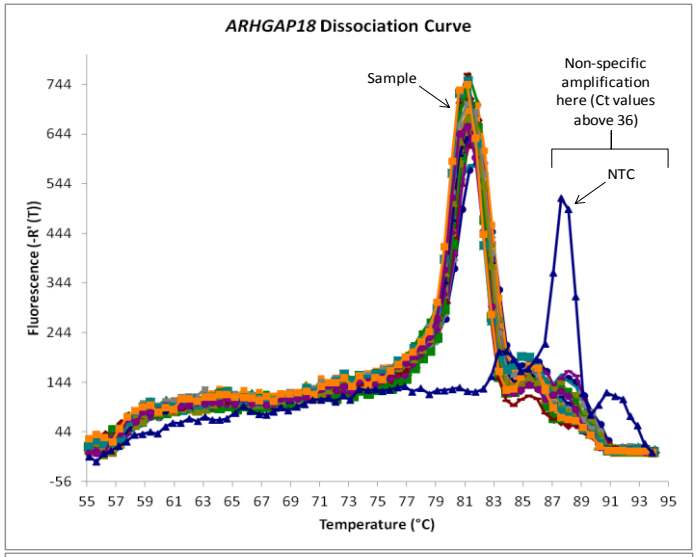

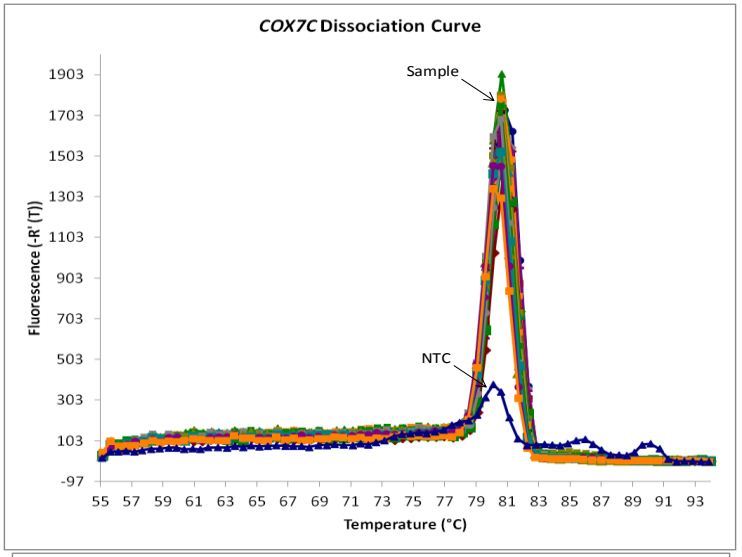

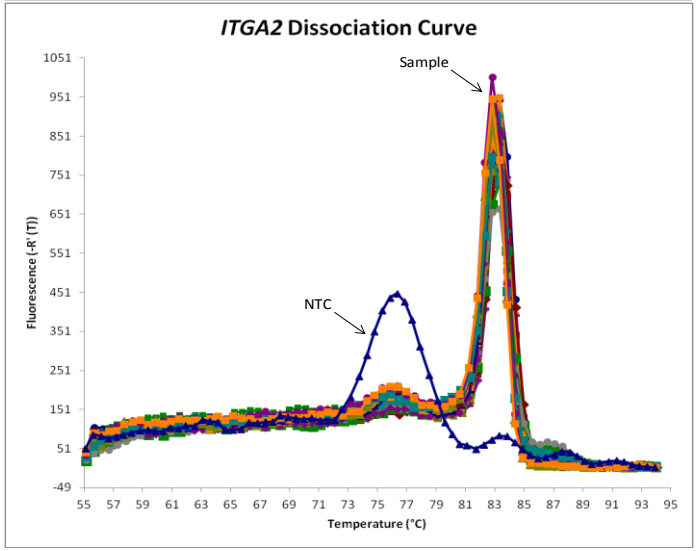

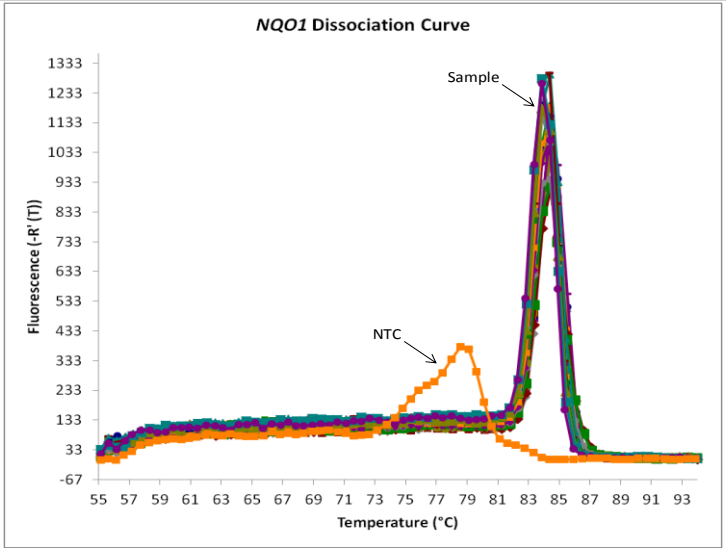

Appendix 2 (continued).

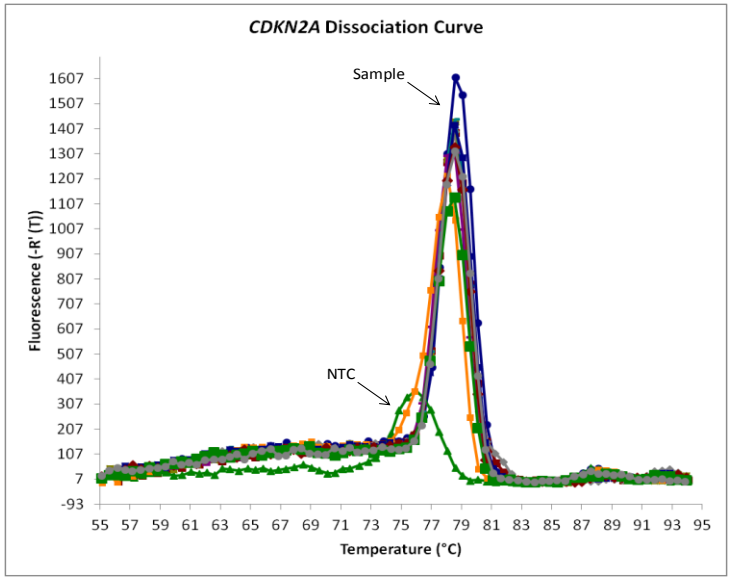

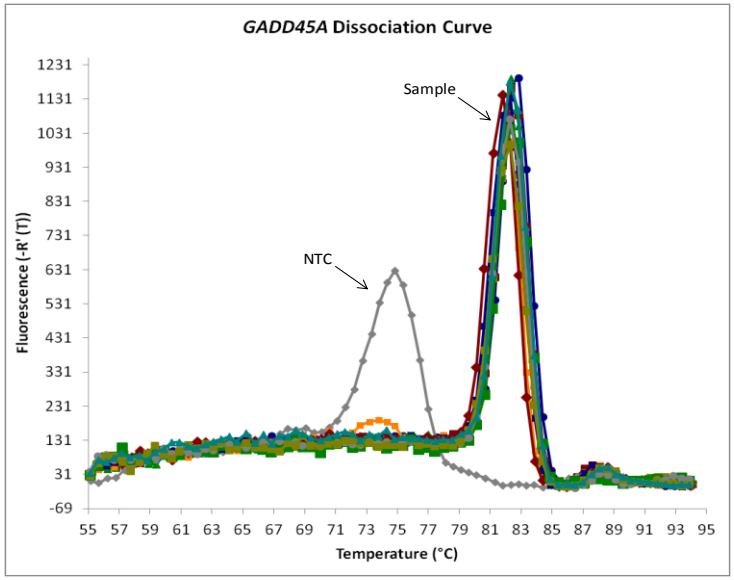

Appendix 2 (continued).

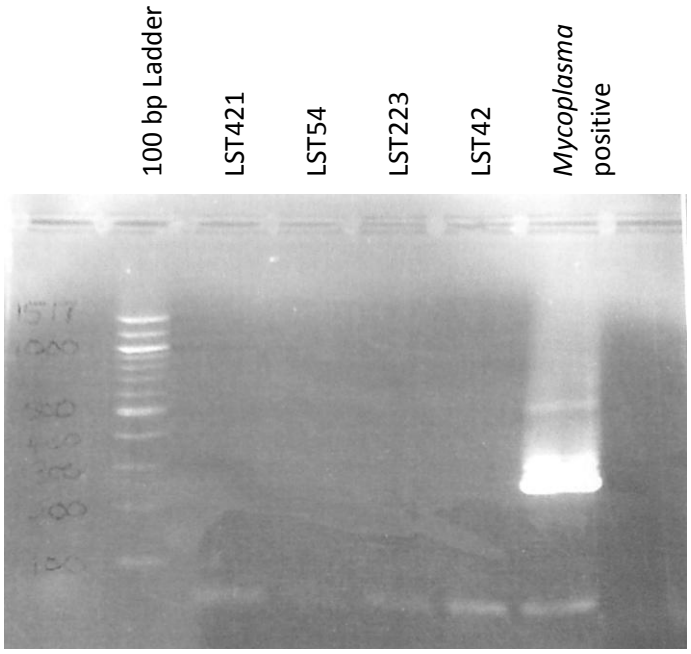

Appendix 3 – Transgenic clones used for experiments were confirmed to be *Mycoplasma sp.* negative prior to cryopreservation.

All clones were tested for the presence of the *Mycoplasma* through PCR. PCR products were separated by 2 % agarose gel electrophoresis and compared to a positive control containing the 270 bp amplicon region of the 16S rRNA gene that characterises *Mycoplasma* species. All clones were screened and none showed any contamination, so several cryostocks were made for each clone.

Description	Max score	Total score	Query cover	E value	Ident	Accession
Homo sapiens cytoglobin (CYGB), mRNA	1626	1626	86%	0.0	97%	NM_134268.4

Alignments

Homo sapiens cytoglobin (CYGB), mRNA
Sequence ID: **ref|NM_134268.4|** Length: 2166 Number of Matches: 1
Range 1: 21 to 964

Score	Expect	Identities	Gaps	Strand	Frame
1626 bits(880)	0.0()	921/945(97%)	8/945(0%)	Plus/Plus	

Features:

```
Query  139  GTCGCCCCCACCCCGCGCAGCCTTCACCTTGCCGGCATTGGCTCTTACCCACACGGGGCT  198
            ||||||||||||||||||||||||||||||||||||||||||||||||||||||||||||
Sbjct  21   GTCGCCCCCACCCCGCGCAGCCTTCACCTTGCCGGCATTGGCTCTTACCCACACGGGGCT  80

Query  199  GGGGGTTTGGAGCGGATTTGttttttttAAAACATTTTCCAGCAGACCACATCCCCGCCCCA  258
            ||||||||||||||||||||||||||||||||||||||||||||||||||||||||||||
Sbjct  81   GGGGGTTTGGAGCGGATTTGTTTTTTTTAAAACATTTTCCAGCAGACCACATCCCCGCCCCA  140

Query  259  CCGCTGGCTGTccccgccccccGCACATATACCCTGcacacacgcgcacgcacacacacac  318
            ||||||||||||||||||||||||||||||||||||||||||||||||||||||||||||
Sbjct  141  CCGCTGGCTGTCCCCCGCCCCCCGCACATATACCCTGCACACACGCACGCACACACACAC  200

Query  319  acacacccggcgcgcacagacacacgctcccctcccctccgcgctctgccccctcgccccgccc  378
            ||||||||||||||||||||||||||||||||||||||||||||||||||||||||||||
Sbjct  201  ACACACCCGGCGCGCACAGACACACGCTCCCTCCCTCCGCGCTCTACCCCTCGCCCGCCC  260

Query  379  gccgcgcacgcagccggccccggctcccggcgccccgcgccccgcgccccgcgccccgcc  438
            ||||||||||||||||||||||||||||||||||||||||||||||||||||||||||||
Sbjct  261  GCCGCGCACGCAGCCGGCCCCGGCTCCCGGCGCCCCGCGCCCCGCGCCCCGCGCCCCGCC  320

Query  439  accgcccgcccgccgagcaaagccgggctgggcttggagctgctcatggagaaagtgccagg  498
            ||||||||||||||||||||||||||||||||||||||||||||||||||||||||||||
Sbjct  321  ACCGCCGCCGCCGAGCAAAGCCGGGCTGGGCTTGGAGCTGCTCATGGAGAAAGTGCCAGG  380

Query  499  CGAGATGGAGATCGAGCGCAGGGAGCGGAGCGAGGAGCTGTCCGAGGCGGAGAGGAAGGC  558
            ||||||||||||||||||||||||||||||||||||||||||||||||||||||||||||
Sbjct  381  CGAGATGGAGATCGAGCGCAGGGAGCGGAGCGAGGAGCTGTCCGAGGCGGAGAGGAAGGC  440

Query  559  GGTGCAGGCTATGTGGGCCCGGCTCTATGCCAACTGCGAGGACGTGGGGGTGGCCATCCT  618
            ||||||||||||||||||||||||||||||||||||||||||||||||||||||||||||
Sbjct  441  GGTGCAGGCTATGTGGGCCCGGCTCTATGCCAACTGCGAGGACGTGGGGGTGGCCATCCT  500

Query  619  GGTGAGGTTCTTTGTGAACTTCCCCTCGGCCAAGCAGTACTTCAGCCAGTTCAAGCACAT  678
            ||||||||||||||||||||||||||||||||||||||||||||||||||||||||||||
Sbjct  501  GGTGAGGTTCTTTGTGAACTTCCCCTCGGCCAAGCAGTACTTCAGCCAGTTCAAGCACAT  560

Query  679  GGAGGATCCCCTGGAGATGGAGCGGAGCCCCCAGCTGCGGAAGCACGCCTGCCGAGTCAT  738
            ||||||||||||||||||||||||||||||||||||||||||||||||||||||||||||
Sbjct  561  GGAGGATCCCCTGGAGATGGAGCGGAGCCCCCAGCTGCGGAAGCACGCCTGCCGAGTCAT  620

Query  739  GGGGGCCCTCAACACTGTCGTGGAGAACCTGCATGACCCCGACAAGGTGTCCTCTGTGCT  798
            ||||||||||||||||||||||||||||||||||||||||||||||||||||||||||||
Sbjct  621  GGGGGCCCTCAACACTGTCGTGGAGAACCTGCATGACCCCGACAAGGTGTCCTCTGTGCT  680

Query  799  CGCCCTTGTGGGGAAAGCCCACGCCCTCAAGCACAAG-TGGRAMCSGGTGTACTTCAAGA  857
            ||||||||||||||||||||||||||||||||||||| ||| | ||||||||||||||||
Sbjct  681  CGCCCTTGTGGGGAAAGCCCACGCCCTCAAGCACAAGGTGGAACC-GGTGTACTTCAAGA  739

Query  858  TCTTCTCTGGGGTCATTCTGGAGGTGGTCGCCGAGGAATTTGCCAGTGACTTCCCA-CTG  916
            ||||||||||||||||||||||||||||||||||||||||||||||||||||||| ||||
Sbjct  740  TCCTCTCTGGGGTCATTCTGGAGGTGGTCGCCGAGGAATTTGCCAGTGACTTCCCACCTG  799

Query  917  AGACGCAGAGAGCCTGGGYCAAGCTGCGTGGCCTCATCTACAGCCACGTGACCGCTGCCT  976
            ||||||||||||||||| |||||||||||||||||||||||||||||||||||||||||||
Sbjct  800  AGACGCAGAGAGCCTGGGCCAAGCTGCGTGGCCTCATCTACAGCCACGTGACCGCTGCCT  859

Query  977  AC-AGGAAGTGKGCTGGKTGCAGCAGKY--CCAACGCCACCACYC-ACGGG-CACACTGC  1031
            || |||||||| |||| |||||||||||  |||||||||||||| | ||||| ||||||||
Sbjct  860  ACAAGGAAGTGGGCTGGGTGCAGCAGGTCCCCAACGCCACCACCCCACCGGCCACACTGC  919

Query  1032  CCTCTTCGGGGCSGTAGGACCCCYCCCTCCACCCCCCTCCYTGGC  1076
             ||||||||||| |||||||||| |||||||||| |||||||||||
Sbjct  920   CCTCTTCGGGGCCGTAGGACCCCTAACTCCACCCCCCTCCCTGGC  964
```

Appendix 4 – Sequencing CYGB cDNA Insert within the pCMV6-AC plasmid.

The human CYGB cDNA sequence incorporated into the pCMV6-AC vector was verified by direct sequencing to ensure that the sequence being introduced was indeed wildtype. BLAST sequence alignment between the amplicon synthesised with the forward VP1.5 primer and the reference CYGB mRNA (NM_134268.4) is shown. There was an observed 97 % identity between the sequences.

(a)

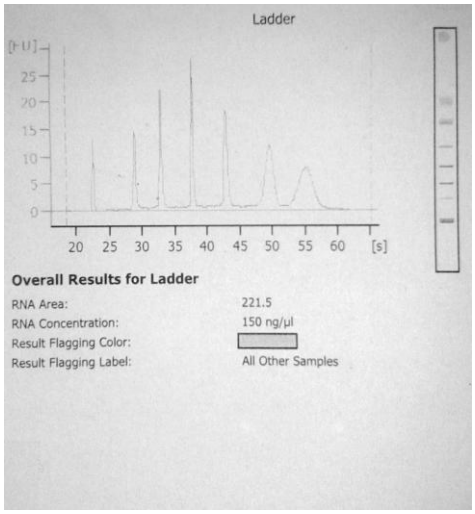

(b)

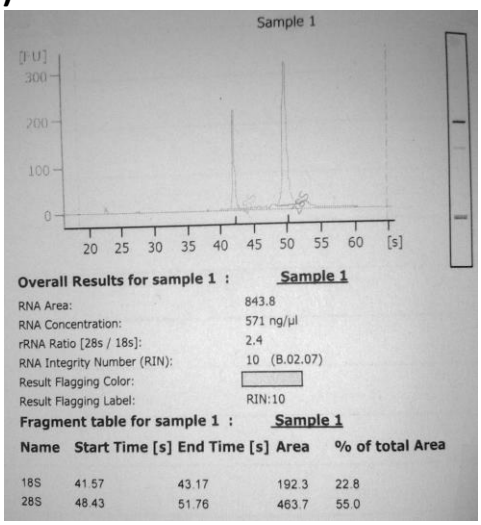

(c)

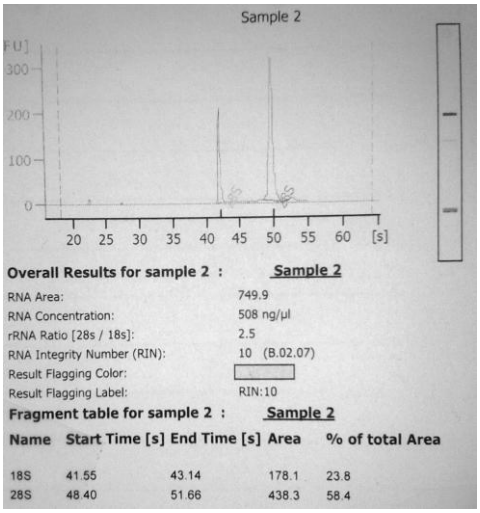

(d)

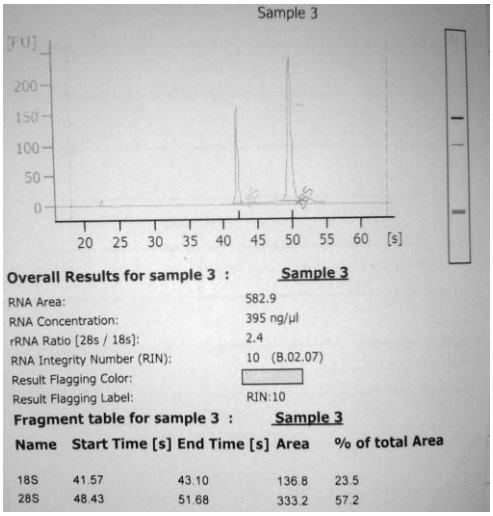

Appendix 5 – Microarray Sample RNA Electropherograms.

LST421 and LST223 RNA isolates were extracted and checked for integrity with the Agilent 2100 Bioanalyser before being cyanine-dye labelled ready for hybridisation. The results here show the RNA extract concentrations, RNA integrity number (RIN) and 28S/18S ratios for each sample, along with their electropherograms that show the ribosomal RNA peaks (a – Ladder, b – LST421 rep 1, c – LST421 rep 2, d – LST421 rep 3, e – LST223 rep 1, f – LST223 rep 2 and g – LST223 rep 3). The baselines in each sample electropherogram have no observable smaller peaks that would have suggested degraded RNA. All samples gave RINs above 8 and were therefore of high quality for hybridisation to the microarray chip.

(e)

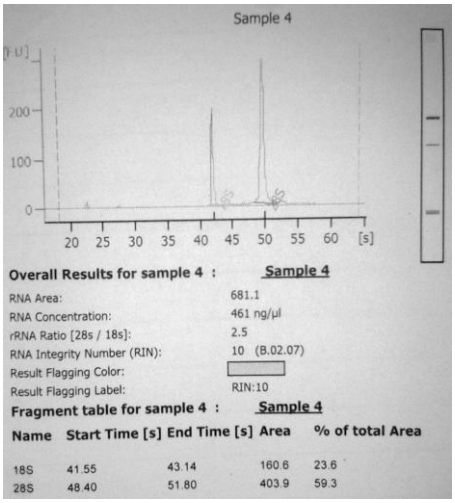

Overall Results for sample 4 : **Sample 4**

RNA Area:	681.1
RNA Concentration:	461 ng/µl
rRNA Ratio [28s / 18s]:	2.5
RNA Integrity Number (RIN):	10 (B.02.07)
Result Flagging Color:	
Result Flagging Label:	RIN:10

Fragment table for sample 4 : **Sample 4**

Name	Start Time [s]	End Time [s]	Area	% of total Area
18S	41.55	43.14	160.6	23.6
28S	48.40	51.80	403.9	59.3

(f)

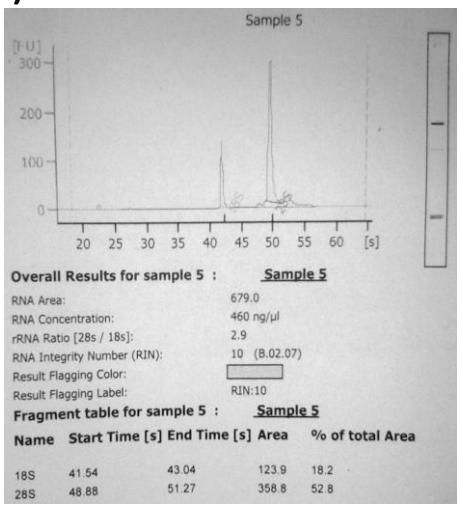

Overall Results for sample 5 : **Sample 5**

RNA Area:	679.0
RNA Concentration:	460 ng/µl
rRNA Ratio [28s / 18s]:	2.9
RNA Integrity Number (RIN):	10 (B.02.07)
Result Flagging Color:	
Result Flagging Label:	RIN:10

Fragment table for sample 5 : **Sample 5**

Name	Start Time [s]	End Time [s]	Area	% of total Area
18S	41.54	43.04	123.9	18.2
28S	48.88	51.27	358.8	52.8

(g)

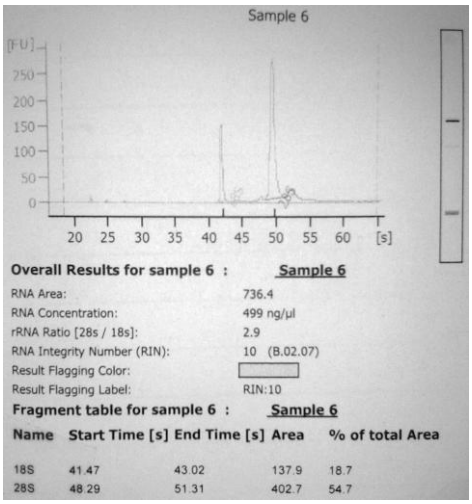

Overall Results for sample 6 : **Sample 6**

RNA Area:	736.4
RNA Concentration:	499 ng/µl
rRNA Ratio [28s / 18s]:	2.9
RNA Integrity Number (RIN):	10 (B.02.07)
Result Flagging Color:	
Result Flagging Label:	RIN:10

Fragment table for sample 6 : **Sample 6**

Name	Start Time [s]	End Time [s]	Area	% of total Area
18S	41.47	43.02	137.9	18.7
28S	48.29	51.31	402.7	54.7

Appendix 5 (continued).

Hybridisation Buffer	1	2	3
	① ❷	③ ❹	⑤ ❻
Cy 3 labelled sample (µl)	9.2	6.13	4.81
Cy 5 labelled sample (µl)	3.23	4.57	4.23
10X blocking agent (µl)	5	5	5
water (µl)	6.57	8.3	9.96
25X fragmentation buffer (µl)	1	1	1
total	25	25	25

Appendix 6 – Microarray Hybridisation Recipe.

cRNA samples (500 ng) were added to a buffer mix as shown prior to hybridisation to the microarray. Samples were as follows: 1 – LST421 rep 1, 3 – LST421 rep 2, 5 – LST421 rep 3, 2 – LST223 rep 1, 4 – LST223 rep 2 and 6 – LST223 rep 3.

Symbol	Gene Name	Accession ID	Fold change	P value
HTRA1	HtrA serine peptidase 1	NM_002775	6.753	4.05E-10
MOXD1	monooxygenase, DBH-like 1	NM_015529	4.806	9.39E-08
MMP1	matrix metallopeptidase 1 (interstitial collagenase)	NM_002421	4.695	1.44E-07
XLOC_008374			4.219	0.000194
CRCT1	cysteine-rich C-terminal 1	NM_019060	4.207	1.48E-06
FSTL3	follistatin-like 3 (secreted glycoprotein)	NM_005860	3.921	7.62E-06
ELL2	elongation factor, RNA polymerase II, 2	NM_012081	3.876	1.65E-07
SERPINA3	serpin peptidase inhibitor, clade A (alpha-1 antiproteinase, antitrypsin), member 3	NM_001085	3.73	6.01E-06
FAM89A	family with sequence similarity 89, member A	NM_198552	3.64	9.22E-07
SPP1	secreted phosphoprotein 1	NM_001040058	3.624	5.95E-06
FAM25A	family with sequence similarity 25, member A	NM_001146157	3.561	1.48E-06
BAIAP2L2	BAI1-associated protein 2-like 2	NM_025045	3.558	1.78E-06
CYP4F11	cytochrome P450, family 4, subfamily F, polypeptide 11	NM_021187	3.461	3.44E-05
CYP4F12	cytochrome P450, family 4, subfamily F, polypeptide 12	NM_023944	3.356	1.38E-06
XLOC_007249			3.317	2.82E-05
IL6	interleukin 6 (interferon, beta 2)	NM_000600	3.185	5.55E-06
LOC728769	hypothetical LOC728769	XR_108586	3.167	4.87E-05
S1PR3	sphingosine-1-phosphate receptor 3	NM_005226	3.149	7.30E-06
XLOC_001856			3.052	7.38E-07
PRICKLE1	prickle homolog 1 (Drosophila)	NM_153026	3.05	2.02E-07
REEP5	receptor accessory protein 5	NM_005669	3.025	8.73E-06
SPRR1B	small proline-rich protein 1B	NM_003125	3.006	4.35E-05
HES5	hairy and enhancer of split 5 (Drosophila)	NM_001010926	3.005	9.39E-08
RDM1	RAD52 motif 1	NM_001034836	3.001	8.93E-06
SQSTM1	sequestosome 1	NM_003900	2.993	8.22E-06
GPRIN1	G protein regulated inducer of neurite outgrowth 1	NM_052899	2.959	4.17E-05
ADRBK2	adrenergic, beta, receptor kinase 2	NM_005160	2.944	6.69E-06
AKR1C3	aldo-keto reductase family 1, member C3 (3-alpha hydroxysteroid dehydrogenase, type II)	NM_003739	2.933	4.45E-06
RPL28	ribosomal protein L28	NM_001136134	2.922	4.38E-07

Appendix 7 – Average fold changes of transcripts up-regulated in CYGB+ clones.

Transcriptional targets that were considered as being significantly up-regulated if they increased by 2 fold or more in CYGB+ (LST421) clones in comparison to the NCE (LST223) background expression of these targets are shown. All fold changes were determined from expression across a biological triplicate set of samples analysed on the Agilent SurePrint G3 Human Gene Expression 8x 60K v1 Microarray.

Symbol	Gene Name	Accession ID	Fold change	P value
PLEKHO1	pleckstrin homology domain containing, family O member 1	NM_016274	2.919	2.49E-05
TRIM37	tripartite motif containing 37	NM_001005207	2.894	2.30E-05
FOLR3	folate receptor 3 (gamma)	NM_000804	2.884	0.000468
TRIML2	tripartite motif family-like 2	NM_173553	2.878	0.000381
SCLY	selenocysteine lyase	NM_016510	2.869	5.32E-06
CAST	calpastatin	NM_001042440	2.844	7.80E-07
NDST2	N-deacetylase/N-sulfotransferase (heparan glucosaminyl) 2	BC018681	2.832	0.000541
METRNL	meteorin, glial cell differentiation regulator-like	NM_001004431	2.81	2.51E-07
PRDX5	peroxiredoxin 5	NM_012094	2.78	1.20E-05
N4BP2L2	NEDD4 binding protein 2-like 2	NM_033111	2.713	5.98E-05
APBB3	amyloid beta (A4) precursor protein-binding, family B, member 3	NM_006051	2.711	1.43E-06
ADSSL1	adenylosuccinate synthase like 1	NM_199165	2.7	2.38E-05
SNHG9	small nucleolar RNA host gene 9 (non-protein coding)	NR_003142	2.687	4.49E-09
XLOC_001775			2.675	2.54E-06
TCOF1	Treacher Collins-Franceschetti syndrome 1	NM_001008657	2.646	1.18E-06
HMOX1	heme oxygenase (decycling) 1	NM_002133	2.597	1.36E-05
CDC23	cell division cycle 23 homolog (S. cerevisiae)	BC010944	2.593	2.94E-05
UIMC1	ubiquitin interaction motif containing 1	NM_016290	2.584	9.81E-06
PITX1	paired-like homeodomain 1	NM_002653	2.584	0.000981
XRCC4	X-ray repair complementing defective repair in Chinese hamster cells 4	NM_022550	2.58	8.01E-05
LIF	leukemia inhibitory factor (cholinergic differentiation factor)	NM_002309	2.563	0.000254
BEX2	brain expressed X-linked 2	NM_001168399	2.558	3.96E-05
SEL1L3	sel-1 suppressor of lin-12-like 3 (C. elegans)	NM_015187	2.556	1.55E-05
ZMYND15	zinc finger, MYND-type containing 15	NM_032265	2.525	8.38E-06
FAM172A	family with sequence similarity 172, member A	NM_032042	2.504	0.001
DPM3	dolichyl-phosphate mannosyltransferase polypeptide 3	NM_018973	2.504	8.70E-07
CXCL2	chemokine (C-X-C motif) ligand 2	NM_002089	2.503	0.000692
C9orf16	chromosome 9 open reading frame 16	NM_024112	2.502	0.00126
CHAC1	ChaC, cation transport regulator homolog 1 (E. coli)	NM_024111	2.494	6.83E-07

Appendix 7 (continued).

Symbol	Gene Name	Accession ID	Fold change	P value
LHFPL2	lipoma HMGIC fusion partner-like 2	NM_005779	2.488	0.000655
LCN2	lipocalin 2	NM_005564	2.485	0.00264
SYTL3	synaptotagmin-like 3	NM_001009991	2.482	0.000119
CCDC80	coiled-coil domain containing 80	NM_199511	2.475	9.20E-06
C2orf89	chromosome 2 open reading frame 89	NM_001080824	2.47	1.62E-07
CSF2	colony stimulating factor 2 (granulocyte-macrophage)	NM_000758	2.462	0.0204
ANKHD1-EIF4EBP3	ANKHD1-EIF4EBP3 readthrough	NM_020690	2.445	0.000205
CYB5R4	cytochrome b5 reductase 4	NM_016230	2.445	0.000192
AOX1	aldehyde oxidase 1	NM_001159	2.444	9.53E-06
GALNT14	UDP-N-acetyl-alpha-D-galactosamine:polypeptide N-acetylgalactosaminyltransferase 14 (GalNAc-T14)	NM_024572	2.44	9.22E-06
JMY	junction mediating and regulatory protein, p53 cofactor	NM_152405	2.418	0.000382
LOC285178	hypothetical protein LOC285178	AK091571	2.416	1.48E-05
GAS6	growth arrest-specific 6	NM_000820	2.413	0.000301
C11orf70	chromosome 11 open reading frame 70	NM_032930	2.402	1.69E-05
MLXIP	MLX interacting protein	NM_014938	2.387	7.71E-05
CYP27B1	cytochrome P450, family 27, subfamily B, polypeptide 1	NM_000785	2.385	0.00243
TXNRD1	thioredoxin reductase 1	NM_003330	2.385	0.000163
GDF15	growth differentiation factor 15	NM_004864	2.384	0.00049
ATG12	ATG12 autophagy related 12 homolog (S. cerevisiae)	NM_004707	2.38	0.000267
FLJ35776	hypothetical LOC649446	NR_024101	2.375	0.000792
HIGD2A	HIG1 hypoxia inducible domain family, member 2A	NM_138820	2.374	0.000638
FER	fer (fps/fes related) tyrosine kinase	NM_005246	2.372	8.96E-05
PXDNL	peroxidasin homolog (Drosophila)-like	NM_144651	2.37	6.75E-05
C9orf130	chromosome 9 open reading frame 130	NR_023389	2.37	0.000112
GRB14	growth factor receptor-bound protein 14	NM_004490	2.365	0.000653
COX7C	cytochrome c oxidase subunit VIIc	NM_001867	2.359	0.000244
ABCC3	ATP-binding cassette, sub-family C (CFTR/MRP), member 3	NM_001144070	2.356	6.54E-07
AOX1	aldehyde oxidase 1	NM_001159	2.351	0.00041
CCDC99	coiled-coil domain containing 99	NM_017785	2.351	0.00112

Appendix 7 (continued).

Symbol	Gene Name	Accession ID	Fold change	P value
FLNC	filamin C, gamma	NM_001458	2.351	0.000151
KRT80	keratin 80	NM_182507	2.344	0.00048
NADK	NAD kinase	NM_023018	2.343	1.75E-05
YAF2	YY1 associated factor 2	NM_001190979	2.337	5.54E-07
PTPRM	protein tyrosine phosphatase, receptor type, M	NM_002845	2.332	3.33E-06
GDA	guanine deaminase	NM_004293	2.331	0.00184
NCRNA00219	non-protein coding RNA 219	NR_015370	2.33	4.08E-05
C11orf70	chromosome 11 open reading frame 70	NM_001195005	2.326	1.98E-06
SLMO1	slowmo homolog 1 (Drosophila)	NM_006553	2.323	6.75E-06
C1orf133	chromosome 1 open reading frame 133	NR_024337	2.322	0.000197
DHFR	dihydrofolate reductase	NM_000791	2.315	0.000258
LMO4	LIM domain only 4	NM_006769	2.315	0.000356
RAB31	RAB31, member RAS oncogene family	NM_006868	2.311	0.000909
IMPA2	inositol(myo)-1(or 4)-monophosphatase 2	NM_014214	2.31	0.000231
DOM3Z	dom-3 homolog Z (C. elegans)	NM_005510	2.307	0.000892
HPS1	Hermansky-Pudlak syndrome 1	NM_000195	2.304	1.43E-06
GADD45G	growth arrest and DNA-damage-inducible, gamma	NM_006705	2.304	0.00254
ZMAT2	zinc finger, matrin-type 2	NM_144723	2.294	0.000721
TMEM222	transmembrane protein 222	NM_032125	2.294	8.10E-06
PHGDH	phosphoglycerate dehydrogenase	NM_006623	2.288	4.23E-06
SLC35E2	solute carrier family 35, member E2	NM_182838	2.284	1.04E-05
NQO1	NAD(P)H dehydrogenase, quinone 1	NM_000903	2.283	8.53E-07
S100A9	S100 calcium binding protein A9	NM_002965	2.268	0.00481
MYO10	myosin X	NM_012334	2.268	6.31E-05
ANGPTL4	angiopoietin-like 4	NM_139314	2.262	0.00784
MSH3	mutS homolog 3 (E. coli)	NM_002439	2.256	0.000918
SNX24	sorting nexin 24	NM_014035	2.256	0.00109
CARD11	caspase recruitment domain family, member 11	NM_032415	2.242	2.44E-05
AP4M1	adaptor-related protein complex 4, mu 1 subunit	NM_004722	2.241	2.27E-05

Appendix 7 (continued).

Symbol	Gene Name	Accession ID	Fold change	P value
TCOF1	Treacher Collins-Franceschetti syndrome 1	NM_001008657	2.241	0.00334
LOC730183	hypothetical LOC730183	XR_109284	2.24	0.00162
CYB5RL	cytochrome b5 reductase-like	BC071735	2.236	7.57E-05
PPP1R14C	protein phosphatase 1, regulatory (inhibitor) subunit 14C	NM_030949	2.228	1.18E-05
GAMT	guanidinoacetate N-methyltransferase	NM_138924	2.222	8.34E-05
CES1	carboxylesterase 1	NM_001025195	2.219	0.00257
UPP1	uridine phosphorylase 1	NM_181597	2.217	0.000124
LRSAM1	leucine rich repeat and sterile alpha motif containing 1	NM_138361	2.215	0.0012
FEM1C	fem-1 homolog c (C. elegans)	NM_020177	2.211	8.09E-06
TMCC1	transmembrane and coiled-coil domain family 1	NM_001017395	2.208	0.00141
C17orf37	chromosome 17 open reading frame 37	NM_032339	2.201	2.47E-06
TGFB1	transforming growth factor, beta 1	NM_000660	2.201	0.00349
EML1	echinoderm microtubule associated protein like 1	NM_001008707	2.199	3.36E-05
AGXT2L2	alanine-glyoxylate aminotransferase 2-like 2	NM_153373	2.199	4.06E-05
TAGLN3	transgelin 3	NM_013259	2.198	0.00177
CFB	complement factor B	NM_001710	2.194	0.00963
CLEC11A	C-type lectin domain family 11, member A	NM_002975	2.19	1.47E-05
C19orf28	chromosome 19 open reading frame 28	NM_001042680	2.188	1.49E-05
SPRR2C	small proline-rich protein 2C (pseudogene)	NR_003062	2.187	0.00256
SYNPO	synaptopodin		2.187	0.00379
TRMU	tRNA 5-methylaminomethyl-2-thiouridylate methyltransferase	NM_018006	2.187	0.000124
MAML1	mastermind-like 1 (Drosophila)	NM_014757	2.184	0.00192
KLK5	kallikrein-related peptidase 5	NM_012427	2.181	0.0133
SGSM3	small G protein signaling modulator 3	NM_015705	2.181	0.000606
C9orf9	chromosome 9 open reading frame 9	NM_018956	2.179	6.56E-05
KIAA0114	KIAA0114	NR_024031	2.179	1.07E-08
NEURL1B	neuralized homolog 1B (Drosophila)	NM_001142651	2.179	0.000544
SMAD7	SMAD family member 7	NM_005904	2.177	0.000301
GDF11	growth differentiation factor 11	NM_005811	2.174	1.18E-06

Appendix 7 (continued).

Symbol	Gene Name	Accession ID	Fold change	P value
PIGL	phosphatidylinositol glycan anchor biosynthesis, class L	NM_004278	2.173	0.00147
RIOK2	RIO kinase 2 (yeast)	NM_018343	2.168	0.0054
CDKN2A	cyclin-dependent kinase inhibitor 2A (melanoma, p16, inhibits CDK4)	NM_058197	2.168	0.000617
MFSD3	major facilitator superfamily domain containing 3	NM_138431	2.165	0.000137
TMEM161B	transmembrane protein 161B	NM_153354	2.155	0.00415
NSA2	NSA2 ribosome biogenesis homolog (S. cerevisiae)	NM_014886	2.154	0.000138
REEP2	receptor accessory protein 2	NM_016606	2.152	3.68E-05
PITX1	paired-like homeodomain 1	NM_002653	2.15	0.00189
SPOCK1	sparc/osteonectin, cwcv and kazal-like domains proteoglycan (testican) 1	NM_004598	2.143	0.000199
HOMER3	homer homolog 3 (Drosophila)	NM_001145724	2.141	1.14E-05
NADK	NAD kinase	NM_023018	2.14	1.20E-05
FAM83A	family with sequence similarity 83, member A	NM_032899	2.139	0.00152
FAM169A	family with sequence similarity 169, member A	NM_015566	2.138	0.00019
SCAF1	SR-related CTD-associated factor 1	NM_021228	2.13	0.0135
WWC1	WW and C2 domain containing 1	NM_015238	2.128	0.00032
SLC36A1	solute carrier family 36 (proton/amino acid symporter), member 1	NM_078483	2.125	0.000594
ACRC	acidic repeat containing	NM_052957	2.122	0.00061
ARSI	arylsulfatase family, member I	NM_001012301	2.119	8.70E-07
TAF8	TAF8 RNA polymerase II, TATA box binding protein (TBP)-associated factor, 43kDa	BC033728	2.118	0.000301
AP3B1	adaptor-related protein complex 3, beta 1 subunit	NM_003664	2.116	3.69E-07
GNAZ	guanine nucleotide binding protein (G protein), alpha z polypeptide	NM_002073	2.115	0.00217
CCDC99	coiled-coil domain containing 99	NM_017785	2.115	0.00103
CHD1	chromodomain helicase DNA binding protein 1	NM_001270	2.114	0.00452
BCR	breakpoint cluster region	NM_004327	2.114	8.68E-05
SLC35E2B	solute carrier family 35, member E2B	NM_001110781	2.114	0.000589
BCR	breakpoint cluster region	NM_004327	2.11	5.61E-07
CLU	clusterin	NM_203339	2.108	3.63E-06
ZNF580	zinc finger protein 580	NM_016202	2.105	0.00439
CDC42EP1	CDC42 effector protein (Rho GTPase binding) 1	NM_152243	2.104	4.56E-07

Appendix 7 (continued).

Symbol	Gene Name	Accession ID	Fold change	P value
RAB11FIP4	RAB11 family interacting protein 4 (class II)	NM_032932	2.102	0.000747
RAMP1	receptor (G protein-coupled) activity modifying protein 1	NM_005855	2.1	8.70E-07
C5orf45	chromosome 5 open reading frame 45	NM_016175	2.097	1.44E-07
SPIRE1	spire homolog 1 (Drosophila)	NM_001128626	2.096	4.03E-05
XLOC_001775			2.092	2.62E-05
TUBA3C	tubulin, alpha 3c	NM_006001	2.087	0.0012
GRK6	G protein-coupled receptor kinase 6	NM_001004105	2.086	0.00751
STK10	serine/threonine kinase 10	NM_005990	2.084	3.92E-06
ASNS	asparagine synthetase (glutamine-hydrolyzing)	NM_001673	2.083	0.000487
CXCL1	chemokine (C-X-C motif) ligand 1 (melanoma growth stimulating activity, alpha)	NM_001511	2.08	0.00565
ISCA1	iron-sulfur cluster assembly 1 homolog (S. cerevisiae)	NM_030940	2.078	0.000196
ZNF76	zinc finger protein 76	NM_003427	2.076	0.000286
MAP4K4	mitogen-activated protein kinase kinase kinase kinase 4	NM_145686	2.072	0.00435
LNPEP	leucyl/cystinyl aminopeptidase	AF178574	2.069	0.000173
CHPF2	chondroitin polymerizing factor 2	NM_019015	2.068	0.00422
SLC3A2	solute carrier family 3 (activators of dibasic and neutral amino acid transport), member 2	NM_001012662	2.068	0.00072
TMEM99	transmembrane protein 99	NM_001195386	2.067	0.00173
RARG	retinoic acid receptor, gamma	NM_000966	2.064	0.00335
IP6K1	inositol hexakisphosphate kinase 1	NM_001242829	2.064	0.00607
RASIP1	Ras interacting protein 1	NM_017805	2.061	0.00166
EGR1	early growth response 1	NM_001964	2.06	5.39E-05
LNPEP	leucyl/cystinyl aminopeptidase	NM_005575	2.059	0.000357
MLST8	MTOR associated protein, LST8 homolog (S. cerevisiae)	NM_022372	2.057	9.86E-05
HYI	hydroxypyruvate isomerase (putative)	NM_031207	2.055	0.000426
TBC1D1	TBC1 (tre-2/USP6, BUB2, cdc16) domain family, member 1	NM_015173	2.055	0.0101
FAM110C	family with sequence similarity 110, member C	NM_001077710	2.054	2.09E-05
DDIT3	DNA-damage-inducible transcript 3	NM_004083	2.051	0.000511
MGC16121	hypothetical protein MGC16121	NR_024607	2.051	0.000947
CDC42SE2	CDC42 small effector 2	NM_020240	2.047	0.0013

Appendix 7 (continued).

Symbol	Gene Name	Accession ID	Fold change	P value
ZFPM1	zinc finger protein, multitype 1	NM_153813	2.047	0.00276
ANKRD57	ankyrin repeat domain 57	NM_023016	2.046	0.00359
THOC3	THO complex 3	NM_032361	2.044	5.94E-06
NAV3	neuron navigator 3	NM_014903	2.043	0.00242
ZNF513	zinc finger protein 513	NM_144631	2.043	0.000288
AGGF1	angiogenic factor with G patch and FHA domains 1	NM_018046	2.043	0.00303
CAB39L	calcium binding protein 39-like	NM_030925	2.039	8.16E-05
CCDC92	coiled-coil domain containing 92	NM_025140	2.036	2.94E-05
SPRY4	sprouty homolog 4 (Drosophila)	NM_030964	2.036	0.000847
FAM120AOS	family with sequence similarity 120A opposite strand	CR618537	2.036	1.49E-05
MAF1	MAF1 homolog (S. cerevisiae)	NM_032272	2.035	0.000234
C3orf78	chromosome 3 open reading frame 78	NM_001124767	2.03	0.00107
SPIRE1	spire homolog 1 (Drosophila)	NM_001128626	2.028	0.00411
IDS	iduronate 2-sulfatase	NM_006123	2.026	0.00297
WDR41	WD repeat domain 41	NM_018268	2.026	0.00127
TLCD1	TLC domain containing 1	NM_138463	2.025	5.90E-06
CDK11B	cyclin-dependent kinase 11B	NM_033489	2.024	0.00421
BSG	basigin (Ok blood group)	NM_001728	2.023	0.00478
FLJ43663	hypothetical LOC378805	NR_015431	2.022	0.00405
FOXP4	forkhead box P4	NM_001012426	2.022	0.0106
RALBP1	ralA binding protein 1	NM_006788	2.02	8.10E-06
UPP1	uridine phosphorylase 1	BC047030	2.018	1.09E-06
SEC31B	SEC31 homolog B (S. cerevisiae)	NM_015490	2.013	0.00209
JUNB	jun B proto-oncogene	NM_002229	2.012	0.000677
IQSEC2	IQ motif and Sec7 domain 2	NR_024449	2.012	0.00321
DHRS11	dehydrogenase/reductase (SDR family) member 11	NM_024308	2.002	0.000943
C1orf213	chromosome 1 open reading frame 213	NR_033690	2.002	0.00565
CTNNA1	catenin (cadherin-associated protein), alpha 1, 102kDa	NM_001903	1.998	0.00576
SLC25A46	solute carrier family 25, member 46	NM_138773	1.997	7.07E-07

Appendix 7 (continued).

Symbol	Gene Name	Accession ID	Fold change	P value
POC5	POC5 centriolar protein homolog (Chlamydomonas)	NM_152408	1.991	0.000519
HSPA6	heat shock 70kDa protein 6 (HSP70B')	NM_002155	1.989	0.00702
B3GAT3	beta-1,3-glucuronyltransferase 3 (glucuronosyltransferase I)	NM_012200	1.985	0.000161
LOC375190	hypothetical protein LOC375190	NM_001145710	1.984	0.0231
IFI27L1	interferon, alpha-inducible protein 27-like 1	NM_206949	1.983	5.50E-06
ASF1B	ASF1 anti-silencing function 1 homolog B (S. cerevisiae)	NM_018154	1.981	0.00191
SLC35F3	solute carrier family 35, member F3	NM_173508	1.981	0.000417
CXCL1	chemokine (C-X-C motif) ligand 1 (melanoma growth stimulating activity, alpha)	NM_001511	1.981	0.0262
RUFY1	RUN and FYVE domain containing 1	NM_025158	1.981	8.53E-07
AKAP12	A kinase (PRKA) anchor protein 12	NM_005100	1.981	0.0085
CC2D1B	coiled-coil and C2 domain containing 1B	NM_032449	1.981	0.0037
NDUFV2	NADH dehydrogenase (ubiquinone) flavoprotein 2, 24kDa	NM_021074	1.98	1.49E-05
PPP4R1	protein phosphatase 4, regulatory subunit 1	NM_001042388	1.978	0.00047
VWCE	von Willebrand factor C and EGF domains	NM_152718	1.978	0.00272
DBN1	drebrin 1	NM_080881	1.976	0.000133
GLS	glutaminase	NM_014905	1.974	0.000318
RNF207	ring finger protein 207	NM_207396	1.972	0.02
SMAP1	small ArfGAP 1	NM_001044305	1.971	0.00535
LMO4	LIM domain only 4	NM_006769	1.969	0.00112
GRK6	G protein-coupled receptor kinase 6	NM_002082	1.966	3.93E-05
NDUFB1	NADH dehydrogenase (ubiquinone) 1 beta subcomplex, 1, 7kDa	NM_004545	1.962	4.59E-05
ADAM12	ADAM metallopeptidase domain 12	NM_003474	1.962	0.00176
SLC35E2	solute carrier family 35, member E2	NM_182838	1.958	0.000278
DUS1L	dihydrouridine synthase 1-like (S. cerevisiae)	NM_022156	1.958	0.000129
TP53I3	tumor protein p53 inducible protein 3	NM_004881	1.953	0.00013
HYI	hydroxypyruvate isomerase (putative)	NM_001190880	1.951	8.94E-06
TUBA4A	tubulin, alpha 4a	NM_006000	1.951	0.00181
HSPB8	heat shock 22kDa protein 8	NM_014365	1.949	0.00036
RUFY1	RUN and FYVE domain containing 1	NM_025158	1.947	3.81E-06

Appendix 7 (continued).

Symbol	Gene Name	Accession ID	Fold change	P value
C1R	complement component 1, r subcomponent	NM_001733	1.947	4.41E-05
RNASEH2C	ribonuclease H2, subunit C	NM_032193	1.945	0.00141
C9orf102	chromosome 9 open reading frame 102	AK095025	1.942	0.000136
MYL5	myosin, light chain 5, regulatory	NM_002477	1.938	9.25E-05
PMS2L2	postmeiotic segregation increased 2-like 2 pseudogene	BC010535	1.936	0.000184
LOC286161	hypothetical protein LOC286161	AK091672	1.936	0.000288
TTC15	tetratricopeptide repeat domain 15	NM_016030	1.934	0.000152
AFP	alpha-fetoprotein	NM_001134	1.933	0.000987
GADD45A	growth arrest and DNA-damage-inducible, alpha	NM_001924	1.932	9.86E-05
KIAA0141	KIAA0141	NM_014773	1.929	7.41E-05
MAT2B	methionine adenosyltransferase II, beta	NM_182796	1.929	0.000586
PDLIM7	PDZ and LIM domain 7 (enigma)	NM_005451	1.927	0.0141
ABHD11	abhydrolase domain containing 11	NM_001145364	1.926	2.97E-06
KRT16P2	keratin 16 pseudogene 2	NR_029392	1.926	0.000296
NEURL	neuralized homolog (Drosophila)	NM_004210	1.926	0.00719
FGFRL1	fibroblast growth factor receptor-like 1	NM_001004356	1.922	0.00332
MPPE1	metallophosphoesterase 1	NM_023075	1.922	0.00549
ABHD14B	abhydrolase domain containing 14B	NM_032750	1.919	0.0211
TTC1	tetratricopeptide repeat domain 1	NM_003314	1.915	0.00051
RAB26	RAB26, member RAS oncogene family	NM_014353	1.914	0.0119
PDLIM7	PDZ and LIM domain 7 (enigma)	NM_005451	1.912	0.0373
LFNG	LFNG O-fucosylpeptide 3-beta-N-acetylglucosaminyltransferase	NM_001040168	1.912	0.0119
CNFN	cornifelin	NM_032488	1.912	0.00115
ZBTB7B	zinc finger and BTB domain containing 7B	NM_015872	1.911	0.00042
ZBED1	zinc finger, BED-type containing 1	NM_001171135	1.911	0.000577
HSD17B1	hydroxysteroid (17-beta) dehydrogenase 1	NM_000413	1.909	1.12E-06
LOC100128737	hypothetical LOC100128737	XR_108797	1.909	2.60E-06
LOC100131607	hypothetical LOC100131607	XR_108637	1.907	0.00791
PYROXD1	pyridine nucleotide-disulphide oxidoreductase domain 1	NM_024854	1.907	0.000361
MPPE1	metallophosphoesterase 1	NM_023075	1.906	0.00227
XLOC_008115			1.903	0.00259
TNKS1BP1	tankyrase 1 binding protein 1, 182kDa	NM_033396	1.902	0.0131
SOCS2	suppressor of cytokine signaling 2	NM_003877	1.901	0.00274

Appendix 7 (continued).

Symbol	Gene Name	Accession ID	Fold change	P value
PRKCE	protein kinase C, epsilon	NM_005400	0.549	0.00054
KHNYN	KH and NYN domain containing	NM_015299	0.549	0.000148
GPR180	G protein-coupled receptor 180	NM_180989	0.549	0.00181
SPEF2	sperm flagellar 2	NM_144722	0.549	0.00262
XLOC_014209			0.548	0.00359
NEK9	NIMA (never in mitosis gene a)- related kinase 9	NM_033116	0.548	0.000232
MEX3D	mex-3 homolog D (C. elegans)	NM_001174118	0.548	0.00693
LSM14B	LSM14B, SCD6 homolog B (S. cerevisiae)	NM_144703	0.547	0.000517
SLC39A8	solute carrier family 39 (zinc transporter), member 8	NM_022154	0.547	0.000102
TRAF6	TNF receptor-associated factor 6	NM_145803	0.547	4.43E-05
FRMD6	FERM domain containing 6	NM_001042481	0.547	0.000937
ATP11C	ATPase, class VI, type 11C	NM_173694	0.547	0.000951
LOC729080	glycine cleavage system H pseudogene	NR_033244	0.547	0.00184
SON	SON DNA binding protein	NM_032195	0.546	7.96E-06
AVP	arginine vasopressin	NM_000490	0.545	0.00387
SH2D2A	SH2 domain containing 2A	NM_003975	0.545	0.00161
TMEM30B	transmembrane protein 30B	NM_001017970	0.545	0.00298
TNFRSF14	tumor necrosis factor receptor superfamily, member 14 (herpesvirus entry mediator)	NM_003820	0.544	0.00449
CPVL	carboxypeptidase, vitellogenic-like	NM_019029	0.544	0.00449
SLC37A1	solute carrier family 37 (glycerol-3-phosphate transporter), member 1	NM_018964	0.544	3.63E-06
HTR7P1	5-hydroxytryptamine (serotonin) receptor 7 pseudogene 1	NR_002774	0.544	0.00367
C14orf118	chromosome 14 open reading frame 118	NM_017972	0.544	2.73E-05
MYL9	myosin, light chain 9, regulatory	NM_181526	0.543	0.00134
CMTM8	CKLF-like MARVEL transmembrane domain containing 8	NM_178868	0.543	9.49E-06
GBP1	guanylate binding protein 1, interferon-inducible	NM_002053	0.542	0.00293
ZNF329	zinc finger protein 329	AK090893	0.542	0.00648
STAT2	signal transducer and activator of transcription 2, 113kDa	NM_005419	0.541	0.00148
JKAMP	JNK1/MAPK8-associated membrane protein	NM_016475	0.54	6.23E-05
USP16	ubiquitin specific peptidase 16	NM_001032410	0.54	0.0183
SRD5A1	steroid-5-alpha-reductase, alpha polypeptide 1 (3-oxo-5 alpha-steroid delta 4-dehydrogenase alpha 1)	NM_001047	0.54	0.00284

Appendix 8 – Average fold changes of transcripts down-regulated in CYGB+ clones.

Transcriptional targets that were considered as being significantly down-regulated if they decreased by 2 fold or more (i.e. 0.5 fold down-regulated or more) in CYGB+ (LST421) clones in comparison to the NCE (LST223) background expression of these targets are shown. All fold changes were determined from expression across a biological triplicate set of samples analysed on the Agilent SurePrint G3 Human Gene Expression 8x 60K v1 Microarray.

Symbol	Gene Name	Accession ID	Fold change	P value
CSRP2BP	CSRP2 binding protein	NM_020536	0.54	0.00623
PROCR	protein C receptor, endothelial	NM_006404	0.54	0.00228
USP48	ubiquitin specific peptidase 48	NM_001032730	0.54	0.00572
ZNF217	zinc finger protein 217	NM_006526	0.539	0.00896
FZD4	frizzled family receptor 4	NM_012193	0.538	0.00927
CNTRL	centriolin	NM_007018	0.538	0.00404
HIPK2	homeodomain interacting protein kinase 2	NM_022740	0.538	0.00105
MAR-4	membrane-associated ring finger (C3HC4) 4	NM_020814	0.537	0.0058
C20orf12	chromosome 20 open reading frame 12	NM_001099407	0.537	0.00173
PEX3	peroxisomal biogenesis factor 3	NM_003630	0.537	0.00425
ZSCAN2	zinc finger and SCAN domain containing 2	NM_181877	0.537	0.02
TBC1D19	TBC1 domain family, member 19	NM_018317	0.536	0.0021
ESRP1	epithelial splicing regulatory protein 1	NM_017697	0.536	8.10E-06
CHFR	checkpoint with forkhead and ring finger domains	NM_018223	0.536	0.0029
E2F8	E2F transcription factor 8	NM_024680	0.536	0.023
RAB2B	RAB2B, member RAS oncogene family	NM_032846	0.536	0.00856
SYTL4	synaptotagmin-like 4	NM_080737	0.536	0.000677
PIGU	phosphatidylinositol glycan anchor biosynthesis, class U	NM_080476	0.536	2.38E-05
VAPB	VAMP (vesicle-associated membrane protein)-associated protein B and C	NM_004738	0.535	0.000233
EPSTI1	epithelial stromal interaction 1 (breast)	NM_033255	0.534	0.000539
CALML4	calmodulin-like 4	NM_033429	0.534	0.000575
SLC35A3	solute carrier family 35 (UDP-N-acetylglucosamine (UDP-GlcNAc) transporter), member A3	NM_012243	0.534	0.0198
ANGEL1	angel homolog 1 (Drosophila)	NM_015305	0.534	0.0252
SEMA6C	sema domain, transmembrane domain (TM), and cytoplasmic domain, (semaphorin) 6C	NM_001178061	0.534	0.00504
CPNE1	copine I	NM_003915	0.534	1.91E-05
C1orf93	chromosome 1 open reading frame 93	NM_001195736	0.534	3.59E-05
CWF19L2	CWF19-like 2, cell cycle control (S. pombe)	NM_152434	0.533	0.00124
ZNF512B	zinc finger protein 512B	NM_020713	0.533	0.00089
ZNF138	zinc finger protein 138	NM_006524	0.533	0.0173

Appendix 8 (continued).

Symbol	Gene Name	Accession ID	Fold change	P value
CHD8	chromodomain helicase DNA binding protein 8	NM_020920	0.533	1.46E-06
PRNP	prion protein	NM_000311	0.531	0.00031
TSPAN4	tetraspanin 4	NM_001025237	0.531	0.000118
CD109	CD109 molecule	NM_133493	0.531	0.000139
LRRC56	leucine rich repeat containing 56	NM_198075	0.531	0.000291
CBR3	carbonyl reductase 3	NM_001236	0.531	0.000894
FAR1	fatty acyl CoA reductase 1	NM_032228	0.531	0.00263
FAM92A3	family with sequence similarity 92, member A3	NR_003612	0.531	0.000453
EMP1	epithelial membrane protein 1	NM_001423	0.53	0.000952
SPOCD1	SPOC domain containing 1	NM_144569	0.529	0.000603
SLCO4A1	solute carrier organic anion transporter family, member 4A1	NM_016354	0.529	0.000433
MCTP2	multiple C2 domains, transmembrane 2	NM_018349	0.529	0.00124
LOC100131096	hypothetical LOC100131096	NR_040071	0.529	0.000269
PRSS23	protease, serine, 23	NM_007173	0.529	0.00428
FMNL3	formin-like 3	NM_175736	0.529	0.000591
KLF2	Kruppel-like factor 2 (lung)	NM_016270	0.528	0.000235
ESCO2	establishment of cohesion 1 homolog 2 (S. cerevisiae)	NM_001017420	0.528	0.00445
MAP1B	microtubule-associated protein 1B	NM_005909	0.528	0.00153
PLEKHF2	pleckstrin homology domain containing, family F (with FYVE domain) member 2	NM_024613	0.527	0.00061
ACSS2	acyl-CoA synthetase short-chain family member 2	NM_018677	0.527	0.000373
MIS18BP1	MIS18 binding protein 1	NM_018353	0.527	4.91E-05
NKX3-1	NK3 homeobox 1	NM_006167	0.527	0.000129
MRPL39	mitochondrial ribosomal protein L39	NM_017446	0.526	6.57E-05
DSTNP2	destrin (actin depolymerizing factor) pseudogene 2	NR_033796	0.526	0.00201
THUMPD1	THUMP domain containing 1	NM_017736	0.525	0.000522
IFNAR2	interferon (alpha, beta and omega) receptor 2	NM_000874	0.525	8.93E-05
APCDD1L	adenomatosis polyposis coli down-regulated 1-like	NM_153360	0.524	0.00119
CSTB	cystatin B (stefin B)	NM_000100	0.523	3.92E-06
SNN	stannin	NM_003498	0.523	0.000291

Appendix 8 (continued).

Symbol	Gene Name	Accession ID	Fold change	P value
AGAP3	ArfGAP with GTPase domain, ankyrin repeat and PH domain 3	NM_001042535	0.523	0.00172
FLJ90757	hypothetical LOC440465	NR_026857	0.523	0.000295
BNIP3L	BCL2/adenovirus E1B 19kDa interacting protein 3-like	NM_004331	0.523	1.56E-05
AMPD3	adenosine monophosphate deaminase 3	NM_001025390	0.522	0.00356
DCAF11	DDB1 and CUL4 associated factor 11	NM_025230	0.521	0.00408
LACTB2	lactamase, beta 2	NM_016027	0.52	0.000334
LGALS8	lectin, galactoside-binding, soluble, 8	NM_006499	0.52	0.00321
BRWD1	bromodomain and WD repeat domain containing 1	NM_001007246	0.52	0.000407
TMEM41B	transmembrane protein 41B	NR_028491	0.52	0.00712
IFNGR2	interferon gamma receptor 2 (interferon gamma transducer 1)	NM_005534	0.519	0.000117
PHLDA1	pleckstrin homology-like domain, family A, member 1	NM_007350	0.519	0.00773
LOC439949	hypothetical LOC439949	NR_036502	0.519	7.83E-05
FAM179B	family with sequence similarity 179, member B	NM_015091	0.518	0.00505
LOC647979	hypothetical LOC647979	NR_027451	0.518	0.000205
HOMEZ	homeobox and leucine zipper encoding	NM_020834	0.517	0.00294
DCBLD2	discoidin, CUB and LCCL domain containing 2	NM_080927	0.516	0.00109
DEPDC7	DEP domain containing 7	NM_139160	0.515	0.0172
CEP250	centrosomal protein 250kDa	NM_007186	0.515	4.08E-05
SRSF1	serine/arginine-rich splicing factor 1	NM_001078166	0.515	0.000247
HMGB3P1	high mobility group box 3 pseudogene 1	NR_002165	0.514	0.000247
NAV1	neuron navigator 1	NM_020443	0.514	4.23E-06
HNRNPA3	heterogeneous nuclear ribonucleoprotein A3	NM_194247	0.514	0.00277
DENND2A	DENN/MADD domain containing 2A	NM_015689	0.513	0.000139
TFAM	transcription factor A, mitochondrial	NM_003201	0.513	0.00946
GANC	glucosidase, alpha; neutral C	NM_198141	0.513	1.70E-07
HOXA9	homeobox A9	NM_152739	0.513	0.0264
DSN1	DSN1, MIND kinetochore complex component, homolog (S. cerevisiae)	NM_024918	0.512	0.00275
STEAP2	six transmembrane epithelial antigen of the prostate 2	NM_152999	0.512	0.000533
BCAR3	breast cancer anti-estrogen resistance 3	NM_003567	0.512	2.63E-05

Appendix 8 (continued).

Symbol	Gene Name	Accession ID	Fold change	P value
C14orf128	chromosome 14 open reading frame 128	NR_027263	0.512	2.28E-05
UGT1A6	UDP glucuronosyltransferase 1 family, polypeptide A6	NM_001072	0.511	0.0021
CASD1	CAS1 domain containing 1	NM_022900	0.511	0.000119
EIF4G2	eukaryotic translation initiation factor 4 gamma, 2	NM_001172705	0.511	1.45E-05
TCF7L1	transcription factor 7-like 1 (T-cell specific, HMG-box)	NM_031283	0.51	1.77E-05
FER1L4	fer-1-like 4 (C. elegans) pseudogene	NR_024377	0.51	0.00968
ZNF626	zinc finger protein 626	NM_145297	0.509	0.00994
CD82	CD82 molecule	NM_002231	0.508	4.87E-05
CDH3	cadherin 3, type 1, P-cadherin (placental)	NM_001793	0.508	9.34E-05
BCAS4	breast carcinoma amplified sequence 4	NM_001010974	0.508	7.58E-06
CAV3	caveolin 3	NM_001234	0.508	0.00819
PDK1	pyruvate dehydrogenase kinase, isozyme 1	NM_002610	0.508	0.00109
C1orf229	chromosome 1 open reading frame 229	NM_207401	0.507	0.00653
MLH3	mutL homolog 3 (E. coli)	NM_001040108	0.507	0.00061
IRS1	insulin receptor substrate 1	NM_005544	0.506	0.00302
B7H6	B7 homolog 6	NM_001202439	0.506	0.0101
RRBP1	ribosome binding protein 1 homolog 180kDa (dog)	NM_001042576	0.505	0.0346
SNX5	sorting nexin 5	NM_014426	0.505	0.00305
C14orf126	chromosome 14 open reading frame 126	NM_080664	0.505	0.00011
HIF1A	hypoxia inducible factor 1, alpha subunit (basic helix-loop-helix transcription factor)	NM_181054	0.505	0.000796
TGM2	transglutaminase 2 (C polypeptide, protein-glutamine-gamma-glutamyltransferase)	NM_198951	0.505	0.00013
GABPA	GA binding protein transcription factor, alpha subunit 60kDa	NM_002040	0.505	0.000833
GART	phosphoribosylglycinamide formyltransferase, phosphoribosylglycinamide synthetase, phosphoribosylaminoi	NM_000819	0.504	4.59E-05
PRMT5	protein arginine methyltransferase 5	NM_001039619	0.504	0.00242
ARVCF	armadillo repeat gene deleted in velocardiofacial syndrome	NM_001670	0.504	0.00295
RRBP1	ribosome binding protein 1 homolog 180kDa (dog)	BC009700	0.504	1.13E-05
PRIC285	peroxisomal proliferator-activated receptor A interacting complex 285	NM_001037335	0.504	5.37E-06
LOC647979	hypothetical LOC647979	NR_027451	0.503	0.0068
PHYH	phytanoyl-CoA 2-hydroxylase	NM_001037537	0.502	0.000249

Appendix 8 (continued).

Symbol	Gene Name	Accession ID	Fold change	P value
SNX16	sorting nexin 16	NM_022133	0.502	0.0174
LOC647070	hypothetical LOC647070	AK001442	0.501	0.0269
SON	SON DNA binding protein	NM_032195	0.5	2.46E-05
PORCN	porcupine homolog (Drosophila)	NM_203473	0.499	7.18E-05
GPR153	G protein-coupled receptor 153	NM_207370	0.499	0.00192
FLRT3	fibronectin leucine rich transmembrane protein 3	NM_198391	0.499	0.00294
VWA1	von Willebrand factor A domain containing 1	NM_022834	0.498	0.000306
CAP2	CAP, adenylate cyclase-associated protein, 2 (yeast)	NM_006366	0.498	1.95E-06
ITGB6	integrin, beta 6	NM_000888	0.497	0.000581
TGDS	TDP-glucose 4,6-dehydratase	NM_014305	0.497	0.00238
PHF14	PHD finger protein 14	NM_014660	0.496	0.00024
APEX1	APEX nuclease (multifunctional DNA repair enzyme) 1	NM_080649	0.496	0.00208
ZCCHC3	zinc finger, CCHC domain containing 3	NM_033089	0.496	5.94E-07
MYLK2	myosin light chain kinase 2	NM_033118	0.495	0.00031
BDKRB1	bradykinin receptor B1	NM_000710	0.494	0.00597
C20orf177	chromosome 20 open reading frame 177	NM_001190826	0.494	0.00134
PM20D2	peptidase M20 domain containing 2	NM_001010853	0.494	0.00147
RAVER1	ribonucleoprotein, PTB-binding 1	NM_133452	0.493	0.0139
SBF2	SET binding factor 2	NM_030962	0.491	0.00042
ZSWIM3	zinc finger, SWIM-type containing 3	NM_080752	0.49	0.0368
ASPH	aspartate beta-hydroxylase	NM_004318	0.49	9.28E-06
SGK494	uncharacterized serine/threonine-protein kinase SgK494	NM_001174103	0.49	0.00419
SUPT16H	suppressor of Ty 16 homolog (S. cerevisiae)	NM_007192	0.489	0.000387
HAS3	hyaluronan synthase 3	NM_005329	0.489	0.00258
C14orf45	chromosome 14 open reading frame 45	NM_025057	0.489	0.0195
GZF1	GDNF-inducible zinc finger protein 1	NM_022482	0.489	0.000375
LDHA	lactate dehydrogenase A	NM_005566	0.489	0.00778
PTGER4	prostaglandin E receptor 4 (subtype EP4)	NM_000958	0.488	0.000901
CRYZL1	crystallin, zeta (quinone reductase)-like 1	NM_145858	0.488	0.000238

Appendix 8 (continued).

Symbol	Gene Name	Accession ID	Fold change	P value
FAM83D	family with sequence similarity 83, member D	NM_030919	0.488	2.40E-05
NGDN	neuroguidin, EIF4E binding protein	NM_001042635	0.488	2.90E-06
AP4S1	adaptor-related protein complex 4, sigma 1 subunit	NM_007077	0.488	0.0032
MIG7	mig-7	DQ080207	0.488	0.000123
ALOX12	arachidonate 12-lipoxygenase	NM_000697	0.487	0.00227
DCAF5	DDB1 and CUL4 associated factor 5	NM_003861	0.487	0.00887
FANCC	Fanconi anemia, complementation group C	AK222871	0.487	2.24E-05
WRB	tryptophan rich basic protein	NM_004627	0.486	0.000434
PXMP4	peroxisomal membrane protein 4, 24kDa	NM_007238	0.486	2.38E-05
SLC7A2	solute carrier family 7 (cationic amino acid transporter, y+ system), member 2	NM_001008539	0.486	0.00085
TXNDC16	thioredoxin domain containing 16	NM_020784	0.484	0.00443
ZBTB1	zinc finger and BTB domain containing 1	NM_014950	0.484	0.000656
GPR68	G protein-coupled receptor 68	NM_003485	0.484	4.60E-05
KIF16B	kinesin family member 16B	NM_001199866	0.484	2.22E-06
METTL3	methyltransferase like 3	NM_019852	0.483	1.48E-06
PFDN4	prefoldin subunit 4	NM_002623	0.481	0.00173
MCM8	minichromosome maintenance complex component 8	NM_182802	0.481	7.88E-06
IL12RB2	interleukin 12 receptor, beta 2	NM_001559	0.481	0.00318
DPY19L4	dpy-19-like 4 (C. elegans)	NM_181787	0.481	0.000629
ITGA6	integrin, alpha 6	NM_000210	0.48	0.000508
SLC37A2	solute carrier family 37 (glycerol-3-phosphate transporter), member 2	NM_198277	0.48	4.17E-07
RBMS2	RNA binding motif, single stranded interacting protein 2	NM_002898	0.479	0.000606
ALG10B	asparagine-linked glycosylation 10, alpha-1,2-glucosyltransferase homolog B (yeast)	NM_001013620	0.478	0.000559
ITSN1	intersectin 1 (SH3 domain protein)	NM_001001132	0.478	0.000385
RUNX1	runt-related transcription factor 1	NM_001001890	0.477	5.07E-06
SYTL1	synaptotagmin-like 1	NM_032872	0.477	2.59E-06
C16orf48	chromosome 16 open reading frame 48	NM_032140	0.476	7.50E-07
IL1RAP	interleukin 1 receptor accessory protein	NM_134470	0.476	0.00781
DUOX1	dual oxidase 1	NM_017434	0.476	0.000199

Appendix 8 (continued).

Symbol	Gene Name	Accession ID	Fold change	P value
API5	apoptosis inhibitor 5	NM_006595	0.476	5.92E-05
ADPRH	ADP-ribosylarginine hydrolase	NM_001125	0.476	0.000116
LOC100128184	hypothetical protein LOC100128184	AK128032	0.476	1.46E-06
SLC13A3	solute carrier family 13 (sodium-dependent dicarboxylate transporter), member 3	NM_001193339	0.476	0.000129
HES2	hairy and enhancer of split 2 (Drosophila)	BC012091	0.475	7.82E-05
ARL6IP6	ADP-ribosylation-like factor 6 interacting protein 6	NM_152522	0.474	0.00754
STRN3	striatin, calmodulin binding protein 3	NM_014574	0.474	0.000195
NDRG2	NDRG family member 2	NM_201535	0.474	4.82E-06
LOC145694	hypothetical LOC145694	XR_109210	0.474	0.00726
NEK11	NIMA (never in mitosis gene a)- related kinase 11	NM_145910	0.473	2.26E-05
PLAGL2	pleiomorphic adenoma gene-like 2	NM_002657	0.473	2.44E-05
G2E3	G2/M-phase specific E3 ubiquitin protein ligase	NM_017769	0.473	0.000116
FAM198B	family with sequence similarity 198, member B	NM_016613	0.472	0.00288
GINS1	GINS complex subunit 1 (Psf1 homolog)	NM_021067	0.472	0.000402
CBFA2T2	core-binding factor, runt domain, alpha subunit 2; translocated to, 2	NM_005093	0.471	0.00788
LOC100133224	hypothetical protein LOC100133224	XM_001716151	0.471	0.0495
RRP1B	ribosomal RNA processing 1 homolog B (S. cerevisiae)	NM_015056	0.471	7.76E-05
MOSC1	MOCO sulphurase C-terminal domain containing 1	NM_022746	0.471	0.000952
RPRD1B	regulation of nuclear pre-mRNA domain containing 1B	NM_021215	0.469	1.65E-05
MAP3K5	mitogen-activated protein kinase kinase kinase 5	NM_005923	0.469	0.000833
LOC100508670	putative high mobility group protein B3-like protein-like	XM_003119674	0.468	6.31E-05
PBX4	pre-B-cell leukemia homeobox 4	NM_025245	0.467	0.000814
ARHGAP18	Rho GTPase activating protein 18	NM_033515	0.467	0.000699
AURKAPS1	aurora kinase A pseudogene 1	NR_001587	0.467	0.00234
CPNE1	copine I	NM_003915	0.467	1.87E-05
CBR1	carbonyl reductase 1	NM_001757	0.466	0.000305
TRAPPC10	trafficking protein particle complex 10	NM_003274	0.464	0.00243
HSPA13	heat shock protein 70kDa family, member 13	NM_006948	0.464	0.00035
LOC441869	hypothetical protein LOC441869	NM_001145210	0.463	1.66E-05

Appendix 8 (continued).

Symbol	Gene Name	Accession ID	Fold change	P value
KLRAQ1	KLRAQ motif containing 1	NM_152994	0.463	0.000516
CLCN5	chloride channel 5	NM_001127899	0.463	0.00577
RIN2	Ras and Rab interactor 2	NM_018993	0.462	0.00118
ITGA2	integrin, alpha 2 (CD49B, alpha 2 subunit of VLA-2 receptor)	NM_002203	0.461	0.00483
PARD6B	par-6 partitioning defective 6 homolog beta (C. elegans)	NM_032521	0.461	0.000235
LGR4	leucine-rich repeat containing G protein-coupled receptor 4	NM_018490	0.46	0.00125
DUOXA1	dual oxidase maturation factor 1	NM_144565	0.459	0.019
OSBPL5	oxysterol binding protein-like 5	NM_020896	0.458	6.74E-08
HNRNPCL1	heterogeneous nuclear ribonucleoprotein C-like 1	NM_001013631	0.458	0.00185
WDR89	WD repeat domain 89	NM_001008726	0.458	0.00053
FNBP1	formin binding protein 1	AK023681	0.458	0.000805
ZDHHC13	zinc finger, DHHC-type containing 13	NM_019028	0.457	0.000245
ITSN1	intersectin 1 (SH3 domain protein)	NM_001001132	0.457	0.000192
EREG	epiregulin	NM_001432	0.457	0.00184
S100A4	S100 calcium binding protein A4	NM_002961	0.457	0.00043
GPR88	G protein-coupled receptor 88	NM_022049	0.457	0.00436
PPARG	peroxisome proliferator-activated receptor gamma	NM_138711	0.456	3.38E-07
PIGP	phosphatidylinositol glycan anchor biosynthesis, class P	NM_153681	0.455	0.00553
SNTA1	syntrophin, alpha 1 (dystrophin-associated protein A1, 59kDa, acidic component)	NM_003098	0.455	0.00304
MORC2-AS1	MORC2 antisense RNA 1 (non-protein coding)	NR_026920	0.455	2.10E-06
DHRS4L2	dehydrogenase/reductase (SDR family) member 4 like 2	NM_001193636	0.455	0.000468
POLE2	polymerase (DNA directed), epsilon 2 (p59 subunit)	NM_002692	0.454	0.000617
WEE1	WEE1 homolog (S. pombe)	NM_003390	0.453	1.75E-05
BACH1	BTB and CNC homology 1, basic leucine zipper transcription factor 1	NM_206866	0.451	0.000669
SON	SON DNA binding protein	NM_032195	0.451	4.87E-05
DZIP1	DAZ interacting protein 1	NM_198968	0.45	6.44E-05
RAD51AP1	RAD51 associated protein 1	NM_006479	0.449	0.000228
FGF7	fibroblast growth factor 7	NM_002009	0.449	0.000229
SSH2	slingshot homolog 2 (Drosophila)	BC011636	0.449	4.43E-05

Appendix 8 (continued).

Symbol	Gene Name	Accession ID	Fold change	P value
AK4	adenylate kinase 4	NM_001005353	0.448	0.000352
TIMP4	TIMP metallopeptidase inhibitor 4	NM_003256	0.448	0.000768
LOC100509022	splicing factor U2AF 35 kDa subunit-like	XM_003119609	0.447	4.06E-05
ZNF395	zinc finger protein 395	NM_018660	0.446	1.10E-08
C11orf74	chromosome 11 open reading frame 74	NM_138787	0.444	3.92E-06
B3GNT3	UDP-GlcNAc:betaGal beta-1,3-N-acetylglucosaminyltransferase 3	NM_014256	0.443	5.30E-05
DHRS4	dehydrogenase/reductase (SDR family) member 4	NM_021004	0.443	0.000145
TIMP3	TIMP metallopeptidase inhibitor 3	NM_000362	0.442	1.87E-05
HKR1	HKR1, GLI-Kruppel zinc finger family member	NM_181786	0.441	2.38E-05
CDS2	CDP-diacylglycerol synthase (phosphatidate cytidylyltransferase) 2	NM_003818	0.441	0.000305
ADAMTS1	ADAM metallopeptidase with thrombospondin type 1 motif, 1	NM_006988	0.439	0.000496
SYT16	synaptotagmin XVI	NM_031914	0.439	0.000407
USP16	ubiquitin specific peptidase 16	NM_001001992	0.439	3.05E-05
GRHL1	grainyhead-like 1 (Drosophila)	NM_198182	0.438	0.000655
HCG11	HLA complex group 11	NR_026790	0.438	0.000901
FLJ42627	hypothetical LOC645644	AK126677	0.438	7.37E-05
ZNF219	zinc finger protein 219	NM_016423	0.437	1.87E-05
CLCN4	chloride channel 4	NM_001830	0.437	4.16E-05
MORC3	MORC family CW-type zinc finger 3	NM_015358	0.436	2.68E-05
PAPLN	papilin, proteoglycan-like sulfated glycoprotein	NM_173462	0.436	2.44E-05
KCNJ15	potassium inwardly-rectifying channel, subfamily J, member 15	NM_170736	0.436	0.000306
C14orf128	chromosome 14 open reading frame 128	NR_027263	0.435	0.000238
DHRS4	dehydrogenase/reductase (SDR family) member 4	NM_021004	0.434	3.13E-07
DSCAM	Down syndrome cell adhesion molecule	NM_001389	0.434	3.15E-05
TMEM67	transmembrane protein 67	NM_153704	0.433	0.000619
GNB4	guanine nucleotide binding protein (G protein), beta polypeptide 4	NM_021629	0.433	2.30E-05
SLC35A3	solute carrier family 35 (UDP-N-acetylglucosamine (UDP-GlcNAc) transporter), member A3	NM_012243	0.432	3.63E-06
PROM2	prominin 2	NM_001165978	0.432	1.45E-05
N6AMT1	N-6 adenine-specific DNA methyltransferase 1 (putative)	NM_013240	0.43	9.13E-06

Appendix 8 (continued).

Symbol	Gene Name	Accession ID	Fold change	P value
HSPA2	heat shock 70kDa protein 2	NM_021979	0.429	9.44E-05
DIP2A	DIP2 disco-interacting protein 2 homolog A (Drosophila)	NM_206890	0.428	0.000156
FANCF	Fanconi anemia, complementation group F	NM_022725	0.427	3.59E-05
LHX6	LIM homeobox 6	NM_014368	0.426	1.04E-05
CCNYL1	cyclin Y-like 1	NM_152523	0.426	0.000489
ADAMTS1	ADAM metallopeptidase with thrombospondin type 1 motif, 1	NM_006988	0.426	0.00299
LOC152225	hypothetical LOC152225	NR_026934	0.426	0.00147
ACCS	1-aminocyclopropane-1-carboxylate synthase homolog (Arabidopsis)(non-functional)	NM_032592	0.425	4.43E-05
SOX7	SRY (sex determining region Y)-box 7	NM_031439	0.425	8.10E-06
TRERF1	transcriptional regulating factor 1	NM_033502	0.425	6.14E-05
FMN1	formin 1	NM_001103184	0.424	0.0122
ANKRD1	ankyrin repeat domain 1 (cardiac muscle)	NM_014391	0.421	0.00173
NRP1	neuropilin 1	NM_001024629	0.421	6.78E-08
PDXK	pyridoxal (pyridoxine, vitamin B6) kinase	NM_003681	0.421	2.63E-07
DYRK1A	dual-specificity tyrosine-(Y)-phosphorylation regulated kinase 1A	NM_130438	0.421	8.34E-05
PECR	peroxisomal trans-2-enoyl-CoA reductase	NM_018441	0.419	0.00145
DYRK1A	dual-specificity tyrosine-(Y)-phosphorylation regulated kinase 1A	NM_130436	0.418	9.09E-06
NUCB2	nucleobindin 2	NM_005013	0.417	0.000192
TRPM4	transient receptor potential cation channel, subfamily M, member 4	NM_017636	0.417	3.18E-05
AGPAT9	1-acylglycerol-3-phosphate O-acyltransferase 9	NM_032717	0.417	0.00047
ITCH	itchy E3 ubiquitin protein ligase homolog (mouse)	NM_031483	0.417	0.000342
CD40	CD40 molecule, TNF receptor superfamily member 5	NM_001250	0.416	6.30E-06
CEP250	centrosomal protein 250kDa	NM_007186	0.415	0.000886
WFDC2	WAP four-disulfide core domain 2	NM_006103	0.414	0.000465
CD163L1	CD163 molecule-like 1	NM_174941	0.413	1.18E-06
TOP1P2	topoisomerase (DNA) I pseudogene 2	NR_001283	0.413	2.16E-05
ARHGAP27	Rho GTPase activating protein 27	NM_174919	0.413	4.75E-05
SLC19A1	solute carrier family 19 (folate transporter), member 1	NM_194255	0.413	5.32E-06
AP1G2	adaptor-related protein complex 1, gamma 2 subunit	NM_003917	0.412	3.34E-06

Appendix 8 (continued).

Symbol	Gene Name	Accession ID	Fold change	P value
PTK6	PTK6 protein tyrosine kinase 6	NM_005975	0.412	4.13E-05
GPX2	glutathione peroxidase 2 (gastrointestinal)	NM_002083	0.411	8.79E-06
C20orf194	chromosome 20 open reading frame 194	NM_001009984	0.411	0.00316
ACOT4	acyl-CoA thioesterase 4	NM_152331	0.41	2.42E-05
SEMA3A	sema domain, immunoglobulin domain (Ig), short basic domain, secreted, (semaphorin) 3A	NM_006080	0.41	7.82E-05
CA13	carbonic anhydrase XIII	NM_198584	0.409	0.00119
C7orf58	chromosome 7 open reading frame 58	NM_024913	0.409	2.14E-06
NDRG2	NDRG family member 2	NM_201535	0.409	1.18E-08
CD40	CD40 molecule, TNF receptor superfamily member 5	NM_001250	0.406	1.62E-07
C7orf58	chromosome 7 open reading frame 58	NM_024913	0.406	3.34E-06
PKIB	protein kinase (cAMP-dependent, catalytic) inhibitor beta	NM_181795	0.404	0.00265
PRPF40B	PRP40 pre-mRNA processing factor 40 homolog B (S. cerevisiae)	NM_001031698	0.404	0.005
TMEM50B	transmembrane protein 50B	NM_006134	0.404	1.48E-06
DKK3	dickkopf homolog 3 (Xenopus laevis)	NM_015881	0.404	0.000306
MAMDC4	MAM domain containing 4	NM_206920	0.403	8.96E-05
TTC5	tetratricopeptide repeat domain 5	NM_138376	0.403	0.000116
LRIG3	leucine-rich repeats and immunoglobulin-like domains 3	NM_153377	0.402	4.54E-05
C21orf59	chromosome 21 open reading frame 59	NM_021254	0.402	0.000125
EPS8L2	EPS8-like 2	NM_022772	0.401	7.07E-07
ITSN1	intersectin 1 (SH3 domain protein)	NM_001001132	0.401	2.10E-06
LOC440525	proline rich 13 pseudogene	BI224516	0.401	0.00025
ZNF573	zinc finger protein 573	NM_152360	0.398	0.000207
AP4S1	adaptor-related protein complex 4, sigma 1 subunit	NM_001128126	0.398	0.000507
SLC7A8	solute carrier family 7 (amino acid transporter light chain, L system), member 8	NM_182728	0.397	0.000205
FAM165B	family with sequence similarity 165, member B	BC045820	0.397	1.82E-05
MMP14	matrix metallopeptidase 14 (membrane-inserted)	NM_004995	0.397	3.26E-08
LOC389831	hypothetical LOC389831	NM_001242480	0.396	1.50E-05
WFDC2	WAP four-disulfide core domain 2	NM_006103	0.395	0.00167
ANKRD5	ankyrin repeat domain 5	NM_022096	0.393	2.03E-05

Appendix 8 (continued).

Symbol	Gene Name	Accession ID	Fold change	P value
RPL27A	ribosomal protein L27a	NM_000990	0.392	0.019
SLC20A1	solute carrier family 20 (phosphate transporter), member 1	NM_005415	0.391	6.52E-05
DSCR3	Down syndrome critical region gene 3	NM_006052	0.389	2.10E-06
DONSON	downstream neighbor of SON	NM_017613	0.388	9.10E-06
NFE2L3	nuclear factor (erythroid-derived 2)-like 3	NM_004289	0.388	2.38E-05
LOC645195	hypothetical LOC645195	AK123450	0.388	0.000183
TSPAN1	tetraspanin 1	NM_005727	0.387	7.58E-08
DCBLD2	discoidin, CUB and LCCL domain containing 2	NM_080927	0.387	9.24E-06
FOXL1	forkhead box L1	NM_005250	0.387	0.000152
LOC389831	hypothetical LOC389831	NM_001242480	0.385	5.33E-05
BTG3	BTG family, member 3	NM_006806	0.384	0.00478
MGC4294	hypothetical MGC4294	XR_109628	0.383	1.03E-05
LMCD1	LIM and cysteine-rich domains 1	NM_014583	0.383	3.63E-06
NEK11	NIMA (never in mitosis gene a)- related kinase 11	NM_024800	0.382	8.10E-06
C20orf54	chromosome 20 open reading frame 54	NM_033409	0.381	0.00369
CBFA2T2	core-binding factor, runt domain, alpha subunit 2; translocated to, 2	JF432662	0.379	3.59E-05
MAMSTR	MEF2 activating motif and SAP domain containing transcriptional regulator	NM_182574	0.378	1.24E-06
SNORD17	small nucleolar RNA, C/D box 17	NR_003045	0.375	7.07E-07
HMGA2	high mobility group AT-hook 2	NM_003483	0.372	0.00035
FOXB1	forkhead box B1	NM_012182	0.368	0.000814
NPAS2	neuronal PAS domain protein 2	NM_002518	0.368	0.00567
LOC644189	acyl-CoA thioesterase 4 pseudogene	NR_033748	0.367	0.000453
ITGB8	integrin, beta 8	NM_002214	0.365	7.76E-05
SNX21	sorting nexin family member 21	NM_001042633	0.364	7.07E-07
DHRS4L1	dehydrogenase/reductase (SDR family) member 4 like 1	NM_001082488	0.363	0.000339
FZD7	frizzled family receptor 7	NM_003507	0.36	6.23E-05
LTN1	listerin E3 ubiquitin protein ligase 1	NM_015565	0.36	0.000117
SLC5A3	solute carrier family 5 (sodium/myo-inositol cotransporter), member 3	NM_006933	0.359	0.000155
JPH2	junctophilin 2	NM_020433	0.358	0.000105

Appendix 8 (continued).

Symbol	Gene Name	Accession ID	Fold change	P value
PPARG	peroxisome proliferator-activated receptor gamma	NM_138711	0.358	9.28E-06
LRRCC1	leucine rich repeat and coiled-coil domain containing 1	NM_033402	0.356	4.03E-05
GCFC1	GC-rich sequence DNA-binding factor 1	NM_013329	0.353	0.000244
SLC22A18AS	solute carrier family 22 (organic cation transporter), member 18 antisense	NM_007105	0.352	0.00013
LCTL	lactase-like	NM_207338	0.352	3.92E-05
CAPRIN1	cell cycle associated protein 1	NM_203364	0.349	7.80E-07
MAP3K5	mitogen-activated protein kinase kinase kinase 5	NM_005923	0.348	6.38E-06
CFH	complement factor H	NM_001014975	0.346	1.77E-07
DCAF5	DDB1 and CUL4 associated factor 5	BC022967	0.346	0.000228
CRYZL1	crystallin, zeta (quinone reductase)-like 1	NM_145858	0.341	0.000389
OXTR	oxytocin receptor	NM_000916	0.341	1.75E-06
UNCX	UNC homeobox	NM_001080461	0.34	0.000114
JAG1	jagged 1	NM_000214	0.338	2.94E-05
XLOC_005764			0.337	0.00497
CXADR	coxsackie virus and adenovirus receptor	NM_001338	0.333	1.55E-05
KCNJ15	potassium inwardly-rectifying channel, subfamily J, member 15	NM_170736	0.331	7.21E-05
C21orf91	chromosome 21 open reading frame 91	NM_017447	0.323	1.78E-07
SLC4A11	solute carrier family 4, sodium borate transporter, member 11	NM_032034	0.317	9.36E-05
HMGB3P24	high mobility group box 3 pseudogene 24	XM_929965	0.313	4.75E-05
ARHGEF40	Rho guanine nucleotide exchange factor (GEF) 40	NM_018071	0.31	1.35E-05
ASB9	ankyrin repeat and SOCS box containing 9	NM_001031739	0.305	0.00107
TEP1	telomerase-associated protein 1	NM_007110	0.304	8.09E-07
HIF1A	hypoxia inducible factor 1, alpha subunit (basic helix-loop-helix transcription factor)	NM_181054	0.304	9.22E-06
PLCB2	phospholipase C, beta 2	NM_004573	0.296	1.44E-07
LOC642852	hypothetical LOC642852	NR_026943	0.293	1.12E-06
FLJ37786	hypothetical LOC642691	XR_108343	0.265	0.00014
CFH	complement factor H	NM_000186	0.264	7.59E-07
MRPL52	mitochondrial ribosomal protein L52	NM_181304	0.26	1.05E-07
MAMDC2	MAM domain containing 2	NM_153267	0.253	8.22E-06
DUOXA1	dual oxidase maturation factor 1	EU927394	0.251	2.30E-05
TNS4	tensin 4	NM_032865	0.218	7.14E-08
LOC645431	hypothetical LOC645431	NR_024334	0.212	8.10E-06
OSGEP	O-sialoglycoprotein endopeptidase	NM_017807	0.208	1.04E-06
DIAPH2	diaphanous homolog 2 (Drosophila)	NM_007309	0.177	0.0001

Appendix 8 (continued).

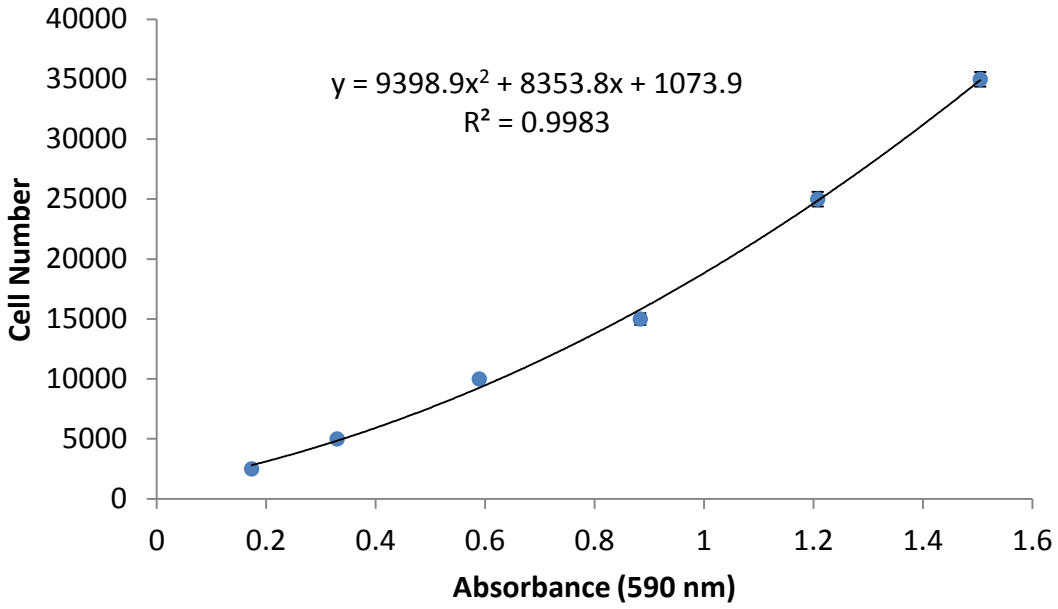

Appendix 9 – Crystal Violet Calibration Curve.

Cells were seeded into 96 well plates at increasing cell densities in quadruplet from 2500 cell per well to 35000 cell per well. After 3 hours, the cells had adhered to the surface of the plastic and were then subject to the crystal violet assay. Absorbances were corrected to the 10 % acetic acid solvent blank and then plotted against the cell number. There was a clear and tight relationship observed between absorbance at 590 nm and cell number, suggesting that the assay would be able to yield an accurate inference of cell number from crystal violet stained cell cultures, using non-linear regression and the equation $y= 9398.9x^2 + 8353.8x + 1073.9$, where y is cell number and x is absorbance at 590 nm.

References

Aghajanian, A., Wittchen, E.S., Campbell, S.L., et al. (2009) Direct Activation of RhoA by Reactive Oxygen Species Requires a Redox-Sensitive Motif. **Plos One,** 4 (11): e8045.

Ajioka, R.S., Phillips, J.D. and Kushner, J.P. (2006) Biosynthesis of heme in mammals. **Biochimica et Biophysica Acta (BBA) - Molecular Cell Research,** 1763 (7): 723-736.

Akhurst, R.J. and Derynck, R. (2001) TGF-beta signaling in cancer - a double-edged sword. **Trends in cell biology,** 11 (11): S44-S51.

Alcolado, R., Arthur, M. and Iredale, J. (1997) Pathogenesis of liver fibrosis. **Clinical science,** 92 (2): 103-112.

Ali, A.Y., Abedini, M.R. and Tsang, B.K. (2012) The oncogenic phosphatase PPM1D confers cisplatin resistance in ovarian carcinoma cells by attenuating checkpoint kinase 1 and p53 activation. **Oncogene,** 31 (17): 2175-2186Andersen, J.L., Kornbluth, S. (2013) The tangled circuitry of metabolism and apoptosis. **Molecular Cell.** 49(3): 399-410.

Andrews, G.A., Xi, S.C., Pomerantz, R.G., et al. (2004) Mutation of P53 in head and neck squamous cell carcinoma correlates with BCL-2 expression and increased susceptibility to cisplatin-induced apoptosis. **Head and Neck-Journal for the Sciences and Specialties of the Head and Neck,** 26 (10): 870-877.

Arthur, W.T. and Burridge, K. (2001) RhoA inactivation by p190RhoGAP regulates cell spreading and migration by promoting membrane protrusion and polarity. **Molecular biology of the cell,** 12 (9): 2711-2720.

Asahina, K., Kawada, N., Kristensen, D.B., et al. (2002) Characterization of human stellate cell activation-associated protein and its expression in human liver. **Biochimica Et Biophysica Acta-Gene Structure and Expression,** 1577 (3): 471-475.

Ascenzi, P., Marino, M., Polticelli, F., et al. (2013) Non-covalent and covalent modifications modulate the reactivity of monomeric mammalian globins. **Biochimica et Biophysica Acta (BBA) - Proteins and Proteomics,** 1834 (9): 1750-1756.

Asher, G., Lotem, J., Kama, R., et al. (2002) NQ01 stabilizes p53 through a distinct pathway. **Proceedings of the National Academy of Sciences of the United States of America,** 99 (5): 3099-3104.

Bachman, K.E. and Park, B.H. (2005) Duel nature of TGF-beta signaling: tumor suppressor vs. tumor promoter. **Current opinion in oncology,** 17 (1): 49-54.

Barr, M.P., Gray, S.G., Hoffmann, A.C., et al. (2013) Generation and Characterisation of Cisplatin-Resistant Non-Small Cell Lung Cancer Cell Lines Displaying a Stem-Like Signature. **Plos One,** 8 (1): e54193.

Baskar, R., Lee, K.A., Yeo, R., et al. (2012) Cancer and Radiation Therapy: Current Advances and Future Directions. **International Journal of Medical Sciences,** 9 (3): 193-199.

Bataller, R. and Brenner, D.A. (2005) Liver fibrosis. **Journal of Clinical Investigation,** 115 (2): 209-218.

Berchner-Pfannschmidt, U., Yamac, H., Trinidad, B., et al. (2007) Nitric oxide modulates oxygen sensing by hypoxia-inducible factor 1-dependent induction of prolyl hydroxylase 2. **Journal of Biological Chemistry,** 282 (3): 1788-1796.

Bernier, J., Domenge, C., Ozsahin, M., et al. (2004) Postoperative irradiation with or without concomitant chemotherapy for locally advanced head and neck cancer. **New England Journal of Medicine,** 350 (19): 1945-1952.

Berridge, M.V. and Tan, A.S. (1993) Characterization of the Cellular Reduction of 3-(4,5-Dimethylthiazol-2-Yl)-2,5-Diphenyltetrazolium Bromide (Mtt) - Subcellular-Localization, Substrate Dependence, and Involvement of Mitochondrial Electron-Transport in Mtt Reduction. **Archives of Biochemistry and Biophysics,** 303 (2): 474-482.

Berry, E.A. and Trumpower, B.L. (1987) Simultaneous Determination of Hemes-A, Hemes-B, and Hemes-C from Pyridine Hemochrome Spectra. **Analytical Biochemistry,** 161 (1): 1-15.

Blaydon, D., Etheridge, S., Risk, J., et al. (2012) RHBDF2 Mutations Are Associated with Tylosis, a Familial Esophageal Cancer Syndrome. **The American Journal of Human Genetics,** 90 (2): 340-346.

Bosselut, N., Housset, C., Marcelo, P., et al. (2010) Distinct proteomic features of two fibrogenic liver cell populations: Hepatic stellate cells and portal myofibroblasts. **Proteomics,** 10 (5): 1017-1028.

Braakhuis, B.J.M., Bloemena, E., Leemans, C.R., et al. (2010) Molecular analysis of surgical margins in head and neck cancer: More than a marginal issue. **Oral oncology,** 46 (7): 485-491.

Brand, M.D., Affourtit, C., Esteves, T.C., et al. (2004) Mitochondrial superoxide: production, biological effects, and activation of uncoupling proteins. **Free Radical Biology and Medicine,** 37 (6): 755-767.

Brown, G.C. and Borutaite, V. (2008) Regulation of apoptosis by the redox state of cytochrome c. **Biochimica et Biophysica Acta (BBA) - Bioenergetics,** 1777 (7–8): 877-881.

Brown, V.L., Harwood, C.A., Crook, T., et al. (2004) P16(INK4a) and p14(ARF) tumor suppressor genes are commonly inactivated in cutaneous squamous cell carcinoma. **Journal of Investigative Dermatology,** 122 (5): 1284-1292.

Brozovic, A., Ambriovic-Ristov, A. and Osmak, M. (2010) The relationship between cisplatin-induced reactive oxygen species, glutathione, and BCL-2 and resistance to cisplatin. **Critical reviews in toxicology,** 40 (4): 347-359.

Bucher, N. and Britten, C.D. (2008) G2 checkpoint abrogation and checkpoint kinase-1 targeting in the treatment of cancer. **British Journal of Cancer**. 98(3): 523-528.

Burhans, W.C. and Heintz, N.H. (2009) The cell cycle is a redox cycle: Linking phase-specific targets to cell fate. **Free Radical Biology and Medicine,** 47 (9): 1282-1293.

Burmester, T., Ebner, B., Weich, B., et al. (2002) Cytoglobin: A novel globin type ubiquitously expressed in vertebrate tissues. **Molecular biology and evolution,** 19 (4): 416-421.

Burmester, T., Gerlach, F. and Hankeln, T. (2007) Regulation and role of neuroglobin and cytoglobin under hypoxia. **Hypoxia and the Circulation,** 618 169-180.

Burmester, T., Haberkamp, M., Mitz, S., et al. (2004) Neuroglobin and cytoglobin: Genes, proteins and evolution. **IUBMB life,** 56 (11-12): 703-707.

Burmester, T., Weich, B., Reinhardt, S., et al. (2000) A vertebrate globin expressed in the brain. **Nature,** 407 (6803): 520-523.

Bussink, J., van der Kogel, A.J. and Kaanders, J.H.A.M. (2008) Activation of the PI3-K/AKT pathway and implications for radioresistance mechanisms in head and neck cancer. **Lancet Oncology,** 9 (3): 288-296.

Carpenter, M. (2010) **The expression profile of cytoglobin in human fibrotic lung, and the protective role of cytoglobin in hypoxia and oxidative stress in vitro.** PhD, University of Birmingham.

Chakravarthi, S., Jessop, C. and Bulleid, N. (2006) The role of glutathione in disulfide bond formation and endoplasmic-reticulum-generated oxidative stress. **EMBO reports,** 7 (3): 271-275.

Chang, C., Chen, Y., Chou, S., et al. (2014a) Distinct Subpopulations of Head and Neck Cancer Cells with Different Levels of Intracellular Reactive Oxygen Species Exhibit Diverse Stemness, Proliferation, and Chemosensitivity. **Cancer research,** 74 (21): 6291-6305.

Chang, G.H.K., Lay, A.J., Ting, K.K., et al. (2014b) ARHGAP18: an endogenous inhibitor of angiogenesis, limiting tip formation and stabilizing junctions. **Small GTPases,** 5 (3): 1-15.

Chen, H., Zhao, X. and Meng, T. (2014) Expression and biological role of cytoglobin in human ovarian cancer.

Chen, X., Zhong, Z., Xu, Z., et al. (2010) 2 ',7 '-Dichlorodihydrofluorescein as a fluorescent probe for reactive oxygen species measurement: Forty years of application and controversy. **Free radical research,** 44 (6): 587-604.

Chiarugi, P., Pani, G., Giannoni, E., et al. (2003) Reactive oxygen species as essential mediators of cell adhesion: the oxidative inhibition of a FAK tyrosine phosphatase is required for cell adhesion. **Journal of Cell Biology,** 161 (5): 933-944.

Chiu, J. and Dawes, I.W. (2012) Redox control of cell proliferation. **Trends in cell biology,** 22 (11): 592-601.

Cho, K., Ju, S., Ryu, K., et al. (2009) Gene expression profile of mesenchymal stromal cells after co-culturing with injured liver tissue. **Molecular Medicine Reports,** 2 (1): 51-61.

Choi, M. and Kim, D. (2006) Platinum transporters and drug resistance. **Archives of Pharmacal Research,** 29 (12): 1067-1073.

Chong, S.J.F., Low, I.C.C. and Pervaiz, S. (2014) Mitochondrial ROS and involvement of Bcl-2 as a mitochondrial ROS regulator. **Mitochondrion,** 19, Part A 39-48.

Chua, P., Yip, G.W. and Bay, B. (2009) Cell Cycle Arrest Induced by Hydrogen Peroxide Is Associated with Modulation of Oxidative Stress Related Genes in Breast Cancer Cells. **Experimental biology and medicine,** 234 (9): 1086-1094.

Chua, Y.L., Dufour, E., Dassa, E.P., et al. (2010) Stabilization of Hypoxia-inducible Factor-1 alpha Protein in Hypoxia Occurs Independently of Mitochondrial Reactive Oxygen Species Production. **Journal of Biological Chemistry,** 285 (41): 31277-31284.

Circu, M.L. and Aw, T.Y. (2012) Glutathione and modulation of cell apoptosis. **Biochimica Et Biophysica Acta-Molecular Cell Research,** 1823 (10): 1767-1777.

Circu, M.L. and Aw, T.Y. (2010) Reactive oxygen species, cellular redox systems, and apoptosis. **Free Radical Biology and Medicine,** 48 (6): 749-762.

Clunn, G.F., Refson, J.S., Lymn, J.S., et al. (1997) Platelet-derived growth factor beta-receptors can both promote and inhibit chemotaxis in human vascular smooth muscle cells. **Arteriosclerosis Thrombosis and Vascular Biology,** 17 (11): 2622-2629.

Cohen–Jonathan, E., Bernhard, E.J. and McKenna, W.G. (1999) How does radiation kill cells? **Current opinion in chemical biology,** 3 (1): 77-83.

Copple, I.M., Goldring, C.E., Kitteringham, N.R., et al. (2008) The Nrf2-Keapl defence pathway: Role in protection against drug-induced toxicity. **Toxicology,** 246 (1): 24-33.

Cui, W., Wang, M., Maegawa, H., et al. (2012) Inhibition of the activation of hepatic stellate cells by arundic acid via the induction of cytoglobin. **Biochemical and biophysical research communications,** 425 (3): 642-648.

Cullen, K.J., Yang, Z., Schumaker, L., et al. (2007) Mitochondria as a critical target of the chemotheraputic agent cisplatin in head and neck cancer. **Journal of Bioenergetics and Biomembranes,** 39 (1): 43-50.

Czabotar, P.E., Lessene, G., Strasser, A., et al. (2014) Control of apoptosis by the BCL-2 protein family: implications for physiology and therapy. **Nature Reviews Molecular Cell Biology,** 15 (1): 49-63.

D'Angio, C.T. and Finkelstein, J.N. (2000) Oxygen regulation of gene expression: A study in opposites. **Molecular genetics and metabolism,** 71 (1-2): 371-380.

Dasari, S. and Tchounwou, P.B. (2014) Cisplatin in cancer therapy: Molecular mechanisms of action. **European journal of pharmacology,** 740 364-378.

Davis, C.A., Nick, H.S. and Agarwal, A. (2001) Manganese superoxide dismutase attenuates cisplatin-induced renal injury: Importance of superoxide. **Journal of the American Society of Nephrology,** 12 (12): 2683-2690.

de Sanctis, D., Dewilde, S., Pesce, A., et al. (2004) Crystal structure of cytoglobin: The fourth globin type discovered in man displays heme hexa-coordi nation. **Journal of Molecular Biology,** 336 (4): 917-927.

De Windt, L.J., Lim, H.W., Taigen, T., et al. (2000) Calcineurin-mediated hypertrophy protects cardiomyocytes from apoptosis in vitro and in vivo - An apoptosis-independent model of dilated heart failure. **Circulation research,** 86 (3): 255-263.

Derdak, Z., Mark, N.M., Beldi, G., et al. (2008a) The mitochondrial uncoupling protein-2 promotes chemoresistance in cancer cells. **Cancer research,** 68 (8): 2813-2819.

Derdak, Z., Mark, N.M., Beldi, G., et al. (2008b) The Mitochondrial Uncoupling Protein-2 Promotes Chemoresistance in Cancer Cells. **Cancer research,** 68 (8): 2813-2819.

Diaz, E. and Barisone, G.A. (2011) DNA Microarrays: Sample Quality Control, Array Hybridization and Scanning. **Jove-Journal of Visualized Experiments,** (49): UNSP e2546.

Dinkova-Kostova, A.T. and Talalay, P. (2010) NAD(P)H:quinone acceptor oxidoreductase 1 (NQO1), a multifunctional antioxidant enzyme and exceptionally versatile cytoprotector. **Archives of Biochemistry and Biophysics,** 501 (1): 116-123.

Dokmanovic, M., Clarke, C. and Marks, P.A. (2007) Histone deacetylase inhibitors: Overview and perspectives. **Molecular Cancer Research,** 5 (10): 981-989.

Duke University and Medical Centre (2015) **Introduction to Sample Preparation: Immunofluorescence.** [Online]. Available from: http://microscopy.duke.edu/sampleprep/if.html [Accessed 06/24 2015]Dutto, I., Tillhon, M., Cazzalini, O. et al. (2015) Biology of the cell cycle inhibitor p21(CDKN1A): molecular mechanisms and relevance in chemical toxicology. **Archives of Toxicology**. 89(2): 155-178.

Emara, M., Turner, A.R. and Allalunis-Turner, J. (2010) Hypoxic regulation of cytoglobin and neuroglobin expression in human normal and tumor tissues. **Cancer Cell International,** 10 33.

Etienne-Manneville, S. (2004) Cdc42 - the centre of polarity. **Journal of cell science,** 117 (8): 1291-1300.

Fago, A., Hundahl, C., Dewilde, S., et al. (2004) Allosteric regulation and temperature dependence of oxygen binding in human neuroglobin and cytoglobin - Molecular mechanisms and physiological significance. **Journal of Biological Chemistry,** 279 (43): 44417-44426.

Fago, A., Mathews, A.J. and Brittain, T. (2008) A role for neuroglobin: Resetting the trigger level for apoptosis in neuronal and retinal cells. **IUBMB life,** 60 (6): 398-401.

Fang, J.Y., Ma, I. and Allalunis-Turner, J. (2011) Knockdown of Cytoglobin Expression Sensitizes Human Glioma Cells to Radiation and Oxidative Stress. **Radiation research,** 176 (2): 198-207.

Fei, P.W., Wang, W.G., Kim, S.H., et al. (2004) Bnip3L is induced by p53 under hypoxia, and its knockdown promotes tumor growth. **Cancer Cell,** 6 (6): 597-609.

Fernandez-Capetillo, O., Chen, H.T., Celeste, A., et al. (2002) DNA damage-induced G(2)-M checkpoint activation by histone H2AX and 53BP1. **Nature cell biology,** 4 (12): 993-997.

Ferreira, J.C., Marcondes, M.F., Icimoto, M.Y., et al. (2015) Intermediate Tyrosyl Radical and Amyloid Structure in Peroxide-Activated Cytoglobin. **PLoS ONE,** 10 (8): e0136554.

Forastiere, A.A., Goepfert, H., Maor, M., et al. (2003) Concurrent chemotherapy and radiotherapy for organ preservation in advanced laryngeal cancer. **New England Journal of Medicine,** 349 (22): 2091-2098.

Fordel, E., Geuens, E., Dewilde, S., et al. (2004) Cytoglobin expression is upregulated in all tissues upon hypoxia: an in vitro and in vivo study by quantitative real-time PCR. **Biochemical and biophysical research communications,** 319 (2): 342-348.

Fordel, E., Thijs, L., Martinet, W., et al. (2006) Neuroglobin and cytoglobin overexpression protects human SH-SY5Y neuroblastoma cells against oxidative stress-induced cell death. **Neuroscience letters,** 410 (2): 146-151.

Freitas, T.A.K., Saito, J.A., Hou, S.B., et al. (2005) Globin-coupled sensors, protoglobins, and the last universal common ancestor. **Journal of inorganic biochemistry,** 99 (1): 23-33.

Friedman, S.L. (2008) Mechanisms of hepatic fibrogenesis. **Gastroenterology,** 134 (6): 1655-1669.

Fujita, Y., Koinuma, S., De Velasco, M.A., et al. (2014) Melanoma transition is frequently accompanied by a loss of cytoglobin expression in melanocytes: a novel expression site of cytoglobin. **PloS one,** 9 (4): e94772-e94772.

Fujiwara, T., Grimm, E.A., Mukhopadhyay, T., et al. (1994) Induction of Chemosensitivity in Human Lung-Cancer Cells In-Vivo by Adenovirus-Mediated Transfer of the Wild-Type P53 Gene. **Cancer research,** 54 (9): 2287-2291.

Galluzzi, L., Senovilla, L., Vitale, I., et al. (2012) Molecular mechanisms of cisplatin resistance. **Oncogene,** 31 (15): 1869-1883.

Gardner, A.M., Cook, M.R. and Gardner, P.R. (2010) Nitric-oxide Dioxygenase Function of Human Cytoglobin with Cellular Reductants and in Rat Hepatocytes. **Journal of Biological Chemistry,** 285 (31): 23850-23857.

Genin, O., Rechavi, G., Nagler, A., et al. (2008) Myofibroblasts in pulmonary and brain metastases of Alveolar Soft-part Sarcoma: A novel target for treatment? **Neoplasia,** 10 (9): 940-948.

Geuens, E., Brouns, I., Flamez, D., et al. (2003) A globin in the nucleus! **Journal of Biological Chemistry,** 278 (33): 30417-30420.

Giono, L.E. and Manfredi, J.J. (2006) The p53 tumor suppressor participates in multiple cell cycle checkpoints. **Journal of cellular physiology,** 209 (1): 13-20.

Glorieux, C., Dejeans, N., Sid, B., et al. (2011) Catalase overexpression in mammary cancer cells leads to a less aggressive phenotype and an altered response to chemotherapy. **Biochemical pharmacology,** 82 (10): 1384-1390.

Godwin, A., Meister, A., Odwyer, P., et al. (1992) High-Resistance to Cisplatin in Human Ovarian-Cancer Cell-Lines is Associated with Marked Increase of Glutathione Synthesis. **Proceedings of the National Academy of Sciences of the United States of America,** 89 (7): 3070-3074.

Gorr, T.A., Wichmann, D., Pilarsky, C., et al. (2011) Old proteins - new locations: myoglobin, haemoglobin, neuroglobin and cytoglobin in solid tumours and cancer cells. **Acta Physiologica,** 202 (3): 563-581.

Guo, X., Philipsen, S. and Tan-Un, K. (2007) Study of the hypoxia-dependent regulation of human CYGB gene. **Biochemical and biophysical research communications,** 364 (1): 145-150.

Guo, X., Philipsen, S. and Tan-Un, K. (2006) Characterization of human cytoglobin gene promoter region. **Biochimica et Biophysica Acta (BBA) - Gene Structure and Expression,** 1759 (5): 208-215.

Gupta, M., Gupta, S.K., Hoffman, B., et al. (2006) Gadd45a and Gadd45b protect hematopoietic cells from UV-induced apoptosis via distinct signaling pathways, including p38 activation and JNK inhibition. **Journal of Biological Chemistry,** 281 (26): 17552-17558.

Hall, G.L., Shaw, R.J., Field, E.A., et al. (2008) P16 Promoter Methylation is a Potential Predictor of Malignant Transformation in Oral Epithelial Dysplasia. **Cancer Epidemiology Biomarkers & Prevention,** 17 (8): 2174-2179.

Halligan, K.E., Jourd'heuil, F.L. and Jourd'heuil, D. (2009) Cytoglobin Is Expressed in the Vasculature and Regulates Cell Respiration and Proliferation via Nitric Oxide Dioxygenation. **Journal of Biological Chemistry,** 284 (13): 8539-8547.

Hamanaka, R.B. and Chandel, N.S. (2010) Mitochondrial reactive oxygen species regulate cellular signalling and dictate biological outcomes. **Trends in Biochemical Sciences.** 35(9): 505-513.

Hamdane, D., Kiger, L., Dewilde, S., et al. (2003) The redox state of the cell regulates the ligand binding affinity of human neuroglobin and cytoglobin. **Journal of Biological Chemistry,** 278 (51): 51713-51721.

Hanahan, D. and Weinberg, R.A. (2011) Hallmarks of Cancer: The Next Generation. **Cell,** 144 (5): 646-674.

Hanna, G.J., Haddad, R.I. and Lorch, J.H. (2013) Induction Chemotherapy for Locoregionally Advanced Head and Neck Cancer: Past, Present, Future? **Oncologist,** 18 (3): 288-293.

Hannun, Y.A. and Obeid, L.M. (2008) Principles of bioactive lipid signalling: lessons from sphingolipids. **Nature Reviews Molecular Cell Biology,** 9 (2): 139-150.

Harada, H., Inoue, M., Itasaka, S., et al. (2012) Cancer cells that survive radiation therapy acquire HIF-1 activity and translocate towards tumour blood vessels. **Nature Communications,** 3 783.

Harris, A.L. (2002) Hypoxia - A key regulatory factor in tumour growth. **Nature Reviews Cancer,** 2 (1): 38-47.

Hauck, C.R., Hsia, D.A. and Schlaepfer, D.D. (2000) Focal adhesion kinase facilitates platelet-derived growth factor-BB-stimulated ERK2 activation required for chemotaxis migration of vascular smooth muscle cells. **Journal of Biological Chemistry,** 275 (52): 41092-41099.

Hayakawa, Y., Hirata, Y., Sakitani, K., et al. (2012) Apoptosis signal-regulating kinase-1 inhibitor as a potent therapeutic drug for the treatment of gastric cancer. **Cancer Science,** 103 (12): 2181-2185.

He, G., Kuang, J., Khokhar, A.R., et al. (2011) The impact of S- and G2-checkpoint response on the fidelity of G1-arrest by cisplatin and its comparison to a non-cross-resistant platinum(IV) analog. **Gynecologic oncology,** 122 (2): 402-409.

He, X. and Ma, Q. (2012) Redox Regulation by Nuclear Factor Erythroid 2-Related Factor 2: Gatekeeping for the Basal and Diabetes-Induced Expression of Thioredoxin-Interacting Protein. **Molecular pharmacology,** 82 (5): 887-897.

He, X., Lv, R., Wang, K., et al. (2011) Cytoglobin Exhibits Anti-Fibrosis Activity on Liver In Vivo and In Vitro. **Protein Journal,** 30 (7): 437-446.

Held, P. (2015) **An Introduction to Reactive Oxygen Species: Measurement of ROS in Cells.** [Online]. Available from: http://www.biotek.com/assets/tech_resources/ROS%20White%20Paper_2015.pdf [Accessed 07/27 2015].

Hildesheim, J., Bulavin, D.V., Anver, M.R., et al. (2002) Gadd45a protects against UV irradiation-induced skin tumors, and promotes apoptosis and stress signaling via MAPK and p53. **Cancer research,** 62 (24): 7305-7315.

Hildesheim, J. and Fornace, A.J. (2002) Gadd45a: An elusive yet attractive candidate gene in pancreatic cancer. **Clinical Cancer Research,** 8 (8): 2475-2479.

Hissin, P.J. and Hilf, R. (1976) Fluorometric Method for Determination of Oxidized and Reduced Glutathione in Tissues. **Analytical Biochemistry,** 74 (1): 214-226.

Hodges, N.J., Innocent, N., Dhanda, S., et al. (2008) Cellular protection from oxidative DNA damage by over-expression of the novel globin cytoglobin in vitro. **Mutagenesis,** 23 (4): 293-298.

Hoffmann, T.K., Sonkoly, E., Hauser, U., et al. (2008) Alterations in the p53 pathway and their association with radio- and chemosensitivity in head and neck squamous cell carcinoma. **Oral oncology,** 44 (12): 1100-1109.

Hollander, M.C., Sheikh, M.S., Bulavin, D.V., et al. (1999) Genomic instability in Gadd45a-deficient mice. **Nature genetics,** 23 (2): 176-184.

Hollstein, M., Sidransky, D., Vogelstein, B., et al. (1991) P53 Mutations in Human Cancers. **Science,** 253 (5015): 49-53.

Holmgren, A. and Lu, J. (2010) Thioredoxin and thioredoxin reductase: Current research with special reference to human disease. **Biochemical and biophysical research communications,** 396 (1): 120-124.

Holmstroem, K.M. and Finkel, T. (2014) Cellular mechanisms and physiological consequences of redox-dependent signalling. **Nature Reviews Molecular Cell Biology,** 15 (6): 411-421.

Hsieh, A.C., Truitt, M.L. and Ruggero, D. (2011) Oncogenic AKTivation of translation as a therapeutic target. **British journal of cancer,** 105 (3): 329-336.

Hundahl, C.A., Allen, G.C., Hannibal, J., et al. (2010) Anatomical characterization of cytoglobin and neuroglobin mRNA and protein expression in the mouse brain. **Brain research,** 1331 58-73.

Hurd, T.R., DeGennaro, M. and Lehmann, R. (2012) Redox regulation of cell migration and adhesion. **Trends in cell biology,** 22 (2): 107-115.

IARC (2010) **Detection of TP53 mutations by direct sequencing.** [Online]. Available from: http://p53.iarc.fr/download/tp53_directsequencing_iarc.pdf [Accessed 07/06/15 2015].

Ibanez, I.L., Policastro, L.L., Tropper, I., et al. (2011) H2O2 scavenging inhibits G1/S transition by increasing nuclear levels of p27(KIP1). **Cancer letters,** 305 (1): 58-68.

Ibidi (2015) **Ibidi Culture-Insert.** [Online]. Available from: http://ibidi.com/fileadmin/products/labware/open_removable/E_8XXXX_CultureInsert/IN_8XXXX_CI.pdf?x6c5f9=e36bc40870174df2e4d465c8b91a5474 [Accessed 07/17 2015].

Imazu, T., Shimizu, S., Tagami, S., et al. (1999) Bcl-2/E1B 19kDa-interacting protein 3-like protein (Bnip3L) interacts with Bcl-2/Bcl-x(L) and induces apoptosis by altering mitochondrial membrane permeability. **Oncogene,** 18 (32): 4523-4529.

Indran, I.R., Tufo, G., Pervaiz, S., et al. (2011) Recent advances in apoptosis, mitochondria and drug resistance in cancer cells. **Biochimica et Biophysica Acta (BBA) - Bioenergetics,** 1807 (6): 735-745.

Itoh, R., Fujita, K., Mu, A., et al. (2013) Imaging of heme/hemeproteins in nucleus of the living cells expressing heme-binding nuclear receptors. **FEBS letters,** 587 (14): 2131-2136.

Janssen-Heininger, Y.M.W., Mossman, B.T., Heintz, N.H., et al. (2008) Redox-based regulation of signal transduction: Principles, pitfalls, and promises. **Free Radical Biology and Medicine,** 45 (1): 1-17.

John, R., Chand, V., Chakraborty, S., et al. (2014) DNA damage induced activation of CYGB stabilizes p53 and mediates G1 arrest. **DNA Repair,** 24 (0): 107-112.

Jourd'heuil, F.L., Zhang, W., Halligan, K., et al. (2012) Loss of the Nitric Oxide Dioxygenase Cytoglobin Exacerbates Smooth Muscle Apoptosis and Inhibits Restenosis during Vascular Injury. **Free Radical Biology and Medicine,** 53 S165-S165.

Kabuyama, Y., Langer, S.J., Polvinen, K., et al. (2006) Functional proteomics identifies protein-tyrosine phosphatase 1B as a target of RhoA signaling. **Molecular & Cellular Proteomics,** 5 (8): 1359-1367.

Kamata, H. and Hirata, H. (1999) Redox regulation of cellular signalling. **Cellular Signalling**. 11(1):1-14.

Kanamori, Y., Kigawa, J., Minagawa, Y., et al. (1998) A newly developed adenovirus-mediated transfer of a wild-type p53 gene increases sensitivity to cis-diamminedichloroplatinum (II) in p53-deleted ovarian cancer cells. **European journal of cancer,** 34 (11): 1802-1806.

Karlsson, R., Pedersen, E.D., Wang, Z., et al. (2009) Rho GTPase function in tumorigenesis. **Biochimica et Biophysica Acta (BBA) - Reviews on Cancer,** 1796 (2): 91-98.

Kartalou, M. and Essigmann, J.M. (2001) Mechanisms of resistance to cisplatin. **Mutation Research-Fundamental and Molecular Mechanisms of Mutagenesis,** 478 (1-2): 23-43.

Kasherman, Y., Sturup, S. and Gibson, D. (2009) Is Glutathione the Major Cellular Target of Cisplatin? A Study of the Interactions of Cisplatin with Cancer Cell Extracts. **Journal of medicinal chemistry,** 52 (14): 4319-4328.

Kastan, M.B. and Bartek, J. (2004) Cell-cycle checkpoints and cancer. **Nature,** 432 (7015): 316-323.

Kawada, N., Kristensen, D.B., Asahina, K., et al. (2001) Characterization of a stellate cell activation-associated protein (STAP) with peroxidase activity found in rat hepatic stellate cells. **Journal of Biological Chemistry,** 276 (27): 25318-25323.

Kelland, L. (2007) The resurgence of platinum-based cancer chemotherapy. **Nature Reviews Cancer,** 7 (8): 573-584.

Kim, H., Yoon, S.C., Lee, T.Y., et al. (2009) Discriminative cytotoxicity assessment based on various cellular damages. **Toxicology letters,** 184 (1): 13-17.

Kim, J.W., Sahm, H., You, J., et al. (2010) Knock-down of Superoxide Dismutase 1 Sensitizes Cisplatin-resistant Human Ovarian Cancer Cells. **Anticancer Research,** 30 (7): 2577-2581.

Kinoshita, H., Hirata, Y., Nakagawa, H., et al. (2013) Interleukin-6 Mediates Epithelial-Stromal Interactions and Promotes Gastric Tumorigenesis. **Plos One,** 8 (4): e60914.

Klaunig, J.E., Wang, Z., Pu, X., et al. (2011) Oxidative stress and oxidative damage in chemical carcinogenesis. **Toxicology and applied pharmacology,** 254 (2): 86-99.

Kleinjan, D.J. and van Heyningen, V. (1998) Position effect in human genetic disease. **Human molecular genetics,** 7 (10): 1611-1618.

Koukourakis, M.I., Bentzen, S.M., Giatromanolaki, A., et al. (2006) Endogenous markers of two separate, hypoxia response pathways (hypoxia inducible factor 2 alpha and carbonic anhydrase 9) are associated with radiotherapy failure in head and neck cancer patients recruited in the CHART randomized trial. **Journal of Clinical Oncology,** 24 (5): 727-735.

Kruiswijk, F., Labuschagne, C.F. and Vousden, K.H. (2015) P53 in Survival, Death and Metabolic Health: a Lifeguard with a Licence to Kill. **Nature Reviews Molecular Cell Biology,** 16 (7): 393-405.

Kugelstadt, D., Haberkamp, M., Hankeln, T., et al. (2004) Neuroglobin, cytoglobin, and a novel, eye-specific globin from chicken. **Biochemical and biophysical research communications,** 325 (3): 719-725.

Kurokawa, K. and Matsuda, M. (2005) Localized RhoA activation as a requirement for the induction of membrane ruffling. **Molecular biology of the cell,** 16 (9): 4294-4303.

Kuwahara, D., Tsutsumi, K., Kobayashi, T., et al. (2000) Caspase-9 regulates cisplatin-induced apoptosis in human head and neck squamous cell carcinoma cells. **Cancer letters,** 148 (1): 65-71.

Kuwahara, D., Tsutsumi, K., Oyake, D., et al. (2003) Inhibition of caspase-9 activity and Apaf-1 expression in cisplatin-resistant head and neck squamous cell carcinoma cells. **Auris Nasus Larynx,** 30 S85-S88.

Langan, J.E., Risk, J.M. and Field, J.K. (2002) Refinement of the tylosis oesophageal cancer (TOC) minimal region to 65KB by haplotype analysis using novel microsatelite markers and SNPS. **British journal of cancer,** 86 S119-S120.

Latina, A., Viticchie, G., Lena, A.M., et al. (2015) Delta]Np63 targets cytoglobin to inhibit oxidative stress-induced apoptosis in keratinocytes and lung cancer. **Oncogene,** .

Le Thi Thanh Thuy, Matsumoto, Y., Tuong Thi Van Thuy, et al. (2015) Cytoglobin Deficiency Promotes Liver Cancer Development from Hepatosteatosis through Activation of the Oxidative Stress Pathway. **American Journal of Pathology,** 185 (4): 1045-1060.

Lechauve, C., Chauvierre, C., Dewilde, S., et al. (2010) Cytoglobin conformations and disulfide bond formation. **Febs Journal,** 277 (12): 2696-2704.

Leemans, C.R., Braakhuis, B.J.M. and Brakenhoff, R.H. (2011) The molecular biology of head and neck cancer. **Nature Reviews Cancer,** 11 (1): 9-22.

Leonarduzzi, G., Arkan, M.C., Basaga, H., et al. (2000) Lipid oxidation products in cell signaling. **Free Radical Biology and Medicine,** 28 (9): 1370-1378.

Leroy, B., Fournier, J.L., Ishioka, C., et al. (2013) The TP53 website: an integrative resource centre for the TP53 mutation database and TP53 mutant analysis. **Nucleic acids research,** 41 (D1): D962-D969.

Li, D., Chen, X.Q., Li, W., et al. (2007) Cytoglobin up-regulated by hydrogen peroxide plays a protective role in oxidative stress. **Neurochemical research,** 32 (8): 1375-1380.

Li, R.C., Lee, S.K., Pouranfar, F., et al. (2006) Hypoxia differentially regulates the expression of neuroglobin and cytoglobin in rat brain. **Brain research,** 1096 173-179.

Liebermann, D.A. and Hoffman, B. (2008) Gadd45 in stress signaling. **Journal of molecular signaling,** 3 15-15.

Liu, X., Follmer, D., Zweier, J.R., et al. (2012) Characterization of the Function of Cytoglobin as an Oxygen-Dependent Regulator of Nitric Oxide Concentration. **Biochemistry,** 51 (25): 5072-5082.

Livak, K.J. and Schmittgen, T.D. (2001) Analysis of relative gene expression data using real-time quantitative PCR and the 2(T)(-Delta Delta C) method. **Methods,** 25 (4): 402-408.

López-Mirabal, H.R. and Winther, J.R. (2008) Redox characteristics of the eukaryotic cytosol. **Biochimica et Biophysica Acta (BBA) - Molecular Cell Research,** 1783 (4): 629-640.

Lu, J. and Holmgren, A. (2014) The thioredoxin antioxidant system. **Free Radical Biology and Medicine,** 66 75-87.

Lustgarten, M.S., Bhattacharya, A., Muller, F.L., et al. (2012) Complex I generated, mitochondrial matrix-directed superoxide is released from the mitochondria through voltage dependent anion channels. **Biochemical and biophysical research communications,** 422 (3): 515-521.

Madesh, M. and Hajnoczky, G. (2001) VDAC-dependent permeabilization of the outer mitochondrial membrane by superoxide induces rapid and massive cytochrome c release. **Journal of Cell Biology,** 155 (6): 1003-1015.

Maeda, M., Hasegawa, H., Hyodo, T., et al. (2011) ARHGAP18, a GTPase-activating protein for RhoA, controls cell shape, spreading, and motility. **Molecular biology of the cell,** 22 (20): 3840-3852.

Mailloux, R.J., Adjeitey, C.N. and Harper, M. (2010) Genipin-Induced Inhibition of Uncoupling Protein-2 Sensitizes Drug-Resistant Cancer Cells to Cytotoxic Agents. **Plos One,** 5 (10): e13289.

Majmundar, A.J., Wong, W.J. and Simon, M.C. (2010) Hypoxia-Inducible Factors and the Response to Hypoxic Stress. **Molecular cell,** 40 (2): 294-309.

Makino, M., Sawai, H., Shiro, Y., et al. (2011) Crystal structure of the carbon monoxide complex of human cytoglobin. **Proteins-Structure Function and Bioinformatics,** 79 (4): 1143-1153.

Man, K.M., Philipsen, S. and Tan-Un, K.C. (2008) Localization and expression pattern of cytoglobin in carbon tetrachloride-induced liver fibrosis. **Toxicology letters,** 183 (1-3): 36-44.

Marchenko, N.D., Zaika, A. and Moll, U.M. (2000) Death signal-induced localization of p53 protein to mitochondria - A potential role in apoptotic signaling. **Journal of Biological Chemistry,** 275 (21): 16202-16212.

Martel, C., Wang, Z. and Brenner, C. (2014) VDAC phosphorylation, a lipid sensor influencing the cell fate. **Mitochondrion,** 19 69-77.

Marullo, R., Werner, E., Degtyareva, N., et al. (2013) Cisplatin Induces a Mitochondrial-ROS Response That Contributes to Cytotoxicity Depending on Mitochondrial Redox Status and Bioenergetic Functions. **Plos One,** 8 (11):.

Mathupala, S.P. and Sloan, A.E. (2009) An agarose-based cloning-ring anchoring method for isolation of viable cell clones. **BioTechniques,** 46 (4): 305-307.

Matsukawa, J., Matsuzawa, A., Takeda, K., et al. (2004) The ASK1-MAP kinase cascades in mammalian stress response. **Journal of Biochemistry,** 136 (3): 261-265.

McCommis, K.S. and Baines, C.P. (2012) The role of VDAC in cell death: Friend or foe? **Biochimica et Biophysica Acta (BBA) - Biomembranes,** 1818 (6): 1444-1450.

McLean, L.S., Watkins, C.N., Campbell, P., et al. (2015) Aryl Hydrocarbon Receptor Ligand 5F 203 Induces Oxidative Stress That Triggers DNA Damage in Human Breast Cancer Cells. **Chemical research in toxicology,** 28 (5): 855-871.

McRonald, F.E., Liloglou, T., Xinarianos, G., et al. (2006) Down-regulation of the cytoglobin gene, located on 17q25, in tylosis with oesophageal cancer (TOC): evidence for trans-allele repression. **Human molecular genetics,** 15 (8): 1271-1277.

McRonald, F.E., Risk, J.M. and Hodges, N.J. (2012) Protection from Intracellular Oxidative Stress by Cytoglobin in Normal and Cancerous Oesophageal Cells. **Plos One,** 7 (2): e30587.

Meek, D.W. (2004) The p53 response to DNA damage. **Dna Repair,** 3 (8-9): 1049-1056.

Menon, S.G. and Goswami, P.C. (2007) A redox cycle within the cell cycle: ring in the old with the new. **Oncogene,** 26 (8): 1101-1109.

Menon, S.G., Sarsour, E.H., Spitz, D.R., et al. (2003) Redox regulation of the G(1) to S phase transition in the mouse embryo fibroblast cell cycle. **Cancer research,** 63 (9): 2109-2117.

Metzen, E., Zhou, J., Jelkmann, W., et al. (2003) Nitric oxide impairs normoxic degradation of HIF-1 alpha by inhibition of prolyl hydroxylases. **Molecular biology of the cell,** 14 (8): 3470-3481.

Mi, H., Muruganujan, A. and Thomas, P.D. (2013) PANTHER in 2013: modeling the evolution of gene function, and other gene attributes, in the context of phylogenetic trees. **Nucleic acids research,** 41 (D1): D377-D386.

Mills, G.B. and Moolenaar, W.H. (2003) The emerging role of lysophosphatidic acid in cancer. **Nature Reviews Cancer,** 3 (8): 582-591.

Mimura, I., Nangaku, M., Nishi, H., et al. (2010) Cytoglobin, a novel globin, plays an antifibrotic role in the kidney. **American Journal of Physiology-Renal Physiology,** 299 (5): F1120-F1133.

Mohammad, D.H. and Yaffe, M.B. (2009) 14-3-3 proteins, FHA domains and BRCT domains in the DNA damage response. **DNA Repair,** 8 (9): 1009-1017.

Monnerat, C., Faivre, S., Temam, S., et al. (2002) End points for new agents in induction chemotherapy for locally advanced head and neck cancers. **Annals of Oncology,** 13 (7): 995-1006.

Moran, J.M., Ortiz-Ortiz, M.A., Ruiz-Mesa, L.M., et al. (2010) Effect of paraquat exposure on nitric oxide-responsive genes in rat mesencephalic cells. **Nitric Oxide-Biology and Chemistry,** 23 (1): 51-59.

Moreira, J.d.V., Peres, S., Steyaert, J., et al. (2015) Cell cycle progression is regulated by intertwined redox oscillators. **Theoretical Biology and Medical Modelling,** 12 10.

Moser, T.L., Pizzo, S.V., Bafetti, L.M., et al. (1996) Evidence for preferential adhesion of ovarian carcinoma cells to type I collagen mediated by the alpha2beta1 integrin. I**nternational Journal of Cance**r. 67 (5): 695-701.

Mukhopadhyay, P., Horvath, B., Zsengeller, Z., et al. (2012) Mitochondrial-targeted antioxidants represent a promising approach for prevention of cisplatin-induced nephropathy. **Free Radical Biology and Medicine,** 52 (2): 497-506.

Mukhopadhyay, P., Rajesh, M., Yoshihiro, K., et al. (2007) Simple quantitative detection of mitochondrial superoxide production in live cells. **Biochemical and biophysical research communications,** 358 (1): 203-208.

Murphy, M., Holmgren, A., Larsson, N., et al. (2011) Unraveling the Biological Roles of Reactive Oxygen Species. **Cell Metabolism,** 13 (4): 361-366.

Myllyharju, J. (2013) Prolyl 4-hydroxylases, master regulators of the hypoxia response. **Acta Physiologica,** 208 (2): 148-165.

Nakatani, K., Okuyama, H., Shimahara, Y., et al. (2004) Cytoglobin/STAP, its unique localization in splanchnic fibroblast-like cells and function in organ fibrogenesis. **Laboratory Investigation,** 84 (1): 91-101.

Nimnual, A.S., Taylor, L.J. and Bar-Sagi, D. (2003) Redox-dependent downregulation of Rho by Rac. **Nature cell biology,** 5 (3): 236-U7.

Nishi, H., Inagi, R., Kawada, N., et al. (2011) Cytoglobin, a Novel Member of the Globin Family, Protects Kidney Fibroblasts against Oxidative Stress under Ischemic Conditions. **American Journal of Pathology,** 178 (1): 128-139.

Nishimura, T., Newkirk, K., Sessions, R.B., et al. (1996) Immunohistochemical staining for glutathione S-transferase predicts response to platinum-based chemotherapy in head and neck cancer. **Clinical Cancer Research,** 2 (11): 1859-1865.

Niture, S.K., Kaspar, J.W., Shen, J., et al. (2010) Nrf2 signaling and cell survival. **Toxicology and applied pharmacology,** 244 (1): 37-42.

NLM, (2015) **Align Sequences Nucleotide Basic Local Alignment Search Tool (BLAST).** [Online]. Available from: http://blast.ncbi.nlm.nih.gov/Blast.cgi?PAGE_TYPE=BlastSearch&BLAST_SPEC=blast2seq&LINK_LOC=align2seq [Accessed 07/06 2015].

Oleksiewicz, U., Liloglou, T., Field, J., et al. (2011) Cytoglobin: biochemical, functional and clinical perspective of the newest member of the globin family. **Cellular and Molecular Life Sciences,** 1-15.

Oleksiewicz, U., Liloglou, T., Tasopoulou, K., et al. (2013) Cytoglobin has bimodal: tumour suppressor and oncogene functions in lung cancer cell lines. **Human molecular genetics,** .

Oliveira, K., da ConceiÃ§Ã£o, R., Piedade, G., et al. (2015) Thyroid hormone modulates neuroglobin and cytoglobin in rat brain. **Metabolic brain disease,** 1-8.

Olivero, O.A., Chang, P.K., LopezLarraza, D.M., et al. (1997) Preferential formation and decreased removal of cisplatin-DNA adducts in Chinese hamster ovary cell mitochondrial DNA as compared to

nuclear DNA. **Mutation Research-Genetic Toxicology and Environmental Mutagenesis,** 391 (1-2): 79-86.

Onumah, O.E., Jules, G.E., Zhao, Y., et al. (2009) Overexpression of catalase delays G(0)/G(1)- to S-phase transition during cell cycle progression in mouse aortic endothelial cells. **Free Radical Biology and Medicine,** 46 (12): 1658-1667.

Ott, M., Zhivotovsky, B. and Orrenius, S. (2007) Role of cardiolipin in cytochrome c release from mitochondria. **Cell death and differentiation,** 14 (7): 1243-1247.

Ou, Y., Chung, P., Sun, T. and Shieh, S. (2005) p53 C-Terminal Phosphorylation by CHK1 and CHK2 Participates in the Regulation of DNA-Damage-induced C-Terminal Acetylation. Molecular Biology of the Cell. 16 (4): 1684-1695.

Pabla, N., Huang, S., Mi, Q., et al. (2008) ATR-CHK2 signaling in p53 activation and DNA damage response during cisplatin-induced apoptosis. **Journal of Biological Chemistry,** 283 (10): 6572-6583.

Pardali, K. and Moustakas, A. (2007) Actions of TGF-beta as tumor suppressor and pro-metastatic factor in human cancer. **Biochimica Et Biophysica Acta-Reviews on Cancer,** 1775 (1): 21-62.

Parri, M. and Chiarugi, P. (2010) Rac and Rho GTPases in cancer cell motility control. **Cell Communication and Signaling,** 8 23.

Patil, M., Pabla, N. and Dong, Z. (2013) Checkpoint kinase 1 in DNA damage response and cell cycle regulation. **Cellular and Molecular Life Sciences,** 70 (21): 4009-4021.

Pesce, A., Bolognesi, M., Bocedi, A., et al. (2002) Neuroglobin and cytoglobin - Fresh blood for the vertebrate globin family. **EMBO reports,** 3 (12): 1146-1151.

Petersen, M.G., Dewilde, S. and Fago, A. (2008) Reactions of ferrous neuroglobin and cytoglobin with nitrite under anaerobic conditions. **Journal of inorganic biochemistry,** 102 (9): 1777-1782.

Pfaffl, M. (2001) A new mathematical model for relative quantification in real-time RT-PCR. **Nucleic acids research,** 29 (9): e45.

Ponka, P. (1999) Cell biology of heme. **American Journal of the Medical Sciences,** 318 (4): 241-256.

Pons, D.G., Nadal-Serrano, M., Torrens-Mas, M., et al. (2015) UCP2 inhibition sensitizes breast cancer cells to therapeutic agents by increasing oxidative stress. **Free Radical Biology and Medicine,** 86 (0): 67-77.

Ralph, S.J., Rodriguez-Enriquez, S., Neuzil, J., et al. (2010) The causes of cancer revisited: "Mitochondrial malignancy" and ROS-induced oncogenic transformation - Why mitochondria are targets for cancer therapy. **Molecular aspects of medicine,** 31 (2): 145-170.

Ray, P.D., Huang, B. and Tsuji, Y. (2012a) Reactive oxygen species (ROS) homeostasis and redox regulation in cellular signaling. **Cellular signalling,** 24 (5): 981-990.

Ray, P.D., Huang, B. and Tsuji, Y. (2012b) Reactive oxygen species (ROS) homeostasis and redox regulation in cellular signaling. **Cellular signalling,** 24 (5): 981-990.

Raychaudhuri, S., Skommer, J., Henty, K., et al. (2010) Neuroglobin protects nerve cells from apoptosis by inhibiting the intrinsic pathway of cell death. **Apoptosis,** 15 (4): 401-411.

Recillas-Targa, F. (2006) Multiple strategies for gene transfer, expression, knockdown, and chromatin influence in mammalian cell lines and transgenic animals. **Molecular biotechnology,** 34 (3): 337-354.

Reeder, B.J., Svistunenko, D.A. and Wilson, M.T. (2011) Lipid binding to cytoglobin leads to a change in haem co-ordination: a role for cytoglobin in lipid signalling of oxidative stress. **Biochemical Journal,** 434 483-492.

Reuter, S., Gupta, S.C., Chaturvedi, M.M., et al. (2010) Oxidative stress, inflammation, and cancer How are they linked? **Free Radical Biology and Medicine,** 49 (11): 1603-1616.

Risk, J.M., Mills, H.S., Garde, J., et al. (1999) The tylosis esophageal cancer (TOC) locus: more than just a familial cancer gene. **Diseases of the Esophagus,** 12 (3): 173-176.

Rohani, M.G., Pilcher, B.K., Chen, P., et al. (2014) Cdc42 Inhibits ERK-Mediated Collagenase-1 (MMP-1) Expression in Collagen-Activated Human Keratinocytes. **Journal of Investigative Dermatology,** 134 (5): 1230-1237.

Roskoski Jr., R. (2012) ERK1/2 MAP kinases: Structure, function, and regulation. **Pharmacological Research,** 66 (2): 105-143.

Santandreu, F.M., Roca, P. and Oliver, J. (2010) Uncoupling protein-2 knockdown mediates the cytotoxic effects of cisplatin. **Free Radical Biology and Medicine,** 49 (4): 658-666.

Santos, C.R. and Schulze, A. (2012) Lipid metabolism in cancer. **Febs Journal,** 279 (15): 2610-2623.

Santos, N.A.G., Catao, C.S., Martins, N.M., et al. (2007) Cisplatin-induced nephrotoxicity is associated with oxidative stress, redox state unbalance, impairment of energetic metabolism and apoptosis in rat kidney mitochondria. **Archives of Toxicology,** 81 (7): 495-504.

Savitsky, P.A. and Finkel, T. (2002) Redox regulation of CDC25C. **Journal of Biological Chemistry,** 277 (23): 20535-20540.

Sawai, H., Makino, M., Mizutani, Y., et al. (2005) Structural characterization of the proximal and distal histidine environment of cytoglobin and neuroglobin. **Biochemistry,** 44 (40): 13257-13265.

Schaakekoning, C., Vandenbogaert, W., Dalesio, O., et al. (1992) Effects of Concomitant Cisplatin and Radiotherapy on Inoperable Non-Small-Cell Lung-Cancer. **New England Journal of Medicine,** 326 (8): 524-530.

Schieber, M. and Chandel, N. (2014) ROS Function in Redox Signaling and Oxidative Stress. **Current Biology,** 24 (10): R453-R462.

Schmidt, M., Gerlach, F., Avivi, A., et al. (2004) Cytoglobin is a respiratory protein in connective tissue and neurons, which is up-regulated by hypoxia. **Journal of Biological Chemistry,** 279 (9): 8063-8069.

Schmitz, A.A.P., Govek, E.E., Bottner, B., et al. (2000) Rho GTPases: Signaling, migration, and invasion. **Experimental cell research,** 261 (1): 1-12.

Schroeder, A., Mueller, O., Stocker, S., et al. (2006) The RIN: an RNA integrity number for assigning integrity values to RNA measurements. **Bmc Molecular Biology,** 7 3.

Schuler, P.J., Trellakis, S., Greve, J., et al. (2010) In Vitro Chemosensitivity of Head and Neck Cancer Cell Lines. **European journal of medical research,** 15 (8): 337-344.

Semenza, G.L. (2000) Expression of hypoxia-inducible factor 1: Mechanisms and consequences. **Biochemical pharmacology,** 59 (1): 47-53.

Sena, L.A. and Chandel, N.S. (2012) Physiological Roles of Mitochondrial Reactive Oxygen Species. **Molecular Cell**. 48(2):158-167.

Shaw, R.J., Liloglou, T., Rogers, S.N., et al. (2006) Promoter methylation of P16, RAR beta, E-cadherin, cyclin A1 and cytoglobin in oral cancer: quantitative evaluation using pyrosequencing. **British journal of cancer,** 94 (4): 561-568.

Shaw, R.J., Omar, M.M., Rokadiya, S., et al. (2009) Cytoglobin is upregulated by tumour hypoxia and silenced by promoter hypermethylation in head and neck cancer. **British journal of cancer,** 101 (1): 139-144.

Shaw, R.J., Hobkirk, A.J., Nikolaidis, G., et al. (2013) Molecular Staging of Surgical Margins in Oral Squamous Cell Carcinoma Using Promoter Methylation of p16(INK4A), Cytoglobin, E-cadherin, and TMEFF2. **Annals of Surgical Oncology,** 20 (8): 2796-2802.

Shen, H., Perez, R.E., Davaadelger, B., et al. (2013) Two 4N Cell-Cycle Arrests Contribute to Cisplatin-Resistance. **Plos One,** 8 (4): e59848.

Shidoji, Y., Hayashi, K., Komura, S., et al. (1999) Loss of Molecular Interaction between Cytochrome c and Cardiolipin Due to Lipid Peroxidation. **Biochemical and biophysical research communications,** 264 (2): 343-347.

Shigematsu, A., Adachi, Y., Matsubara, J., et al. (2008) Analyses of expression of cytoglobin by immunohistochemical studies in human tissues. **Hemoglobin,** 32 (3): 287-296.

Shivapurkar, N., Stastny, V., Okumura, N., et al. (2008) Cytoglobin, the newest member of the globin family, functions as a tumor suppressor gene. **Cancer research,** 68 (18): 7448-7456.

Siddik, Z.H. (2003a) **Cisplatin: mode of cytotoxic action and molecular basis of resistance.**. **Oncogene,** 22 (47): 7265.

Siddik, Z.H. (2003b) Cisplatin: mode of cytotoxic action and molecular basis of resistance. **Oncogene,** 22 (47): 7265-7279.

Siddiqui, W.A., Ahad, A. and Ahsan, H. (2015) The mystery of BCL2 family: Bcl-2 proteins and apoptosis: an update. **Archives of Toxicology,** 89 (3): 289-317.

Simons, K. and Toomre, D. (2000) Lipid rafts and signal transduction. **Nature Reviews Molecular Cell Biology,** 1 (1): 31-39.

Singh, M., Chaudhry, P., Fabi, F., et al. (2013) Cisplatin-induced caspase activation mediates PTEN cleavage in ovarian cancer cells: a potential mechanism of chemoresistance. **Bmc Cancer,** 13 233.

Singh, S., Canseco, D.C., Manda, S.M., et al. (2014) Cytoglobin modulates myogenic progenitor cell viability and muscle regeneration. **Proceedings of the National Academy of Sciences of the United States of America,** 111 (1): E129-E138.

Singh, S., Manda, S.M., Sikder, D., et al. (2009) Calcineurin Activates Cytoglobin Transcription in Hypoxic Myocytes. **Journal of Biological Chemistry,** 284 (16): 10409-10421.

Singh, S., Wu, S., Canseco, D.C., et al. (2010) Cytoglobin Regulates Proliferation and Differentiation by Homeostatic and Stress Induced Repression of p53 Transcriptional Activity. **Circulation,** 122 (21):.

Skehan, P., Storeng, R., Scudiero, D., et al. (1990) New Colorimetric Cytotoxicity Assay for Anticancer-Drug Screening. **Journal of the National Cancer Institute,** 82 (13): 1107-1112.

Smagghe, B.J., Trent, J.T.,III and Hargrove, M.S. (2008) NO Dioxygenase Activity in Hemoglobins Is Ubiquitous In Vitro, but Limited by Reduction In Vivo. **Plos One,** 3 (4): e2039.

So, M.Y., Tian, Z., Phoon, Y.S., et al. (2014) Gene expression profile and toxic effects in human bronchial epithelial cells exposed to zearalenone. **PloS one,** 9 (5): e96404-e96404.

Soussi, T. and Wiman, K.G. (2015) TP53: an oncogene in disguise. **Cell death and differentiation,** 22 (8): 1239-1249.

Stagner, J.I., Parthasarathy, S.N., Wyler, K., et al. (2005) Protection from ischemic cell death by the induction of cytoglobin. **Transplantation proceedings,** 37 (8): 3452-3453.

Stagner, J.I., Seelan, R.S., Parthasarathy, R.N., et al. (2009) Reduction of ischemic cell death in cultured islets of Langerhans by the induction of cytoglobin. **Islets,** 1 (1): 50-54.

Steenbergen, R.H.G., Drummen, G.P.C., Op den Kamp, J.A.F., et al. (1997) The use of cis-parinaric acid to measure lipid peroxidation in cardiomyocytes during ischemia and reperfusion. **Biochimica et Biophysica Acta (BBA) - Biomembranes,** 1330 (2): 127-137.

Stockholm, D., Benchaouir, R., Picot, J., et al. (2007) The Origin of Phenotypic Heterogeneity in a Clonal Cell Population In Vitro. **Plos One,** 2 (4): e394.

Stone, L.C., Thorne, L.S., Weston, C.J., et al. (2015) Cytoglobin expression in the hepatic stellate cell line HSC-T6 is regulated by extracellular matrix proteins dependent on FAK-signalling. **Fibrogenesis & tissue repair,** 8 15-15.

Tajeddine, N., Galluzzi, L., Kepp, O. et al (2008) Hierarchical involvement of Bak, VDAC1 and Bax in cispaltin-induced cell death. **Oncogene,** 27(30): 4221-4232.

Tangar, A. (2015) Probing the Role of Cytoglobin's Extended Termini. **Biophysical journal,** 108 (2, Supplement 1): 219a.

Tateaki, Y., Ogawa, T., Kawada, N., et al. (2004) Typing of hepatic nonparenchymal cells using fibulin-2 and cytoglobin/STAP as liver fibrogenesis-related markers. **Histochemistry and cell biology,** 122 (1): 41-49.

Taylor, W. and Stark, G. (2001) Regulation of the G2/M transition by p53. **Oncogene,** 20 (15): 1803-1815.

Teranishi, Y., Matsubara, T., Krausz, K. W., Le ,T. T.T. et al. (2015) Involvement of hepatic stellate cell cytoglobin in acute hepatocyte damage through the regulation of CYP2E1-mediated xenobiotic metabolism. **Laboratory Investigation**. 95 (5): 515-524.

Thomas, G.T., Lewis, M.P. and Speight, P.M. (1999) Matrix metalloproteinases and oral cancer. **Oral oncology,** 35 (3): 227-233.

Thomas, P.D., Kejariwal, A., Guo, N., et al. (2006) Applications for protein sequence-function evolution data: mRNA/protein expression analysis and coding SNP scoring tools. **Nucleic acids research,** 34 W645-W650.

Thuy, L.T.T., Morita, T., Yoshida, K., et al. (2011) Promotion of liver and lung tumorigenesis in DEN-treated cytoglobin-deficient mice. **The American Journal of Pathology,** 179 (2): 1050-60.

Thuy, L.T.T., Matsumoto, Y., Thuy, T.T.V., et al (2015) Cytoglobin Deficiency Promotes Liver Cancer Development from Hepatosteatosis through Activation of the Oxidative Stress Pathway. **The American Journal of Pathology.** 185(4):1045-1060.

Tian, S.F., Yang, H., Xiao, D., et al. (2013) Mechanisms of Neuroprotection from Hypoxia-ischemia (HI) Brain Injury by Up-regulation of Cytoglobin (CYGB) in a Neonatal Rat Model. **Journal of Biological Chemistry,** 288 (22): 15988.

Tobiume, K., Matsuzawa, A., Takahashi, T., et al. (2001) ASK1 is required for sustained activations of JNK/p38 MAP kinases and apoptosis. **EMBO reports,** 2 (3): 222-228.

Tortora, V., Quijano, C., Freeman, B., et al. (2007) Mitochondrial aconitase reaction with nitric oxide, S-nitrosoglutathione, and peroxynitrite: Mechanisms and relative contributions to aconitase inactivation. **Free Radical Biology and Medicine,** 42 (7): 1075-1088.

Trachootham, D., Lu, W., Ogasawara, M.A., et al. (2008) Redox regulation of cell survival. **Antioxidants & Redox Signaling,** 10 (8): 1343-1374.

Trandafir, F., Hoogewijs, D., Altieri, F., et al. (2007) Neuroglobin and cytoglobin as potential enzyme or substrate. **Gene,** 398 (1-2): 103-113.

Trent, J.T. and Hargrove, M.S. (2002) A ubiquitously expressed human hexacoordinate hemoglobin. **Journal of Biological Chemistry,** 277 (22): 19538-19545.

Tsiftsoglou, A.S., Tsamadou, A.I. and Papadopoulou, L.C. (2006) Heme as key regulator of major mammalian cellular functions: Molecular, cellular, and pharmacological aspects. **Pharmacology & therapeutics,** 111 (2): 327-345.

Tsujino, H., Yamashita, T., Nose, A., et al. (2014) Disulfide bonds regulate binding of exogenous ligand to human cytoglobin. **Journal of inorganic biochemistry,** 135 20-7.

Uchino, H., Kuroda, Y., Morota, S., et al. (2008) Probing the molecular mechanisms of neuronal degeneration: importance of mitochondrial dysfunction and calcineurin activation. **Journal of Anesthesia,** 22 (3): 253-262.

Valko, M., Rhodes, C.J., Moncol, J., et al. (2006) Free radicals, metals and antioxidants in oxidative stress-induced cancer. **Chemico-biological interactions,** 160 (1): 1-40.

Van Slambrouck, S., Jenkins, A.R., Romero, A.E., et al. (2009) Reorganization of the integrin alpha 2 subunit controls cell adhesion and cancer cell invasion in prostate cancer. **International journal of oncology,** 34 (6): 1717-1726.

Vasiliou, V., Ross, D. and Nebert, D.W. (2006) Update of the NAD(P)H:Quinone oxidoreductase (NQO) gene family. **Human Genomics,** 2 (5): 329-335.

Vermorken, J.B. and Specenier, P. (2010) Optimal treatment for recurrent/metastatic head and neck cancer. **Annals of Oncology,** 21 252-261.

Vichai, V. and Kirtikara, K. (2006) Sulforhodamine B colorimetric assay for cytotoxicity screening. **Nature Protocols,** 1 (3): 1112-1116.

Vinogradov, S.N. and Moens, L. (2008) Diversity of globin function: enzymatic, transport, storage, and sensing. **Journal of Biological Chemistry,** 283 (14): 8773-8777.

Vurusaner, B., Poli, G. and Basaga, H. (2012) Tumor suppressor genes and ROS: complex networks of interactions. **Free Radical Biology and Medicine,** 52 (1): 7-18.

Wagner, J.M. and Karnitz, L.M. (2009) Cisplatin-Induced DNA Damage Activates Replication Checkpoint Signaling Components that Differentially Affect Tumor Cell Survival. **Molecular pharmacology,** 76 (1): 208-214.

Wajcman, H., Kiger, L. and Marden, M.C. (2009) Structure and function evolution in the superfamily of globins. **Comptes Rendus Biologies,** 332 (2-3): 273-282.

Wang, D.B., Kinoshita, C., Kinoshita, Y., et al. (2014) p53 and mitochondrial function in neurons. **Biochimica et Biophysica Acta (BBA) - Molecular Basis of Disease,** 1842 (8): 1186-1197.

Wang, S., Yu, H. and Wickliffe, J.K. (2011) Limitation of the MTT and XTT assays for measuring cell viability due to superoxide formation induced by nano-scale TiO2. **Toxicology in Vitro,** 25 (8): 2147-2151.

Wang, T., Zhang, X. and Li, J. (2002) The role of NF-kappa B in the regulation of cell stress responses. **International immunopharmacology,** 2 (11): 1509-1520.

Waridel, F., Estreicher, A., Bron, L., et al. (1997a) Field cancerisation and polyclonal p53 mutation in the upper aerodigestive tract. **Oncogene,** 14 (2): 163-169.

Waridel, F., Estreicher, A., Bron, L., et al. (1997b) Field cancerisation and polyclonal p53 mutation in the upper aerodigestive tract. **Oncogene,** 14 (2): 163-169.

Wawrowski, A., Gerlach, F., Hankeln, T., et al. (2011) Changes of globin expression in the Japanese medaka (Oryzias latipes) in response to acute and chronic hypoxia. **Journal of Comparative Physiology B-Biochemical Systemic and Environmental Physiology,** 181 (2): 199-208.

Weber, R.E. and Fago, A. (2004) Functional adaptation and its molecular basis in vertebrate hemoglobins, neuroglobins and cytoglobins. **Respiratory Physiology & Neurobiology,** 144 (2-3): 141-159.

Will, O., Gocke, E., Eckert, I., et al. (1999) Oxidative DNA damage and mutations induced by a polar photosensitizer, Ro19-8022. **Mutation Research-Dna Repair,** 435 (1): 89-101.

Wilson, M.T. and Reeder, B.J. (2008) Oxygen-binding haem proteins. **Experimental physiology,** 93 (1): 128-132.

Wojnarowicz, P.M., Provencher, D.M., Mes-Masson, A., et al. (2012) Chromosome 17q25 genes, RHBDF2 and CYGB, in ovarian cancer. **International journal of oncology,** 40 (6): 1865-1880.

Wright, T.J. and Davis, R.W. (2015) Myoglobin oxygen affinity in aquatic and terrestrial birds and mammals. **The Journal of experimental biology,** 218 (Pt 14): 2180-9.

Wurtele, H., Little, K.C.E. and Chartrand, P. (2003) Illegitimate DNA integration in mammalian cells. **Gene therapy,** 10 (21): 1791-1799.

Wystub, S., Ebner, B., Fuchs, C., et al. (2004) Interspecies comparison of neuroglobin, cytoglobin and myoglobin: Sequence evolution and candidate regulatory elements. **Cytogenetic and Genome Research,** 105 (1): 65-78.

Xi, Y., Obara, M., Ishida, Y., et al. (2007) Gene expression and tissue distribution of cytoglobin and myoglobin in the Amphibia and Reptilia: Possible compensation of myoglobin with cytoglobin in skeletal muscle cells of anurans that lack the myoglobin gene. **Gene,** 398 (1-2): 94-102.

Xiao, G., Chicas, A., Olivier, M., et al. (2000) A DNA damage signal is required for p53 to activate gadd45. **Cancer research,** 60 (6): 1711-1719.

Xinarianos, G., McRonald, F.E., Risk, J.M., et al. (2006) Frequent genetic and epigenetic abnormalities contribute to the deregulation of cytoglobin in non-small cell lung cancer. **Human molecular genetics,** 15 (13): 2038-2044.

Xu, H., Huang, Y., Xie, Z., et al. (2013) The expression of cytoglobin as a prognostic factor in gliomas: a retrospective analysis of 88 patients. **Bmc Cancer,** 13 247-247.

Xu, R., Harrison, P.M., Chen, M., et al. (2006) Cytoglobin overexpression protects against damage-induced fibrosis. **Molecular Therapy,** 13 (6): 1093-1100.

Xu, W.S., Parmigiani, R.B. and Marks, P.A. (2007) Histone deacetylase inhibitors: molecular mechanisms of action. **Oncogene,** 26 (37): 5541-5552.

Yamamoto, T., Suzuki, T., Kobayashi, A., et al. (2008) Physiological significance of reactive cysteineteine residues of keap1 in determining Nrf2 activity. **Molecular and cellular biology,** 28 (8): 2758-2770.

Yang, C.Q., Zeisberg, M., Lively, J.C., et al. (2003) Integrin alpha 1 beta 1 and alpha 2 beta 1 are the key regulators of hepatocarcinoma cell invasion across the fibrotic matrix microenvironment. **Cancer research,** 63 (23): 8312-8317.

Yang, Z., Schumaker, L.M., Egorin, M. J., et al . (2006) Cisplatin preferentially binds mitochondrial DNA and voltage-dependent anion channel protein in the mitochondrial membrane of head and neck squamous cell carcinoma: Possible role in apoptosis. **Clinical Cancer Research.** 1 (12): 5817-5825.

Ye, Q., Manda, S.M., Gallardo, T.D., et al. (2006) Mitochondrial localization and cellular function of cytoglobin: A novel calcineurin-dependent stress-responsive globin in the cardiovascular system. **Circulation,** 114 (18): 329-329.

Yoshimura, K., Meckel, K.F., Laird, L.S., et al. (2009) Integrin alpha 2 Mediates Selective Metastasis to the Liver. **Cancer research,** 69 (18): 7320-7328.

Yu, P., Yan, M., Lai, H., et al. (2014) Downregulation of miR-29 contributes to cisplatin resistance of ovarian cancer cells. **International Journal of Cancer,** 134 (3): 542-551.

Zeekpudsa, P., Kukongviriyapan, V., Senggunprai, L., et al. (2014) Suppression of NAD(P)H-quinone oxidoreductase 1 enhanced the susceptibility of cholangiocarcinoma cells to chemotherapeutic agents. **Journal of Experimental & Clinical Cancer Research,** 33 11.

Zhang, Y., Xiong, Y. and Yarbrough, W.G. (1998) ARF Promotes MDM2 Degradation and Stabilizes p53: ARF-INK4a Locus Deletion Impairs Both the Rb and p53 Tumor Suppression Pathways. **Cell,** 92 (6): 725-734.